

**DEVELOPMENT OF SOLID ACID CATALYSTS FOR BIODIESEL
PRODUCTION FROM HIGH FREE FATTY ACID FEEDSTOCK**

YAHAYA MUHAMMAD SANI

**THESIS SUBMITTED IN FULFILMENT OF THE
REQUIREMENTS FOR THE DEGREE OF DOCTOR OF
PHILOSOPHY**

**FACULTY OF ENGINEERING
UNIVERSITY OF MALAYA
KUALA LUMPUR**

2015

UNIVERSITY OF MALAYA
ORIGINAL LITERARY WORK DECLARATION

Name of Candidate: YAHAYA MUHAMMAD SANI (Passport No: A01534062)

Matric No: KHA110068

Name of Degree: DOCTOR OF PHILOSOPHY

Title of Thesis ("this Work"): DEVELOPMENT OF SOLID ACID CATALYSTS
FOR BIODIESEL PRODUCTION FROM HIGH FREE FATTY ACID
FEEDSTOCK

Field of Study: REACTION ENGINEERING (CHEMICAL ENGINEERING)

I do solemnly and sincerely declare that:

- (1) I am the sole author/writer of this Work;
- (2) This Work is original;
- (3) Any use of any work in which copyright exists was done by way of fair dealing and for permitted purposes and any excerpt or extract from, or reference to or reproduction of any copyright work has been disclosed expressly and sufficiently and the title of the Work and its authorship have been acknowledged in this Work;
- (4) I do not have any actual knowledge nor do I ought reasonably to know that the making of this work constitutes an infringement of any copyright work;
- (5) I hereby assign all and every rights in the copyright to this Work to the University of Malaya ("UM"), who henceforth shall be owner of the copyright in this Work and that any reproduction or use in any form or by any means whatsoever is prohibited without the written consent of UM having been first had and obtained;
- (6) I am fully aware that if in the course of making this Work I have infringed any copyright whether intentionally or otherwise, I may be subject to legal action or any other action as may be determined by UM.

Candidate's Signature

Date:

Subscribed and solemnly declared before,

Witness's Signature

Date:

Name: Prof. Dr. Wan Mohd Ashri Wan Daud

Designation: Professor/Supervisor

ABSTRACT

Numerous energy crises have been confronting the world due to excessive utilization of the world's depleting oil reserves by the ever-increasing human population. Concerns such as deteriorating health standards and environmental degradations have led to the search for sustainable biofuel alternatives. However, the recent nose-diving of the Brent crude oil price makes the search for sustainable catalysts more arduous. Consequently, the present study investigated two distinct catalytic routes for producing biodiesel from a cheap feedstock, which could have competitive edge with fossil diesel. Firstly, the study explored the potentials of converting wastes from oil palm biomass such as empty fruit bunch (EFB), palm frond (PTF), spikelet (PTS) and waste fruit (WPF) into sulfonated mesoporous solid acids *via* carbonization-sulfonation method. Brunauer-Emmet-Teller (BET), powder X-ray diffraction (XRD), Energy dispersive X-ray (EDX), and field emission scanning emission microscopy (FE-SEM) analyses elucidated the structural and textural properties of the catalysts. Further, Fourier transform-infrared (FT-IR) spectroscopy and titrimetric analyses measured the strong acid value and acidity distribution of the materials. These evidenced large mesopore volumes, large surface areas, uniform pore sizes, and high acid densities on the catalysts. The catalytic activity exhibited in esterifying used frying oil (UFO) containing high (48%) free fatty acid (FFA) further confirmed these properties. Interestingly, sEFB/300 and sPTS/400 converted more than 98% FFA into fatty acid methyl esters (FAMES). This is outstanding considering the lower reaction parameters of 3 h, 5:1 methanol-to-oil ratio, and moderate temperature range between 100 and 200 °C.

Equally, the study delved into a process considered to have attained state-of-the art status; sulfated zirconia (SZ), which has been the subject of numerous reports since its discovery in 1979. The catalytic activity of SZ in esterifying FFA and transesterifying triglycerides

(TG) simultaneously from high-FFA containing feedstocks into biodiesel has led to claims that SZ are superacids, or at least very strong acids. However, SZ has some inherent limitations such as slow reaction rates. Similarly, despite the numerous advantages of zeolite catalysts, microporosity hinders their industrial applicability for biodiesel production. Evidently, several reports on optimal preparative conditions that produced superacidic materials abound *via* carefully controlled procedures. Nonetheless, to date, no study has reported the effect of grafting zeolite on SZ for biodiesel production. Further, there is no information from open literature regarding biodiesel production over SZ doped with ytterbium, Yb. Consequently, this study investigated the prospects of combining mesoporous zeolite and SZ; and effect of doping SZ with Yb for biodiesel production. The study synthesized different composite catalysts that have potential to maximize activity and minimize adsorbate-induced surface reconstruction, with consequent reduction in net energy consumption. Remarkably, large mesoporosity, high amount, and dispersion of active sites on Yb-doped SZ ensured significant activity despite low specific surface area that was due to short aging period. However, different sulfation methods showed marginal effect on SZ. Interestingly, the catalyst achieved more than 99% conversion under moderate conditions. These findings will definitely help to further the biofuel central policy of replacing petrodiesel in the possible near future.

ABSTRAK

PEMBANGUNAN PEMANGKIN ACID PEPEJAL UNTUK PENGELUARAN BIODIESEL DARI BAHAN MENTAH ASID LEMAK BEBAS YANG TINGGI

Pelbagai krisis tenaga telah dihadapi dunia disebabkan oleh penggunaan berlebihan simpanan minyak dunia yang semakin berkurangan dan peningkatan populasi manusia. Kebimbangan terhadap tahap kesihatan yang semakin merosot dan kemusnahan alam sekitar telah membawa kepada pencarian alternatif biofuel yang mampan. Walaubagaimanapun, harga minyak mentah Brent yang menurun secara mendadak baru-baru ini menjadikan pencarian pemangkin yang mampan menjadi lebih sukar. Oleh itu, kajian ini dijalankan melalui dua kaedah yang berbeza untuk menghasilkan biodiesel yang mempunyai daya saing dengan diesel fosil. Salah satu kaedah kajian adalah mengeksplorasi potensi menukar sisa biomas kelapa sawit seperti tandan kelapa sawit kosong (EFB), pelepah sawit (PTF), *spikelet* (PTS) dan sisa buah (WPF) kepada pemangkin *mesoporous Sulfonated* melalui kaedah karbonisasi-sulfonation. Analisis melalui Brunauer-Emmet-Teller (BET), *powder X-ray diffraction* (XRD), *Energy dispersive X-ray* (EDX), dan *field emission scanning emission microscopy* (FE-SEM) telah dilakukan untuk mengenal pasti ciri-ciri struktur dan tekstur pemangkin. FT-IR dan analisis titrimetric mengukur nilai asid kuat dan serakan keasidan bahan tersebut. Analisis ini menunjukkan bahawa pemangkin mempunyai sejumlah besar *mesopore*, luas permukaan yang tinggi, saiz liang yang seragam, dan ketumpatan asid yang tinggi. Aktiviti pemangkin yang dipamerkan oleh *esterifying* minyak goreng yang telah digunakan (UFO) mengandungi asid lemak bebas (FFA) yang tinggi (48%) mempunyai ciri-ciri tersebut. Lebih menarik, sEFB/300 dan sPTS/400 menukar lebih daripada 98% FFA kepada *fatty acid methyl esters* (FAMES). Ini memberangsangkan jika diambilkira

parameter reaksi lebih rendah iaitu 3 jam dengan nisbah 5:1 untuk metanol-minyak, dan julat suhu sederhana antara 100 dan 200 °C.

Kajian ini turut menjurus kepada satu proses yang boleh dianggap mempunyai status pembangunan yang tinggi (*state-of-art*), di mana *Sulfated Zirkonia* (SZ) merupakan subjek yang kerap dilaporkan sejak penemuannya pada tahun 1979. Aktiviti memangkin SZ dalam proses serentak untuk *esterifying FFA* dan *transesterifying* trigliserida (TG) daripada bahan mentah yang mengandungi FFA yang tinggi kepada biodiesel telah membawa kepada dakwaan bahawa SZ merupakan *superacids* atau asid yang sangat kuat. Walaubagaimanapun, SZ mempunyai beberapa kelemahan seperti keasidan lemah dan kadar tindak balas yang perlahan. Walaupun mempunyai kelebihan pemangkin zeolite, mikrokeliangan mereka menghalang perindustrian bersesuaian bagi pengeluaran biodiesel. Terdapat beberapa laporan mengenai keadaan persiapan optimum yang menghasilkan bahan-bahan *superacidic* banyak terdapat melalui prosedur terkawal. Namun begitu, sehingga kini tiada lagi kajian melaporkan kesan cantuman zeolite pada SZ bagi pengeluaran biodiesel. Di samping itu, tiada maklumat daripada kajian lepas mengenai pengeluaran biodiesel lebihan SZ digabungkan dengan ytterbium, Yb. Oleh itu, kajian ini menyiasat prospek penggabungan *mesoporous zeolite* dan SZ dan kesan gabungan SZ dan Yb terhadap pengeluaran biodiesel. Pemangkin komposit berbeza yang mempunyai potensi untuk memaksimum dan meminimumkan aktiviti bahan terjerap yang disebabkan oleh pembinaan semula permukaan dengan mengurangkan penggunaan tenaga bersih telah dihasilkan. Kajian ini mengenalpasti cantuman, kelembapan yang baru jadi dan teknik *sol-gel* dalam proses menghasilkan pemangkin komposit. Kaedah sulfation berbeza mempunyai kesan yang sangat sedikit terhadap SZ yang dihasilkan. Seperti jangkaan, semua pemangkin menghasilkan penukaran lebih daripada 98% dalam

keadaan sederhana. Penemuan ini akan dapat membantu untuk mencapai dasar *biofuel* pusat bagi menggantikan *petrodiesel* dalam masa terdekat.

ACKNOWLEDGEMENTS

Verily, all praise is for Allaah, we seek His help and forgiveness. We seek refuge with Allaah from the evil of our own souls (and from our deeds). Whomsoever Allaah guides will never be led astray, and whomsoever Allaah leaves astray, no one can guide such a person. I bear witness that there is no god but Allaah (alone and without partner), and I testify that Muhammad ﷺ is His Slave and Messenger.

Most of the experimental studies during the progression of this study, from February 2012 to January 2015 were carried out in *Makmal Pemindahan Jisim* (Mass Transfer Process Laboratory) and *Makmal Unit Operasi* (Unit Operation Laboratory), and *Makmal Instrumentasi* (Instrumentation Laboratory), at the Department of Chemical Engineering, University of Malaya, 50603, Kuala Lumpur, Malaysia. Others were partly at the *Pusat Perkhidmat Penyelidikan* (Centre for Research Service, Institute of Research Management & Monitoring), and Department of Chemistry of University of Malaya. High Impact Research, HIR under University of Malaya funded the research from HIR project number D000011-16001. I am also grateful to the valuable assistance provided from the Project No: PG144-2012B, and the Tertiary Education Trust Fund (TETFund), Ahmadu Bello University, Zaria, Nigeria.

I am grateful to my supervisors, Prof. Dr. Wan Mohd Ashri Wan Daud and Prof. Ir. Dr. Abdul Raman Abdul Aziz for their advice, patience, support, and encouragement. I am also thankful to Prof. Dr. Idris Muhammad Bugaje, Prof. Dr. Nurudeen Biola Oladoja, Dr. Muhammad Tijjani Isa, Dr. Nurudeen Yusuf, Dr. Abdulaziz Atta, Dr. Umar Shehu, Dr. Kamil Bello, Dr. Idris Musa Atadashi, and Murtala Tijjani, Ismail Adedeji, for their valuable contributions, financial support, concerns, and prayers. Warm regards also go to my co-authors, especially My Alter'ego for all the help in the research and *in the* research,

for your support and most of all, for your unflinching understanding friendship. Many thanks also go to Messrs. Sharafadeen Gbadamasi, Abdulaziz Isa and Ahmad Khalil, Idris Saeed, Murtala Ambursa, Dr. Babangida Sarkin Yandoka, Abdulwasiu Abdulhameed, Ma'ruf Ibitoye, Mushaffa Oke, Isa Yakub Muhammad, and Peter Adeniyi Alaba for their help in the research work.

My warmest thanks to my colleagues at Chemical Engineering Department, Ahmadu Bello University, Zaria Nigeria for providing a motivating working atmosphere, for kind support and social encouragement. Especially, I thank Mrs. Samson, Mrs Dodo, Dr. Hamza, Dr. Maina, Dr. Waziri, Dr. Mohammed-Dabo, Mal. Ibrahim, Dr. Olawale, Dr. Aderemi, Dr. Momoh, Prof. Ahmed, Dr. Nurudeen Salahudeen and all others too numerous to mention for her support and friendship during many years.

I saved the last part of my acknowledgement to my family because they are my greatest assets. To my mother, Hajiya Binta for mentoring and being catalysts of my growth for many years. For always having faith in me and my capabilities right from my youthful age – your love radiates in me always which makes people wonder the source of my ever-happy and smiley mood. Thank you for being the inspiration and miracle of my life. Alhaji Sani, my deceased father, I pray that Allah forgive you and join us all in Jannatul Firdaus, amin! To my 2nd mother, Hajiya Adama (I pray that Allah grant you Raudatul Jannah, amin!); thank you for your love, presence, and support. Daddy, may Allah be pleased with you and reunite us in Jannatul Firdaus so I could narrate to you all that you missed. Special appreciation to my 2nd Dad; many things wouldn't have been possible were it not for your Allah-endowed foresight. To my wife – you deserve a second mention; I thank most lovingly Ayeashah for your presence and patience. To my lovely, intelligent and obedient children; Sumayyaah, Abdallaah, Abdurrahman, and 'Umar Al-Qaqa, I pray that Allah elevates you and love you. May the love of His Noble messenger

be your guiding principle in life. I also share my warmest thanks to my siblings; Adama – my pseudo-mum, Muhammad Sani, Hajarrah, Abidah, Hussayn, Suwaibah, and Abdulaziz and all our extended family members – I love you all.

“As a catalyst, I have learnt that the fastest way of being perpetually happy is by striving to put a smile on others!”

Yahya M. Sani

“If we knew what it was we were doing, it would not be called research, would it?”

~ Albert Einstein

TABLE OF CONTENTS

ORIGINAL LITERARY WORK DECLARATION	ii
ABSTRACT	iii
<i>ABSTRAK</i>	v
ACKNOWLEDGEMENTS	viii
TABLE OF CONTENTS	xi
LIST OF FIGURES.....	xvi
LIST OF TABLES	xxii
APPENDIX	xxiv
CHAPTER 1: GENERAL INTRODUCTION	1
1.1 Importance of the present study	4
1.2.1 Research background	8
1.2.2 Statement of the research problem	10
1.2.3 Justification for the study	11
1.2.4 Aim and objectives of the research	11
1.2.5 Scope of the research	13
1.2.6 Outline of the thesis	14
1.2.7 Synopsis, findings and contributions of the study.....	18
CHAPTER 2: LITERATURE REVIEW	20
2.1 Overview	20
2.2 Composition of vegetable oil	23
2.3 Reasons why vegetable oil is not suitable for direct usage in diesel engines	24
2.4 Methods of reducing viscosity of vegetable oil for diesel engines	25
2.4.1 Direct use and blending (dilution).....	25
2.4.2 Thermal cracking (pyrolysis)	26

2.4.3	Micro-emulsion or co-solvency	27
2.4.4	Transesterification or alcoholysis.....	27
2.5	Oil yields of various feedstocks	29
2.6	Energy balance of biodiesel	30
2.7	Present scope of biodiesel production.....	30
2.8	Performance, handling, storage, and usage comparisons – biodiesel and diesel ...	32
2.9	Issues surrounding conventional processes for biodiesel production	32
2.10	Solid acid catalysts	34
2.10.1	The concept of acidity	34
2.10.2	Amorphous mixed oxides	37
2.10.3	Catalysts with sulfonic acid groups.....	41
2.10.4	Heteropoly acids and polyoxometalates (isopoly and heteropoly anions)	41
2.10.5	Zeolites and zeotype materials	42
2.11	Biodiesel production <i>via</i> solid acid catalysis	44
2.11.1.	Effect of preparation and structure promoters.....	45
CHAPTER 3: PALM FROND AND SPIKELET AS ENVIRONMENTALLY BENIGN ALTERNATIVE SOLID ACID CATALYSTS FOR BIODIESEL PRODUCTION		
3.1	Introduction	51
3.2	Literature review	54
3.3	Materials and catalyst preparation.....	58
3.4	Methods.....	59
3.4.1	Catalyst characterization	60
3.4.2	Production of fatty acid methyl esters.....	61

3.4.3	Acid density analysis.....	62
3.3.4	Determination of acid value	63
3.4	Results and discussion.....	64
3.4.1	Catalytic performance of the solid acid catalysts in biodiesel production	72
3.4	Conclusions	78
CHAPTER 4: OIL PALM BIOMASS AS CHEAP PRECURSOR TO EFFICIENT MESOPOROUS SOLID ACID CATALYSTS FOR ESTERIFYING USED FRYING OIL CONTAINING HIGH FREE FATTY ACIDS		80
4.1	Introduction	80
4.2	Literature review	83
4.3	Materials and methods	85
4.3.1	Preparation of mesoporous carbon catalysts from palm empty palm fruit bunches (EFB) and waste palm fruits (WPF).....	85
4.3.2	Catalyst characterizations.....	86
4.3.3	Acid density analysis.....	86
4.3.4	Production of free fatty methyl esters from FFA-containing feedstock	87
4.3.5	Determination of acid value	88
4.4	Results and discussion.....	88
4.4.1	Characterization of palm biomass and catalysts	88
4.4.2	Catalytic performance of the catalysts in esterifying feedstock containing high FFA	97

4.6	Conclusions	101
CHAPTER 5: ACIDITY AND CATALYTIC PERFORMANCE OF Yb-DOPED $\text{SO}_4^{2-}/\text{Zr}$ IN COMPARISON WITH $\text{SO}_4^{2-}/\text{Zr}$ CATALYSTS SYNTHESIZED <i>via</i> DIFFERENT PREPARATORY CONDITIONS FOR BIODIESEL PRODUCTION		
		103
5.1	Introduction	103
5.2	Literature review	106
5.2.1	Structure and chemistry of sulfated zirconium	106
5.3	Materials and methods	111
5.3.1	Catalyst characterization	114
5.3.2	Production of fatty acid methyl esters from used frying oil.....	115
5.4	Results and discussion.....	117
5.4.1	X-ray diffraction analysis.....	117
5.4.2	Surface physical property measurements.....	121
5.4.4	Activity of mesoporous SZ catalysts in transesterifying high FFA-containing feedstock.....	132
5.5	Conclusion.....	135
CHAPTER 6: FACILE SYNTHESIS OF SULFATED MESOPOROUS $\text{Zr}/\text{ZSM-5}$ WITH IMPROVED BRØNSTED ACIDITY AND SUPERIOR ACTIVITY OVER SZr/Ag, SZr/Ti, AND SZr/W IN TRANSFORMING USED FRYING OIL INTO BIODIESEL.....		
		137
6.1	Introduction	137
6.2	Literature review	141
6.2.1	Superacidity of SZ and other modified aluminosilicate catalysts	141
6.2.3	Sulfated zirconia supported on zeolite – the way forward?	144

6.3 Materials and methods	144
6.3.1 Catalyst preparation.....	145
6.3.2 Catalyst characterization	145
6.3.3 Production of fatty acid methyl esters.....	147
6.4 Results and discussion.....	148
6.4.1 Results of catalyst characterization	148
6.4.2 Comparative transesterification activity over the composite sulfated zirconia catalysts	164
6.4.3 Palmitic acid transesterification kinetics SZr/ZSM-5	167
6.5 Conclusion.....	171
CHAPTER 7: OVERALL CONCLUSION	174
7.1 Recommendations for future works.....	178
REFERENCES	180
List of publications and papers presented	207
List of other related publications.....	209

LIST OF FIGURES

Figure 1.1: Diagrammatical representation of the logical and coordinated progression of chapters 3 to 6	17
Figure 2.1: Total renewable energy supply (Mtoe) in year 2008.....	21
Figure 2.3: Transesterification of triglyceride with methanol in the presence of catalyst.....	28
Figure 2.4: Liquid fuel supply by type (Millions of oil-equivalent barrel per day).....	29
Figure 2.5: Determinants for selecting a particular catalyst.....	36
Figure 3.1: Molecular structures of carbohydrate derivatives.....	56
Figure 3.2: Diagrammatic representation of amorphous polycyclic carbon sheets with -OH -COOH, and -SO ₃ H, groups bonded on the carbon precursor	57
Figure 3.3: Field emission scanning electron microscope	61
Figure 3.4: Double 100 mL stainless steel autoclave (250 °C, 100 bar) reactor.....	62
Figure 3.5: XRD patterns of sPTS/400, sPTF/400, sPTF/SA/300, and sPTF/SA/400 ..	65
Figure 3.6: N ₂ adsorption-desorption isotherm and pore size distribution of sPTF/SA/400 and sPTF/400	68
Figure 3.4: (a) Results of the surface microstructural analysis of the sPTF/SA/400 <i>via</i> FE-SEM, and (b) surface elemental composition of the sPTF/SA/400 determined <i>via</i> EDX analysis.....	69
Figure 3.8 (a) Results of the surface microstructural analysis of the sPTF/SA/300 <i>via</i> SEM, and (b) surface elemental composition of the sPTF/SA/300 determined <i>via</i> EDX analysis.....	70
Figure 3.9: (a) Results of the surface microstructural analysis of the sPTS-400 <i>via</i> SEM, and (b) surface elemental composition of the sPTS-400 determined <i>via</i> EDX analysis.....	70

Figure 3.10: FT-IR spectra of sPTF/300 catalysts, sPTS/400 catalysts, and unsulfonated-PTS/400 mesoporous carbon.....	71
Figure 3.12: Mechanism of esterification catalyzed by mesoporous sulfonated carbon catalyst.....	73
Figure 3.11: Catalytic activities of mesoporous (a) sPTF/SA/400 and (b) sPTS/400 catalysts prepared under different conditions.....	75
Figure 3.11: Catalytic activities of mesoporous (c) sPTF/400, and (d) sPTF/SA/300 catalysts prepared under different conditions.....	76
Figure 3.12: Activity of sPTS/400 after regeneration and recycling for esterification reaction.....	77
Figure 4.1: XRD pattern of sEFB/400 and sWPF/400.....	90
Figure 4.2: N ₂ adsorption–desorption isotherms for sEFB/300, sEFB/400 and sWPF/400	92
Figure 4.3: Pore size distribution curves for sEFB/300, sEFB/400 and sWPF/400.....	93
Figure 4.4: (a) Results of the surface microstructural analysis of the sEFB/400 <i>via</i> FE-SEM, and (b) surficial elemental composition of the sEFB/400 <i>via</i> EDX analysis.....	93
Figure 4.5: (a) Results of the surface microstructural analysis of the sEFB/300 <i>via</i> SEM, and (b) surficial elemental composition of the sEFB/300 <i>via</i> EDX analysis.....	94
Figure 4.6: (a) Results of the surface microstructural analysis of the sWPF/400 <i>via</i> SEM and (b) surficial elemental composition of the sWPF/400 <i>via</i> EDX analysis.....	95
Figure 4.7: FTIR spectra for sWPF/300, sEFB/300, sEFB/400 mesoporous carbon catalysts, and unsulfonated EFB.	96
Figure 4.7: Comparative catalytic activity of mesoporous (a) sEFB/400 and (b) sEFB/300 catalysts prepared at different conditions.....	99

Figure 4.7: Comparative catalytic activity of mesoporous (c) sWPF/SA/400 catalysts prepared at different conditions.....	99
Figure 4.8: Activity of sEFB/300 after regeneration and recycling for esterification reaction.....	100
Figure 5.1: Two structures of SZ at moderate coverage with possibility of residing on different crystal planes	107
Figure 5.2: Equilibrium structures of the $\text{H}_2\text{O}/\text{ZrO}_2$ (101) complexes for the two possible Zr sites with selected bond lengths given in angstroms	108
Figure 5.3: Equilibrium structure of the $(\text{H}^+, \text{HSO}_4^-)/\text{ZrO}_2$ (101) adsorption complex showing bond lengths in angstroms and the two outermost ZrO_2 layers	110
Figure 5.4: Equilibrium structure of the $(2\text{H}^+, \text{SO}_4^{2-})/\text{ZrO}_2$ (101) complex with selected bond lengths in angstroms.....	111
Figure 5.5: Preliminary optimization on (a) temperature, (b) time and (c) methanol-to-oil molar ratio	116
Figure 5.6: X-ray diffraction patterns for SZr-Ti-Yb-500-4/s, SZr-500/e, SZr-500-4/s, SZr-Ti-500-4/e, and SZr-Ti-500-4/s.	119
Figure 5.7: X-ray diffraction patterns for (a) SZr-500-5/7, (b) SZr-500-5/14, and (c) SZr-500-5/10.	120
Figure 5.8(a): N_2 adsorption-desorption isotherms of mesoporous SZ synthesized from different conditions	122
Figure 5.8(b): N_2 adsorption-desorption isotherms of mesoporous SZ synthesized from different conditions	123
Figure 5.9: Pore size distribution curves of mesoporous SZ prepared from different preparatory conditions.....	124
Figure 5.10: Pore size distribution curves of mesoporous SZ prepared from different preparatory conditions.....	125

Figure 5.11: (a) Results of the surface microstructural analysis of the SZr-500-4/e <i>via</i> FE-SEM and (b) surface elemental composition of the SZr-500-4/e determined <i>via</i> EDX analysis.....	126
Figure 5.12: (a) Results of the surface microstructural analysis of the SZr-500-4/s <i>via</i> SEM and (b) surficial elemental composition of the SZr-500-4/s <i>via</i> EDX analysis	127
Figure 5.13: (a) Results of the surface microstructural analysis of the SZr-500-1/e (15 min) <i>via</i> SEM and (b) surficial elemental composition of the SZr-500-1/e (15 min) <i>via</i> EDX analysis.....	127
Figure 5.14: (a) Results of the surface microstructural analysis of the SZr-Ti-500/e (15 min) <i>via</i> SEM and (b) surficial elemental composition of the SZr-Ti-500/e <i>via</i> EDX analysis.....	128
Figure 5.15: (a) Results of the surface microstructural analysis of the SZr-Ti-500/s (15 min) <i>via</i> SEM and (b) surficial elemental composition of the SZr-Ti-500/s <i>via</i> EDX analysis.....	128
Figure 5.16: (a) Results of the surface microstructural analysis of the SZr-Ti-Yb/500-4/s <i>via</i> SEM and (b) surficial elemental composition of the SZr-Ti-Yb/500-4/s <i>via</i> EDX analysis.....	128
Figure 5.17: (a) Results of the surface microstructural analysis of the SZr-500-5/7 <i>via</i> SEM and (b) surficial elemental composition of the SZr-500-5/7 <i>via</i> EDX analysis	129
Figure 5.18: (a) Results of the surface microstructural analysis of the SZr-500-5/7R <i>via</i> SEM and (b) surficial elemental composition of the SZr-500-5/7R <i>via</i> EDX analysis.....	129

Figure 5.19: (a) Results of the surface microstructural analysis of the SZr-500-5/10 <i>via</i> SEM and (b) surficial elemental composition of the SZr-500-5/10 <i>via</i> EDX analysis.....	130
Figure 5.20: NH ₃ -temperature-programmed desorption profiles for the synthesized catalysts	131
Figure 5.12: Different activity of SZ employed at 200 °C for 5 h	133
Figure 5.12: Performance of regenerated SZ employed at 200 °C for 5 h.....	135
Figure 6.1: Presence of Bronsted and Lewis acid sites on SZ	142
Figure 6.1: (a) NH ₃ -temperature-programmed desorption profiles for the parent ZSM-5, and (b) SZr/Ag, SZr/Ti, SZr/W, SZr/ZSM-5 synthesized catalysts.....	151
Figure 6.2: X-ray diffraction patterns for the parent ZSM-5 and the optimized SZr/Ag, SZr/Ti, SZr/W, SZr/ZSM-5 catalysts synthesized under the same conditions .	155
Figure 6.3: (a) N ₂ adsorption-desorption isotherms for SZr/Ag, SZr/Ti, SZr/W, SZr/ZSM-5, and ZSM-5 respectively, synthesized under the same conditions	157
Figure 6.3: (b) Pore size distribution curves for mesoporous SZr/Ag, SZr/Ti, SZr/W, SZr/ZSM-5, and ZSM-5 respectively, synthesized under the same conditions	158
Figure 6.5: (a) Results of the surface microstructural analysis of the ZSM-5 <i>via</i> FE-SEM and (b) surface elemental composition of the ZSM-5 determined <i>via</i> EDX analysis	161
Figure 6.6: (a) Results of the surface microstructural analysis of the SZr/ZSM-5 <i>via</i> FE-SEM and (b) surface elemental composition of the SZr/ZSM-5 determined <i>via</i> EDX analysis.....	161
Figure 6.7: (a) Results of the surface microstructural analysis of the AgNO ₃ <i>via</i> FE-SEM and (b) surface elemental composition of the AgNO ₃ determined <i>via</i> EDX analysis	162

Figure 6.8: (a) Results of the surface microstructural analysis of the SZr/Ag <i>via</i> FE-SEM and (b) surface elemental composition of the SZr/Ag determined <i>via</i> EDX analysis	163
Figure 6.9: (a) Results of the surface microstructural analysis of the S/Zr/Ti <i>via</i> FE-SEM and (b) surface elemental composition of the S/Zr/Ti determined <i>via</i> EDX analysis	163
Figure 6.10: (a) Results of the surface microstructural analysis of the $(\text{NH}_4)_6\text{H}_2\text{W}_{12}\text{O}_{40} \cdot x\text{H}_2\text{O}$ <i>via</i> FE-SEM and (b) surface elemental composition of the $(\text{NH}_4)_6\text{H}_2\text{W}_{12}\text{O}_{40} \cdot x\text{H}_2\text{O}$ determined <i>via</i> EDX analysis	164
Figure 6.11: (a) Results of the surface microstructural analysis of the SZr/W <i>via</i> FE-SEM and (b) surface elemental composition of the SZr/W determined <i>via</i> EDX analysis	164
Scheme 6.1: The Langmuir-Hinshelwood mechanism.....	165
Figure 6.12: Catalytic activities of 2 wt.% mesoporous catalysts at 5:1 methanol-to-oil ratio and 200 °C	167

LIST OF TABLES

Table 2.1: Fatty acid composition of common oils and fats.....	24
Table 2.2: Estimated oil content, yields and required land of different biodiesel feedstocks	30
Table 2.3: Main advantages and disadvantages of solid acid catalysts	35
Table 2.4: Catalytic effect of superacids on esterification and transesterification as function of calcination temperature.....	45
Table 2.5: Effect of calcination temperature on catalytic activity of $\text{ZrO}_2/\text{WO}_3^{2-}$ during esterification	46
Table 2.6: Catalyst reactivity supported on alumina and functionalized mesoporous silicates	48
Table 2.7: Problems and potential solutions for using solid acid catalysts for biodiesel production	49
Table 3.1: Selected properties of B100 and typical No. 2 diesel fuels.....	60
Table 3.2: Methods for analyzing vegetable oils.....	64
Table 3.3: Surface properties and total acid ($-\text{SO}_3\text{H}$) density of the catalysts	67
Table 4.1: Surface properties and total acid density ($-\text{SO}_3\text{H}$) of the tested catalysts	92
Table 5.1: Variable parameters employed for synthesizing mesoporous sulfated zirconia	112
Table 5.2: Textural properties and acidity of synthesized sulfated zirconia	121
Table 6.1: Textural properties and acidity of synthesized sulfated zirconia	149
Table 6.2: Wave number frequencies and extinction coefficients of IR absorption spectra designated to typical probe molecules adsorbed on acid sites	153
Table 6.3: Working conditions for the GC analyzer	168
Table 6.4: Physical properties and biodiesel yield obtained from UFO compared to diesel	169

Table 6.5: Comparative FFA pretreatment cost	171
Table 7.1: Summary of the different catalysts and their respective performances.....	177

APPENDIX

Appendix A: Energy dispersive X-ray, EDX analysis.....	204
---	-----

CHAPTER 1: GENERAL INTRODUCTION

This chapter gives the overall perspective of the research problem and explains why the problems are worth investigating. It sets out the aim and objectives of the study and it serves as orientation for the reader. The chapter gave general introduction to the field of study, as well as to the present study. The increasing prices on the limited petroleum reserves exacerbate the growing public concerns on human and animal health, and the environmental impact caused by petroleum exploration and excessive utilization. These issues compelled researchers to explore energy alternatives, which are cheaper, “greener”, and sustainable. In this regard, biodiesel is receiving great attention because of its renewability, cheap feedstock sources, and its promising potential to replace petroleum-based diesel. Vegetable oils, animal fats, or other sources such as used cooking oil, grease, algae, etc. containing triglyceride, TG serve as the primary building block for long-chain fatty acid methyl esters, FAME known as “biodiesel”. Biodiesel is defined as fuel obtained from reacting alcohols such as methanol or ethanol with TGs derived from vegetable oils or fats in a (trans)esterification reaction catalyzed by acid, base, or enzyme. Esterification is the chemical reaction in which two reactants (typically, an alcohol and an acid) form an ester. On the other hand, transesterification is the transformation of an ester into another ester *via* interchange of the alkoxy moiety. In other words, it involves the exchange of the alkoxy groups of an ester with an alcohol often catalyzed.

Further, pollution caused from combusting biodegradable liquid biodiesel fuel is less than petroleum diesel combustion. This is because biodiesel is sulfur- and aromatic-free, and it has high oxygen content. Moreover, it is possible to apply directly in diesel engines without modifications or mixed in any proportion with petroleum diesel (Hassan, et al., 2015). Consequently, this chapter presents a detailed overview of the current state-of-the-art on biodiesel production, the challenges current development, and the need for newer

advances. Subsequent chapters present detailed discussions and analyses on catalyst synthesis from palm biomass, and advances in the activity of zirconia-based catalysts.

The numerous challenges such as cost of feedstock, separation problems, wastage of reagents, disposal, and environmental issues posed by corrosive mineral acids such as HF, H₂SO₄, AlCl₃, etc. in the industry have become the driving force for developing environmentally benign solid acid catalysts. These promising alternatives have the potential to minimize the large volumes of acids utilized as catalysts and waste generated from such harmful acids from neutralization and decomposition processes. Further, substituting such liquid acids and bases, and heterogeneous bases with solid acid catalysts for organic reactions will serve as the prime requisite in ensuring preserved environments. This is because solid acid catalysts have high activity advantage and good selectivity, which suppresses unwanted side reactions. Other major advantages of solid acid catalysts include: (a) higher selectivity of desired product, (b) product yield maximization, (c) environmentally benign and non-stoichiometric catalysts replaces stoichiometric reagents, (d) ease of separation and handling of final products from the reaction mixture, (e) fast and efficient catalyst recovery, (f) minimized waste disposal and associated costs, and (g) enhanced reusability and recycling options.

Evidently, solid acid catalysts are efficient in producing biodiesel from feedstocks with high FFA contents. However, the scarcity of licensed processes is an indication that solid acid catalysis needs new advances *via* comprehensive experimentations. These will help to establish the numerous potentials of these catalysts as well as ensuring biodiesel prominence. Despite these challenges, last century witnessed catalysis as the major backbone for most industrial processes such as petrochemistry (especially, petroleum catalytic refining) and bulk chemistry. However as earlier highlighted, recent environmental and socioeconomic challenges have brought about new demands that

require novel catalytic solutions. Inherent with these new challenges are the potentials for greater efficiency and sustainability of such systems (Reddy, et al., 2006). Moreover, the searches for newer solutions have led experts to explore in minute details, the attributes of different materials, systems and devices (Garcia, et al., 2008). One key task is in achieving phase-homogeneous solids with uniform morphological and chemical properties. This challenge is a fundamental prerequisite to any rational catalyst design.

Conventionally, selection of catalytic performance is from a large library of synthesized catalytic materials under predefined conditions. One consequence of such method is that the resulting materials possess complex phase mixtures. Further, the desired outcome is only a small and mostly unidentified fraction, while most of the solid is only spectator or even of detrimental function. Moreover, deactivation could easily occur on the catalytic sites because of the structural conversion they facilitate. These may limit the existence of high-energy sites that are essential for the performance of the solid acids. Hence, a way out of this key obstacle is the use of *in situ* observation techniques. This is because the high-energy sites of a catalyst cannot be predetermined *via* synthesis because their formation occurs only during the catalytic process. Consequently, the era of catalysis research, characterized primarily by trial-and-error, is becoming history (Reddy, et al., 2006). Techniques such as quantum mechanics calculations, density functional theory simulation, solid-state nuclear magnetic resonance, *in situ* fluorescence microscopy and computational-real-time technology aid in deciphering the in-depths of heterogeneous catalysis and surface science (Mitchell, et al., 2013; Holewinski, et al., 2013; Gladden, 2013; Al-Rifai, et al., 2013; Garcia, et al. 2008; Dutch National Research School, NRSC-Catalysis, April 2009).

Achieving these fundamental insights into the mechanisms of catalysis *via* breakthroughs in theoretical insights and computational methods will enhance predicting catalysts performance under real reaction conditions. These important tools will in turn, be utilized in the design of novel solid acid catalysts and the control of catalytic processes (Hara, et al. 2004). These will have tremendous applications in unraveling the challenges encountered in synthesizing efficient catalysts. Further, these facilitate the determination of the active sites of surface reactions, the barrier(s) encountered in such reactions and the rate at which they occur even within picoseconds. These might involve combining such techniques and utilizing probe molecules augmented with multifarious nuclei such as ^1H , ^{13}C and ^{31}P for investigating surface acidities of the solid acid catalysts (Dal Santo, et al., 2010) which is outside the scope of this study.

1.1 Importance of the present study

Homogeneous acid catalysts received wide acceptability because of their fast reaction rates. However, postproduction costs incurred from aqueous quenching, wastewater and loss of catalysts led to the search for alternatives. Until recently, heterogeneous base catalyzed-biodiesel production also gained the attention of most researchers. This was because the process minimized the problems of homogeneous catalysis in terms of catalyst regeneration and recycling in continuous processes. However, despite these advances, the ultimate aim of producing biodiesel at affordable cost is yet to be realized. Further, the process requires refined feedstocks which account for as high as 88% of the final production costs. Thus, the focus of many research efforts is towards the rational design and development of solid acid catalysts aimed at reducing biodiesel production costs. Therefore, there is a need to exploit the activities and advantages of solid acid catalysts for efficient biodiesel production.

Recently, many researchers reported the use of several catalysts such as zirconia, titania, zeolites and other mesoporous materials in transforming oils and fats into fatty acid methyl esters, FAME. However, most of the acid catalyzed reactions require very higher reaction conditions such methanol-to-oil ratio and temperature (Sani, et al., 2015a). Incidentally, cheap and abundant biomass that could form a highly versatile class of catalytic material because of the ease with which their properties are amenable to desired properties. On the other hand, despite the wide acceptability of zirconium as efficient catalysts for transesterification reactions, numerous challenges await the ingenuity of the research community (Sani, et al., 2015). Consequently, the underlying theme of this study is to develop two different sets of active catalytic materials; first set from waste palm biomass and the second *via* process variables modification of zirconium-based catalysts.

(i) Sulfonated mesoporous carbon catalyst

The production of most biodiesel fuels is currently from the transesterification reaction of virgin or refined vegetable oils and expensive catalysts. However, this has proved uneconomical because feedstock cost remains the overriding factor when compared with 7% capital cost from the total production cost of biodiesel. It is imperative to formulate cheaper biodiesel production procedures. Incidentally, several cheaper feedstocks and sources for catalyst synthesis abound. These include, but not limited to used frying oils/fats and palm fatty acid distillate (PFAD) and biomass. These low-quality resources are gaining popularity due to their abundance, low production cost, benign nature, as well as reusability. Moreover, wastes such as waste oils and factory by-products and wastes generated from palm plantations constitute a major problem. The utilization of these wastes and by-products is one appropriate means of reducing pollution as well as production costs.

The discovery of sugar catalysts showed that carbon-based solid acids are promising alternatives to homogeneous alkaline and liquid acid catalysts (Toda et al. 2005). Recently, the incorporation of -SO₃H into carbon biomass sources such as cellulose, corn straw, starch, glucose, and sucrose (Zhang et al. 2015; Lou et al. 2008), *via* carbonization-sulfonation method exhibited significant performances (Toda et al., 2005; Takagaki et al., 2006; Budarin et al., 2007; Zong et al., 2007; Agulló et al., 2010; Dehkhoda et al., 2010; Maciá-Liu et al., 2013). This is in spite of their low surface area and porosity, which limit reactant diffusion to active sites (Zhang et al., 2015).

However, numerous groups have recently synthesized sulfonated, ordered, mesoporous carbons *via* nanocasting with SBA-15 as a template and phenolic resol and Pluronic F127 self-assemblies under acidic conditions, respectively (Wang et al. 2007; Xing et al. 2007; Liu et al. 2008; Peng et al. 2010; Janaun and Ellis 2011; Suganuma et al. 2011; Geng et al. 2012). Similarly, Peng et al. (2005) and Yu et al. (2008), describe how to prepare catalysts for esterification *via* the high temperature sulfonation of carbon nanotubes. The acidity, large pore size, and high surface area of these materials ensure accessibility of long-chain FFA molecules and high catalytic activity. However, a literature survey revealed that no reports are available regarding acid-catalyzed reactions using palm tree biomass.

Developing efficient solid catalysts from low-value biomass is essential to making the process ecologically friendly and economical. Malaysia, the world's second largest producer and exporter of palm oil, generates a deluge of biomass from oil palm production. According to Sulaiman et al. 2012, oil palm production generates 85.5% of the total biomass produced from a variety of crops, including but not limited to rubber,

rice, and oil palm. This accounts for the highest percentage with little to no economic value.

(ii) Zirconium-based catalyst

A catalyst that has remained in the research realm is zirconia. However, zirconia has weak activity for transesterifying triglycerides into methyl esters in its normal state. The first report on sulfated zirconia (SZ) was in 1979 by Hino, et al. in 1979. The authors reported SZ as an active catalyst for the low-temperature isomerization of isobutane. This triggered numerous investigations. Expectedly, since then, several reports abound on this promising catalyst. For instance, Yamaguchi et al. (1990) and Tanabe et al. (1991) reviewed a wide range of reactions catalyzed by SZ. Similarly, (Arata and Hino, 1990; Moles, 1992; Morterra et al., 1993, 1995; Ward and Ko, 1994; Corma et al., 1994a, and 1994b) reported the importance and dependence of acidity and catalytic properties of SZ on preparative variables such as precursor type and concentration, sulfation procedure, and sulfate concentration and activation temperature. Further, Sani et al. (2014) reviewed the activity of solid acid catalysts such as SZ for producing biodiesel.

However, despite the numerous reports, scholars in this field are yet to address the weak acidity and slow reaction rate of SZ adequately. This is because despite the presence of sulfate anions, the hydroxyl groups on the SZ surface are less acidic than bridged hydroxyls in zeolites. Moreover, in addition to Lewis sites, the surface of zirconia contains basic sites in the form of coordinated unsaturated oxygen atoms. This explains the rationale of viewing the interaction between zirconia and H_2SO_4 as acid-base reaction as posited by Haase and Sauer (1998). Therefore, this study investigated the combined advantages of mesoporous zeolite and superacidic zirconium by synthesizing a catalyst that has the potential to maximize activity and minimize adsorbate-induced surface

reconstruction with reduced net energy consumption. This chapter also discussed in details how the preparation method and prevailing reaction conditions affect the catalytic activity of the catalyst. To achieve the biofuel central policy, the study also developed green catalysts from palm tree biomass and suggested way forward from the traditional trial-and-error method to a rational means of determining catalytic activities.

1.2.1 Research background

It is not surprising that numerous researches tailor their catalytic synthesis towards resolving the energy crisis confronting the world for several decades due to the excessive utilization of the world's depleting oil reserves (Agrawal, 2007). On one hand, the world's economy is largely dependent on the transportation of goods and services (Sarkar, et al., 2012; Jothiramalingam & Wan, 2009); while on the other hand, transportation is mainly dependent on energy from petroleum. In fact, the transportation sector is 96% dependent on fossil fuels with an annual worldwide fuel consumption of 62% (Pirou & Vaitilingoma, 2013). This is despite other sources of energy such as coal, natural gas, hydroelectricity and nuclear power (Clark & Macquarrie, 2002; Luque, et al., 2010). Apart from the ever-increasing prices of petroleum fuels, more worrying issues associated with utilizing these fuels include deteriorating health standards and environmental degradations. These concerns have led to the search for sustainable biofuel alternatives (Knothe, 2010). These researches aimed at curbing the menace of climate changes while sustaining a stable world economy with reduced health problems.

A renewable and sustainable fuel currently receiving renewed interests and intensive experimentations since the work of Rudolf Diesel is biodiesel (Cheng & Timilsina, 2011; Zhang, et al., 2012; Giarola, et al., 2012; Karatepe, et al., 2012; Zabeti, et al, 2009). It is increasingly becoming attractive as an alternative to petrodiesel. It is worthy to note that

biodiesel is considered the fastest growing industry worldwide (Lam, et al. 2010; Luque, et al., 2010). This is evident from the deluge of publications available from both the open and patent literature (Karatepe, et al., 2012; Luque, et al., 2010; Borges & Díaz, 2012; Lou, et al., 2008; Di Serio, et al., 2008; Loreto, et al., 2005). Nonetheless, achieving the central policy of biodiesel in replacing petrodiesel is still a challenge (Nigam & Singh, 2011; Sani, et al., 2012). This is notwithstanding the tax reliefs and subsidies (Knothe, 2010) the biodiesel industry enjoys from governmental agencies. Evidently, to achieve this target, certain technological advancements and sustained governmental policies are essential (Atadashi, et al., 2011). These include:

- (1) Affordable biodiesel feedstocks produced in vast quantities *via* the establishment of proficient production and distribution systems.
- (2) Greater yields obtained under shorter time and lesser refining difficulties catalyzed by novel catalysts with higher activities.
- (3) Efficient processes for separating and refining crude biodiesel *via* radical innovations.
- (4) Enacting new policies that will favor sustained biodiesel production.
- (5) Implementing the excellent findings from the research communities for minimizing costs, energy and water usage.

In line with these, several attempts are ongoing to improve biodiesel production processes (McNeff, et al., 2008). Prominent amongst them is the prospects of solid acid catalysts for the simultaneous esterification and transesterification of feedstocks especially those containing high amounts of free fatty acids (FFAs). Report by West et al. (2008) showed that solid acid-catalyzed process is more economical than supercritical processes, homogeneous acid, and alkali catalysis. The study also highlighted it as having the least capital investment with the highest return on investment, while technically being

a simple process. Consequently, to overcome the disadvantages of heterogeneous alkaline catalysts currently used in the industries, last decade witnessed the synthesis of several solid acid catalysts. The challenging feat however is in attaining a breakthrough on the mechanism of fatty acids (FAs) esterification by solid acid catalysts. This is because it is more difficult to develop suitable solid acid catalysts for esterifying long-chain acids compared to the shorter acids such as acetic acids (McNeff, et al., 2008; Hideshi, 2010). Accordingly, the aim of numerous recent research efforts is to develop novel solid acid catalysts. Certainly, these catalysts must be active, selective, reusable, stable, and reproducible *via* simple economically viable procedures (López, et al., 2007; Carrero, et al., 2011).

1.2.2 Statement of the research problem

Though some of the biodiesel central policy of protecting the environment and protecting and/or creating jobs have become reality, the aim of replacing petroleum diesel economically is facing some challenges. To overcome challenges such feedstock cost and catalytic activity, fundamental understanding of catalysis is required for the development of novel, robust, and affordable catalysts. Usually, turnover frequency (TOF), strength, and concentration of the catalytic sites, surface area, Brønsted/Lewis acidity, and porosity (morphology) of the catalyst and its support are the variables used in describing solid acid catalysts. Manipulating these properties can lead to enhanced activity and product selectivity (Clark, 2002; Wilson, et al., 1999). The best description of heterogeneous catalysts is ‘non-equilibrium’ or ‘dynamic’ catalysts. This is due to the intimate dependency of the catalytic structures on the prevailing reaction conditions. Consequently, small changes in the reaction medium may result in large or complete morphological changes on the catalyst surface structure because of the adsorbate-induced surface-reconstruction relationship. These have the possibility of affecting the

performance of the catalyst significantly. Thus, the assertion that the active state of a solid acid catalyst is solely predominant during the catalytic process becomes plausible. Hence, the usual assumption that the state and number of active sites remain constant under varying reacting conditions becomes inadequate (Topsøe, 2003). Therefore, it is pertinent to decipher the optimal factors regarding the adsorbate-induced surface-reconstruction relationship that will aid in developing robust catalysts with better activities on cheaper feedstocks, which contains high FFA.

1.2.3 Justification for the study

Processing alternative cheaper feedstocks with solid acid catalysts under fast reaction rates and less expensive processes will no doubt, improve biodiesel production economics. Therefore, synthesis of novel solid catalysts that possess high activity and selectivity will ensure cheaper biodiesel production and commercialization against petrodiesel. Interestingly, the traction gained by published articles from the present study is receiving wider readership and increasing citations. Further, two of the articles received recognition as the “most downloaded articles”, while one is the “most cited” for more than two years, and counting. These justifies the rationale behind present study. A list of publications, and papers presented at conferences is provided at the end of the thesis.

1.2.4 Aim and objectives of the research

The aim of this study is twofold: first, is to synthesize solid acid catalysts, while the second, is to investigate the activities of the synthesized catalysts for biodiesel production. The synthesis of robust catalysts with interconnected system of mesopores and fast transesterification reaction rates (*i.e.*, shorter reaction time; lower alcohol-to-oil molar ratio at moderate temperature), at acceptable cost (high FFA feedstock) would ascertain the novelty of this study.

The main research objectives of this study are as follows:

1. To synthesize and characterize solid acid catalysts from palm tree biomass as environmentally benign alternative for biodiesel production.
2. To investigate the effect of different precursors on activating active sites of sulphated zirconia.
3. To synthesize and characterize new composite zirconia/zeolite catalysts by combining precipitation, impregnation and sol-gel techniques for simultaneous transesterification and esterification process in biodiesel synthesis.

The specific activities underlying the research objectives of the study include:

- a. To synthesize, characterize and evaluate the use of sulfonated mesoporous catalysts from palm frond and spikelets in the esterification of free fatty acids for biodiesel production.
- b. To synthesize, characterize and evaluate the use of sulfonated mesoporous catalysts from palm empty fruit bunch and palm waste fruits in the esterification of free fatty acids for biodiesel production.
- c. To synthesize and modify sulfated zirconia and compare the effect of doping SZ with ytterbium, and the variation in preparatory methods on acidity and catalytic activity for simultaneous esterification and transesterification reactions in biodiesel production.
- d. To synthesize and characterize sulfated Zr/ZSM-5 with improved Brønsted acidity and compare its activity over SZr/Ag, SZr/Ti, and SZr/W for the transesterification reaction of used frying oil to form its methyl ester.

1.2.5 Scope of the research

The present study is limited to the synthesis of catalytic materials from waste palm biomass and investigating their activity in esterifying used cooking oil, which contains high free fatty acids. The aim is to reduce the overall biodiesel production costs. The major theme of the present research is synthesis of solid acid catalysts majorly for cheaper biodiesel production. Thus, the study also investigated the possibility of improving the acceptability of sulfated zirconia (SZ) by enhancing its activity. It is an established fact that a solid catalyst that has been receiving a lot of research is SZ. This is due to its high activity and selectivity for hydrocarbon transformation. Moreover, it is also eco-friendly especially with regard to heterogeneous acid catalysts. Addition of a promoter to SZ achieves high initial activity. However, rapid deactivation of the active sites often follows this high activity.

Some researchers studied other metal oxides with higher stability under oxidizing and reducing conditions such as tungstated zirconia as alternatives to SZ in ameliorating this shortcoming. Nonetheless, these did not yield the desired catalytic activity compared to SZ. Despite numerous advances on catalysis, industrial biodiesel production is yet to surpass petrodiesel economically. This is majorly due to limited fundamental understanding of the mechanism for the structure-activity relationship during catalysis. In this study, the simultaneous esterification and transesterification of high free fatty acid (FFA) containing feedstock helped to assess the catalytic performance of the catalysts. The acidic sites on the surface of the material were prominent in catalyzing the reaction. Consequently, the present study investigated the relationship between catalytic performance and material properties, with emphasis on the influence of promoters in the structure of the material and its catalytic properties.

1.2.6 Outline of the thesis

The general layout of the present thesis follows the University of Malaya's Article Style Format comprising of articles written as separate chapters in a cohesive manner with logical and coordinated progression. A consortium of catalysts synthesized from different precursors and under different conditions converted waste feedstock, used frying oil obtained from household in Malaysia. Figure 1.1 puts the cohesion of the different s into perspective.

Chapter 1

The initial chapter consists of a general introduction that gave a detailed research overview including the research objectives, novelty, as well as questions addressed by the research.

Chapter 2

Chapter 2 presents a review of literature surrounding biodiesel production with solid acid catalysts, including but not limited to vegetable oil composition, challenges limiting direct use of vegetable oils in diesel engines, methods for reducing viscosity of vegetable oil for diesel engines, and oil yields of various feedstocks. Others reviewed aspects include energy balance of biodiesel, performance, handling, storage and usage comparisons – biodiesel and diesel, issues surrounding conventional processes for biodiesel production, current status, future challenges and prospect of solid acid catalysts in achieving biodiesel prominence, and biodiesel production *via* solid acid catalysis.

Chapter 3

This chapter described the study of sulfonated mesoporous catalysts from palm frond and spikelets in the esterification of free fatty acids for biodiesel production. The Chapter is available as a reproduced Article 1. This chapter and the next, addressed the general research objective number 1: to develop solid acid catalysts from palm tree biomass as environmentally benign alternative for biodiesel production.

Chapter 4

The chapter describes the superiority of of sulfonated mesoporous catalysts from palm empty fruit bunch and palm waste fruits in the esterification of free fatty acids for biodiesel production compared to existing sulfonated carbon catalysts.

Chapter 5

Apparently, the options available for promoting sustainability are not mutually exclusive. Therefore, aside biomass-derived catalysts, the present study investigated the possibility of improving the status of sulfated zirconium-based catalysts for the same purpose. Chapter 5 presents Article 3, which investigated the effect of doping SZ with Ytterbium and further showed how preparative procedures affected catalytic activity and acidity of SZ.

Chapter 6

Chapter 6 described the synthesis and characterization of a new sulfated Zr/ZSM-5 with improved Brønsted acidity and compared its activity over SZr/Ag, SZr/Ti, and SZr/W for the transesterification reaction of used frying oil to form biodiesel. This is chapter is a representation of Article 4. This article investigated an innovative approach of enhancing acidity of SZ composite catalysts that could withstand unfavorable constituents

highlighted above. The basis of the interplay between metal function of modified oxo-anions and pore structure of zeolites and its strong acidic properties premised this research. Each article (Chapter) consisted of its own different sections; namely Introduction, Literature Review, Results and Discussion, and Conclusion.

Chapter 7

Finally, Chapter 7 presents the Conclusions and Recommendations. The chapter summarized the overall research findings from all the four articles and offered recommendations for future research.

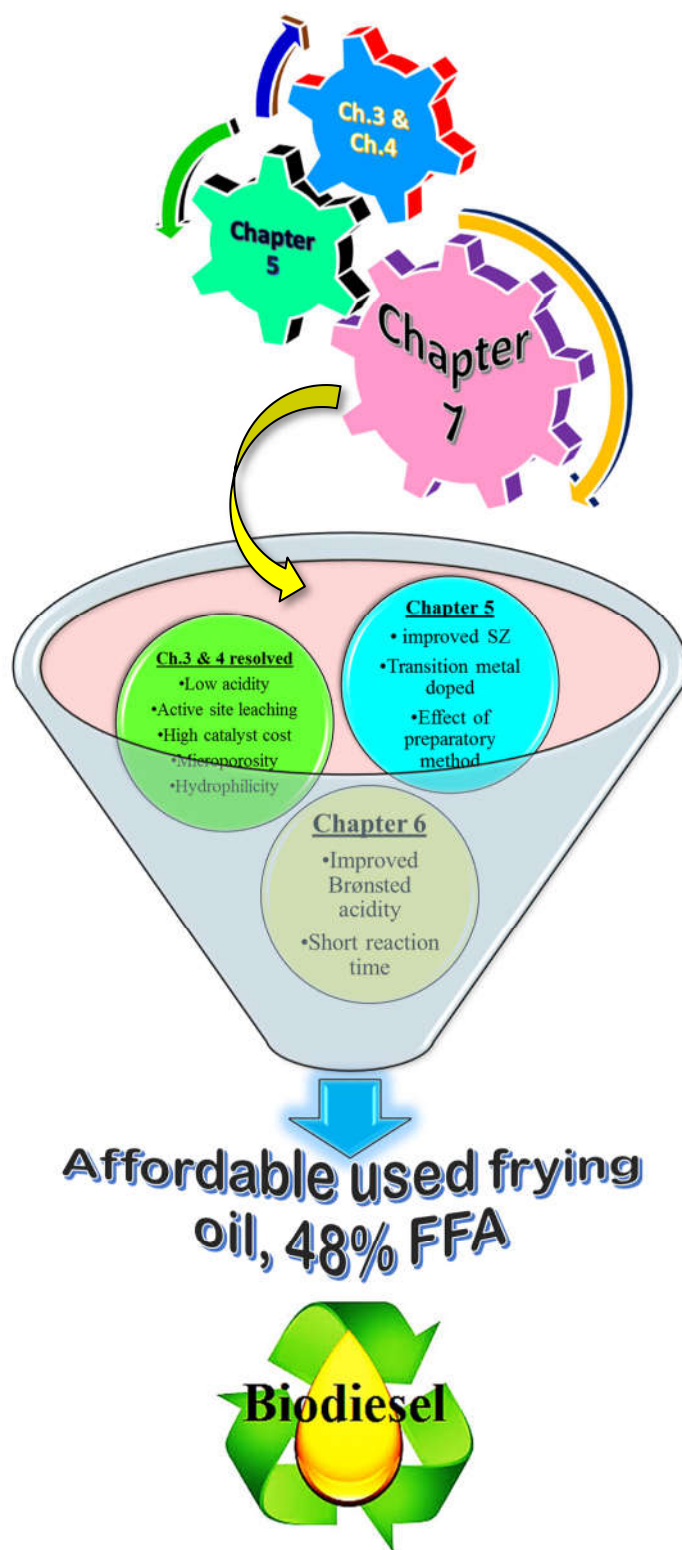


Figure 1.1: Diagrammatical representation of the logical and coordinated progression of chapters 3 to 6

1.2.7 Synopsis, findings and contributions of the study

- a) The novel aspect of this research is synthesis of robust catalysts with interconnected system of mesopores and fast transesterification reaction rates (*i.e.*, shorter reaction time; lower alcohol-to-oil molar ratio at moderate temperature), at acceptable cost from feedstock containing high FFA.
- b) This is timely because the main issue challenging biodiesel production is the rational design and development of affordable and efficient catalysts for low-value feedstocks.
- c) Evaluating green precursors, unconventional promoters, and supports for the catalyst synthesis are some of the crucial research decisions taken. The study put into cognizance that research involves thinking out-of-the-box, and doing the ‘unconventional’ though backed with plausible philosophical and technical-know to achieve novelty. We also considered alternative procedures for investing the same synthesis technique. These exhibited positive impacts on the activities of the catalysts.
- d) The findings of this research compared favorably with peer-reviewed data from the open-literature. The aspect that sets the outcomes of this study apart from others is faster reaction rates from cheaper precursors.
- e) The research outcomes indicate the possibility of synthesizing the desired catalysts that could ensure a cheaper biodiesel production, which translate to a profitable and sustainable biodiesel industry in the long run. However, despite the successes of this study, it is pertinent to highlight that there is need for improvement. This is especially in the aspect of *in situ* analysis of the catalytic reactions (*i.e.*, the precise determination of activity and reactivity of the catalyst during catalysis.), and acid recovery.
- f) Expectedly, the results obtained from this study would remain innovative for a couple of years. However, this brilliance would diminish in the next 5 years specifically due to advances that will emerge.

g) It is our conviction that the recommendations given at the end of this thesis are appropriate for future researches.

CHAPTER 2: LITERATURE REVIEW

This chapter presents a comprehensive review of literature surrounding biodiesel production with solid acid catalysts, including but not limited to vegetable oil composition, challenges limiting direct use of vegetable oils in diesel engines, methods for reducing viscosity of vegetable oil for diesel engines, and oil yields of various feedstocks. Others reviewed aspects include energy balance of biodiesel, performance, handling, storage and usage comparisons – biodiesel and diesel, issues surrounding conventional processes for biodiesel production, current status, future challenges and prospect of solid acid catalysts in achieving biodiesel prominence, and biodiesel production *via* solid acid catalysis.

2.1 Overview

Industrialization and transportation are two indicators used in reflecting the global civilization status (Serrano-Ruiz, et al., 2012; Haung, et al., 2012). Human civilization transformed from using animal forces (which relied on biomass from plants) to external combustion engines (which relied on solid coal). After steam engines, internal combustion engines (ICE) which relied on liquid diesel and gasoline, revolutionized transportation (Zhang, 2008). Currently, ICE and liquid fuels such as jet fuel, diesel, and gasoline propel jet planes, trains, ships, and vehicles. However, the lower price advantage that made these fuels popular (Zhang, 2009) is becoming history. The current scenario is an inverse relationship with petroleum becoming depleted and more expensive (Luque, et al., 2010; Kafuku and Mbarawa, 2010). Concomitantly, it is estimated that the world would require 50% more energy in 2030 than it does today (Shahid and Jamal 2011; IEA, 2007). Besides, environmental degradation due to the emissions of CO₂ is becoming increasingly worrisome. In 2007 and 2008, the transportation sector alone accounted for 22% and 23% of the total CO₂ emissions respectively. About 50% of this greenhouse gas

(GHG) emission comes from road transport (Zhang, 2009; JFS, 2010). The panacea to these challenges confronting the world today is the provision of alternative renewable fuels (Lee & Wilson 2015). These fuels will ensure a global energy security with reduced environmental impacts as well as compete favorably with petroleum diesel (Atadashi, et al., 2011).

Concerns for the environment and biodiversity have made biofuels the most attractive sources of alternative energy (Metcalf, et al., 2010; Koberg and Gedanken, 2012). Other factors that contributed to their acceptability against other sources are sustainability, seasonal fluctuations, and geographical locations (Shahid and Jamal, 2011). Combustible renewables and wastes have the highest potentials to supply the global energy requirements. They accounted for more than three quarters of the global energy supply in 2007 and 2008 (Figure 2.1) (Kafuku and Mbarawa, 2010). From the several energy alternatives identified, biodiesel is the most promising due to its similar properties to petrochemical diesel. Producing biodiesel in large quantities will no doubt help to meet the increasing global energy demands.

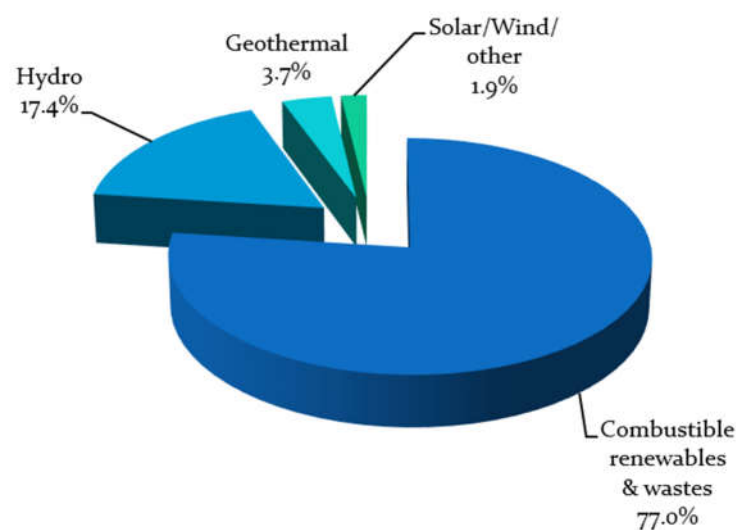


Figure 2.1: Total renewable energy supply (Mtoe) in year 2008.
Total: 100 million tonnes of oil equivalent (Mtoe).

The concept of producing fuel from bio-resources is fascinating, and achieving a sustainable one at an affordable cost is compelling. To date, the most appropriate option to these requirements is biodiesel. Biodiesel have been produced from used oil and high-yield non-edible oil crops such as *Jatropha* from non-arable (arid) and dispensable lands. Recent studies are exploring a much-conceived sustainable alternative from microalgae. Biodiesel production from algal oil is eliminates the completion of land-use and food-for-fuel. Generally, biodiesel is a clean renewable source of energy produced both locally and commercially. It has a high considerable production capacity and energy output ratio. These factors made exploring biodiesel production methods attractive, interesting and a worthy proposition.

Biodiesel is a mixture of fatty acid alkyl esters produced from vegetable oils or animal fats usually *via* transesterification reaction. Triglyceride esters react with alcohol (methanol or ethanol) in the presence of a catalyst producing glycerol as the by-product (Ma and Hanna, 1999). The structure and properties of the produced methyl and ethyl esters are similar to petroleum diesel. This accords biodiesel suitability for direct use in present day diesel engines or as a blend with petroleum diesel (Ma and Hanna, 1999). Therefore, the need to modify engines for the utilization of biodiesel is not necessary. In fact, it is worthy of mention that the engine specifications designed by Rudolf Diesel was meant to combust peanut oil. Recent report by the USDA showed that the cost of biodiesel is approximately 50 to 70 cents to gasoline prices (NREL; Shay, 1993). The current skyrocketing prices of gasoline will serve as catalyst for the research of biodiesel (Agrawal and Das, 2001).

However, there is need for advancement to the current methods of biodiesel production. Presently, the popular approach of producing biodiesel is *via* soluble alkali catalysts (Ma and Hanna, 1999). The alkali reacts with the acids from the free fatty acids (FFAs). This consequently leads to tedious problem of separation after the transesterification reaction. Furthermore, there is need for repeated washing with water to the purify product from dissolved catalyst and soap. This generates about 8 gallons of wastewater for every gallon of biodiesel produced, which leads to unwanted environmental impact. The costs implications from separation, purification environmental impact, batch process, and loss of catalyst have hindered the commercial production of biodiesel from this approach. Currently, researches are ongoing in search for alternative methods. Solid acid catalysts have received renewed interests in this regards. The acidic and heterogeneous nature eliminates the separation and purification steps. Additionally, the catalysts are reusable, amenable to regeneration many times without loss in activity, and suitable for continuous processes (Lam, et al., 2010). The processes for development of heterogeneous acid catalysts for biodiesel production are vast and there is lot of scope for work in this area.

2.2 Composition of vegetable oil

Oils and fats from natural biological sources are generally comprised of a mixture of fatty acid (FA) glycerol esters (Sonntag, 1979). The compositions of FA vary in carbon chain length and number of double bonds (Balat and Balat, 2008). Typical examples of these natural oils and fats are palm oil, soybean oil, corn oil, rapeseed oil, castor oil, sunflower oil, jatropha oil, beef tallow, coconut oil chicken fat, and algae oil. The compositions of fatty acid vary with different sources (Table 2.1).

Table 2.1: Fatty acid composition of common oils and fats

Fatty acid, %*	Soybean	Palm	Lard	Corn	Tallow	Coconut	Cottonseed	Rapeseed	Linseed	Yellow grease	Olive
Lauric (12.0)	0.1	0.1	0.1		0.1	46.4					
Myristic (14.0)	0.1	1.0	1.4	1-2	2.8	19.2	0-2			2.43	
Palmitic (16.0)	10.2	42.8	23.6	8-12	23.3	9.8	20-25	3.0	4-7	23.24	9-10
Stearic (18.0)	3.7	4.5	14.2	2-5	19.4	3.0	1-2	0.8	2-4	12.96	2-3
Oleic (18.1)	22.8	40.5	44.2	19-49	42.4	46.9	23-35	13.1	25-40	44.32	73-84
Linoleic (18.2)	53.7	10.1	10.7	34-62	2.9	2.2	40-50	14.1	35-40	6.97	10-12
Linolenic (18.3)	8.6	0.2	0.4	trace	0.9	0.0	trace	9.7	25-60	0.67	trace
Arachidic (20.0)		0.2						7.4			

**Number of carbons and double bonds in parentheses*

2.3 Reasons why vegetable oil is not suitable for direct usage in diesel engines

Over the years, diesel engine has developed to suit petroleum fuel-combustion engines perfectly. However, direct utilization of vegetable oils encountered some problems because of difference in the composition of hydrocarbons. Petroleum diesel consists of non-branched hydrocarbon molecules with 12 to 18 carbon atoms. Vegetable oil molecules on the other hand, comprises of triglycerides having carbon atoms three times greater in number (Agarwal and Das, 2001). Consequently, vegetable oil has higher viscosity than that of petroleum diesel oil. Agarwal and Das (2001) reported that at 40 °C, the viscosity of vegetable oil is 35 to 45 centistokes as compared to 4.0 centistokes of petroleum diesel oil. The internal combustion engine (ICE) finds it difficult during pumping and atomization in the injection system. Apart from these difficulties, there is incomplete combustion that leads to high carbon deposits and emission of heavy smokes.

Additionally, because of its high molecular weight, vegetable oil has low volatility. This makes it easy for the oil to stick to the cylinder and injector walls (Krawczyk, 1996). The sticky layer polymerizes into a films, which continues to trap more oil forming more deposit formation. This obstruct smooth combustion that leads to carbonization of injector

tips, ring sticking, and lubricating oil dilution and degradation. Incomplete combustion becomes the result of the limited access and inefficient mixing of air in the combustion unit. Other problems as result of low volatility and high viscosity are poor cold engine start-up, misfire, and ignition delay (Balat and Balat, 2008).

2.4 Methods of reducing viscosity of vegetable oil for diesel engines

The methods for minimizing the viscosity of vegetable oils for practical applications in internal combustion engines include pyrolysis, micro-emulsification, blending (diluting), and transesterification (Ma and Hanna, 1999; Agarwal and Das, 2001).

2.4.1 Direct use and blending (dilution)

This involves blending vegetable oil with diesel fuel in varying quantities. This is generally unsatisfactory for use in diesel engines. Blending is not a production process. It involves mixing vegetable oil with existing diesel fuel. This method is good in minimizing viscosity problems in biodiesel. The Caterpillar Co., Brazil used a blend of 10% vegetable oil and diesel fuel in 1980 in the pre-combustion chamber engine. Two years later, a fleet of diesel engines used a blend of 5% diesel and 95% waste cooking oil (Pramanik, 2003). Narayan (2002) reported the optimum blend to be 80% diesel and 20% oil. B100 stands for pure biodiesel while B20 is fuel containing 20% biodiesel. The minimum standard blend that meets the of the federal EPA minimum requirements for clean air is B20. B20 is also the highest recommended blend for best performance in diesel engines. Blending prevents the biodiesel from gelling in extreme cold weather. However, blending is not suitable for commercial production. BX represents the percentage blend in biodiesel. Other problems associated with direct and indirect use include high viscosity, FFAs, carbon deposits and gum formation because of oxidation. Polymerization also occurs during combustion and storage (Ramadhas, et al., 2004).

2.4.2 Thermal cracking (pyrolysis)

It is possible to process vegetable oil, fats, and soap in a technique similar to thermal cracking of petroleum. Pyrolysis is heating of organic matter in the absence of air to produce gas, a liquid, and a solid (Uzun, et al., 2006). Heat or a combination of heat and catalyst break the heavy molecules from vegetable oils and animal fats into smaller constituents. This produces olefins and paraffins with similar properties to petroleum diesel, where such products derived the name “*diesel-like-fuel*” (Sonntag, 1979). Other molecules found in the product include water, particulate matter, sulfur, alkanes, alkenes, and carboxylic acids (Sharma, et al., 2008; Pinto, et al., 2005). Consequently, it is difficult to characterize fuel obtained from pyrolysis because of its heterogeneity (Sonntag, 1979). This process is energy consuming, inefficient, and needs expensive distillation units. Moreover, the sulfur and ash contents make it less eco-friendly (Lotero, et al., 2005).

Sensoz, et al., (2000) researched the effect of rapeseed particle size (range from 0.224 mm to 1.8 mm) on the yield of biodiesel. Their report and a similar conclusion by Uzun et al., (2006) showed the product yield is independent of the rapeseed and soybean particle size. Report by Senzos and co-researchers (2000) confirmed 400 °C to 450 °C to be the maximum temperature range for conversion of bio-oil. Rapid devolatilization of cellulose and hemicellulose occur at this temperature. They also showed that heating rate and temperature have significant effects on bio-oil yields, char, and gas released from olive. When 150 cm³/min flow rate of nitrogen heated at 10 °C min⁻¹, 37.7 % was the maximum yield obtained at 500 °C (Sensoz, et al., 2006). The viscosity, flash and pour points and equivalent calorific values of the oil are lower than diesel fuel. However, the pyrolyzate has increased cetane number, which is lower than diesel oil. Apart from reducing the viscosity of the vegetable oil, pyrolysis enables de-coupling of the unit operation

equipment in shorter time, place, and scale. It produces clean liquids, which needs no additional washing, drying, or filtering.

2.4.3 Micro-emulsion or co-solvency

One of the potential solutions in resolving the viscosity problem of vegetable oil is micro-emulsions (or co-solvency). It addresses the high viscosity problem to some extent. Mixture of alcohol, surfactants, and cetane improvers or vegetable oil as ester and dispersant (co-solvent), and additives in suitable proportions, with or without diesel fuels produces micro-emulsion. Under vigorous stirring, the oil disperses into the solvent such as methanol to produce the emulsions. These become transparent solution dispersed with thermodynamically stable colloids. The diameters of the droplets range from 100 to 1000 Å, which easily passes through fuel filters. The additives used for reducing the fuel viscosity as well as increasing its cetane number are alcohols such as methanol, ethanol, and propanol (Lotero, et al., 2005). The surfactants for improving the cetane number include higher alcohols and alkyl nitrates (Ranganathan, et al., 2008). Ma and Hanna, (1999) reported that biodiesel micro-emulsions produce carbon deposits because of the incomplete combustion, while injector needle sticking occurs after prolong usage due to high viscosity. Fukuda and co-researchers (2001), reported incomplete combustion of biodiesel micro-emulsions after a 200 h endurance test.

2.4.4 Transesterification or alcoholysis

This is the most preferred method. It transforms the vegetable oil into fatty methyl esters biodiesel or (FAMES) for efficient utilization in diesel engines. Transesterification is the most widely employed process for commercial production of biodiesel. It involves heating the oil to a designated temperature with alcohol (often methanol or ethanol) and a catalyst, thereby restructuring its chemical structure. This conversion reduces the high

viscosity of the oils and fats. Transesterification of TG molecule requires three consecutive reactions where the triglyceride from the alcohol neutralizes the free fatty acid. Figure 2.1 depicts esterification while Figure 2.2 depicts the transesterification reaction where all types of glyceride species take part. A completion net reaction produces one mole of glycerol and three moles of alkyl esters for each mole of TG converted. These separate into three layers, with glycerol at the bottom, a middle layer of soapy substance, and biodiesel on top (Lotero, et al., 2005). Transesterification is a reversible reaction. To obtain reasonable conversion rates therefore, it requires a catalyst. The nature of the catalyst predetermines the reaction conditions, feedstock compositional limits, and post-separation requirements. Currently, base catalysts are preferred over other catalysts because of their ability to enhance faster reaction rates (Freedman, et al., 1984). This is because they are readily available at affordable prices.



Figure 2.2: Esterification reaction

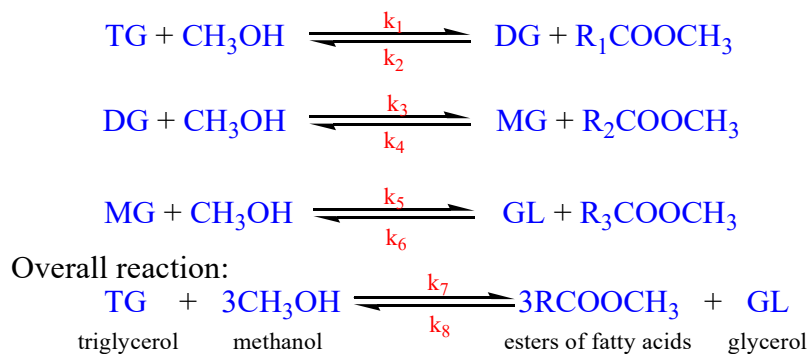


Figure 2.3: Transesterification of triglyceride with methanol in the presence of catalyst; where k1-8 are rate constants.

2.5 Oil yields of various feedstocks

Figure 2.4 shows the world's liquid fuel supply by type, while Table 2.2 lists the estimated oil content yields, and required land for different biodiesel feedstocks. Microalgae, which require the minimum land for cultivation, have the highest oil yield. Though it does not thrive well in all geographic locations, palm tree has the highest yield amongst oil crops. Jatropha that thrives in arid and marginal land requiring minimal irrigation produces inedible oil. Economically, some of the most favorable where Jatropha thrives are Africa, India, Pakistan, Caribbean, and the Philippines. Soybean has lower yield compared to rapeseed, but its fertilizer requirements are considerably less than that of rapeseed since it can fix nitrogen.

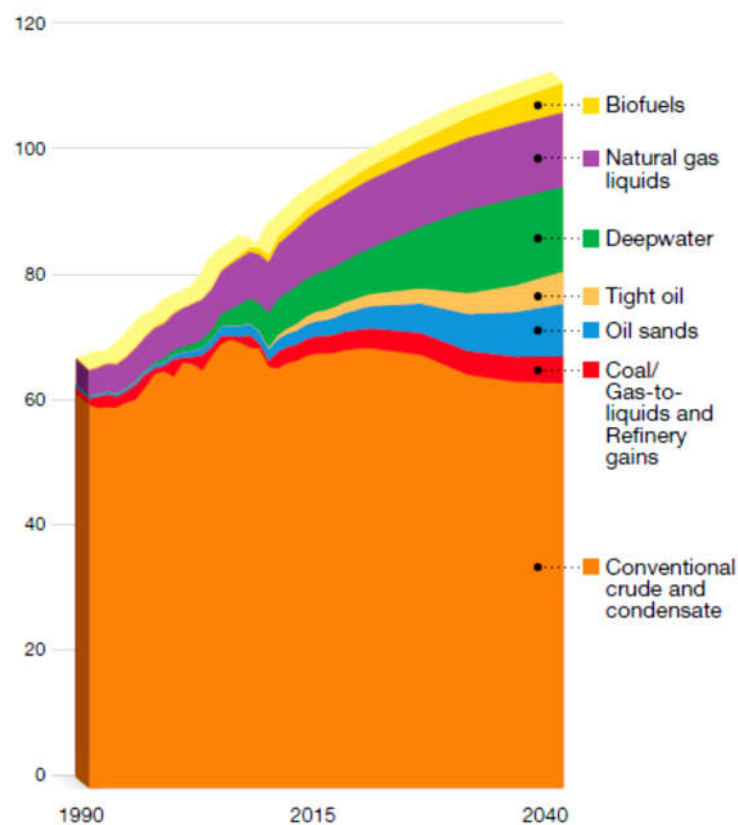


Figure 2.4: Liquid fuel supply by type (Millions of oil-equivalent barrel per day)

Source: http://www.exxonmobil.com/Corporate/files/news_pub_eo.pdf

2.6 Energy balance of biodiesel

Sheehan, et al. (1998) estimated the ratio of the energy output of biodiesel as 3.2:1. This is the quantity of fuel energy per unit of energy used in producing biodiesel. This ratio of biodiesel energy output is high when compared to that of bioethanol, estimated at 1.05:1 to 1.25:1 (Shapouri, et al., 2002; Hill, et al., 2006).

Table 2.2: Estimated oil content, yields and required land of different biodiesel feedstocks (Chisti, 2007)

Microalgae	Oil content (% dry wt)	Oil yield (g.L ⁻¹)	Biomass (g.L ⁻¹)	
<i>Schizochytrium</i> sp.	50 to 77			
<i>Botryococcus braunii</i>	25 to 75			
<i>Chlorella</i> sp.	28 to 32			
<i>Nitzschia</i> sp.	45 to 47			
<i>Nannochloropsis</i>	31 to 68			
<i>Cylindrotheca</i> sp.	16 to 37			
<i>Trichosporon fermentans</i>	35.3	12.8	36.4	
<i>Lipomyces starkeyi</i>	68.0	6.4	9.4	
<i>Mortierella</i>	36.0	3.7	10.4	
<i>Isabellina</i>	24.0	2.0	8.4	
<i>Cunninghamella</i>	28.0	3.8	13.5	
<i>Echinilata</i>	10.0	0.4	4.1	
Microalgae/Plant	Oil yield (L/ha/year)	Oil content (% wt in biomass)	Required land (M ha ^a)	Biodiesel productivity (kg biodiesel/ha/year)
Microalgae ^b	136,900	70	2	121,104
Microalgae ^c	58,700 to 97,800	30 to 50	4.5	51,927 to 85,515
Oil palm	5,950	30 to 60	45	4,747
<i>Jatropha C.</i>	1,892	Seed: 35 to 40 Kernel: 50 to 60	140	656
Canola/Rapeseed	1,190	38-46	223	862
Soybean	446	15-20	594	562
Corn (Germ)	172	48	1540	152

^aTo meet 50 % of all current US transport consumption.

^b70 % (W/W) oil yield in biomass.

^c50-30 % (W/W) oil yield in biomass

2.7 Present scope of biodiesel production

The advancement of biofuels as energy source for industrial and transport sectors encountered serious criticisms from some scientific and policy communities. Some of the arguments emanated based on priority in using food crops as energy sources for biofuels. These biofuels include bioethanol from fermentation of sugar and starch-based feedstocks

and biodiesel from transesterification of vegetable oil TGs. This issue raised the questions of food availability and prices, land-use, environmental degradation and related socio-economic implications. The preliminary data obtained from biofuels produced from biomass and wastes provided leeway to this argument. The results indicated reduced environmental degradation, especially GHG emissions and deforestation. (Luque, 2010; Luque, et al., 2008; Antizar-Ladislao and Turrion-Gomez, 2008; Antizar-Ladislao and Turrion-Gomez, 2010) The major key players that attracted the attention of many researchers from these biofuels are algal and lignocellulosic fuels. This is because these fuels are readily available, and easily processed. While lignocellulosic biomass is currently the frontrunner, the great potential for mass production of biofuel that microalgae have, has attracted the attention of many researchers (Luque, et al., 2008; Yan, et al., 2010).

Concerns over diminishing oil reserves, skyrocketing crude oil prices, increase in GHG emissions and associated environmental impact have made biodiesel emerged as the fastest growing industries worldwide. It is the second most abundant combustible renewable fuel. Biodiesel is a non-toxic, clean-burning fuel, regarded as a viable alternative (or additive) to petrochemical diesel (Luque, et al., 2010; Lam, et al., 2010; Armaroli and Balzani, 2007). Yet, to remain sustainable, it is necessary to produce biodiesel from non-food crops that require minimal cultivation, without competing with the traditional arable land or cause deforestation. However, *Jatropha curcas*, *Miscanthus*, switch grass and non-edible plant parts such as husks, stems, leaves, and used cooking oils are good sources in this regards, a more reliable and efficient source is yet to be established. The potential to produce biodiesel yields > 100 times those attainable per hectare from plant feedstock has attracted current growing interests for algal oil (Mata, et al., 2010; Luque, 2010).

2.8 Performance, handling, storage, and usage comparisons – biodiesel and diesel

Compared to diesel, biodiesel has poor cold-weather properties and higher cloud point (soy biodiesel: 2 °C against No. 2 diesel: -23 °C). Consequently, it forms gel at a lower temperature during cold weather. Blending with diesel or kerosene or the use of anti-gelling agents minimizes this problem. Agarwal and Das (2001) reported that B20 has the same cloud point as diesel. Due to its higher molecular weight, the lubricity of biodiesel is better than that of diesel. Blending biodiesel with diesel improves its lubricity. For instance, diesel blended with as low-level blends of biodiesel as 1% or 2% exhibited high lubricity. This is particularly important for diesel oils with poor lubricating properties such as ultra-low sulfur content. Diesel has 8% more energy content than biodiesel (Pacheco, 2006). B100 degrades gaskets and hoses made of nitrile, buna N or rubber. To prevent this, materials which are resistant to degradation such as VitonTM were designed (NREL, 2006). The cetane number of biodiesel (48-65) is better than that of petroleum diesel (40 to 55). This also implies better engine performance because of efficient combustion and better cold start properties. The tail pipe of biodiesel and petroleum diesel emits lesser (50%) particulate matter. CO₂, partially burned hydrocarbons were 50% and 50% less respectively for biodiesel than petroleum diesel. However, due to high temperature in the ICE, biodiesel has 15 % higher emissions of NO_x than petroleum diesel. Catalytic converters designed to reduce the NO_x into oxygen and nitrogen minimizes this problem (EPA, 2002; Schwab, et al., 1987).

2.9 Issues surrounding conventional processes for biodiesel production

The use of soluble alkaline catalyst (NaOH, KOH) is the major limitation with the conventional process. Apart from the high amount of glycerol as by-product, other impurities contaminate the biodiesel produced at the end of the reaction. Soluble base methoxide in the presence of water produced by the reaction saponifies a fraction of the

triglycerides. Repeated water washing separates the soap and sodium methoxide from the product mixture. Catalysts consumption at the end of the reaction is another economic challenge aside these tedious and cumbersome tasks. It is very uneconomical to try regenerating the catalyst. Therefore, fresh catalysts are required for each transesterification. Furthermore, the wash water also constitutes environmental impact from waste disposal. Each kilogram of biodiesel produced generates about 8 kg of wastewater. Unfortunately, water is one of the most expensive resources employed in biodiesel production plants. Additional heating is required to remove any trace water from the biodiesel. After all these extra processing steps, the product proceeds to the final polishing unit. All these incur unnecessary costs and thereby hindering the economic competitiveness of biodiesel to petroleum diesel (Ma and Hanna, 1999). Extra processing units such as FFA pretreatment and catalyst-alcohol pre-mixing units help in minimizing these problems. However, the overall production costs are high. Apart from a neat, efficient, and robust process for commercial production, a simple process affordable to the subsistent farmer especially in developing countries is also required. The purity of the by-product of the transesterification reaction is only about 80% pure. This is because it contaminated with water, soluble catalyst, and soap. The purification of such product requires expensive equipment such as vacuum distillation units. This depreciates its market value while disposal of unwanted impurities and wastewater incur strict legislations and extra charges. However, numerous researches are exploring means of valorizing such products into value-added products such as organic synthesis, food, medicine, personal care, pharmaceuticals and cosmetics.

2.10 Solid acid catalysts

The focus of most recent advances is towards the use of recyclable heterogeneous acid as alternative to the solid base catalysts and unrecyclable homogeneous acid and base catalysts. Heterogeneous acid catalysts are heterogeneous; hence, they are analogous to their base counterparts. This helps in eliminating the costs of product separation while ensuring the advantage of regeneration and reusability. Furthermore, acid catalysts are less susceptible to FFAs. The support matrix of solid acid catalyst sterically hinders solvation of the active sites by water. Thus, deactivation of the catalyst is comparatively lower than liquid catalyst. Consequently, cheaper and readily available feedstock could be employed (Nusterer, et al., 1996; Veljkovic, et al., 2006; Smith, et al., 2003; Clark, et al., 2002; Misano, et al., 2000).

2.10.1 The concept of acidity

Arrhenius (1880 to 1890) defined acids as substances that dissociate in water to yield H^+ . In 1923, J.N. Brønsted modified this definition to include all species that have the capability of donating H^+ while he referred to bases as species with the capacity to accept the proton. This proton donor (often OH-group) became the Brønsted-Lowry concept. However, G.N. Lewis postulated the electron acceptor concept. He defined acids as substances that can accept electrons while he regarded those capable of donating as bases. Consequently, electron deficient ions or molecules became Lewis acids, otherwise called carbocations. Similarly, Lewis bases are substances having readily available non-bonded electron pairs such as ethers and amines. Interestingly, James Bryant Conant coined the term “superacids” in 1927 to denote materials with acid strength higher than strong mineral acids (10^7 to 10^{19}), such as H_2SO_4 and Lewis acids such as $AlCl_3$. Superacids are capable of protonating certain weak bases such as carbonyl compounds. The initial discoveries of carbocation, acidic halonium ions, and halogen cations on these materials

indicated their electron deficiency, stability, and longevity. The concept of acidity is viewed as the hydrogen nucleus with the *1s* orbital empty (H^+). Within this concept, the nucleus has a powerful polarizing effect because it is not prone to electronic repulsion. Further, it is always associated with one or more molecules because of its strong electron affinity that makes it impossible to exist freely in condensed state. However, free “naked” proton exists in gas phase. Solid acid catalysts are gaining the attention of researchers because of the inherent limitations of liquid acids and heterogeneous bases (Table 2.3).

Table 2.3: Main advantages and disadvantages of solid acid catalysts

Advantages	Disadvantages
Highly selective (specific activity)	Heterogeneity makes acidity measurement difficult
Suitable for continuous operation	Acidity measurement not always accurate
Ease of separation at end of reaction	Acidity measurement are difficult to interpret
Fully recoverable at the end of reaction	Mostly, well-known acid catalyzed reaction estimates acidity
Easily regenerated for recycling	Requires higher temperature to achieve activity
Reutilization of catalyst	Requires enhancers such as treatment with suitable co-acid or binding a liquid acid physically or chemically on the otherwise inert surface to activate the intrinsic acidity

Theoretically, high surface area gives the highest activity. However, materials with high surface areas are (a) difficult to prepare, (b) difficult to maintain because of their susceptibility to sintering and, (c) associated with high porosity. This makes them prone to mass transfer limitations that subsequently render them into weaker catalysts. In some cases, high porosity enhances faster reaction rates. Consequently, it is instructive to factor out the desirable factors when developing catalytic materials for specific targets (Figure 2.5).

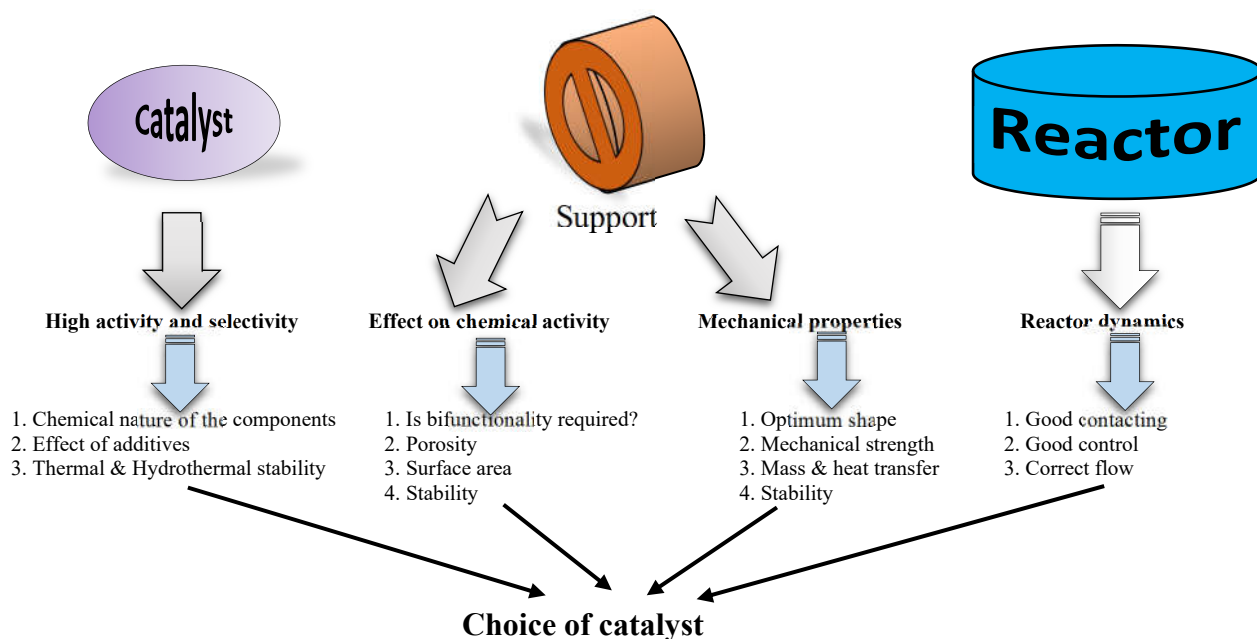


Figure 2.5: Determinants for selecting a particular catalyst

Theoretically, high surface area gives the highest activity. However, materials with high surface areas are (a) difficult to prepare, (b) difficult to maintain because of their susceptibility to sintering and, (c) associated with high porosity. This makes them prone to mass transfer limitations that subsequently render them into weaker catalysts. In some cases, high porosity enhances faster reaction rates. Consequently, it is instructive to factor out the desirable factors when developing catalytic materials for specific targets (Figure 2.5). Solid acids include acidic clays (Campanati, et al., 2003; Vaccari, 1998 and 1999), mixed oxides such as silica-alumina, oxides such as SO_4 , sulfonated polystyrene ion exchange resins and sulfated zirconia, (Sharma, 1995; Chakrabarti and Sharma, 1993). Others include zeolites (van Bekkum, et al., 1991; Corma, 2003), polyoxometalates acids (Sheldon and van Bekkum, 2008), and hybrid organic-inorganic materials such as mesoporous oxides containing suspended organic sulfonic acid moieties (Valkenberg and Hölderich, 2002; Sheldon and van Bekkum, 2001).

Usually, the strength and concentration of catalytic sites, the surface area and porosity (morphology) of the support and Brønsted/Lewis acidity are the variables used for describing solid acids. Manipulating these properties enhances higher product selectivity (Clark, et al., 1994). Pore constraints influences product selectivity because the sizes of the reacting species, intermediates, or the products formed determine accessibility and adsorption (Clark, 2002). The various types of solid acid catalysts are subdivided into three classifications. Amorphous mixed oxides (typified by acidic clays), solid acids having sulfonic acid groups on their surfaces (typified by the sulfonated polystyrene ion exchange resins), heteropoly acids, zeolites, and zeotype materials (Sheldon and van Bekkum, 2001).

2.10.2 Amorphous mixed oxides

(i) Acidic montmorillonite (pillared) clays

Clays are naturally occurring amorphous, pillared, or layered aluminosilicates produced in huge quantities for various processes. Solid acid catalysts extensively catalyzed oil refining during the period from 1930s to the mid-1960s. It was the higher selectivity and activity exhibited by zeolites that brought about the replacement of acid clay catalysts. Polymerization between the basic building blocks (i.e., tetrahedral SiO_4 and octahedral MO_6 where $\text{M} = \text{Al}^{3+}, \text{Mg}^{2+}, \text{Fe}^{3+}, \text{Fe}^{2+}, \text{Sn}^{4+}, \text{Ti}^{4+}, \text{Sc}^{3+}$) produces two-dimensional sheets. Octahedral sheet is sandwiched by these tetrahedral silicate sheets (Sheldon, et al., 2007; Sheldon and van Bekkum, 2001; Smith, et al., 2003; Misano, et al., 2000; Izumi and Onaka, 1992).

The clay's Brønsted and/or Lewis acidity and catalytic properties are dependent on the electronegativity of interlamellar exchangeable cations attached to the negatively charged aluminosilicate sheets. More electronegative cations produce stronger acidic catalysts.

Consequently, cation exchange or acid treatment enhances the amount and strength of Brønsted and Lewis acid sites. The synthesis of active and commonly used KSF and K-10 acid catalysts developed from natural montmorillonite by Fluka and Sud-Chemie respectively, was after treatment with sulfuric acid. Usually, the octahedral sheets consist typically of oxygen atoms attached to multivalent metal cations with lower valency such as Mg^{2+} . The difference in electronic configuration gives the overall sheets a net negative charge. Presence of hydrated cations in the interlamellar spaces compensates for this negative charge. As a result, the clay swells when immersed in water and exposes the intercalated cations. This phenomenon makes the exchange of cation in clays easily accessible.

Brønsted acids (or acidic protons) are produced when water molecules dissociates from the hydration sphere. Consequently, multivalent metal cations exchanged clay can exhibit both Brønsted and Lewis acidity depending on the nature of the reacting species (Kawabata, et al, 2005; Shimizu, et al., 2005; Clark, et al., 1994). It is worthy to mention that the activity of catalysts treated with concentrated sulfuric acids in promoting acid-catalyzed reactions does not surpass that of Al^{3+} -exchanged montmorillonite. The ester yields obtained from transesterified crude oils are usually lower. This is because of extraneous constituents such as gums present in the oil (Sheldon, et al., 2007; Kaneda, et al., 2006; Clark and Macquarrie, 1996; Izumi and Onaka, 1992). These typified lower yields are majorly because of the interference of the clay's interlamellar acid activity by these extraneous materials.

(ii) Mixed metal oxides

Metal oxides consist of Lewis acids (cations) and Brønsted (anions). This provides the required catalytic sites for methanol during methanolysis. O-H bond rupture forms hydrogen cations and methoxides readily. TG molecules react with methoxide anions to form FAMES (Chorkendorff & Niemantsverdriet, 2003; Yan, et al., 2009). Numerous studies elucidated the effects of various transition metal oxides for heterogeneous acid transesterification of TG to FA alkyl esters. These include titanium oxides, zirconium oxides, and zinc oxides. Among these oxides, sulphated or tungstated zirconia stands out as prominent. Zirconia is a well-known industrial catalyst (Clark, et al., 2000). It is thermally stable and possesses strong acidic sites. This catalyst minimizes diffusional limitations because it has large pores that accommodate fatty acid molecules (Damyanova, et al., 2008; Ni and Meunier, 2007). Despite the fact that it leaches in water, sulphated zirconia does not leach during esterification. It is also not susceptible to side reactions such as dehydration or etherification (Kiss, et al., 2006a).

Depending on the treatment, it acts as a superacid or highly acidic when modified with sulphate ions (Sun, et al., 2005; Ardizzone, et al., 2004; Furuta, et al., 2004). The esterification of fatty acids from 2-ethylhexanol with methanol and SZ exhibited high selectivity and activity. Chorkendorff and Niemantsverdriet (2003), reported a good correlation between acidity and high activity of SZ. However, higher conversion requires higher temperatures, and higher catalyst concentrations. Although the activity, robustness, and reusability of the catalyst dropped to 90 % after five runs, there was no need for treatment in between the runs. A different study by Furuta et al., (2004) showed that tungstated zirconia remained stable after 100 h of use. A 40:1 alcohol/oil molar ratio after 8 h converted 94 % of the feedstock. Calcination restores the activity of the catalyst to almost 100 % (Di Serio, et al., 2007; Kiss, et al., 2006a). Jitputti et al. (2006), compared

the catalytic performance of zirconium oxide and zinc oxide in transesterification of palm kernel oil to that of sulfated zirconia. The yields obtained were 64.5%, 86.1%, and 90.3% respectively. The sulfonic acid on the surface of the zirconia provided higher acidic strength and hence, increased yield (Zabeti, et al., 2009).

Studies by López, et al., in 2005, showed that active site concentration and specific surface area have significant influence on catalytic activity of super acid catalysts such as $\text{ZrO}_2/\text{WO}_3^{2-}$ and $\text{ZrO}_2/\text{SO}_4^{2-}$. SZ showed surface area of $134 \text{ m}^2/\text{g}$ and $94 \text{ } \mu\text{mol}/\text{g}$ active site concentration, while tungstated zirconia had $89 \text{ m}^2/\text{g}$ and $54 \text{ } \mu\text{mol}/\text{g}$. The results showed that the activity of sulfated zirconia was higher towards transesterification of triacetin. It gave a conversion of 57% against 10% of the tungstated zirconia after 8 h. However, another study showed sulfated titanium oxide has more specific surface area ($99.5 \text{ m}^2/\text{g}$) than sulfated zirconia ($91.5 \text{ m}^2/\text{g}$). The methyl ester yields obtained in the transesterification of cottonseed oil from sulfated titanium oxide was 90% against 85% by sulfated zirconia after 8 h. Though these catalysts are active for both esterification and transesterification, they require higher calcination temperature ($500 \text{ }^\circ\text{C}$ to $800 \text{ }^\circ\text{C}$) to attain high Brønsted acidic sites (Ramu, et al., 2004; López, et al., 2007). Furthermore, conversions with these catalysts require long reaction time (López, et al., 2007; He, et al., 2007). Another promising heterogeneous acid catalyst is vanadium phosphate. Methyl ester yield of 80% was obtained with 0.2 wt.% loading and 1:1 alcohol/oil molar ratio 1 hour transesterification reaction. Any attempt to increase the yield by raising the temperature result in the reduction of vanadium from V^{5+} to V^{3+} . This causes a slow deactivation of the catalyst as it reacts with methanol (Di Serio, et al., 2007). This is despite the mild reaction parameters and a low specific surface area of 2 to $4 \text{ m}^2/\text{g}$.

2.10.3 Catalysts with sulfonic acid groups

Of the ion exchange family, the ion-exchange resin Nafion and Amberlyst are most common. Nafion resin is non-porous, while large pores characterize Amberlyst. The polymer chain governs the hydrophobicity of these catalysts. Conversely, the polymer backbone has strong affinity towards the tails of the alcohol and fatty acid. This enhances the catalytic activity of these catalysts. Besides, these catalysts have sulphonic acid groups grafted on their polymer chain. These strong sulphonic acids have better acid sites when compared to the hydroxy groups on metal oxides or zeolites. These properties make resins good catalytic candidates for biodiesel production. However, their poor thermal stability is limiting their industrial applications (Kiss, et al., 2006b).

2.10.4 Heteropoly acids and polyoxometalates (isopoly and heteropoly anions)

A promising field of growing significance in catalysis is the use of polyoxometalate compounds and heteropoly acids (HPAs). The incorporation of polyoxometalate anions forms complex proton acids otherwise known as HPA. The basic structure of these acids comprises of a XO_4 central tetrahedron surrounded by octahedra of metal-oxygen (Maksimov, 1995; Tsigdinos, 1978; Keggin, 1934). The first characterized HPA was the keggian heteropoly anion. It is yet the best of these polyoxometalates represented as $\text{XM}_{12}\text{O}_{40}^{x-8}$. X denotes the central atom such as Si^{4+} and P^{5+} , e.g., $\text{H}_4\text{SiW}_{12}\text{O}_{40}$ and $\text{H}_3\text{PW}_{12}\text{O}_{40}$. M represents the metal ions usually W^{6+} or Mo^{6+} which are easily substituted by other metal ions such as Co^{2+} , Zn^{2+} , and V^{5+} .

The strength of these catalysts approaches that of superacids in the Brønsted acidity region. The release of water of hydration on heating increases this strength as exhibited by ionic structure of solid HPAs (Kozhevnikov, 1998). The discrete structure is comprised of heteropoly anions and counter-cations (e.g., H^+ , H_3O^+ , H_5O_2^+) which are

fairly mobile. This property gives the HPAs great proton mobility and a reacting medium resembling highly concentrated solutions termed “pseudoliquid phase”. Almost all the mobile protons partake in the catalysis. Adsorption of polar molecules is thus easy, while catalytic activity occurs on both the surface and bulk of the crystalline network.

High density of substrate adsorption reduces the high temperature requirement of solid acid catalyst. However, nonpolar molecules such as hydrocarbons, which are excluded from the HPA crystalline bulk network, interact only on the catalyst surface. This enhances the unique selectivity of HPA catalysts. Furthermore, the pseudoliquid phase uniformity facilitates online study of the catalytic progression (Misano, et al., 2000; Lee, et al., 1992; Misano, 1987). HPAs have also showed fair thermal stability. Stabilization of organic intermediates by polyanions, the absence of side reactions, and the pseudoliquid phase increases reactivity of HPAs. Solubility of HPAs in polar medium, low surface area (5-10 m²/g) and low thermal stability are their major limitations. Supporting them on appropriate promoter solves these limitations (Caetano, et al., 2008; Sunita, et al., 2008; Xu, et al., 2008; Pizzio, et al., 1998; Blanso, et al., 1998; Dupont and Lefebvre, 1996; Rocchiccioli-Deltcheff, et al., 1990). However, a setback deserving further research is the effect of promoters on HPAs. Interactions between the structure promoter and HPA usually results in weaker acidic strength on the supported HPA (Kozhevnikov, 1998 and 2002). It is therefore necessary to evaluate the reactivity of these catalysts and compare them with other hydrophobic solid catalysts. Such data will provide a proper perspective concerning the catalysts (Helwani, et al., 2009).

2.10.5 Zeolites and zeotype materials

Zeolite is a naturally occurring crystalline aluminosilicate interlinked by oxygen atoms. It has a three-dimensional framework structure with molecular pores and channels of uniform sizes. These pores (maximum pore diameter = UTD-1 with 1.0×0.75 nm) absorb molecules that fit into them while preferentially excluding larger ones; thus, acting as molecular sieves. Al^{3+} replaces Si^{4+} within the crystalline silica (SiO_2) framework. This gives a negative charge to the framework. Zeolites are able to maintain electroneutrality from the loosely held and exchangeable cations present in their cavities. Polar molecules interact reversibly with these cations. These properties allow the synthesis of synthetic zeolites and recently discovered zeotypes (silicoaluminophosphates). Crystalline structures of zeotypes are synthesized with coordinated Al, Si, P, transition metals and other elements such as Fe, Ti, B, Mn, Zn, Co, Be, Cu, etc. (Corma, 2003; Maesen and Marcus, 2001).

Examples of zeotype molecular sieves include SAPO, ALPO_4 , MeAPSO, and MeAPO (Corma, 2003; Maesen and Marcus, 2001). The loosely held cations create robust electric field with the framework making it possible to fine-tune adsorption. These properties and the ability to introduce active sites within the pores and channels enhance the activity and selectivity of zeolites and zeotypes. Other special properties that make these materials to be termed as catalytic microreactors include pores of molecular dimensions with high surface area. They have high adsorption capacity and ability to confine products from the reacting species. In addition, they have the ability of pre-activate molecules by modulating the strong electric fields. However, conversions from reactions catalyzed by zeolites are of minimal increase (1 to 4%) when compared with noncatalyzed reactions. This is because of diffusion limitations by the bulky reactants. These species suppress reactions within the pores while only few reactions take place on the external surface of

the catalyst (Okuhara, 2002; Zhang, et al., 2001; Lobo, et al., 1997; Freyhardt, et al., 1996).

Zeolites with larger pores (Y530 and Y756) exhibited higher activity that increases with increasing temperature. Brito, et al. (2007) reported poor activity for zeolites with high aluminium contents, such Y307 and Y411. Advancements in zeolitic design with larger channels and pores are requirements for better yields. In addition, optimal performance requires a tradeoff between hydrophobicity and acid strength of the zeolite. This is because at higher ratios of $\text{SiO}_2/\text{Al}_2\text{O}_3$, hydrophobicity of the catalyst increases. On the other hand, lower ratios of $\text{SiO}_2/\text{Al}_2\text{O}_3$, increases the acidic strength (Rahimi, & Karimzadeh 2011; Okuhara, 2002; van de Waal and van Bekkum, 2001). Conversely, chemical equilibrium is the limiting factor for achieving maximum conversion during esterification (Kiss, et al., 2006b).

2.11 Biodiesel production *via* solid acid catalysis

The enhancements of many industrial reactions in the last decade became possible with solid acid catalysis (Clark, 2002; Harmer and Sun, 2002). One major advantage these catalysts have is the diversity of acid sites in contrast to the definite acidic properties possessed by liquid acids (Wilson, et al., 2000). In principle, the mechanism of reaction is similar for both homogeneous and heterogeneous acid-catalyzed esterification (Koster, et al., 2001). However, the interaction between the activity of the catalyst and its surface hydrophobicity makes heterogeneous acid-catalyzed esterification distinct from the homogeneous one (Kiss, et al., 2006a; Sreeprasanth, et al., 2006).

Omota, et al. (2003a & 2003b) proposed a continuous method for producing biodiesel by a catalytic reactive distillation. However, deactivation of the solid catalyst by the aqueous phase became a major limitation. This is because of the phase segregation that occurs in nonideal mixtures. Catalysts that possess many hydrophilic acidic sites are more prone to the effect of phase separation. Water sorption inhibits the catalytic activities of these sites. One way of avoiding this problem is designing a water-tolerant catalyst (Okuhara, 2002). Another possible way is by using excess alcohol. This is because alcohol mixes better than the acid in the esterification reaction. Accordingly, a monophasic solution favors maximum conversion (Kiss, et al., 2006a).

2.11.1. Effect of preparation and structure promoters

The method of preparation and type of support employed has significant effect on the physiochemical properties and activity of a solid acid catalyst. Catalyst support minimizes lower reaction rates caused by mass transfer (diffusion) limitations. These supports provide more pores and channels, and hence more specific surface area. These increase the activity of the catalysts especially in liquid phase reactions. Tanabe and Yamaguchi (1994) studied the effect of calcination on $\text{ZrO}_2/\text{WO}_3^{2-}$, $\text{SnO}_2/\text{SO}_4^{2-}$ and $\text{ZrO}_2/\text{SO}_4^{2-}$ for transesterification of soybean oil and esterification of n-octanoic acid. The results indicated these catalysts as good structure promoters (Table 2.4). The acid strength of tungstated and sulfated zirconia (superacid) catalysts corresponds more than 100% H_2SO_4 which is stronger than Hammett acidity function, $H_0 = -12$.

Table 2.4: Catalytic effect of superacids on esterification and transesterification as function of calcination temperature

Catalyst	Calcination temperature (°C); Time (h)	Conversion, % (n-octanoic acid) – Esterification		Conversion, % (Soybean oil) - Transesterification
		175 °C	200 °C	
$\text{ZrO}_2/\text{WO}_3^{2-}$	800; 1	94	100	> 90
$\text{SnO}_2/\text{SO}_4^{2-}$	500; 3	99	100	> 78
$\text{ZrO}_2/\text{SO}_4^{2-}$	675; 1.5	100	100	> 66

The authors observed an inverse relationship is between calcination temperature, time, and conversion of n-octanoic acid. The plausible explanation for this is the formation of oxides on the catalytic sites of the catalysts at higher calcination temperature. The study conducted by López, et al. (2007 and 2008) confirmed this observation. Their results indicated a decrease in surface area of $\text{ZrO}_2/\text{WO}_3^{2-}$ with increase in calcination temperature. WO_x are formed which significantly inhibit the surface area of the catalyst.

Other properties also affected include acid site density and strength, and the metal oxide molecular and crystalline structure. After calcination at 900 °C, the catalyst surface area reduced to about 20% (58 m^2/g) of the initial catalyst precursor (325 m^2/g). The monomeric oxide deposited on the surface of the catalyst transformed into polymeric species. Ramu et al. (2004), investigated the catalytic performance of $\text{ZrO}_2/\text{WO}_3^{2-}$ as a heterogeneous acid catalyst during methanolysis of palmitic acid. A phase transformation occurs during the calcination as shown on Table 2.5.

Table 2.5: Effect of calcination temperature on catalytic activity of $\text{ZrO}_2/\text{WO}_3^{2-}$ during esterification

Calcination temperature, °C	Phase	Conversion, %
500	Tetragonal	98
900	Monoclinic	8

The findings by Kiss, et al., (2006a) corroborated these phase transformational change in the surface structure of sulfated zirconia. The report also showed that temperature of calcination plays significant role in the activity of the catalyst. Optimum temperature reported for $\text{ZrO}_2/\text{WO}_3^{2-}$ esterification of FAs is between 600 and 700 °C. In a similar report, López, et al. (2008), compared the catalytic activities of three modified zirconia catalysts in the esterification of carboxylic acids (FFAs) and transesterification of TGs with ethanol. Each catalyst had different optimum calcination temperature. The optimum

calcination temperatures reported were titanium zirconia (400 to 500 °C), sulfated zirconia (500 °C), and tungstated zirconia (800 °C).

Despite higher calcination temperature, tungstated zirconia showed higher catalytic activity and ease of *in situ* regeneration in a fixed bed reactor. This is probably because the high calcination temperature had minimal effect on the Brønsted acid sites, or the residual water vapour caused re-hydration of the catalyst surface during cooling. Re-impregnation with H₂SO₄ makes the reusability of SZ expensive. This leads to leaching which hinders biodiesel production. On the other hand, although titanium zirconia showed good catalytic activity, FFAs easily poisoned its active basic sites. Consequently, it is unsuitable for catalyzing feedstocks with high FFA content. However, mesoporous and macroporous structures (pore diameter > 2 nm) were exhibited by all the catalysts. Mass transfer limitations because of bulky TG molecules (2 to 4 nm) are significantly minimized (López, et al., 2008).

Garcia, et al., (2008) investigated the effect of preparation method on the activity of sulfated zirconia. Solvent-free precipitation method gave the highest conversion when compared to precipitation and impregnation methods. Alcoholysis with methanol and ethanol gave conversion of 98.6% and 92% respectively, at 120 °C after 1 hr from soybean oil. The presence of 0.44% water was attributed to the lower conversion obtained with ethanol. Extending the reaction time to 6.5 h increased the conversion to 96%. However, catalysts prepared by precipitation and impregnation methods gave $8.5 \pm 3.8\%$ conversions under the same reaction conditions. This report also highlighted the sulfate ion leaching effect and the significant poisoning of the catalyst after regeneration.

Various catalyst supports have the ability to reduce pore diffusion limitations by providing higher surface area. Silicates and alumina have received greater attention in this regard. Lin and Radu, (2006), and Delfort, et al. (2006) independently patented the activity of functionalized mesoporous silicates and titanium zinc oxide and titanium oxide-bismuth, respectively. Furuta, et al., (2006), also reported the comparative promoter catalytic performance of $\text{Al}_2\text{O}_3/\text{ZrO}_2/\text{WO}_3$ solid acid catalyst (Table 2.6). Higher density of sulfonic acid group enhances the activity of the mesoporous silicates significantly. This improved performance is observed from SBA-15- SO_3H -P123 because of higher acidic activity (H^+) and pore diameter (D_p).

Table 2.6: Catalyst reactivity supported on alumina and functionalized mesoporous silicates

Catalyst	Preparation method	Calcination temp (°C); time (h)	Textural properties of support	Reaction conditions	Performance	Oil	Ref
CDAB-SO_3H-C12^a	CDAB	-	$\text{H}^+ = 0.6 \text{ meq/g}$ $\text{BET} = 778 \text{ m}^2/\text{g}$ $V_p = 0.39 \text{ cm}^3/\text{g}$ $D_p = 2.8 \text{ nm}$	85 °C, 3 h, 10 wt%, 20:1	55 % conversion	Palmitic acid	Lin and Radu, 2006
SBA-15-SO_3H-L64	Pluronic L64	-	$\text{H}^+ = 0.84 \text{ meq/g}$ $\text{BET} = 820 \text{ m}^2/\text{g}$ $V_p = 0.58 \text{ cm}^3/\text{g}$ $D_p = 2.7 \text{ nm}$	85 °C, 3 h, 10 wt%, 20:1	Not reported	-	Lin and Radu, 2006
SBA-15-SO_3H-P123	Pluronic L123	-	$\text{H}^+ = 1.44 \text{ meq/g}$ $\text{BET} = 735 \text{ m}^2/\text{g}$ $V_p = 0.67 \text{ cm}^3/\text{g}$ $D_p = 3.5 \text{ nm}$	85 °C, 3 h, 10 wt%, 20:1	85 % conversion	-	Lin and Radu, 2006
SBA-15-ph-SO_3H-P123	Pluronic L123	-	$\text{H}^+ = 0.92 \text{ meq/g}$ $\text{BET} = 540 \text{ m}^2/\text{g}$ $V_p = 0.71 \text{ cm}^3/\text{g}$ $D_p = 5.0 \text{ nm}$	85 °C, 3 h, 10 wt%, 20:1	Not reported	-	Lin and Radu, 2006
Alumina supported titanium zinc oxide	Co-mixing	600;3	$\text{SSA} = 62 \text{ m}^2/\text{g}$	200 °C, 50 bar, 8 h	94 % yield	Colza oil	Delfort, et al, 2006
Alumina supported titanium oxide-bismuth	Co-mixing	600;3	$\text{SSA} = 54 \text{ m}^2/\text{g}$	200 °C, 50 bar, 7 h	88 % yield	Colza oil	Delfort, et al, 2006
$\text{Al}_2\text{O}_3/\text{ZrO}_2/\text{WO}_3$	Co-precipitation	800;1	-	175 °C, 4g, 40:1	100 % conversion	Soybean oil	Delfort, et al, 2006

^aCDAB = cetyltrimethylammonium bromide

Interestingly, polyaniline supported carbon carrier, as heterogeneous acid catalyst possesses all the features lacking on sulfated zirconia such as simple preparation and easy handling. It does not swell in methyl esters and methanol and it is insoluble in most inorganic solvents. It has thus exhibited minimal leaching. However, its characteristic low

surface area requires high molar ratio (29:1) of acid for high conversion. The catalyst also has regeneration and reusability limitations (Zieba, et al., 2010).

Table 2.7 highlights the summary of the literature review on activity and reaction conditions for various types of heterogeneous acid catalysts used in esterification and transesterification. It recapitulates the current challenges facing the commercial utilization of solid acid catalysts and serves as the theoretical framework for this study.

Table 2.7: Problems and potential solutions for using solid acid catalysts for biodiesel production

Problem	Possible cause	Possible solution(s)
1. Deactivation of solid acid catalyst	a) Phase segregation as a result of non-ideal nature of mixture b) Impurities present in unrefined feedstocks	a) Water-tolerant catalyst
2. Mass transfer (diffusion) limitation	Formation of three phases with oil, water and alcohol	a) Use of catalyst support with more specific surface area and interconnected system of larger pore sizes b) Use of co-solvents, e.g. dimethyl sulfoxide (DMSO), Tetrahydrofuran (THF), n-hexane
3. High catalyst concentration required and larger reacting vessels	By-product water from esterification adsorbed onto catalyst surface	a) Water-tolerant catalyst
4. High temperature requirement	Catalytic site covered by adsorbed by-product water from esterification reaction (organic reaction in water)	a) Water-tolerant catalyst c) Use of catalysts with pseudoliquid phase ability
5. Lower reaction rates	catalysis occurs on the external surface of the pores (reaction suppressed by diffusion limitation as a result of bulky alcohol molecules)	a) Use of catalyst support with more specific surface area and interconnected system of larger pore sizes b) catalysts with high concentration of strong acid sites
6. Leaching and product contamination	Ionic group hydrolyzed by water	Ensure good catalyst preparation method
7. Formation of side reactions such as alcohol dehydration or ether formation	Use of excess alcohol	Use minimal acid-to-alcohol ratio

This chapter is available as been published articles in:

- a) The Journal of Applied Catalysis A: General 470, 140-161 (Sani, Abdul Aziz & Daud, 2014).
- b) The Journal of Environmental Chemical Engineering 1 (3), 113-121 (Sani, Abdul Aziz & Daud, 2013).
- c) Biodiesel - Feedstocks, Production and Applications, Prof. Zhen Fang (Ed.), ISBN: 978-953-51-0910-5, InTech, DOI: 10.5772/52790. (Sani, Abdul Aziz & Daud, 2013).

CHAPTER 3: PALM FROND AND SPIKELET AS ENVIRONMENTALLY BENIGN ALTERNATIVE SOLID ACID CATALYSTS FOR BIODIESEL PRODUCTION

This chapter describes the study of sulfonated mesoporous catalysts from palm frond and spikelets in the esterification of free fatty acids for biodiesel production. Article 1 represents Chapter 3 as *Palm frond and spikelet as environmentally benign alternative solid acid catalysts for biodiesel production*. This chapter and the next, addressed the general research objective number 1: the synthesis of solid acid catalysts from palm tree biomass as environmentally benign alternative for biodiesel production. This chapter is available as a published research article in: Sani, Y. M., Raji, A. O., Alaba, P. A., Abdul Aziz, A. R. and Daud, W. M. A. W. (2015). Palm frond and spikelet as environmentally benign alternative solid acid catalysts for biodiesel production. *BioResources* 10(2), 3393-3408.

3.1 Introduction

Despite the recent fall in the price of Brent crude oil, the search for a sustainable and ecologically benign alternative persists. This is due to the pollution caused by crude oil exploration and the combustion of refined oil products (Sani et al., 2013; Hassan et al., 2015), coupled with weaker demand for petroleum fuels. The transesterification of triglycerides (TG) with methanol into biodiesel or fatty acids methyl esters is an alternative under aggressive evaluation (Ghadge and Raheman, 2006). However, feedstocks for this process containing large amounts of free fatty acids (FFAs), such as used frying oil (UFO), animal fats, and vegetable oils, usually incur postproduction costs in soap separation after alkali-catalyzed transesterification. This substantially decreases the biodiesel yield (Park et al., 2010). Reducing the FFA content of these feedstocks to

approximately 1% (acid value of less than 2 mg KOH/g) is necessary before transesterification (Lotero et al., 2005; Zhang and Jiang, 2008).

Similarly, there are several drawbacks to the two-step process of acid-catalyzed pre-esterification of FFA into esters with H_2SO_4 followed by alkali-catalyzed transesterification (Ramadhas et al., 2005; Ghadge and Raheman, 2006; Veljkovic et al., 2006; Wang et al., 2006; Berchmans and Hirata, 2008; Zhang and Jiang, 2008). These include equipment corrosion, difficulty in product separation from homogeneous mixtures, non-recyclability of the catalysts, and high-energy consumption during purification (Sani et al., 2012). These highlight the increasingly urgent need for affordable acid catalysts with good catalytic performance that could alleviate the mentioned issues. The discovery of sugar catalysts showed that carbon-based solid acids are promising alternatives to homogeneous alkaline and liquid acid catalysts (Toda et al., 2005).

The incorporation of $-\text{SO}_3\text{H}$ unto carbon biomass sources such as cellulose, corn straw, starch, glucose, and sucrose *via* the carbonization-sulfonation method (Zhang et al., 2015; Lou et al., 2008) exhibited good catalytic performance during esterification (Toda et al., 2005; Takagaki et al., 2006; Budarin et al., 2007; Zong et al., 2007; Agulló et al., 2010; Dehkhoda et al., 2010; Maciá-Liu et al., 2013). This is in spite of their low surface area and porosity, which limit reactant diffusion to active sites (Zhang et al., 2015). However, numerous groups have recently synthesized sulfonated, ordered, mesoporous carbons *via* nanocasting with SBA-15 as a template and phenolic resol and Pluronic F127 self-assemblies under acidic conditions, respectively (Wang et al., 2007; Xing et al., 2007; Liu et al., 2008; Peng et al., 2010; Janaun and Ellis, 2011; Suganuma et al., 2011; Geng et al., 2012). Similarly, Peng et al. (2005) and Yu et al. (2008), describe how to prepare catalysts for esterification *via* the high temperature sulfonation of carbon nanotubes. The

acidity, large pore size, and high surface area of these materials ensure accessibility of long-chain FFA molecules and high catalytic activity. However, a literature survey revealed that no reports are available regarding acid-catalyzed reactions using palm tree biomass.

Developing efficient solid catalysts from low-value biomass is essential to making the process ecologically friendly and economical. Malaysia, the world's second largest producer and exporter of palm oil, generates a deluge of biomass from oil palm production. According to Sulaiman et al. (2012), oil palm production generates 85.5% of the total biomass produced from a variety of crops, including but not limited to rubber, rice, and oil palm. This accounts for the highest percentage with little to no economic value.

These include palm trunks, palm mesocarp fibre (PMF), empty fruit bunches (EFB), palm fronds, spikelets, and kernel shells (PKS) (Hassan et al., 1997; Aziz et al., 2011). Incidentally, agricultural residues from renewable sources, which are both abundant and inexpensive, can serve as remarkable feedstocks for fuel production and catalyst development (Prauchner and Rodríguez-Reinoso, 2012). Incidentally, the availability of oil palm frond and spikelets is increasing. According to data obtained from <http://www.bfdic.com/en/Features/Features/79.html>, 75 to 80% of emptied fruit bunch is spikelets while the main stalk makes up the remaining 20 to 25%. An estimated average of 2.856 million tones (dry basis) of empty fruit bunches will be produced per year from 2007 to 2020 from the current and expanding planting area of ca. 4.0 million hectares. Similarly, an estimated 10.4 tons.ha⁻¹ of fronds equates to an average of 6.97 and 54.43 million tons per year during pruning activity and replanting process respectively, within the same period. Further, it is important to highlight that despite the mass production,

only ca. 10% of the total biomass produced is made of oil. It is therefore necessary to transform the remaining large amount of waste biomass to useful resources. This chapter demonstrates the synthesis of sulfonated, mesoporous carbon catalysts with concentrated H_2SO_4 (98%) as the sulfonating reagent and palm tree frond and spikelet from oil palm (*Elaeis guineensis*) as the carbon precursors. The study investigated the effects of the resultant catalysts in simultaneously esterifying FFA into FAME.

3.2 Literature review

Basiron, et al. (2000), reported that oil palm tree (*Elaeis guineensis*) was initially introduced to Indonesia (Bogor Botanical Garden) in 1848 and later in 1871 to Malaysia as ornamental plant from the indigenous West African tropical forests. Since then, oil palm tree plantation is on the rapid increase. For instance, the planting area expanded to 4.85×10^6 ha in 2010 from 3.37×10^6 ha in 2005, making Malaysia one of the largest exporter of palm oil in the world. The tree is currently amongst the most valuable cash crops in Malaysia. However, such large oil palm tree plantations generate significant amount of biomass that constitutes environmental challenges. During pruning or harvesting time (i.e., replanting time), oil palm fronds are made available in excess. Though their weights vary, (Chan, et al., 1980) reported annual pruning of up to 24 fronds of 82.5 kg/palm. Efforts in utilizing all the co-products obtained from the oil palm industry paved way for zero-waste policy (Gurmit, et al., 1999). Some researchers have converted some of the biomass, such oil palm trunk into cheaper lignocellulosic feedstock compared to wood (Sulaiman, et al., 2012).

However, in spite of the relatively high activities exhibited by the numerous solid acid catalysts, newer advances are required for the catalysts to be applicable for industrial production. These should necessarily include cheaper, readily available, and sustainable

feedstock sources such as waste biomass and used frying oil, non-edible oils such as grease, and byproduct of vegetable oil refinery (soapstock). This is especially because of the environment concerns caused by the exploration and combustion of, fluctuating prices and finite nature of fossil fuels. In this regard, mesoporous sulfonated carbon catalysts have promising activity for reducing free fatty acid in the esterification reaction from low-grade feedstocks. Aside their promising catalytic performances, sulfonate carbon catalysts have the potential of ameliorating the environmental impact and reduction in catalyst and production costs. Carbon-based solid acids are ideal catalysts for many reactions because they are thermally inert, have good thermal and mechanical stability. Further, they resolve the inherent problems associated with some heterogeneous acid catalysts, viz.:

- (a) Low acid site density,
- (b) Microporosity,
- (c) Hydrophilicity, and
- (d) Leaching of active sites.

The prospects of these new class of sulfonated carbon-based solid acid catalysts has opened new vistas for synthesizing highly active solid acid catalysts for the efficient production of biodiesel at (Toda, et al., 2005; Takagaki, et al., 2006). This is premised on the simple procedure involved in their synthesis, which could be from sulfonating a carbonized inorganic/organic compound, or *via* carbonizing sulfopolycyclic aromatic hydrocarbons such as the sulfonate derived from reacting concentrated with H_2SO_4 naphthalene (Nakajima, et al., 2007, Hao, et al., 2008; Liu et al., 2008).

Two widely accepted methods for incorporating $\text{-SO}_3\text{H}$ groups on the structure of the catalytic material during the preparation of incomplete carbon-based materials are:

- i. Sulfonating incompletely carbonized organic materials such as starch, D-glucose, sucrose, and cellulose (see Figure 3.1) (Toda, et al., 2005; Okamura, et al., 2006); and
- ii. Incomplete carbonization of sulfo-aromatic compounds (Hara, et al., 2004).

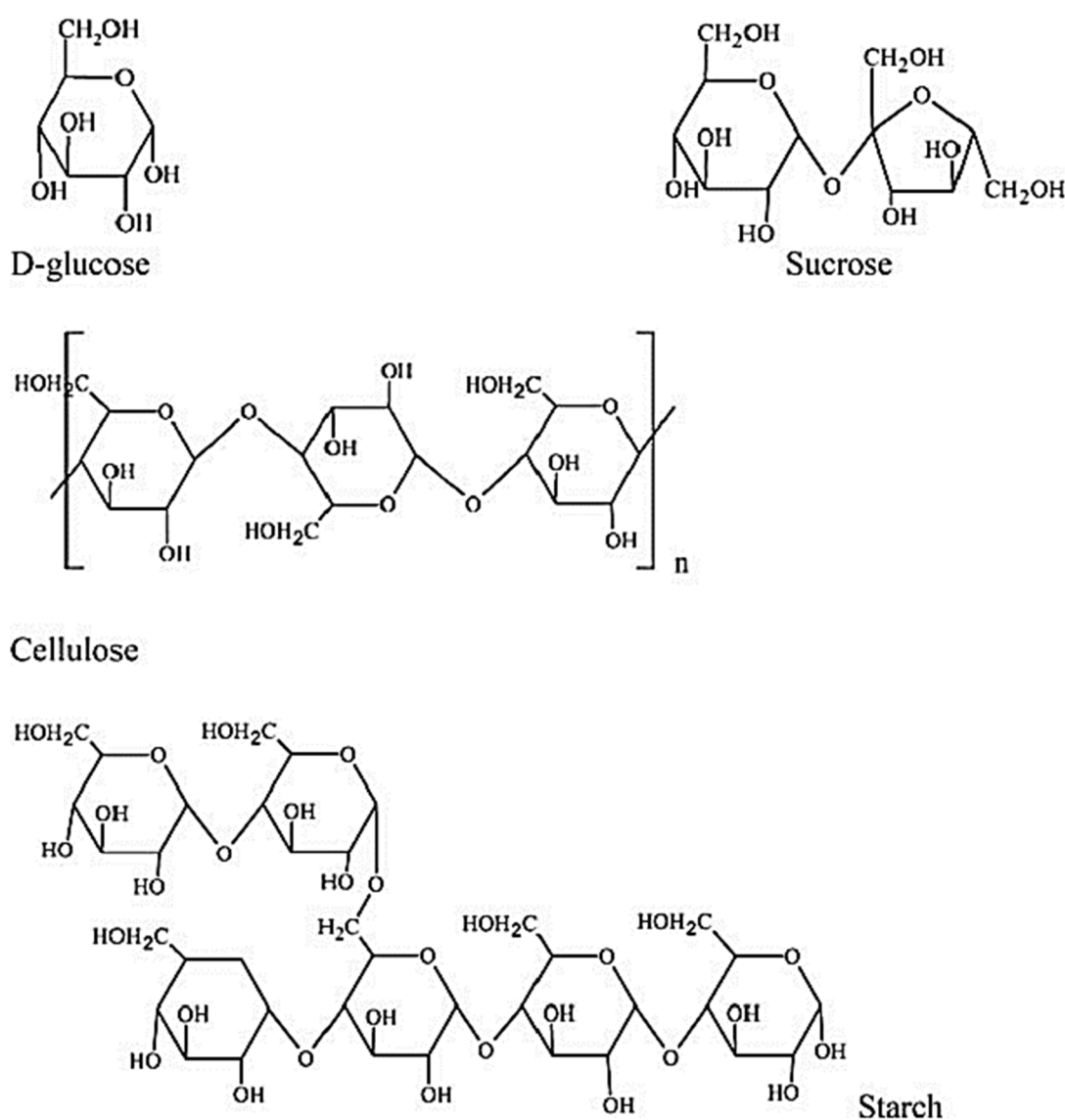


Figure 3.1: Molecular structures of carbohydrate derivatives.

The process of incompletely carbonizing carbohydrate and subsequent sulfonating with strong acid generates a robust structure with high surface area (200 to 1500 m^2/g) on the sulfo-polycyclic aromatic hydrocarbons (see Figure 3.2). Carbonization temperature is

crucial during the process. For instance, the optimal temperature for ensuring the formation of stable polyaromatic carbon ring must not exceed 200 °C during the carbonization. This is because according to Nakajima and Hara (2012), above this temperature, the sulfo-aromatic compound carbonizes. Contrarily, for direct incomplete carbonization of carbohydrate organic materials in inert environment, the optimal temperature is 400 °C. The inert environment such as in flowing N prevents the carbon precursor from burning to ash (Zong, et al., 2007). Slow pyrolysis between 400 to 600 °C, facilitates the synthesis of multi-ringed aromatic structure anchor, which is highly cross-linked. The slow carbonization also enhances the functionalization of catalytic material with active acidic or basic groups. However, hydrolysis, dehydration, partial decomposition, and molecular rearrangement occur and transforms the carbon material into a polycyclic aromatic structure under prolong pyrolysis (Kastner, et al., 2012).

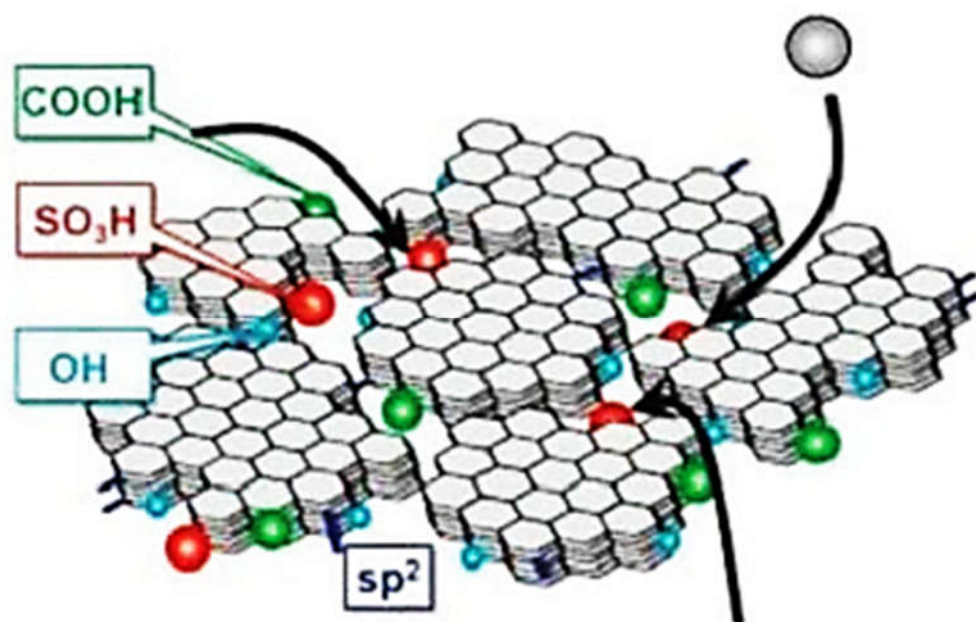


Figure 3.2: Diagrammatic representation of amorphous polycyclic carbon sheets with -OH - COOH, and -SO₃H, groups bonded on the carbon precursor (Nakajima and Hara, 2012)

Shu, et al. (2010), investigated the effect of carbonization temperature on the structure of a carbon-based catalyst. The same researcher group (Shu, et al., 2009) synthesized strong recoverable solid acid catalyst that exhibited high activity for transesterification of vegetable oil asphalt *via* carbonization-sulfonation method. Highly dispersed sulfonic acid groups decked the material of the flexible carbon-based framework. The authors ascribed the high performance to large mesopores, loose irregular network, high acid site density and the electron-withdrawing force exerted by polycyclic aromatic hydrocarbon, HC. Furthermore, the catalyst withstood 270 °C without denaturing nor losing its active acid sites, while its hydrophobicity prevented the –OH hydration. Incidentally, most acid-catalyzed transesterification requires these attributes for efficient conversion at high reaction temperatures

3.3 Materials and catalyst preparation

Room temperature drying for one week ensured steady moisture loss from the oil palm residues (fronds and spikelets). This was measured using the oven-dry basis mass, OD (Eq. 3.1) before oven drying at 120 °C for 24 h followed by milling and sieving (mesh size, 0.5 mm). Catalyst preparation was done according to a modified procedure previously documented (Toda et al., 2005; Dawodu et al., 2014). Low-temperature, incomplete carbonization induced polycyclic aromatic carbon ring formation from cellulosic palm residues. Heating the dried powder in a tubular furnace at 400 °C, with temperature increasing at 2 °C/min, for 24 h under a nitrogen (N₂) atmosphere produced incompletely carbonized materials. Treatment with concentrated sulfuric acid introduced sulfonate groups (-SO₃H) into the material. This was done by heating the solids (20 g) in 200 cm³ of concentrated H₂SO₄ (98%) at 150 °C. Adding distilled water (1000 cm³) after heating for 10 h and then cooling the mixture to room temperature yielded a black precipitate. Washing the precipitate with hot distilled water (temperature above 80 °C)

ensured the absence of impurities such as sulfate ions. The material was then oven dried at 70 °C before it was homogenized with succinic acid (SA). Mixing the carbon material (10 g) with 5 g of succinic acid and 40 cm³ of de-ionized water, then heating at 150 °C for 5 h, achieved proper sulfonation. After filtering and washing with distilled water and methanol, oven drying the resulting product at 100 °C for 5 h produced rigid carbon materials. The sulfonated palm fronds were designated sPTF/SA/T, where T denotes the carbonization temperature (300 or 400 °C). A non-homogenized reference material, designated sPTF/400, was synthesized to evaluate the effects of SA addition. Catalyst prepared from palm tree spikelet was designated sPTS/T without SA addition. These differences in reaction conditions helped to create the optimum sulfonated catalyst synthesized from oil palm residues for esterification.

$$\text{Moisture content (\%; OD basis)} = \frac{\text{weight of water}}{\text{dry weight of wood}} \times 100 \quad (3.1)$$

3.4 Methods

Esterification reaction was employed to obtain biodiesel designated B100 or a fuel made up of mono-alkyl esters of long chain fatty acids which meets the ASTM D 6751 specifications derived from feedstock containing high (48 wt%) free fatty acid; used frying oil. Table 3.1 presents selected properties of B100 and typical No. 2 diesel fuels. Methanol (Molecular Weight - 32.04, Density - 0.792 g/cc, Boiling Point - 64.7 °C) was used for the solid acid-catalyzed methanolysis of the direct esterification of free fatty acids from the high FFA feedstock.

Table 3.1: Selected properties of B100 and typical No. 2 diesel fuels.

Fuel Property	Biodiesel	Diesel
Fuel Standard	ASTM D6751	ASTM D975
Composition	FAME (C ₁₂ to C ₂₂)	HC (C ₁₀ – C ₂₁)
Lower Heating Value, Btu/gal	ca. 118,170	ca.129,050
Kinematic Viscosity, (mm ² /s) @ 40 °C	4.0 to 6.0	1.3 to 4.1
Specific Gravity kg/l @ 60 °F	0.88	0.85
Density, lb/gal @ 15 °C	7.328	7.079
Water and Sediment, vol%	0.05 max	0.05 max
Carbon, wt %	77	87
Hydrogen, wt %	12	13
Oxygen, by difference wt %	11	0
Sulfur, wt %	0.0 to 0.0024	0.05 max
Boiling Point, °C	315 to 350	180 to 340
Flash Point, °C	100 to 170	60 to 80
Cloud Point, °C	-3 to 12	-15 to 5
Pour Point, °C	-15 to 10	-35 to -15
Cetane Number	48 to 65	40-55
Lubricity SLBOCLE*, grams	>7,000	2000 to 5000
Lubricity HFRR*, microns	<300	300 to 600

*SLBOCLE = scuffing load ball on cylinder lubricity evaluator

*HFRR = high frequency reciprocating rig test

3.4.1 Catalyst characterization

A FEI QUANTATM 450 FEG type 2033/14 (Czech Republic) unit with 30 kV accelerating voltage (Figure 3.3) was used for field emission scanning electron microscopy (FE-SEM) to analyze the surface morphology and topology of the catalysts. An energy dispersive X-ray spectrometer (EDX) from the same unit revealed the surface elemental composition of the catalysts. Further, X-ray diffraction (XRD) and BET analyses were used to determine the structural and textural properties of the catalysts. The XRD patterns were analyzed with a Phillips X'pert diffractometer (The Netherlands) using CuK α radiation ($\lambda = 1.54056 \text{ \AA}$) at a scanning speed of 0.05°/s within a 2θ range of 5 to 70° at 40 mA and 40 kV. Micromeritics TriStar II (USA) with accelerated surface area porosity (ASAP)-3020 at minus 196.15 °C was used to determine the specific surface area of the catalytic materials using liquid nitrogen. Degassing the catalysts at 120 °C for 3 h under a vacuum eliminated any physisorbed volatiles and impurities. Rapid (scan speed 3 velocities, 2.2 to 20 kHz) identification and quantification of the catalysts was performed with a Bruker Fourier transform infrared (FT-IR) Tensor 27 IR (Germany).

The apparatus has a spectral range of 7500 to 370 cm^{-1} with more than 1 cm^{-1} apodized resolution and a standard KBr beam splitter.



Figure 3.3: Field emission scanning electron microscope

3.4.2 Production of fatty acid methyl esters

The catalysts were heated at 150 °C for 1 h before the reaction to evacuate adsorbed water and other volatiles. Methanol, with the aid of the catalyst, was used to transesterify used frying oil (UFO) at 100 to 200 °C in a 100 mL autoclave (250 °C, 100 bar) reactor supplied by AmAr Equipment Pvt., Ltd. Mumbai (Figure 3.4). Constant stirring ensured contact between the catalyst and the reaction mixture. A water bath attached to the autoclave maintained the reaction temperature in the range of 190–200 °C during the reaction. Preliminary optimization showed that a 5:1 methanol-to-oil molar ratio and 1 wt.% catalyst loading are optimal reaction conditions. Simple decanting was done to recover the FAME at the end of the 3 to 15 h reaction. Drying, methanol washing, and heating at 120 °C for 1 h regenerated the catalyst. The catalyst retained its activity after regeneration for up to 8 recycles.



Figure 3.4: Double 100 mL stainless steel autoclave (250 °C, 100 bar) reactor.

3.4.3 Acid density analysis

Exchanging Na^+ with H^+ in the form of $-\text{SO}_3\text{H}$ by mixing 0.1 g of sulfonated material with 30 mL of 0.6-M NaCl solution for 2 h facilitated determination of the acid strength of the catalysts. The filtrate from this mixture was titrated with 0.1001 M NaOH standard solution and methyl orange indicator to indicate when the NaOH was consumed. A change from slightly red to bright yellow maintained for 30 s was defined as the end-point. To determine the initial, unconsumed volume of the NaOH standard solution, a blank titration was performed. Equation 3.2 was used to accurately calculate the strong acid ($-\text{SO}_3\text{H}$) density.

$$D_{-\text{SO}_3\text{H}} = \frac{C_{\text{OH}^-} \times [V_1 - V_0]}{m_{\text{cat.}}} \quad (3.2)$$

The strong acid (-SO₃H) density of the catalyst (in mmol/g) and the concentration of standard NaOH solution are represented by $D_{\text{-SO}_3\text{H}}$ and $C_{\text{OH-}}$, respectively. The volume of NaOH standard solution consumed during the blank and catalyst titrations are represented by V_0 and V_1 , respectively; m_{cat} represents the mass of catalyst used for the acid density analysis.

3.3.4 Determination of acid value

The oil's acid value was determined by titration analysis according to DIN EN ISO 660 (2009) while Table 3.1 presents other methods usually employed for the analyzing oil samples (Nakpong, & Wootthikanokkhan, 2010). The expected acid value of used frying oil is between 15 and 75 mg KOH/g. The titrant, 0.1 M KOH, neutralizes the solvent mixture comprised of 50 mL of ethanol-diethyl ether (1:1 ratio, v/v) mixed with 0.5 g of catalyst sample. Equations 3.3, 3.4, and 3.5 were used to calculate the titre value, acid value, and FFA conversion, respectively:

$$\text{Titre value} = \frac{m_s}{V_{EP_1} \times c(\text{KOH}) \times M_A} \quad (3.3)$$

$$\text{Acid value} = \frac{V_{EP_1} \times f \times c(\text{KOH}) \times M_A}{m_s} \quad (3.4)$$

$$\text{FFA conversion, \%} = \frac{V_{EP_1} \times f \times c(\text{KOH}) \times M_A}{10 \times m_s} \quad (3.5)$$

where V_{EP_1} represents the titrant consumed at end of the first equivalent point in mL, $c(\text{KOH})$ represents the concentration of KOH titrant (0.1 M), M_A represents the molecular weight of the analyte (112.12 g/mol), f represents the correction factor obtained from the titre value, M_A represents the molecular weight of palmitic acid (256 g/mol), and m_s represents the sample size in g.

Table 3.2: Methods for analyzing vegetable oils (Nakpong & Wootthikanokkhan, 2010).

Analysis Method	Analysis Method
Fatty acid composition	AOAC (2000), 963.22, 969.33
Saponification value	AOAS (1997)
Density	ASTM D 4052-96
Kinematic viscosity	ASTM D 445-06
Acid value	AOAC (2000), 940.28
Water content	AOAC (1990) 984.20 (for coconut oil)
Total acid number	ASTM D 664-01
Carbon residue	ASTM D 4530-00
Iodine value	EN 14111
Gross heat of combustion	ASTM D 240
Oxidation stability	EN 14112
Mono-, di-, and tri-glycerides	EN 14105

3.4 Results and discussion

A previous study (Aziz et al. 2011) described the approximate oil palm biomass composition from oil palm (*Elaeis guineensis*) as 45 to 50% carbon, 43 to 48% oxygen, 0.5% nitrogen, 5% hydrogen, and 0.4% sulfur. Similarly, proximate analysis revealed that the oil palm biomass consisted of 72 to 75% volatile matter, 14 to 16% fixed carbon, 6 to 8% moisture, and 2 to 5% ash. Specifically, petiole, leaflets, and rachis are the three main parts of the palm fronds. The petiole consists of about 70% of the dry matter in the palm fronds, while the leaves and rachis make up the remaining percentage. The dry matter content of palm fronds is about 31% (Ishida and Abu Hassan, 1992). Depending on age, a palm frond contains *ca.* 15 to 26% hemicellulose. It also contains 4.7 MJ/kg crude proteins, 38.5 MJ/kg crude fibre, 2.1 MJ/kg ether extract, 78.7 MJ/kg neutral-detergent fibre, and 3.2 MJ/kg ash (Wong and Wan Zahari, 1997; Wan Zahari et al., 2000). Similarly, (Rabumi, 1998) reported 70.9 to 90.1 C/N ratio, 25.0 to 29.9% lignin, 16.2 to 21.3% cellulose, 1.52 to 2.46% soluble polyphenols, as the chemical composition of spikelets.

A previous report by Chen et al. (2010) identified 2θ peaks ranging from 22° to 23° as the major diffraction peaks for cellulose crystallography. Figure 3.5 shows the XRD pattern for all the samples. The figure displays one broad XRD peak at about a 2θ value of 24° with d value, calculated using the Bragg equations, of 3.86 nm. The noticeable peak confirmed the presence of crystallinity within the amorphous structure of the cellulosic constituents (Lai and Idris 2013). Further, Liu et al. (2012) posited the prominent I_{002} peak with the maximum intensity of 002-lattice diffraction as the primary as well as crystalline.

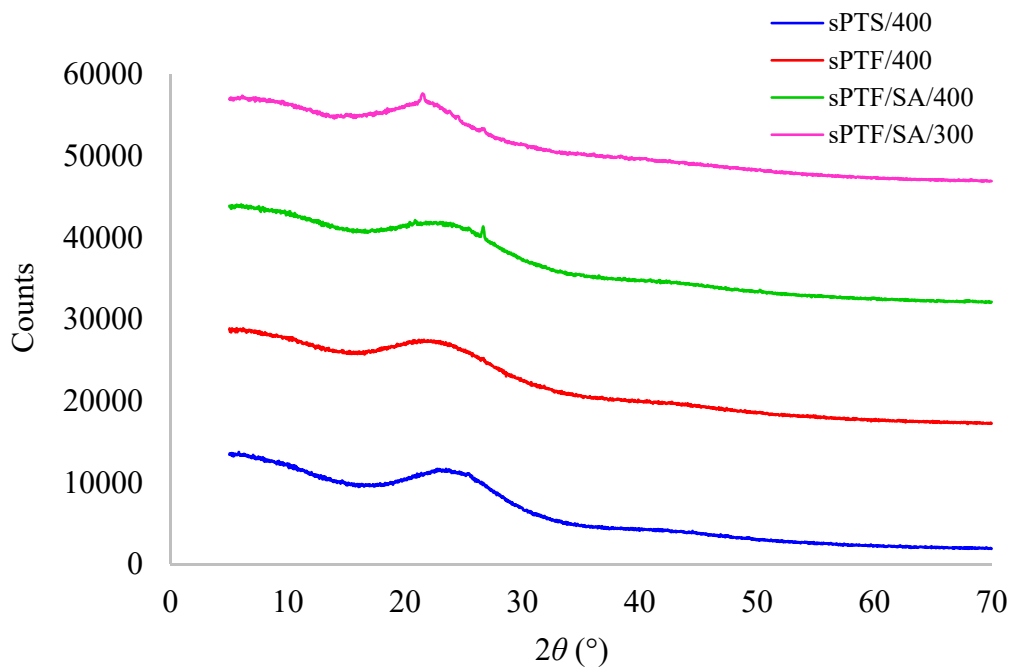


Figure 3.5: XRD patterns of sPTS/400, sPTF/400, sPTF/SA/300, and sPTF/SA/400

The broad nature of the peak is reflective of the cellulosic molecular hydrogen bond transformation during heat treatment. However, the low crystallinity indicated the presence of larger amounts of amorphous cellulose in the catalytic materials (Kuo and Lee, 2009). Certainly, from the representation on Figure 3.5, one may recognize the correlation between the good performance of sPTS/400 and the crystal structure. The material exhibited a spike at 2θ value of 24° , which falls within the range reported for

cellulose crystallography by Chen et al. (2010). The next in line after sPTS/400 is sPTF/400 with a spike at 2θ value of 25.44° and a d -spacing of 3.498\AA . Evidently, crystallinity and the total acid ($-\text{SO}_3\text{H}$) density of these materials facilitated their observed catalytic performances over sPTF/SA-300 and sPTF/SA-400.

The N_2 adsorption results presented in Table 3.3 and Figure 3.6, confirmed the presence of mesopores ($2 < dp < 50\text{ nm}$) on the prepared catalytic materials, consistent with aromatic sheets of amorphous carbon orientation. The clear nitrogen condensation steps on Figure 3.6 evidenced this. Further, the figure shows the N_2 adsorption-desorption isotherm and pore size distribution curves of mesoporous carbon obtained at $400\text{ }^\circ\text{C}$ carbonization temperature. The pore size distribution curves of the two materials (with and without SA) show similar shapes with high pore size uniformity with a highly uniform pore diameter centered at about 17.8 nm . The large mesopores are advantageous because they minimize diffusion limitation and facilitate easier access to the reacting molecules to the active sites within the materials. Additionally, the large mesopores enhance the stability of the ordered mesoporous carbon framework (Zhang et al., 2015).

The adsorption isotherm of all samples followed a type-IV IUPAC classification for mesoporous materials with capillary condensation taking place at higher pressures of adsorbate depicting a hysteresis loop (Sing et al., 1985). At higher pressures, the slope showed increased uptake of adsorbate as pores become filled, with the inflection point typically occurring near completion of the first monolayer. The H_4 -type hysteresis loop fit well to the inkbottle pores expected for the voids between the materials. At lower pressures, an adsorbate monolayer forms on the pore surface, which leads to a multilayer formation. However, it is interesting to note that mesoporosity alone did not determine

the extent of catalytic activity or turnover. Other factors, such as acid sites and type, acid density, carbon precursor and crystal structure, all played significant roles.

Titrimetric, structural, and surface analyses revealed strong acid (-SO₃H) densities (Table 3.3) and amorphous carbon sheets bearing hydroxyl (-OH) and carboxyl (-COOH) groups. Interestingly, the carbon catalysts remained insoluble even above the boiling temperatures of water, methanol, oleic acid, benzene, and hexane (Toda et al., 2005). Furthermore, the presence of low crystallinity also indicates the catalysts' affinity for anchoring -SO₃H groups.

Table 3.3: Surface properties and total acid (-SO₃H) density of the catalysts

Catalyst	Surface Area (m ² /g)	Pore Size (nm)	Pore Volume (cm ³ /g)	Total Acid (-SO ₃ H) Density (mmol/g)
sPTF/SA/400	28.1057	10.1712	0.033078	0.7851
sPTF/SA/300	27.7805	10.0154	0.030178	1.1283
sPTF/400	17.8048	9.1975	0.028308	1.0873
sPTS/400	12.7037	5.1565	0.019907	1.2974

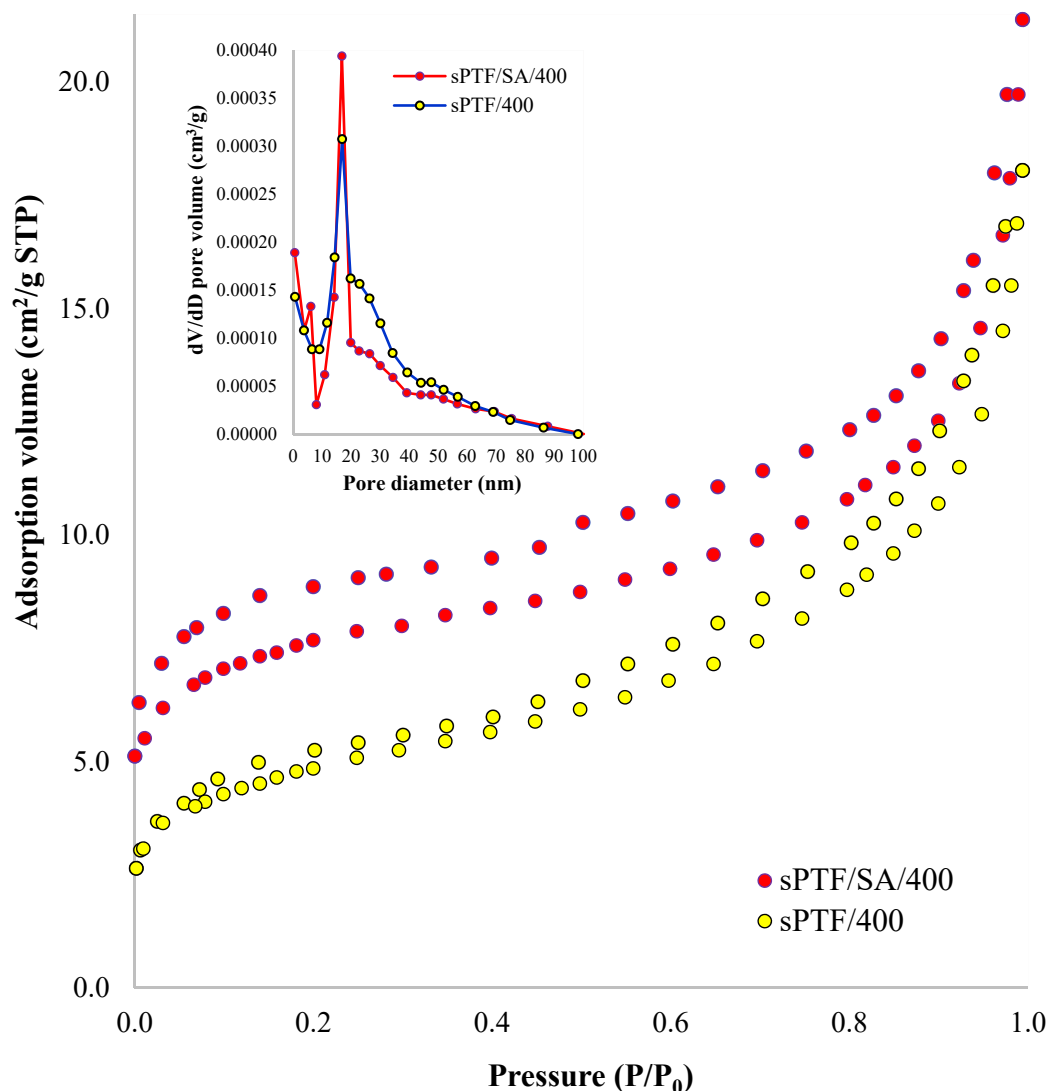


Figure 3.6: N_2 adsorption-desorption isotherm and pore size distribution of sPTF/SA/400 and sPTF/400

Figure 3.6 also highlights the effect of adding SA to the surface properties of the mesoporous carbon materials. Both materials showed similar N_2 adsorption-desorption isotherm and pore size distribution curves. However, sPTF/SA/400 exhibited a larger hysteresis loop than sPTF/400 because of the thermal exchange with the SA. This could reduce the performance of sPTF/SA/400 by giving rise to complex pore structure and network effects. Conversely, the smaller hysteresis exhibited by sPTF/400 confirms the effect of only internal friction in the absence of SA. Consequently, the resultant large hysteresis loop of the material could limit the catalytic activity of sPTF/SA/400. Further, the FE-SEM analysis revealed large pores, sharp edges, and agglomeration on the surface

of the catalysts. Figure 3.7a illustrates the surface microstructure of the sulfonated sPTF/SA-400 carbon catalyst as studied using FESEM. The different constituents appear to have been homogeneously processed into solid particles of varying dimensions. The EDX analysis of the surface elemental composition revealed the presence of carbon, oxygen, and sulfur (Figure 3.7b; Appendix F).

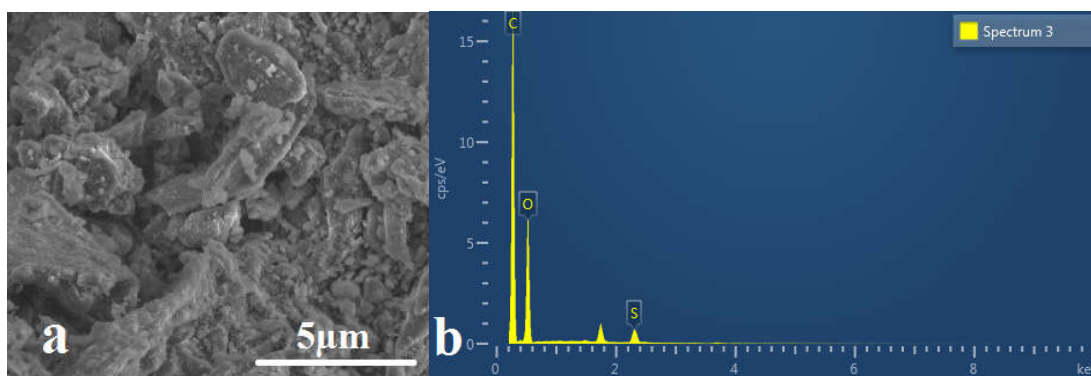


Figure 3.4: (a) Results of the surface microstructural analysis of the sPTF/SA/400 *via* FE-SEM, and (b) surface elemental composition of the sPTF/SA/400 determined *via* EDX analysis

Similarly, Fig. 3.8a illustrates the surface microstructure (size and shape of topographic features) of the sulfonated sPTF/SA-300 as studied using FE-SEM. The surface morphology appears to have been heterogeneously processed into solid particles into which succinic acid was not fully incorporated. The surface elemental composition (Fig. 3.8b) revealed the presence of carbon, oxygen, nitrogen, and sulfur. Further, FE-SEM analysis revealed large pores with sharp edges on the agglomerated catalyst surface.

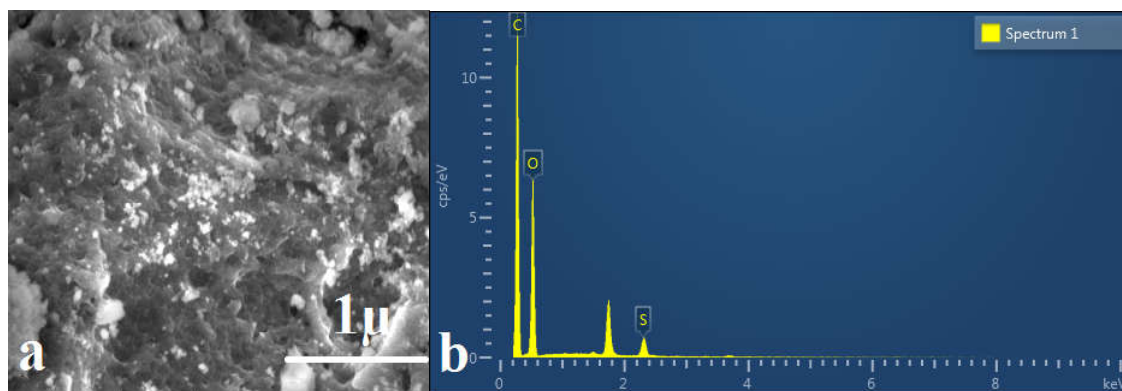


Figure 3.8 (a) Results of the surface microstructural analysis of the sPTF/SA/300 *via* SEM, and (b) surface elemental composition of the sPTF/SA/300 determined *via* EDX analysis

Figure 3.9a presents the surface microstructure of the sulfonated sPTS-400 carbon catalyst studied using FE-SEM. Figure 3.9b shows a cross-sectional surface composition and the distribution of elements on sPTS-400. The result also revealed the presence of carbon, oxygen, and sulfur (Appendix F). However, large pores with sharp edges were not evident in the FE-SEM images. The analysis indicated an agglomerated, amorphous solid with nearly uniform protrusions on its surface.

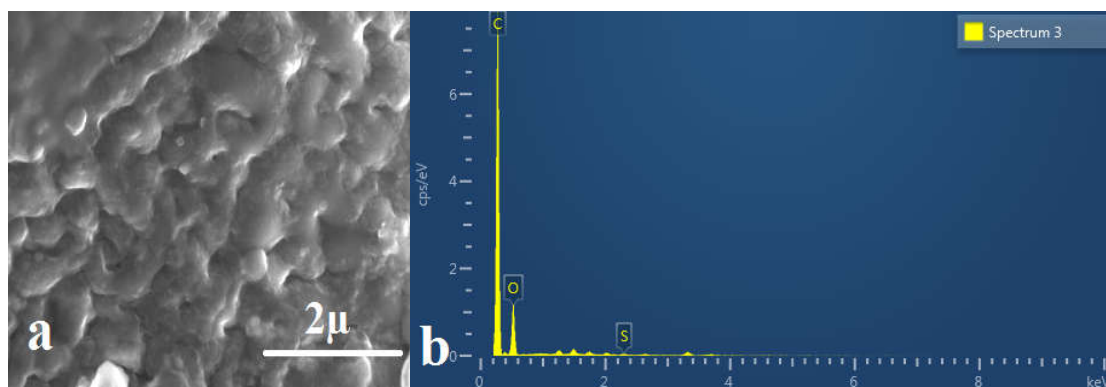


Figure 3.9: (a) Results of the surface microstructural analysis of the sPTS-400 *via* SEM, and (b) surface elemental composition of the sPTS-400 determined *via* EDX analysis

Sulfonating cellulosic materials resulted in the production of highly stable solids with strong acid density and many active sites. This is because sulfonating the carbonized organic or inorganic compounds facilitates the formation of rigid carbon material is comprised of small, three dimensional sp^3 -bonded polycyclic aromatic carbon sheets. Such an approach can simplify the synthesis of highly active catalysts from inexpensive, naturally occurring molecules. Figure 3.10 presents the FT-IR spectra of unsulfonated mesoporous carbon from palm tree spikelet and sulfonated catalysts. These results confirm the findings of Zhang et al. (2015) and Peng et al. (2010). Successful incorporation of $-SO_3H$ groups onto the sulfonated catalysts was observed in the form of FT-IR spectrum bands in the stretching mode at 1008 cm^{-1} . This vibration, attributed to symmetric $S=O$ bonds, is absent in the spectra of unsulfonated material.

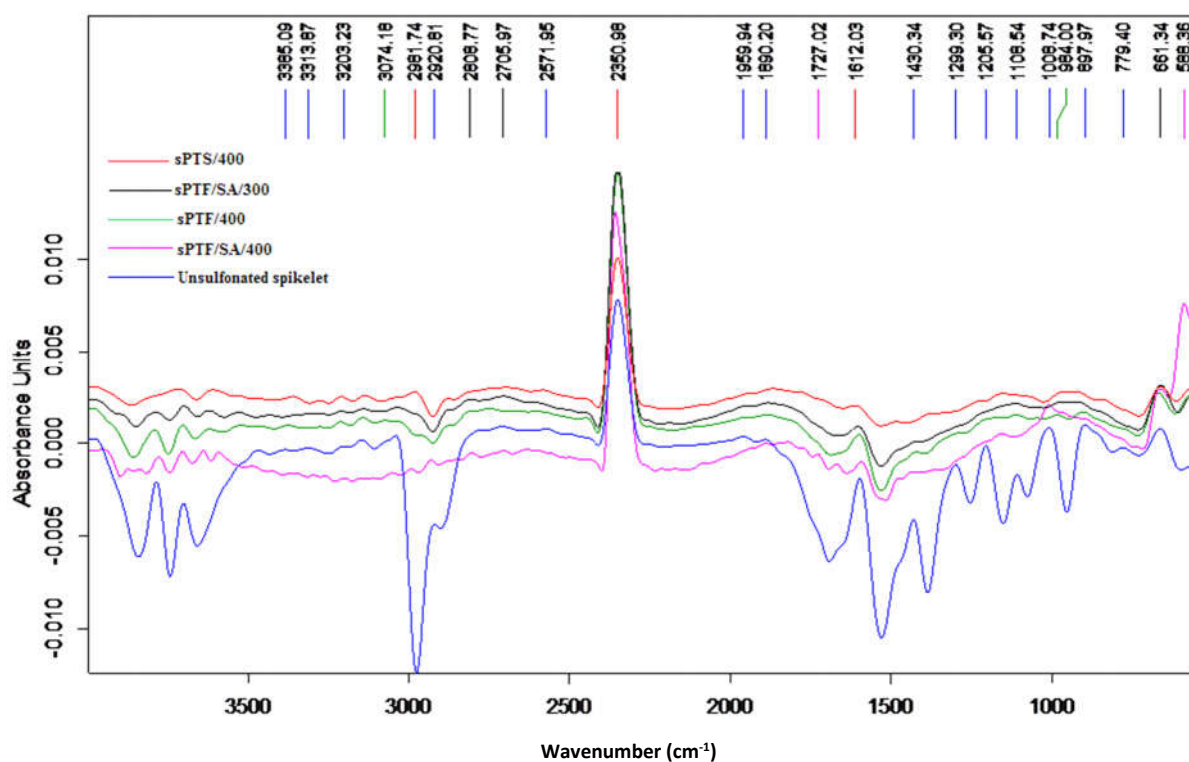


Figure 3.10: FT-IR spectra of sPTF/300 catalysts, sPTS/400 catalysts, and unsulfonated-PTS/400 mesoporous carbon

It was observed that the $S=O$ bond, represented by the peak at 1080 cm^{-1} , is asymmetric. The FT-IR spectra also reveal symmetric $O=S=O$ bonds, as shown by the vibration bands

at 1027 and 1167 cm^{-1} and those for -OH bonds at 3424 and 3429 cm^{-1} . The node stretching at 3440 cm^{-1} was assigned to the O-H stretching mode of phenolic -OH and -COOH groups. Similarly, node stretching at 1719 cm^{-1} is representative of C=O bonds due to -COO- and -COOH group stretching vibrations. The aromatic C=C stretching mode, similar to graphite-like, polyaromatic materials, was ascribed to the broad, intense bands centered at 1610 cm^{-1} . The effect of carbonization was observed from the disappearance of C-H stretching peaks at 675 cm^{-1} , 700 to 900, and 3046 cm^{-1} , ascribed to polycyclic aromatic and aromatic hydrocarbons, respectively. High carbonization temperatures dehydrogenate and graphitize the mesoporous carbon skeleton. Low carbonization temperature thus appears favorable in synthesizing sulfonated carbon catalysts rich in C-H bonds. This is evident from the gradual disappearance of C-H stretching peaks and the difference in the -SO₃H incorporated on sPTF/SA/400 (0.7851 mmol/g) and sPTF/SA/300 (1.1283 mmol/g).

3.4.1 Catalytic performance of the solid acid catalysts in biodiesel production

This section sets out its purpose, *viz.* to evaluate the catalytic activity of the catalysts synthesized from palm frond and spikelet. The study employed 1 wt.% catalyst loading and a methanol-to-oil molar ratio of 5:1 within a temperature range of 100 to 200 °C. The mesoporous sulfonated solid acid catalysts exhibited high activity compared to conventional solid acid catalysts. They were able to convert a high-FFA content (48%) UFO feedstock obtained from a household in Malaysia to more than 98.51% FAMES. Figures 3.11a to 3.11d show the catalytic activity of the sulfonated solid acid catalysts prepared under different conditions. Figure 3.12 shows the reaction mechanism of esterification catalyzed by mesoporous sulfonated carbon catalyst. Despite the low alcohol molar ratio, this procedure achieved more than 80% conversion with each catalyst

after 5 h reaction time. This is encouraging, considering that Zhang et al. (2015) used an 18:1 molar ratio in a study, though at lower temperature.

This trend was similar for all reactions, with equilibrium achieved after 5 h reaction time. The catalyst, sPTS/400 with 1.2974 mmol/g total $\text{-SO}_3\text{H}$ acid density produced the highest catalytic activity (98.51% FAME) the reaction. Next in performance to sPTS/400 was sPTF/SA/300, with 1.1283 mmol/g total $\text{-SO}_3\text{H}$ acid density. Interestingly, despite proper sulfonation and higher surface area and pore size ($27.78 \text{ m}^2/\text{g}$ and 10.02 nm), the performance of sPTF/SA/300 was slightly less than what was obtained from sPTS/400. However, it is interesting to note that mesoporosity alone does not determine the extent of catalytic activity or turnover.

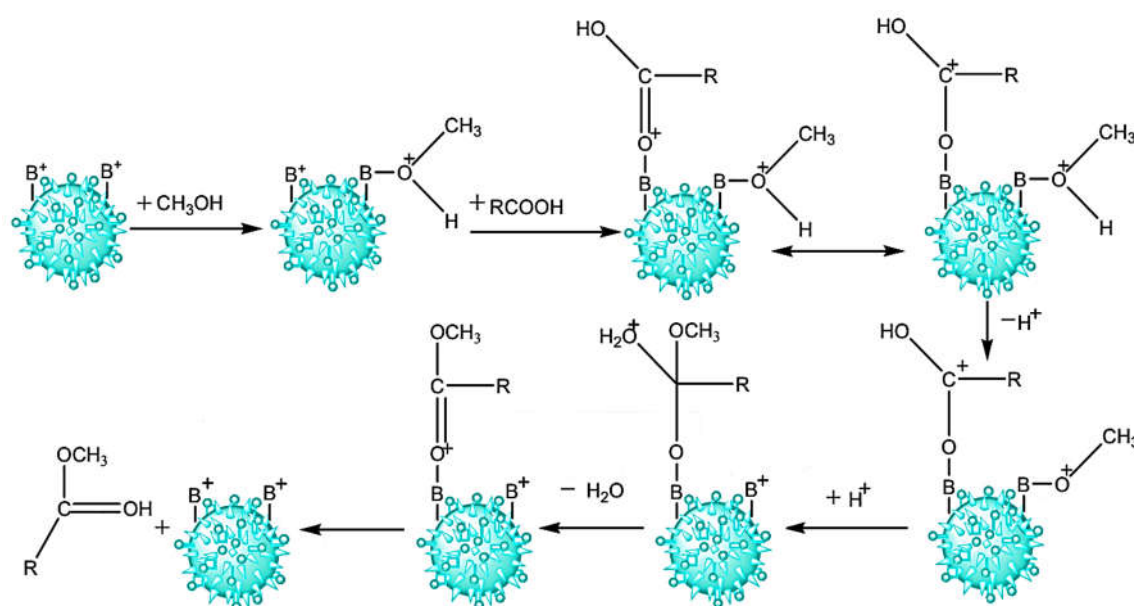


Figure 3.12: Mechanism of esterification catalyzed by mesoporous sulfonated carbon catalyst (Zeng et al. 2012)

Other factors such as acid sites and type, acid density, carbon precursor, and crystal structure all play significant roles. This plausibly explains the reason behind the slightly lower activity of sPTF/SA-300 and sPTF/SA-400 against sPTS/400 is sPTF/400 despite possessing larger surface area, S_{BET} . Another plausible explanation is that chemical equilibrium limits the extent of esterification in isolating SA in the form of esters formed

with sPTF/SA/300 (Orjuela et al. 2012). This probably disrupts the usual five-step Fischer-Speier esterification mechanism (Hernández-Montelongo et al., 2015; Aguilar-Garnica et al., 2014) in the presence of SA and -SO₃H acid catalysts. These steps include (Larock 1989):

- (a) Transfer of proton to carbonyl oxygen from acid catalyst increases the electrophilicity on carbonyl carbon.
- (b) Nucleophilic oxygen atom from the methanol attacks the carbonyl carbon.
- (c) Formation of activated complex molecule as proton transfers to the second alcohol from the oxonium ion.
- (d) A new oxonium ion formed from the protonation of a hydroxyl group within the activated complex.
- (e) Loss of water from the oxonium ion produces ester with consequent deprotonation.

To solve this problem, it is necessary to remove the product from the reacting vessel. However, the batch system employed for this study does not permit efficient product separation without further complications. Furthermore, hydroxyl groups formed during esterification and the low solubility and volatility of SA in methanol, which requires fast esterification kinetics to avoid precipitation or accumulation in the reactor, exacerbate this situation (Orjuela et al. 2011). Similarly, Yu et al. (2011) suggested a stepwise addition of alcohol with excess acid during the synthesis of polyester polyol. However, the performance of sPTF/SA/300 exceeded those without SA after regeneration. This signifies the beneficial effects of SA homogenization after elimination of many of the hydroxy groups. It also implied that both acids neither inhibit each other's rate nor compete for active sites during esterification. Again, this highlights that successful

incorporation of surface strong acid density, combined with well-ordered mesoporosity, are essential for FFA conversion.

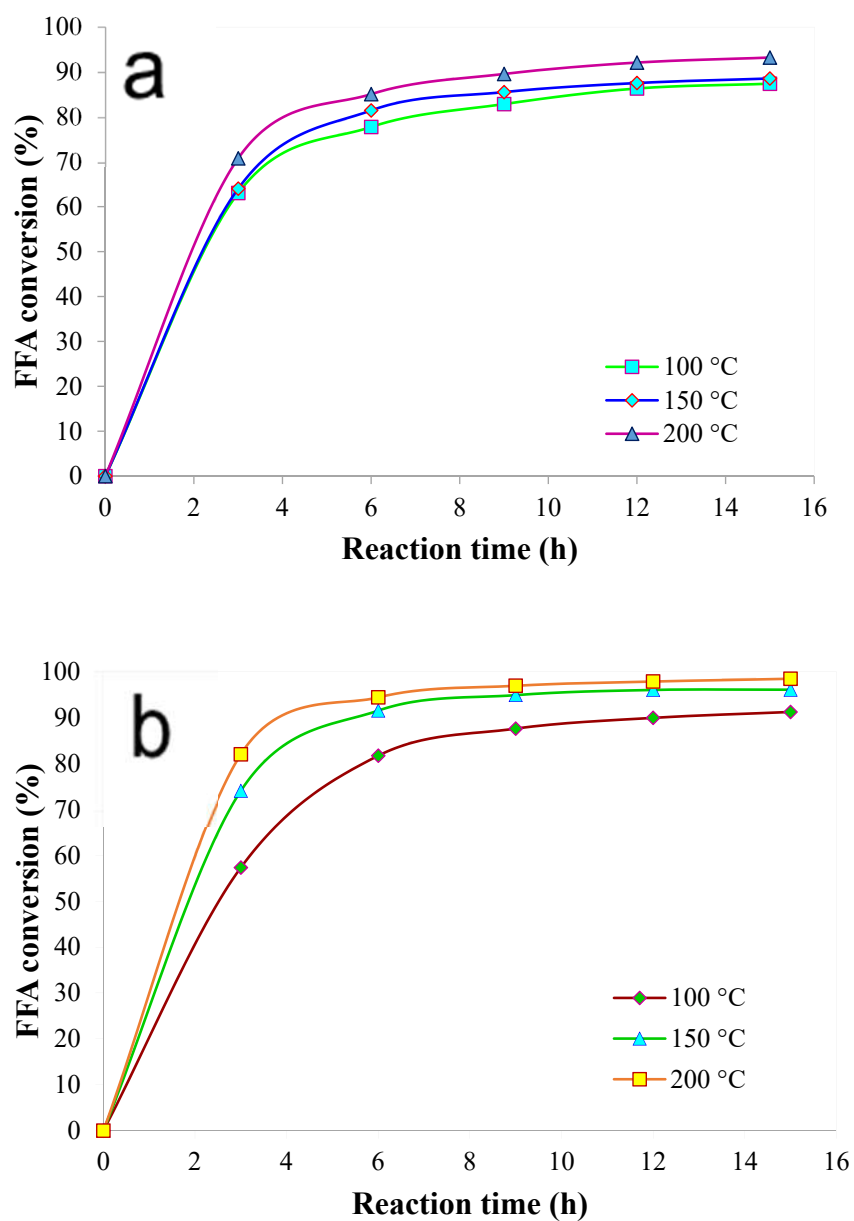


Figure 3.11: Catalytic activities of mesoporous (a) sPTF/SA/400 and (b) sPTS/400 catalysts prepared under different conditions

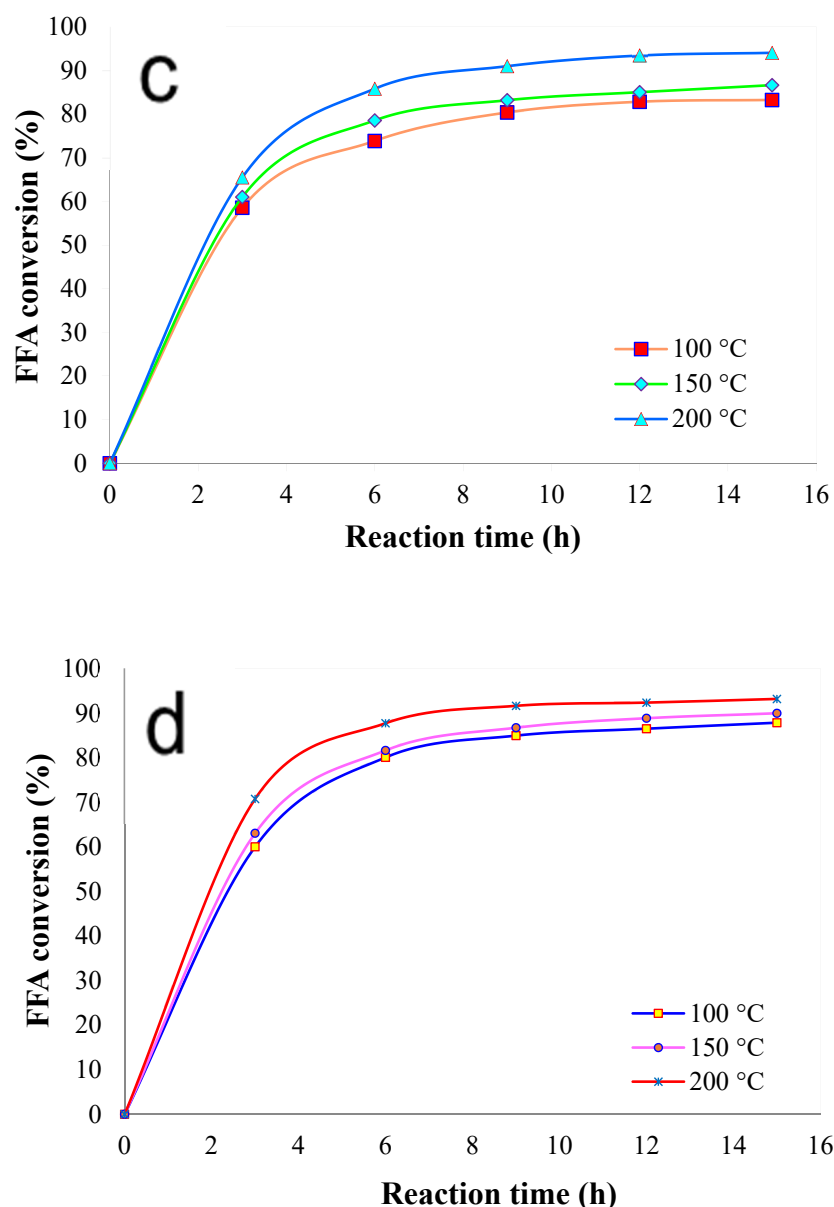


Figure 3.11(cont'd): Catalytic activities of mesoporous (c) sPTF/400, and (d) sPTF/SA/300 catalysts prepared under different conditions

Further, the catalyst retained most of its activity after 8 recycles without significant leaching of its strong (-SO₃H) groups (Figure 3.12). Evidently, incorporation of strong sulfonite groups, mesoporosity, and high stability ensured the good reusability of the synthesized catalysts. Deactivation sets in as the active sites loose the strong sulfonite groups from the material after several cycles. Simple decantation, washing, and drying regenerated the catalyst. This highlights the potential to produce alternative, environmentally benign catalysts from waste palm biomass.

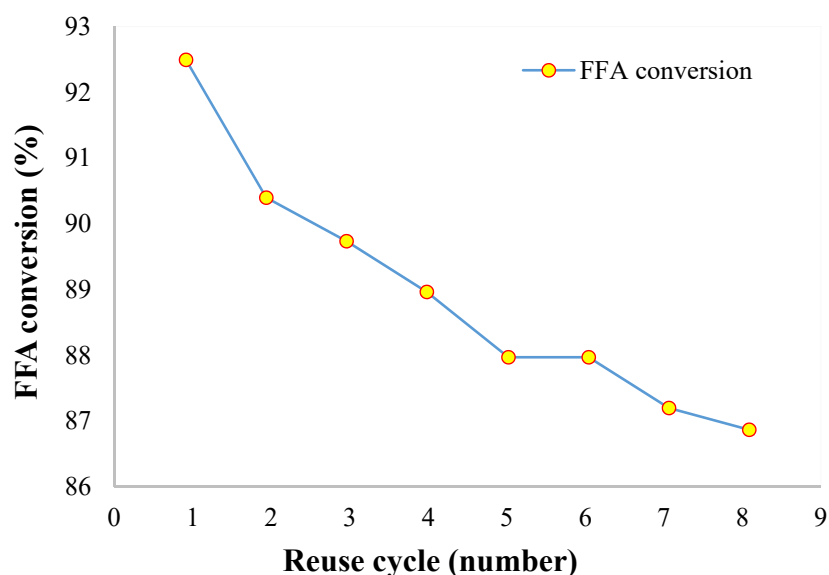


Figure 3.12: Activity of sPTS/400 after regeneration and recycling for esterification reaction

Converting feedstocks of low economic value into high yield methyl esters shows the superiority of solid acid catalyst. In this regard, the present process is economical, as it employed moderate reaction conditions such as relatively low catalyst-loading, low temperature (100 °C), and a 5:1 alcohol-to-oil ratio to convert more than 98% high FFA feedstock. Furthermore, the deluge of waste generated from palm tree cultivation and palm oil production could be easily converted into alternative catalysts, with potential wide ranges of applications in other acid-catalyzed reactions. This is interesting when compared with other carbon-bearing solid acid catalysts. For instance, Dawodu et al., (2014) synthesized catalyst from the cake of *C. inophyllum* and converted 96.6 wt% of the oil extracted therefrom, which contained 18.9 wt.% FFA. This was achieved with a 30:1 methanol-to-oil molar ratio at 180 °C for 5 h and a catalyst loading of 7.5 wt.%. Similarly, Dehkhoda et al., (2010) obtained 92% conversion from 12.25 wt.% FFA-containing feedstock with 5 wt.% sulfonated pyrolysis biochar catalyst after 3 h under 18:1 methanol-to-oil molar ratio. It is noteworthy to mention the close to 100% conversion obtained with Ph-SO₃H-modified mesoporous carbon by Geng et al. (2012)

with 66 times more methanol than oleic acid. For a comprehensive comparison on biodiesel production from palm oil, *Jatropha curcas*, and *Calophyllum inophyllum*, the reader is referred to an article by Ong et al. (2011).

3.4 Conclusions

1. Sulfonated, mesoporous carbon catalysts prepared from waste biomass from palm tree with concentrated H_2SO_4 (98%) as the sulfonating reagent converted more than 98.51% of FFA into biodiesel.
2. This study employed 400 and 150 °C carbonization and sulfonation temperatures, respectively, to avoid destroying the well-ordered mesostructure of the carbon materials, ensuring good catalytic activity by retaining high acid density on the catalysts. The catalysts in this study functioned well at the moderate process conditions of 100 °C, 5 h reaction time, 5:1 methanol-oil ratio, and 1 wt.% catalyst loading.
3. The sPTS/400 catalyst, with specific surface area 12.7037 m^2/g , average pore size 10.02 nm, mesopore volume 0.02 cm^3/g , and 1.2974 mmol/g total $-\text{SO}_3\text{H}$ acid density, exhibited the highest activity (98.51%). Further, it converted more than 90% of FFA after 8 consecutive regeneration cycles.
4. The observed high catalytic performance is attributed to the large pores, uniform pore size, good surface area, large mesopore volume, high $-\text{SO}_3\text{H}$ density, and hydrophobic surface of the sulfonated catalysts. The large mesostructure effectively accommodated the long FFA chains. In addition, the catalysts' mesostructure hinders water molecules from both the UFO feedstock and those formed during the reaction from accessing the interior of the catalysts.

The catalysts generated from palm waste biomass in this study have the potential for application as solid acid catalysis with good prospects in other related acid-catalyzed reactions.

CHAPTER 4: OIL PALM BIOMASS AS CHEAP PRECURSOR TO EFFICIENT MESOPOROUS SOLID ACID CATALYSTS FOR ESTERIFYING USED FRYING OIL CONTAINING HIGH FREE FATTY ACIDS

This chapter sets out its purpose, *viz.* the continuation of Chapter 3. It presents the study as an article, which described the superiority of sulfonated mesoporous catalysts synthesized from palm empty fruit bunches and palm waste fruits in the esterification of free fatty acids for biodiesel production compared to existing sulfonated carbons. The study is currently under consideration for publication by RSC Advances.

4.1 Introduction

High production costs accruing from cost of purchasing feedstock as well as catalyst development hamper the establishment of biodiesel as commercial alternative to petroleum diesel (Sani et al, 2013; Hassan et al., 2015). Incidentally, deluge of agricultural waste materials such as biomass, which are potential feedstock for catalyst synthesis and energy source, end up dumped in landfills at avoidable costs. A promising source of renewable energy is biomass, and it falls under the following categories: (a) agricultural residues, (b) dedicated energy crops, (c) wood residues, and (d) municipal solid wastes. Agricultural residue constitutes the third largest primary source of energy after oil and coal. Thus, developing efficient solid catalyst from low-value biomass is essential in making biodiesel production process fully ecologically friendly and economical. Malaysia being the world's second largest producer and exporter of palm oil generates deluge amount of biomass with little or no economic value from oil palm production (Sulaiman et al., 2012). These include palm trunks, mesocarp fibre (PMF), empty fruit bunches (EFB) and kernel shells (PKS) (Aziz et al., 2011; Hassan et al., 1997). Oil palm production alone generates about 85.5% of the total biomass produced from a

variety of crops, including but not limited to rubber, rice, and oil palm in Malaysia. In this regard, agricultural residues from renewable sources which are both abundant and inexpensive will come-in handy as remarkable feedstocks for fuel production and catalyst development (Prauchner and Rodríguez-Reinoso, 2012).

However, to achieve high activity, the catalyst should possess high density of well-dispersed active phase and provide channels for faster diffusion of the reactants and products (Sani et al, 2014). New heterogeneous materials based on their stable sulphonated amorphous carbon from inexpensive biomass have attracted much research interest. This recent method incorporates $\text{-SO}_3\text{H}$ into biomass carbon; thereby producing efficient alternative solid acid catalysts with good catalytic performances (Zhang et al., 2015). These materials exhibited high acidity, large pore size, and high BET area. These attributes ensure accessibility of long-chain FFA molecules and high catalytic activity. The prospects of these materials have opened new vistas for synthesizing highly active solid acid catalysts. This is premised on the benign and economic aspect of the starting materials. Expectedly, these materials provide promising opportunity for ensuring a sustainable bioenergy (Toda et al., 2005, Takagaki et al., 2006, Budarin et al., 2007, Dehkhoda et al., 2010, Maciá-Agulló et al., 2010 and Liu et al., 2013). Studies showed the prospects of effectively replacing mineral acids in several catalytic reactions with sulfonic acid functionalized porous carbons. Among the sulfonating agents reported for synthesizing these stable, reusable, and environment-friendly solid acid catalysts include H_3PO_2 , conc. H_2SO_4 , 4-benzene-diazoniumsulfonate, hydroxyethylsulfonic acid, and *p*-toluenesulfonic acid (TsOH).

Carbonization-Sulfonation method facilitates high surface area with interconnected porosity, which reduces diffusion limitation of reactants to active sites (Zhang et al., 2015). Hou et al. (2012) synthesized sulfonated ordered mesoporous carbons under acidic condition from self-assembly phenolic resol and Pluronic F127. Similarly, (Xing et al., 2007; Wang et al., 2007; Liu et al., 2008; Peng et al., 2010; Suganuma et al., 2011; Janaun and Ellis, 2011; Geng et al., 2012) employed nanocasting synthesizing sulfonated ordered mesoporous catalysts with SBA-15. Dawodu et al. (2014) produced biodiesel (96.6 wt.%) *C. inophyllum* oil with catalyst derived from its residue. Chen and Fang (2011) obtained 90% biodiesel after 12 h from waste cottonseed oil (FFA 55.2 wt.%) with glucose and corn powder (ratio 1:1) solid acid catalyst. Similarly, Poonjarernsilp et al. (2014) respectively obtained high-grade biodiesel from esterifying oleic acid and stearic acid (vegetable oil) with sugar by Toda et al. (2005) and palmitic acid with single-walled carbon nanohorns. However, limitations such as high alcohol-to-oil molar ratio from these encouraging results prompted the motivation for this study. For instance, Dawodu et al. (2014) employed a 30:1 methanol-to-oil molar ratio in synthesizing catalyst from the cake of *C. inophyllum*.

Similarly, Dehkhoda et al. (2010) utilized 18:1 methanol-to-oil molar ratio to obtained sulfonated pyrolysis biochar catalyst. It is also noteworthy to mention the close to 100% conversion obtained with Ph-SO₃H-modified mesoporous carbon by Geng et al. (2012) with 66 times more methanol than oleic acid. Recently, we reported the catalytic performance *via* preliminary characterization of palm fronds and spikelets for biodiesel production from feedstock containing higher fatty acids (Sani et al., 2015). To the best of knowledge, aside this preliminary report, no study reported in detail, the valorization of low quality waste frying oils into biodiesel with solid acid catalysts derived from palm tree wastes. Consequently, the present study illustrated prospects of converting

inexpensive palm biomass wastes into highly efficient, benign, and recyclable solid acid catalysts for producing biodiesel under moderate conditions such as 5:1 methanol-to-oil molar ratio. This was achieved by investigating the effect of carbonizing and sulfonating empty fruit bunches (EFB) and waste palm fruit (WPF) in esterifying FFA into FAME.

4.2 Literature review

Despite the importance of solid acid catalysts in cracking processes and fine chemicals production, and their employment in about 180 industrial processes (Misono, and Nojiri, 1990; Armor, 1991 and 2001), conventional acids such as AlCl_3 and H_2SO_4 are still employed for numerous acid-catalyzed reactions, such as esterification, hydrolysis, hydration, and Friedel–Crafts reactions (Tanabe & Hölderich, 1999). However, problems such as large amounts of catalyst requirement, separation and recovery difficulty, catalyst waste, corrosion, high toxicity, costs and environmental concerns associated with conventional acids made the search for alternatives imperative (Sani et al., 2015). Incidentally, solid acids are replacement of these liquid acids because they are easily separated, recovered and regenerated, environmentally friendly with respect to safety and corrosiveness. Further, industrial processes in the chemical industry generate less waste with solid acids. Nonetheless, to meet the desired challenge of substituting fossil fuels, advances are required in enhancing the acidity, activity, and durability of solid acid catalysts. This is especially true considering the problem of the high cost of feedstock.

Several approaches such as replacing refined vegetable oil with refurbished oils and fats, used frying oil, and animal fats which contains varying amount of FFAs from 3 to 50% addressed the high cost of feedstock. This is because high FFA-containing feedstocks are readily available, inexpensive, and are obtained from renewable resources. These highlight the promising potentials of such feedstocks for biodiesel production. Moreover,

traditional homogeneous base catalysts are not suitable for transesterification when the amount of FFA in the feedstock exceeds 0.5%. This is because saponification reaction consumes the alkaline catalyst and FFA raw material. The significance of solid acid catalyst lies majorly in resolving this particular problem because of its insensitivity to FFA.

Another strategy currently gaining prominence is the synthesis of solid acid catalysts from wastes and low-value biomass such as corn straw, vegetable oil asphalt, starch, glucose, naphthalene and other carbon-bearing materials *via* incomplete carbonization-sulfonation procedure (Lou et al., 2008). Hou et al. (2012) synthesized sulfonated ordered mesoporous carbons under acidic condition from self-assembly phenolic resol and Pluronic F127. Similarly, (Maciá-Agulló, et al., 2010, Peng, et al.s, 2010, Poonjarernsilp, et al., 2014, Prauchner and Rodríguez-Reinoso, 2012, Rabumi, 1998, Sani, et al., 2013 and 2014) employed carbonization-sulfonation method in synthesizing sulfonated ordered mesoporous catalysts. Dawodu et al. (2014) produced biodiesel (96.6 wt.%) from oil extracted from *C. inophyllum* with catalyst derived from its residue.

Similarly, the preparation and activity studies of amorphous carbon with sulfonic ($-\text{SO}_3\text{H}$) groups as a solid Brønsted acid catalyst by Nakajima and Hara (2012). The small polycyclic aromatic carbon sheets of the catalyst were covalently bonded to the sulfonite ($-\text{SO}_3\text{H}$) groups. The sulfonite groups ensured efficient esterification of high FFA feedstocks while the carbon rings provided strength and stable structure to the insoluble solid acid material. Interestingly, such catalysts remained active even after more than 50 cycles (Zong, et al., 2007) after regeneration. This evidenced the highly stable structure of carbon-derived solid acid catalysts. Furthermore, aside having no toxicity or corrosion

effect and low cost of preparation, the catalysts exhibited strong acid site density, high hydrophobic surface area, and large pores (Lotero, et al., 2005).

4.3 Materials and methods

4.3.1 Preparation of mesoporous carbon catalysts from palm empty palm fruit bunches (EFB) and waste palm fruits (WPF)

The oil palm residues obtained from Sime Darby Plantation in Malaysia, initially dried at room temperature for one week. The steady moisture loss was measured using the oven-dry basis mass, OD (Eq. 4.1) before oven drying at 120 °C for 24 h followed by milling and sieving (mesh size: 0.5 mm). The catalysts were prepared following a modified procedure (Toda et al., 2005 and Dawodu et al., 2014). Heating the dried powder in tubular furnace at 300 °C and 400 °C, 2 °C/min for 12 h under N₂ produced incomplete carbonized material. This facilitated the formation of polycyclic aromatic carbon rings on the cellulosic palm residues. The brown-black solid (20 g) was heated in 200 cm³ conc. H₂SO₄ (98%) at 150 °C. This acid treatment incorporates sulphonite groups (-SO₃H) into mesopores of the carbon material. After heating for 10 h, and cooling to room temperature, 1000 cm³ distilled water was added to form a black precipitate. To ensure the absence of impurities and sulfate ions, the precipitate was washed with hot (> 80 °C) distilled water. The resulting product was oven dried at 100 °C for 5 h. To ensure reproducibility, all the catalysts were prepared in replicates. The sulfonated palm empty fruit bunch (EFB) and waste palm fruit (WPF) were designated sEFB/T and sWPF/T, respectively; where T stands for carbonization temperature (300 or 400 °C). To compare the activity of the materials, different esterification reaction conditions were investigated.

$$\text{Moisture content (\%; OD basis)} = \frac{\text{weight of water}}{\text{dry weight of wood}} \times 100 \quad (\text{Eq. 4.1})$$

4.3.2 Catalyst characterizations

A FEI QUANTA™ 450 FEG type 2033/14 (Czech Republic) unit with 30 kV accelerating voltage was used for field emission scanning electron microscopy (FE-SEM) to analyze the surface morphology and topology of the catalysts. An energy dispersive X-ray spectrometer (EDX) from the same unit revealed the surface elemental composition of the catalysts. Further, X-ray diffraction (XRD) and BET analyses were used to determine the structural and textural properties of the catalysts. The XRD patterns were analyzed with a Phillips X'pert diffractometer (The Netherlands) using $\text{CuK}\alpha$ radiation ($\lambda = 1.54056 \text{ \AA}$) at a scanning speed of $0.05^\circ/\text{s}$ within a 2θ range of 5 to 70° at 40 mA and 40 kV . Micromeritics TriStar II (USA) with accelerated surface area porosity (ASAP)-3020 at minus 196.15°C was used to determine the specific surface area of the catalytic materials using liquid nitrogen. Degassing the catalysts at 120°C for 3 h under a vacuum eliminated any physisorbed volatiles and impurities. Rapid [scan speed of 20 spectra/sec (8 cm^{-1} resolutions, expandable to 100 spectra/sec , with 16 computer selectable mirror velocities between 0.055 and 10 cm/sec , 16-bit-200kHz)] identification and quantification of the catalysts was performed with a Bruker Fourier transform infrared (FT-IR) IFS 66/S (Germany) equipped with OPUS/IR software for data acquisition and manipulation. The apparatus has a spectral range of 7500 to 370 cm^{-1} (standard) with more than 0.25 cm^{-1} apodized resolution and a Ge multilayer coating on KBr beam splitter.

4.3.3 Acid density analysis

Exchanging Na^+ with H^+ in the form of $-\text{SO}_3\text{H}$ by mixing 0.1 g of sulfonated material with 30 mL of 0.6-M NaCl solution for 2 h facilitated determination of the acid strength of the catalysts. The filtrate from this mixture was titrated with 0.1001 M NaOH standard solution and methyl orange indicator to indicate the consumption of NaOH . A change

from slightly red to bright yellow maintained for 30 s defines the endpoint. A blank titration determined the initial, unconsumed volume of the NaOH standard solution. Equation 4.2 was used to accurately calculate the strong acid (-SO₃H) density.

$$D_{-SO_3H} = \frac{C_{OH^-} \times [V_1 - V_0]}{m_{cat.}} \quad (4.2)$$

The strong acid (-SO₃H) density of the catalyst (in mmol/g) and the concentration of standard NaOH solution are represented by D_{-SO_3H} and C_{OH^-} , respectively. The volume of NaOH standard solution consumed during the blank and catalyst titrations are represented by V_0 and V_1 , respectively; m_{cat} represents the mass of catalyst used for the acid density analysis.

4.3.4 Production of free fatty methyl esters from FFA-containing feedstock

The catalysts were heated at 150 °C for 1 h before the reaction to evacuate adsorbed water and other volatiles. Methanol, with the aid of the catalyst, was used to transesterify used frying oil (UFO) at 100 to 200 °C in a 100 mL autoclave (250 °C, 100 bar) reactor supplied by AmAr Equipment Pvt., Ltd. (Mumbai). Constant stirring ensured contact between the catalyst and the reaction mixture. A constant-flow water bath attached to the autoclave maintained the temperature during the reaction. Preliminary optimization showed that a 5:1 methanol-to-oil molar ratio and 1 wt.% catalyst loading are optimal reaction conditions. Simple decanting recovered the FAME at the end of the 3 to 15 h reaction. Drying, methanol washing, and heating at 120 °C for 1 h regenerated the catalyst. The catalyst retained its activity after regeneration for up to 8 recycles.

4.3.5. Determination of acid value

The oil's acid value was determined by titration analysis according to DIN EN ISO 660 (2009). The expected acid value of used frying oil is between 15 and 75 mg KOH/g. The titrant (0.1 M KOH), neutralizes the solvent mixture comprised of 50 mL of ethanol-diethyl ether (1:1 ratio, v/v) mixed with 0.5 g of catalyst sample. Equations 4.3, 4.4, and 4.5 were used to calculate the titre value, acid value, and FFA conversion, respectively.

$$\text{Titre value} = \frac{m_s}{V_{EP_1} \times c(KOH) \times M_A} \quad (4.3)$$

$$\text{Acid value} = \frac{V_{EP_1} \times f \times c(KOH) \times M_A}{m_s} \quad (4.4)$$

$$\text{FFA conversion, \%} = \frac{V_{EP_1} \times f \times c(KOH) \times M_A}{10 \times m_s} \quad (4.5)$$

where V_{EP_1} represents the titrant consumed at end of the first equivalent point in mL, $c(KOH)$ represents the concentration of KOH titrant (0.1 M), M_A represents the molecular weight of the analyte (112.12 g/mol), f represents the correction factor obtained from the titre value, M_A represents the molecular weight of palmitic acid (256 g/mol), and m_s represents the sample size in g.

4.4 Results and discussion

4.4.1 Characterization of palm biomass and catalysts

Proximate analysis of oil palm (*Elaeis guineensis*) biomass by Aziz et al. (2011) revealed the composition as carbon (45-50%), oxygen (43-48%), hydrogen (5%), nitrogen (0.5%) and sulfur (0.4%). The petiole consists of about 70% of the dry matter in the palm fronds, while the leaves and rachis make up the remaining percentage. The dry matter content of palm fronds is about 31% (Ishida and Abu Hassan, 1992). Depending on age, palm fronds contain *ca.* 15 to 26% hemicellulose. It also contains 4.7 MJ/kg crude proteins, 38.5

MJ/kg crude fibre, 2.1 MJ/kg ether extract, 78.7 MJ/kg neutral-detergent fibre, and 3.2 MJ/kg ash (Wong and Wan Zahari, 1997; Wan Zahari and Mohd Ariff, 2000). Similarly, Rabumi (1998) reported 70.9 to 90.1 C/N ratio, 25.0 to 29.9% lignin, 16.2 to 21.3% cellulose, and 1.52 to 2.46% soluble polyphenols, as the chemical composition of spikelets.

A previous report by Chen et al. (2010) identified 2θ peaks ranging from 22° to 23° as the major diffraction peaks for cellulose crystallography. Figure 4.1 shows XRD patterns for sEFB/400 and sWPF/400. The figure displayed one broad XRD peak at 2θ value of 25.33° and 25.20° with d values calculated from Bragg equations as 3.51 and 3.53 Å for the 2 materials respectively. The lower reflection intensities exhibited by the materials highlights the amount of amorphous impurities contained in them. However, XRD pattern for sWPF/400 revealed other peaks absent from sEFB/400 at 2θ values of 10, 18, 21, and 30. These peaks are indicative of low crystallinity from the palm kernel shell. This agrees to Liu et al. (2012) who posited the prominent I_{002} peak with the maximum intensity of 002-lattice diffraction as the primary as well as crystalline. The broad nature of the peak is reflective of the cellulosic molecular hydrogen bond transformation during heat treatment. However, the low crystallinity indicated the presence of larger amounts of amorphous cellulose in the catalytic materials (Kuo and Lee, 2009). However, the general absence of crystallinity indicates the affinity for anchoring $-\text{SO}_3\text{H}$ groups.

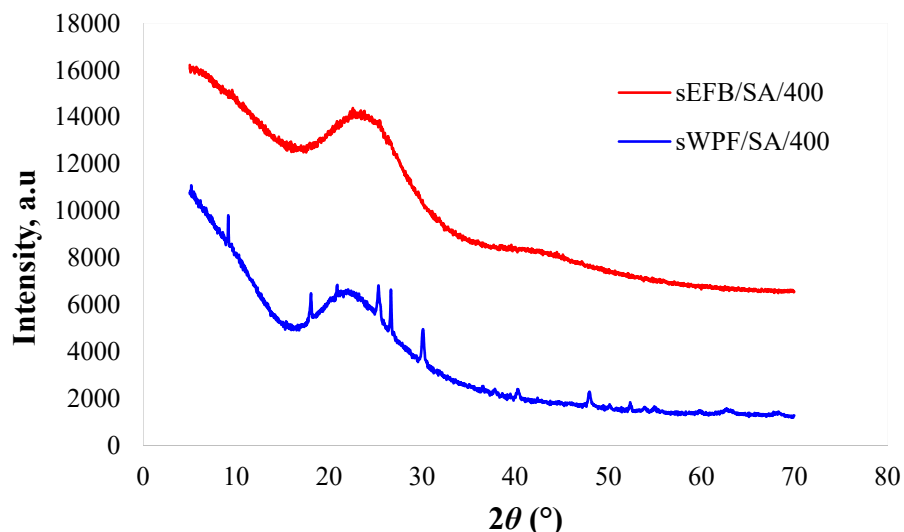


Figure 4.1: XRD pattern of sEFB/400 and sWPF/400.

Certainly, from the representation on Fig. 4.1 and Table 4.1, one may recognize the correlation between the catalytic performance of the synthesized materials and their crystal structures. sEFB/400 exhibited no spikes, but had S_{BET} of 236.37 m²/g. However, sWPF/400 exhibited spike at 2θ value of 25.20° and a d -spacing of 3.53 Å, which falls within the range reported for cellulose crystallography by Chen et al. (2010). However, the S_{BET} , 28 m²/g of the material was comparatively lower than that of sEFB/400. Consequently, despite the observed crystallinity, the total surface area available for acid (-SO₃H) groups is limited. Evidently, this will affect the overall catalytic performance.

The N₂ adsorption results presented in Table 4.1 and Figure 4.2 further confirmed the presence of mesopores on the prepared catalytic materials, which are consistent with aromatic sheets of amorphous carbon orientation. The clear nitrogen condensation steps highlighted in Figure 4.2 evidenced this. Further, the figure shows the N₂ adsorption-desorption isotherm and pore size distribution curves of mesoporous carbon obtained at 300 and 400 °C carbonization temperatures. The pore-size distribution curves of the two materials show similar shapes with high pore size uniformity with a uniform pore diameter centered at about 17.8 nm. The large mesopores are advantageous because they

minimize diffusion limitation and facilitate easier access to the reacting molecules to the active sites within the materials. Additionally, the large mesopores enhance the stability of the ordered mesoporous carbon framework (Zhang et al., 2015). Expectedly, because of the higher temperature employed, sEFB/400 exhibited lower S_{BET} and amount of sulfonate groups ($236.37 \text{ m}^2/\text{g}$; 1.8579 mmol/g) than sEFB/300 (2.3373 mmol/g ; $246.46 \text{ m}^2/\text{g}$). Similarly, Figure 4.2 shows the comparatively much lower BET surface area exhibited by the catalyst synthesized from the waste palm fruits, sWPF/400 against sEFB/400. This is probably because of the homogenization of the different constituents such as mesocarp fibre, kernel, and kernel shell. These noticeable peaks confirmed the presence of crystallinity within the amorphous structure of the cellulosic constituents. Further, FE-SEM analysis revealed large pores, sharp edges, and agglomeration on surface of the catalysts.

The adsorption isotherms of all the samples followed the type-IV IUPAC classification for mesoporous materials with capillary condensation taking place at higher pressures of adsorbate depicting a hysteresis loop (Sing et al., 1985). At higher pressures, the slope showed increased uptake of adsorbate as gas fills the pores, with the inflection point typically occurring near completion of the first monolayer. The H_4 -type hysteresis loop fit well to the inkbottle pores expected for the voids between the materials. At lower pressures, an adsorbate monolayer formed on the pore surface, which leads to a multilayer formation. However, it is interesting to note that mesoporosity alone did not determine the extent of catalytic activity or turnover. Other factors, such as acid sites and type, acid density, carbon precursor and crystal structure, all played significant roles. Titrimetric, surficial and structural analysis (Table 4.1, Figures 4.2 and 4.3) revealed high strong acid ($-\text{SO}_3\text{H}$) densities and amorphous carbon sheets bearing carboxyl ($-\text{COOH}$) and hydroxyl ($-\text{OH}$) groups. Interestingly, even at boiling temperatures of water, methanol, oleic acid,

benzene, and hexane, the mesoporous carbon catalysts remained insoluble as observed by (Toda et al., 2005).

Table 4.1: Surface properties and total acid density (-SO₃H) of the tested catalysts

Catalyst	Surface area (m ² /g)	Pore size (nm)	Pore volume (cm ³ /g)	Total acid (-SO ₃ H) density (mmol/g)
sEFB/400	236.37	4.1511	0.113332	1.8579
sEFB/300	246.46	4.1835	0.115955	2.3373
sWPF/400	28.11	10.0893	0.033078	1.5460

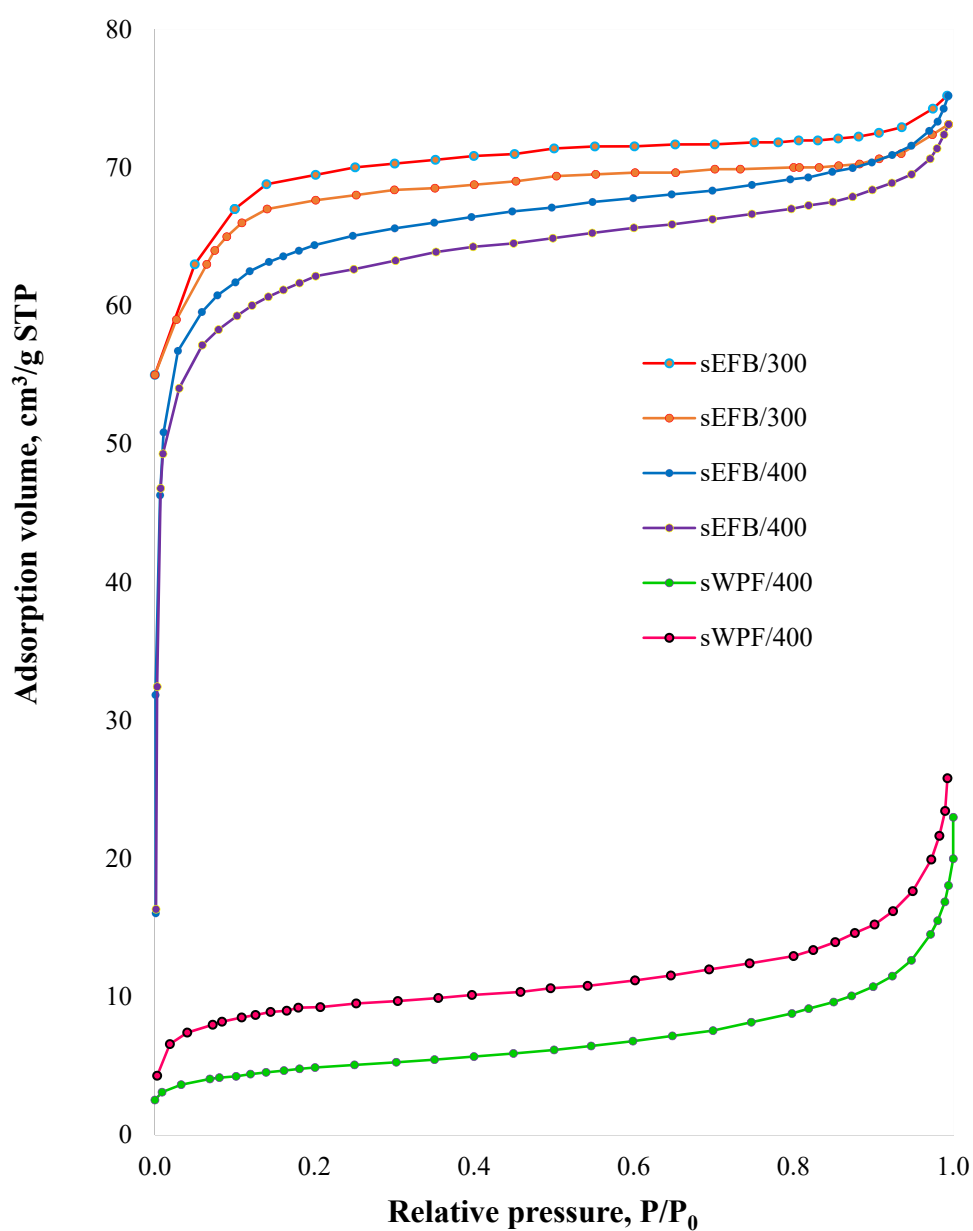


Figure 4.2: N₂ adsorption–desorption isotherms for sEFB/300, sEFB/400 and sWPF/400

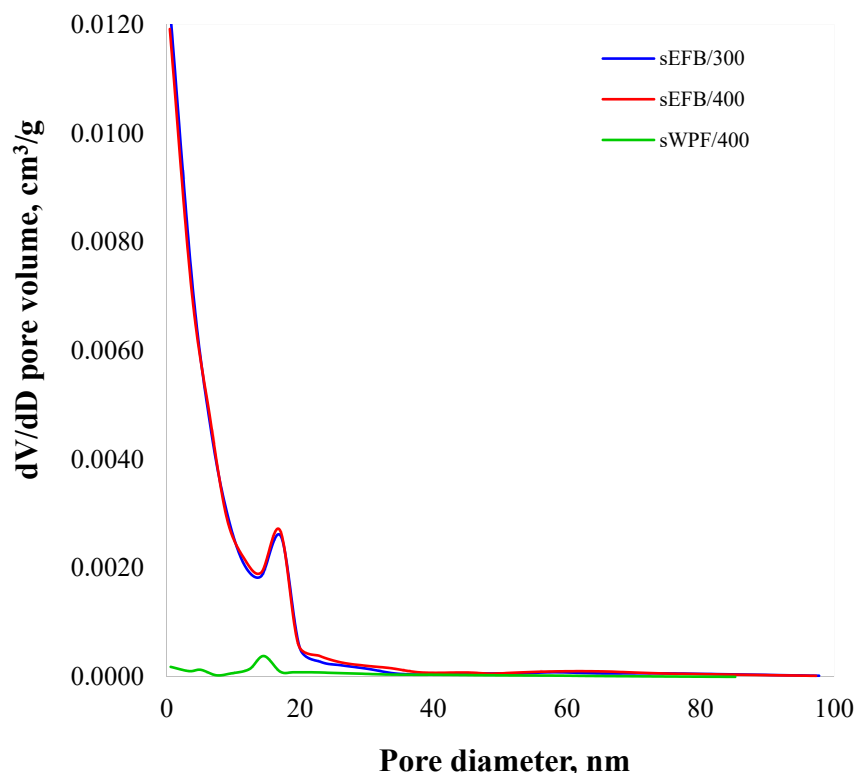


Figure 4.3: Pore size distribution curves for sEFB/300, sEFB/400 and sWPF/400

Figure 4.4a presents the FE-SEM analysis highlighting the surface microstructure of sulfonated sEFB/400 carbon catalyst. The different constituents appeared homogeneously processed into solid particles of varying dimensions. The figure also shows the presence of large uniform mesopore longitudinally along the fibre. The surficial elemental composition by EDX analysis confirmed earlier reports by revealing the presence of carbon, oxygen, and sulfur (Figure 4.4b; Appendix A).

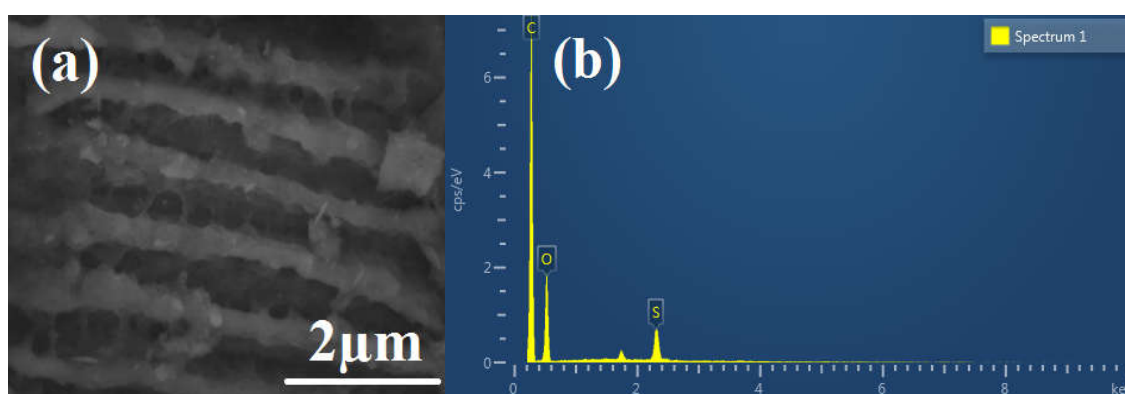


Figure 4.4: (a) Results of the surface microstructural analysis of the sEFB/400 *via* FE-SEM, and (b) surficial elemental composition of the sEFB/400 *via* EDX analysis

Similarly, Figure 4.5(a) presents the surface microstructure (size and shape of topographic features) of sulfonated sEFB/300 carbon catalyst studied using FE-SEM. The surface morphology appeared heterogeneously processed into solid particles. Further, hexagonal large mesopores appear intact compared to sEFB/400 indicating the preference of milder carbonization temperature. However, the presence of carbon, oxygen (Appendix A), and sulfur revealed surficial elemental composition by EDX analysis (Figure 4.5b) are similar to that of sEFB/400.

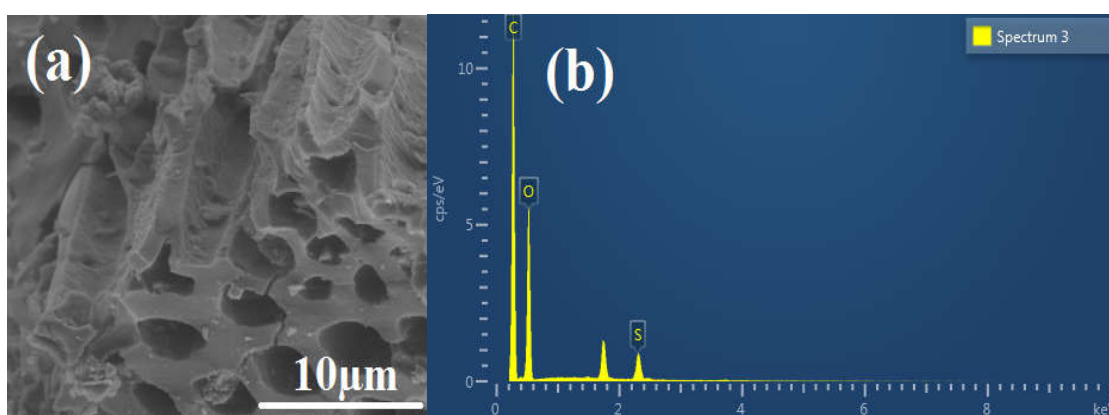


Figure 4.5: (a) Results of the surface microstructural analysis of the sEFB/300 *via* SEM, and (b) surficial elemental composition of the sEFB/300 *via* EDX analysis

Figure 4.6(a) presents the surface microstructure (size and shape of topographic features) of sulfonated sWPF/400 carbon catalyst studied using FE-SEM. High carbonization temperature opened the pore structure of the carbon material. However, the presence of large pores and sharp edges were not evident from the FE-SEM analysis. The analysis only revealed agglomerated amorphous solid with almost uniform protrusions on the catalyst surface. Figure 4.6(b) presents a cross-sectional surficial composition and distribution of elements on sWPF/400 by EDX analysis. The result also revealed the presence of carbon, oxygen, (Appendix A), and sulfur.

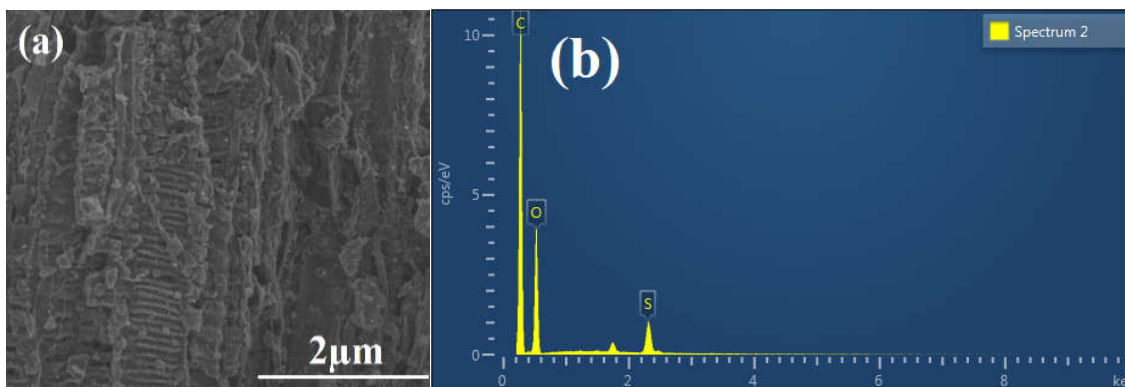


Figure 4.6: (a) Results of the surface microstructural analysis of the sWPF/400 *via* SEM and (b) surficial elemental composition of the sWPF/400 *via* EDX analysis

The process of sulfonation produces stable solids with strong acid density constituting high active sites on the cellulosic materials. This opens a vista for synthesizing highly active catalytic materials from waste biomass with little or no economic value and inexpensive naturally occurring molecules. For comparison, Figure 4.7 shows the FT-IR spectra of unsulfonated palm tree empty fruit bunch and sulfonated catalysts evaluated for this study and our previous report. The spectra revealed successful incorporation of $\text{-SO}_3\text{H}$ groups on the mesoporous catalysts *via* sulfonation. This is evident from the FT-IR spectrum bands stretching mode at 1040 cm^{-1} .

The observed S=O bond represented by the 1080 cm^{-1} spectra appears asymmetric while the vibration attributed to symmetric S=O is absent from the unsulfonated material. This confirms the presence of sulphonite ($\text{-SO}_3\text{H}$) groups on the sulfonated catalysts. Further, the symmetric O=S=O bonds were revealed by the FT-IR spectra from vibration band at 1031 and 1162 cm^{-1} while those of -OH bond at 2924 and 2855 cm^{-1} stretch respectively. On the other hand, the assigned O-H stretching mode of phenolic OH and -COOH groups to the node stretch at 3440 cm^{-1} . Correspondingly, C=O bonds due to -COO- and -COOH groups stretching vibrations are assigned to the node stretching at 1693 cm^{-1} .

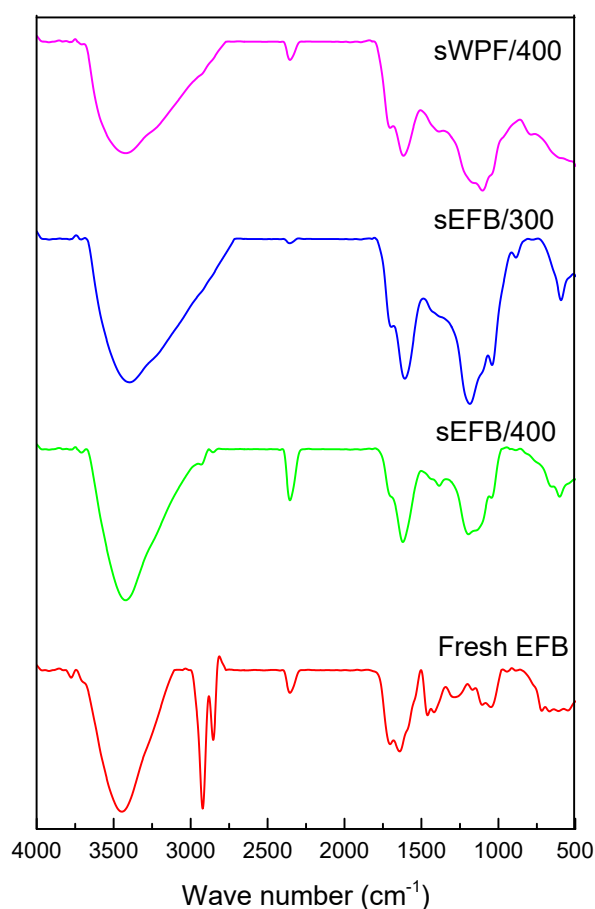


Figure 4.7: FT-IR spectra for sWPF/300, sEFB/300, sEFB/400 mesoporous carbon catalysts, and unsulfonated EFB.

The broad and intense bands centered at 1610 cm^{-1} are representative of the aromatic C=C stretching mode similar to graphite-like polyaromatic materials. Evidently, carbonization temperature affects the structure of the mesoporous material and the subsequent $\text{-SO}_3\text{H}$ incorporation. This is because relatively high carbonization temperature dehydrogenates and graphitizes mesoporous carbon skeleton. The disappearance of C-H peaks stretching at 670 cm^{-1} and $700\text{ to }900\text{ cm}^{-1}$ ascribed to polycyclic aromatic and aromatic hydrocarbons respectively evidenced this. This means that low carbonization temperature is preferable for synthesizing sulfonated carbon catalysts rich in C-H. This is manifest from the difference in $\text{-SO}_3\text{H}$ incorporated on sEFB/400 (1.8579 mmol/g) and sEFB/300 (2.3373 mmol/g) and the gradual disappearance of C-H stretching.

4.4.2 Catalytic performance of the catalysts in esterifying feedstock containing high FFA

The acidic function of the catalysts synthesized from palm empty fruit bunch and waste (whole) fruit were evaluated in esterifying UFO with methanol. Reaction conditions employed by the study were 5:1 methanol-to-oil molar ratio, 1 wt.% catalyst loading within a temperature range of 100 to 200°C. All the sulphonated solid acid catalysts exhibited mesoporosity and high activity comparable to conventional solid acid catalysts. The UFO feedstock containing 48% FFA obtained from household in Malaysia was converted to more than 98% FAMEs. Figures 4.8(a) to (c) present the catalytic activity of the sulfonated solid acid catalysts investigated at different conditions. A similar trend is observed for all the reactions with equilibrium setting in after 3 h reaction time. It is instructive to note that all the catalysts except sEFB/300 achieved more than 60% conversion. This is encouraging considering the 3 h reaction time and low alcohol molar ratio. A study by Zhang et al. (2015) employed a molar ratio of 18:1 but at lower temperature than the present report.

Mesoporous sEFB/300 displayed the highest catalytic activity by catalyzing a 98.72% FAME conversion. The catalyst showed the fastest rate in esterification reaction from the materials investigated. This is plausibly because the material possessed the strongest total -SO₃H acid density of 2.3373 mmol/g. Further, the catalyst exhibited the highest surface area (246 m²/g), pore volume and pore size (4.1835 nm). Similarly, sEFB/400 exhibited high catalytic activity though not as high as sEFB/300. This is evident from the slightly lower total -SO₃H acid density of 1.8579 mmol/g and surface area (236 m²/g). However, sEFB/400 was carbonized at a higher temperature. This is probably the reason for the lower activity. It is therefore logical to state that milder carbonization temperature is more

effective than carbonizing at higher temperatures in producing efficient solid acids from biomass.

Interestingly, sWPF/400 also displayed high catalytic activity by producing 94.32% conversion despite its low surface area ($28 \text{ m}^2/\text{g}$). Intriguingly however, the pore size of sWPF/400 (10.0893 nm) is twice that of sEFB/300 (4.1835 nm) and sEFB/400 (4.1511). Furthermore, sWPF/400 showed comparative total $-\text{SO}_3\text{H}$ acid density of 1.5460 mmol/g . Again, this highlights that successful incorporation of surface strong acid density combined with well-ordered mesoporosity are essential for FFA conversion.

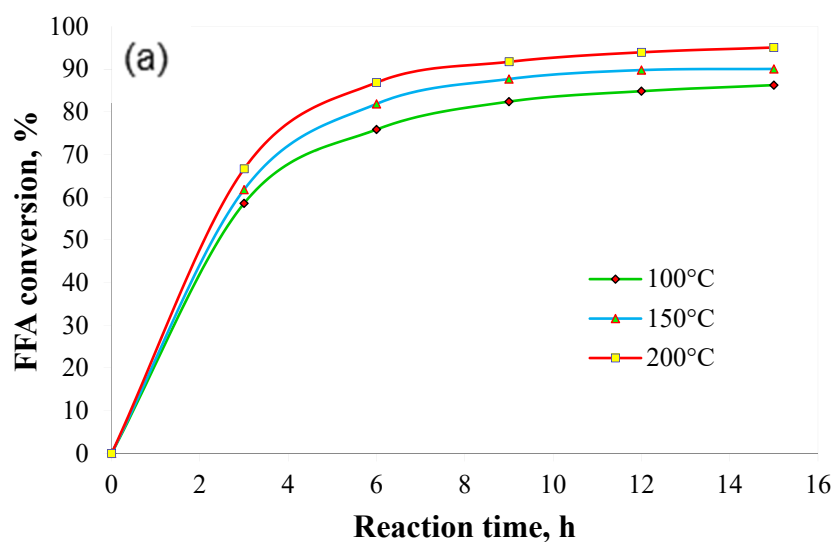


Figure 4.7(a): Comparative catalytic activity of mesoporous sEFB/400 under different reaction conditions

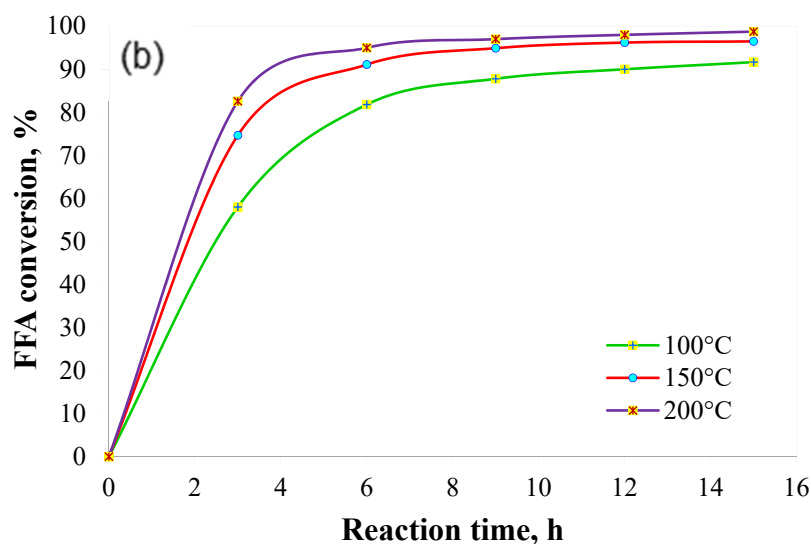


Figure 4.7 Cont'd: (b) Comparative catalytic activity of mesoporous sEFB/300 catalysts under different reaction conditions

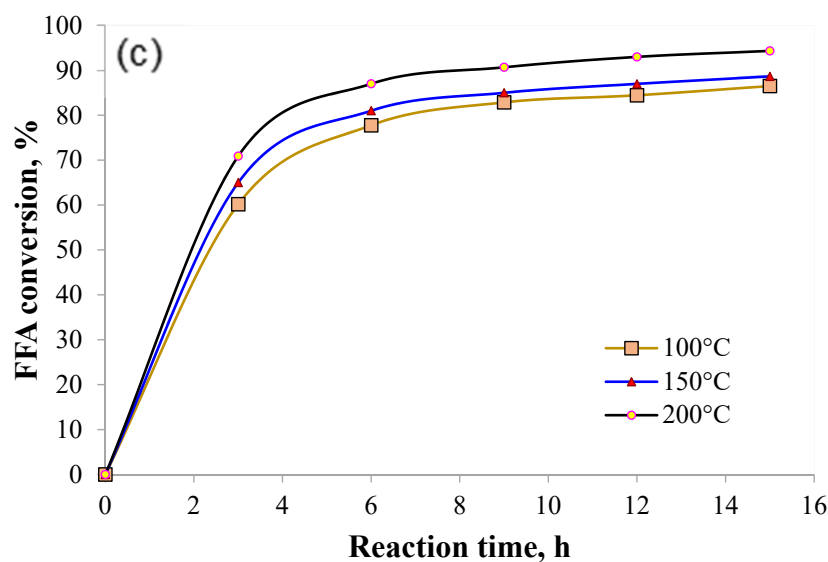


Figure 4.7 Cont'd: (c) Comparative catalytic activity of mesoporous sWPF/SA/400 catalysts prepared under different conditions.

Further, the catalyst retained most of its activity after 8 recycles without significant leaching of its strong ($-\text{SO}_3\text{H}$) groups (Fig. 4.8). Evidently, incorporation of strong sulfonite groups, mesoporosity, and high stability ensured the good reusability of the synthesized catalysts. Deactivation sets in as the active sites loose the strong sulfonite groups from the material after several cycles. Simple decantation, washing, and drying

regenerated the catalyst. This highlights the potential to produce alternative, environmentally benign catalysts from waste palm biomass.

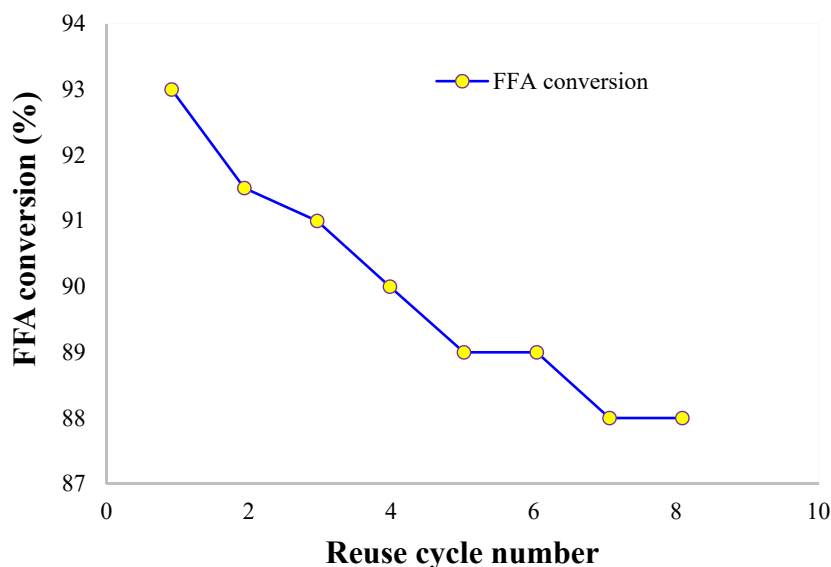


Figure 4.8: Activity of sEFB/300 after regeneration and recycling for esterification reaction

Consequently, this study highlights the prospects of producing efficient and environmentally benign alternative catalysts from waste palm biomass. Further, lower reaction conditions such as 1% catalyst loading, 100 °C, and 5:1 alcohol-to-oil ratio indicate the economic potential of the process. Converting feedstocks of low economic value into high yield methyl esters shows the superiority of solid acid catalyst. Furthermore, the deluge of waste generated from palm tree cultivation and palm oil production could be easily converted into alternative catalysts, with potential wide ranges of applications in other acid-catalyzed reactions. This is interesting when compared with other carbon-bearing solid acid catalysts. For instance, Dawodu et al. (2014), synthesized catalyst from the cake of *C. inophyllum* and converted 96.6 wt% of the oil extracted therefrom, which contained 18.9 wt.% FFA. This was achieved with a 30:1 methanol-to-oil molar ratio at 180 °C for 5 h and a catalyst loading of 7.5 wt.%. Similarly, Dehkhoda et al. (2010), obtained 92% conversion from 12.25 wt.% FFA-containing feedstock with 5 wt.% sulfonated pyrolysis biochar catalyst after 3 h under 18:1 methanol-to-oil molar

ratio. It is noteworthy to mention the close to 100% conversion obtained with Ph-SO₃H-modified mesoporous carbon by Geng et al. (2012), with 66 times more methanol than oleic acid. Additionally, the process is “green” because it has potential of converting the deluge of waste generated from cultivating palm trees and the subsequent palm oil production, as well as UFO. The mesoporous catalyst also has the possibility of wider applications in other acid-catalyzed reactions.

4.6 Conclusions

The interesting implication of the study is the interrelationship between sustainable development and environmental concerns ways of alleviating the barriers to economic competitiveness of biodiesel by utilizing cheaper resources. Catalysts synthesized from waste biomass showed promising results in the application of solid acid catalysis with good prospects in other acid-catalyzed reactions. In spite of transforming wastes into wealth especially in regional sustainable development, the following specific conclusions could be drawn from the synthesis and application of a new family of mesoporous carbon catalysts developed *via* simple carbonization-sulfonation process.

1. Carbonization temperature determines the strength of the sulphonite groups (-SO₃H) incorporated onto the carbon material. Moderate carbonization temperature (300 °C) is preferable because higher temperature affects the well-ordered mesostructure of the carbon.
2. It is instructive to highlight low process parameters such as 1 wt.% catalyst loading, 3 h reaction time, 100 °C and 5:1 methanol-oil molar ratio employed by the study against similar results by other authors. For instance, [8] employed 18:1 methanol-oil molar ratio to obtain ca. 80% conversion after 3 h.

3. The highest activity of 98.72% conversion was exhibited by sEFB/300 with specific surface area of 246.4616 m²/g, average pore size of 4.1835 nm, mesopore volume of 0.12 cm³/g and 2.3373 mmol/g total -SO₃H acid density. Further, it converted more than 90% FFA after regenerating for 8 consecutive cycles. The observed high catalytic performance is attributed to the large and uniform pore size, high surface area, large mesopore volume, high -SO₃H density and hydrophobic surface of sulfonated catalyst. The large mesostructure effectively accommodated the long FFA chains. Additionally, the mesostructure of the catalysts hindered any water molecules from the UFO feedstock or formed in the course of reaction from accessing the active sites. The catalyst from waste biomass is promising in the application of solid acid catalysis with good prospects in other acid-catalyzed reactions.

CHAPTER 5: ACIDITY AND CATALYTIC PERFORMANCE OF Yb-DOPED $\text{SO}_4^{2-}/\text{Zr}$ IN COMPARISON WITH $\text{SO}_4^{2-}/\text{Zr}$ CATALYSTS SYNTHESIZED *via* DIFFERENT PREPARATORY CONDITIONS FOR BIODIESEL PRODUCTION

Apparently, the options available for promoting sustainability are not mutually exclusive. Therefore, aside biomass-derived catalysts, Chapter 5 sets out its purpose, *viz.* to elucidate the possibility of improving the status of sulfated zirconium-based catalysts for transforming low-value feedstock. This chapter therefore, presents Article 3 as *Acidity and catalytic performance of Yb-doped $\text{SO}_4^{2-}/\text{Zr}$ in comparison with $\text{SO}_4^{2-}/\text{Zr}$ catalysts synthesized via different preparatory conditions for biodiesel production*. It investigated the effect of doping SZ with Ytterbium and further showed how preparative procedures affected catalytic activity and acidity of SZ. This was achieved by exploring how slight changes in incipient wetness and co-precipitation method affect acidity and activity of SZ in biodiesel production. This study is available as a research article published by the Journal of the Taiwan Institute of Chemical Engineers.

5.1 Introduction

The potency of public concern in the 21st century forces decision makers to enact policies not primarily based on science and technology. Concerns such as environmental impacts and socioeconomical challenges help to shape public opinion towards new demands that require novel catalytic solutions (Hassan, et al., 2015; Guldhe, et al., 2014). Inherent with these new challenges are the potentials for greater efficiency and sustainability of such systems (Xie and Wang, 2013). Moreover, the searches for newer solutions have led experts to explore in details, the attributes of different materials, systems and devices (Farooq, et al., 2013). One key task is in achieving phase-homogeneous solids with

uniform morphological and chemical properties. This challenge is a fundamental prerequisite to any rational catalyst design. Further, the current dwindling price of crude oil is an indication that catalysis needs extensive experimentation to give biofuel the needed competitive edge. Consequently, it is necessary to devise catalytic processes with ca. 100% yields. These will help to establish the potentials of catalysts as well as ensure the prominence of biofuels such as biodiesel.

Despite these challenges, last century witnessed catalysis as the major backbone for most industrial processes such as petrochemistry (especially, petroleum catalytic refining) and bulk chemistry. Incidentally, the high activity of sulfated zirconia (SZ) attracted substantial attention for converting triglycerides (TGs) into biodiesel at moderate to high temperatures. SZ is the subject of numerous reports since its discovery in 1979 (Furuta, Matsushashi, & Arata, 2004). It is therefore, plausible to assert that SZ has reached a ‘state-of-the-art’ status considering reports too numerous to mention available in the open literature. Further, most reports considered SZ as superacids because of their catalytic activity in simultaneously esterifying free fatty acids (FFA) and transesterifying triglycerides (TG) from high-FFA containing feedstocks into biodiesel.

However, despite numerous encouraging results, some aspects of SZ catalytic activity and physicochemical properties remain debatable. Some authors (Park, et al., 2008, Refaat, 2011, and Shu, et al., 2007) argue that despite the presence of sulfate anions, the hydroxyl groups on the SZ surface is less acidic than the bridged hydroxyls in zeolites. They further claimed that besides Lewis sites, the surface of zirconia contains basic sites in the form of coordinated unsaturated oxygen atoms. They attributed this rationale by viewing the interaction between zirconia and H_2SO_4 as acid-base reaction. Contrarily, proponents (Chung, & Park, 2009, Danuthai, et al., 2009; Kiss, et al., 2006) to its acidity

provided evidences that showed superacidity of SZ contains two types of acid sites. A strong acidic site (24 μmol) with up to 31.2 kcal/mol strength and a weaker site (52 μmol) having a strength of 25.8 kcal/mol. The latter explains the claim by the opponents to the acidity of SZ. This is because 25.8 kcal/mol is lower than 34 kcal/mol and 41 kcal/mol that represent the acidity of HY and HZSM-5 respectively. The latter acidity explains the observation reported by the opposing authors. However, these conflicting reports are not surprising because heterogeneity and site accessibility of solid acid catalysts render direct measurement elusive. Moreover, acidity of SZ is sensitive to preparatory conditions and preparation method employed (Hassan, et al., 2015).

Two decades ago, a detailed report by Breck (1984), evidenced the negligible effect that sulfation procedure has on the final SZ product. Despite this and the extensive attention on the factors affecting the acidity of SZ, there is no information from open literature regarding biodiesel production over SZ doped with ytterbium. Consequently, the present contribution aims to demonstrate the superior acidity and catalytic activity of SZ doped with ytterbium over SZ catalysts prepared by varying preparative procedures. To achieve this, the study evaluated how slight changes during incipient wetness and co-precipitation methods, and sulfate dispersion on SZ affect its acidity and performance in biodiesel production. The report aims at providing insight to the arduous task of making biodiesel economically competitive *via* transesterifying UFO containing 48 wt.% FFA. It is instructive to highlight the significance of employing UFO especially with current dwindling price of crude oil. Rather than dump the waste material into landfills, UFO simultaneously eliminates the food-for-fuel competition (Lotero, et al., 2005) and reduces the cost of biodiesel production (Narasimharao, et al., 2007). The cooking process causes the vegetable oil, TGs, to breakdown to form, DGs, MGs, and free fatty acids (FFAs).

5.2 Literature review

High-resolution spectroscopic techniques that are surface sensitive reveal indirect information on the structure of the sulfur surface species. For instance, Yamaguchi et al. (1986), and Jin et al. (1986), employed X-ray photoelectron spectroscopy (XPS) and IR studies to proposed that zirconia surface (bidentate) is doubly coordinated to surface sulfate species containing a O=S=O moiety (Figure 5.1). Bensitel, et al. (1988), postulated the possibility of the existence of two structures residing on different crystal planes at moderate coverage. The authors showed that SZ surface is attached to both species, each containing only one S=O bond *via* three S-O bonds (See Figure 5.1a). Interestingly, however, Morterra et al. (1995), showed that samples used by Bensitel et al. (1988) contained mainly monoclinic crystal phase. Unfortunately, sulfated monoclinic zirconia has no practical activity in isomerization of hydrocarbons. Nonetheless, (Riemer et al., 1994) accepted the suggestion by Bensitel et al. with slight modification. They observed the sulfate-free material has no O-H stretching band at 3650 cm^{-1} . This prompted the authors to suggest the presence of a HSO_4^- group on the surface (Figure 5.1b).

5.2.1 Structure and chemistry of sulfated zirconium

White, Sikabwe, Coelho, & Resasco (1995), suggested a different possibility where the zirconia tetragonal (001) plane adsorbs SO_3 molecule with only one S=O bond. In this scenario, five different oxygen atoms interact with the sulfur atom (Figure 5.1d). Similarly, depending on the dehydration state of the material, Babou, Coudurier, & Vedrine (1995), postulated as many as four (SO_3 , H_2SO_4 , HSO_4^- and SO_4^{2-}) different surface species on the surface of SZ. Finally, Haase, & Sauer (1998), provided a perspicuous structure representation of the surface sulfur species on SZ. The authors applied periodic plane wave pseudo-potential calculations based on density functional theory (DFT) to achieve this feat as well as proved that two Zr sites react differently with adsorbed molecules (Figures 5.2 to 5.4).

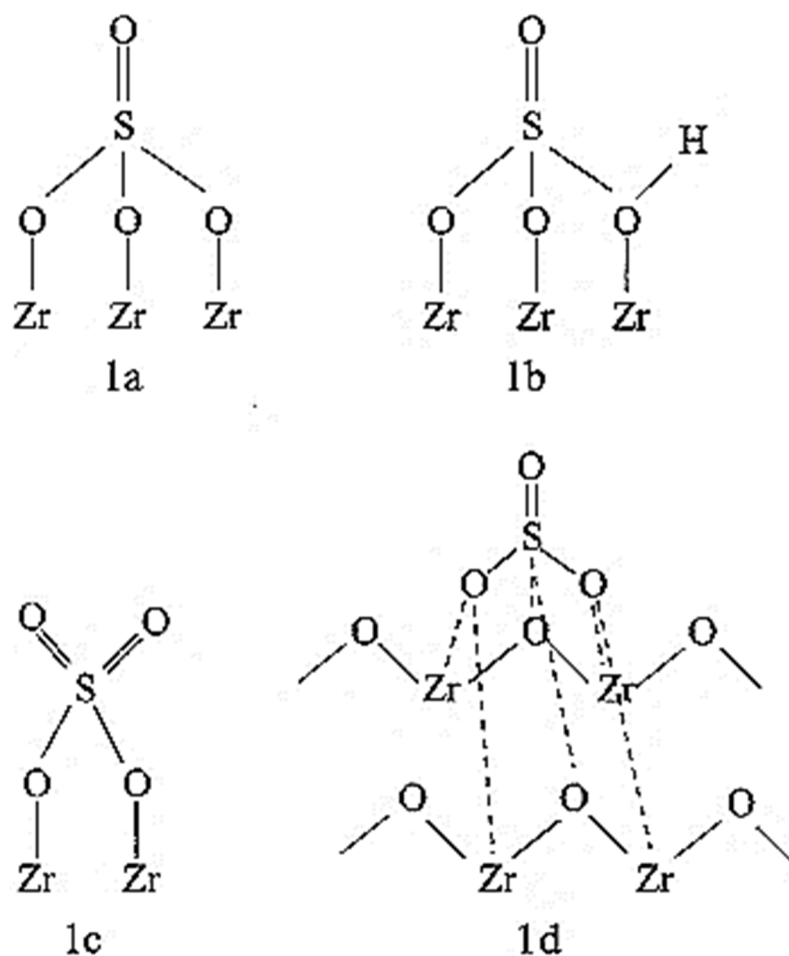


Figure 5.1: Two structures of SZ at moderate coverage with possibility of residing on different crystal planes.

Figure 5.2 presents the evidence depicting the equilibrium position of two structures after adsorbing water at the two possible Zr sites. Chemisorbed water restores 8-fold of the surface Zr sites by coordination and bonds to the strong site with an interaction energy of -194 kJ/mol (bottom of Figure 5.2). However, contrary to the strong (short) Zr-O bond restored by the chemisorbed molecules, only a weak (long) Zr-O bond is facilitated by physisorbed molecules (bottom of Figure 5.2). An interaction energy of -105 kJ/mol bonds the physisorbed complex and water together. Consequently, length (2.30 Å) of Zr-O bond in the physisorption complex obtained by Haase, & Sauer (1998) was commensurate to that of the long Zr-O bond in bulk zirconia (2.37 Å). Consequently, the H-bond interaction elongates the O-H bond of water that is between the one of the protons

and Zr surface oxygen atom. However, the strong bond of Zr-OH₂ dissociates the water molecule on the strong adsorption site and consequently, transfers H⁺ to adjacent surface oxygen atom in its vicinity. This generates a ZrO-(H)Zr hydroxyl bridging group and leaves a terminal hydroxyl group (Haase, & Sauer, 1998).

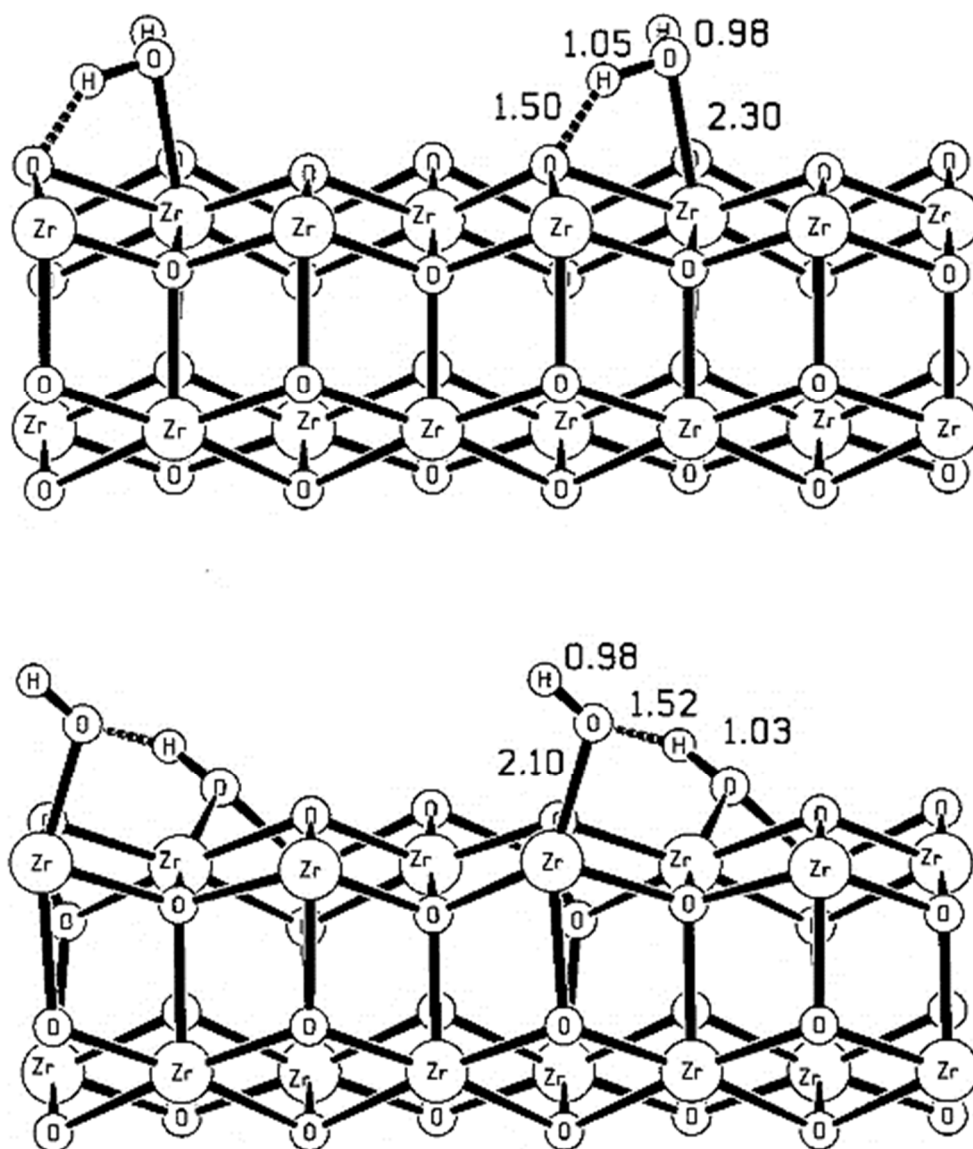


Figure 5.2: Equilibrium structures of the H₂O/ZrO₂ (101) complexes for the two possible Zr sites with selected bond lengths given in angstroms. The figure shows only the first two ZrO₂ layers.

Figure 5.3 illustrates some selected equilibrium bond lengths together with the adsorption complex. The figure depicts the three Zr-O bonds that hydrogen sulfate ion forms with the surface which contains one S=O double bond and three S-O single bonds. Evidently, the electrostatic interaction is very strong because the interaction energy of the bare ZrO_2 (101) surface and the isolated sulfuric acid molecule is -243 kJ/mol. Moreover, the evidence that supports this conclusion is the fact that length of the long Zr-O bonds in the bulk ZrO_2 system is proportionate to the Zr-O bond lengths of the adsorbed anion. Nevertheless, the complete dissociation of the H_2SO_4 molecule in the second adsorption structure formed two surface hydroxyl groups and a sulfate anion. Pauling (1960), used the information regarding the second acid constant of H_2SO_4 (strong polyprotic acid) being ca. 100,000 times smaller than the first one to calculate the first and the second deprotonation energies to be 1316 kJ/mol and 3,200 kJ/mol respectively. The loss of both protons from H_2SO_4 onto the surface of ZrO_2 indicates the remarkably strong interaction of the surface Zr atoms with sulfate ion as well as the base strength of the surface oxygen atoms.

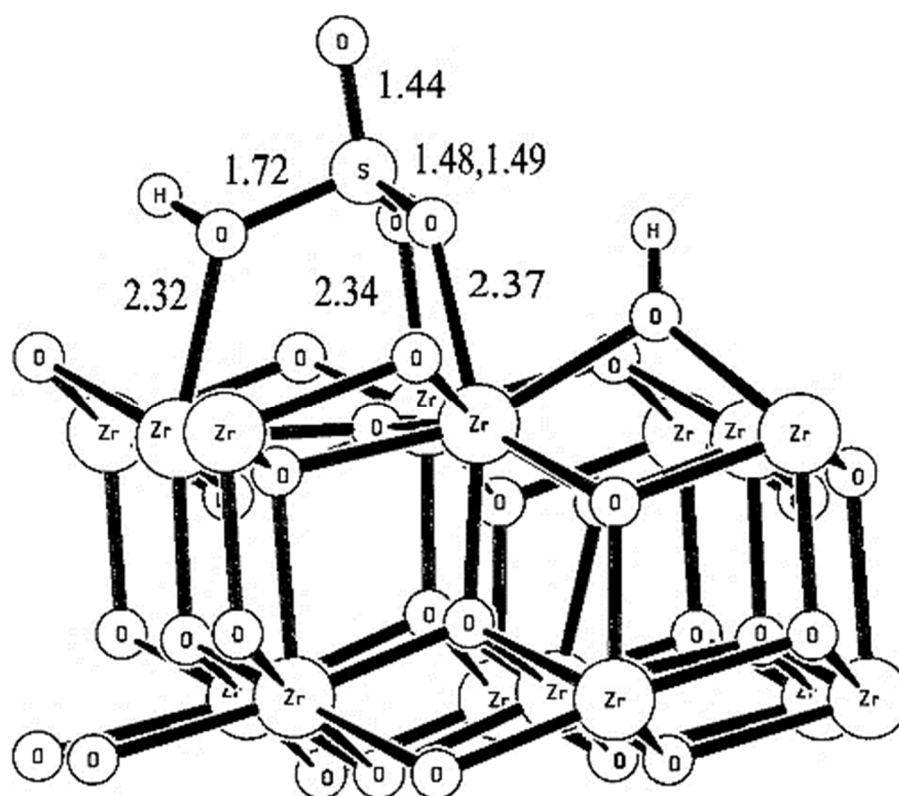


Figure 5.3: Equilibrium structure of the (H^+ , HSO_4^-)/ ZrO_2 (101) adsorption complex showing bond lengths in angstroms and the two outermost ZrO_2 layers.

Interestingly, the length of the only “free” S-O bond is comparable to that of the S=O double bond (1.44 Å) as depicted from the structure of the resulting adsorption complex (Figure 5.5). Similarly, the calculated bond lengths of the isolated SO_4^{2-} gas-phase anion (1.52 Å) were virtually equal to the remaining three S-O bonds attached to surface Zr atoms (1.53 Å). This adsorption complex is far more stable than the hydrogen-sulfate surface complex because its adsorption energy is -322 kJ/mol.

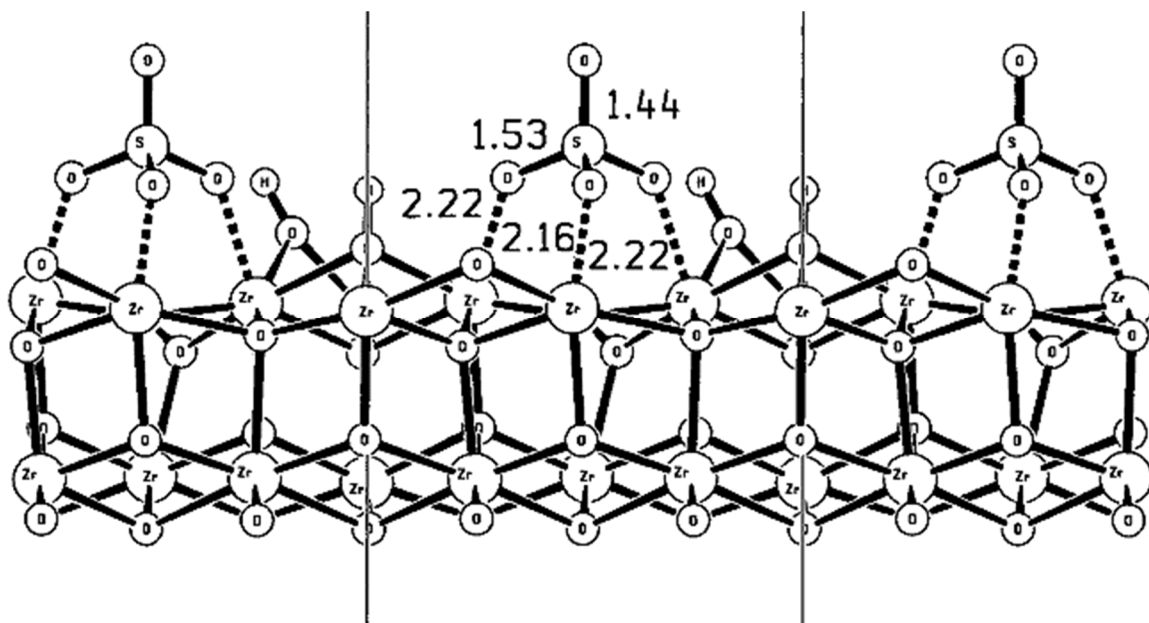


Figure 5.4: Equilibrium structure of the $(2\text{H}^+, \text{SO}_4^{2-})/\text{ZrO}_2$ (101) complex with selected bond lengths in angstroms. The unit cell is translated in the $+x$ and $-x$ directions, and the c vectors (z -axis) are indicated by two perpendicular lines.

5.3 Materials and methods

Sigma-Aldrich supplied all the reagents for this study. To ensure better comparative analyses, the study synthesized three different batches of catalytic materials. These are (a) catalysts prepared *via* incipient method, (b) ytterbium doped catalysts and doping method, (c) materials synthesized *via* co-precipitation. The required amount of ZrO_2 ($5\ \mu\text{m}$, 99%) was soaked in excess 0.5-M H_2SO_4 ($\geq 98\%$) and stirred for 120 min. Fritted glass filtered the resultant solution prior to drying of the solid for 20 h in open-air inside a fume cupboard; and at $130\ ^\circ\text{C}$ for 16 h in an oven. Calcination was for 4 h at $500\ ^\circ\text{C}$. The acronym SZr-T-t/x represents the synthesized materials. Where T denotes calcination temperature, t signifies time, while x denotes sufficient soaking (s), soaking in excess (e), or aging period (days). These preparatory variables were varied (see Table 1) to elucidate their effects on acidity and activity.

Further, homogeneous co-precipitation was the route employed for synthesizing the second batch of catalytic materials. Aqueous solutions of 1:2 wt.% of $\text{ZrOCl}_2 \cdot 8\text{H}_2\text{O}$ ($\geq 99.5\%$) and TiO_2 (*ReagentPlus*[®], $\geq 99\%$, 4.26 g/mL at 25 °C) were thoroughly mixed with urea. The mixture was heated at 95 °C under vigorous stirring for 12 h. Repeated washing of the precipitate with distilled water after filtering ensured negligible Cl^- concentration. The solid was initially oven-dried for 12 h at 120 °C, and then stored in dry N_2 atmosphere. Immersing 6 g of Zr-Ti composite in 0.5-M H_2SO_4 facilitated sulfation, while water bath evaporated the excess moisture. The resultant solid was oven-dried at 130 °C for 16 h and calcined at 500 °C for 4 h. This sample was designated as SZr-Ti-500-4/e. To investigate the effect that transition metal has on activity, Ytterbium (III) nitrate pentahydrate, $\text{Yb}(\text{NO}_3)_3 \cdot 5\text{H}_2\text{O}$ (crystals and lumps; 99.9% trace metals basis) was added to the third batch of catalysts. NH_4OH ($\geq 99.99\%$ trace metals basis; 28% NH_3 in H_2O) was added to aqueous mixture of Zr and Ti and stirred for 2 h. The resultant solid was oven-dried at 110 °C for 24 h and ground into powder. A thorough mixing of the samples with aqueous 0.5-M H_2SO_4 incorporated sulfate ions, while heating at 110 °C for 12 h prior to calcination at 500 °C for 4 h ensured stability on the materials. The material was designated SZr-Ti-Yb-500-4/s.

Table 5.1: Variable parameters employed for synthesizing mesoporous sulfated zirconia

Sample ID	0.5-M H_2SO_4	pH	Aging (h)
SZr-500-4/e	Excess	-	2
SZr-500-4/s	Sufficient	-	2
SZr-500-1/e	Excess	-	0.25
SZr-Ti-500-4/e	Excess	-	0.25
SZr-Ti-500-4/s	sufficient	-	0.25
SZr-Ti-Yb-500-4/s	0.323	-	2
SZr-500-5/7	0.034	1.25	168
SZr-500-5/7R	0.039	2	168
SZr-500-5/14	0.071	5	336
SZr-500-5/10	0.038	4	240

The third batch of catalytic materials was prepared according to a modified procedure previously documented by (Suharto, 2009). Distilled water and continuous stirring for 5 min, dissolved the required amount of $\text{ZrOCl}_2 \cdot 8\text{H}_2\text{O}$ to 0.34-M concentration. Adding urea in drop-wise manner to the required pH, precipitated the active species from the solution. While adding 0.5M $(\text{NH}_4)_2\text{SO}_4$ produced a gel-like acidic solution. This was aged for 1 to 14 days in closed polyethylene (PE) bottles at 90 °C. The solution underwent filtration after cooling to room temperature, and subsequent washing with excess distilled water (6 times, each with 200 ml). Calcination of the solid in air at 500 °C for 5 h followed drying in open-air for 20 h, and heating at 90 °C for 4 h in a fume cupboard. These samples were designated as SZr-500-5/7. To evaluate the effect strong acid sites, a portion of SZr-500-4/7, designated SZr-500-4/7R underwent a re-sulfation procedure again.

After drying, kneading, mixing with 0.5M- H_2SO_4 for 2 h, filtering through fritted glass, and drying at 130 °C for 16 h, the solids were calcined at 500 °C for 4 h. The procedure was repeated for sample SZr-500-5/14 except that required amount of $\text{ZrOCl}_2 \cdot 8\text{H}_2\text{O}$ was dissolved in distilled water before adding urea to a pH value of 5. Similarly, the procedure was repeated for SZr/500-5/10 except required amount of $\text{ZrO}(\text{NO}_3)_2 \cdot x\text{H}_2\text{O}$ was dissolved in 400 ml distilled water before adding urea to pH value of 3 and mixing with required amount $\text{Al}(\text{NO}_3)_3 \cdot 9\text{H}_2\text{O}$. Continuous stirring under 210 rpm at 50 °C for two hours aided homogeneity. Adding ammonia solution and stirring for 40 min preceded aging at room temperature for 10 days. Subsequently, after filtering, drying in fume cupboard at 90 °C for 24h, and calcining at 500 °C for 5 h, the catalysts were stored in airtight vials inside a desiccator. All catalysts and experimental runs were prepared in replicates to ensure repeatability.

5.3.1 Catalyst characterization

Analyzing isolated catalytic materials, precursors, or intermediates facilitates circumventing the high complexities of catalytic systems. It provides important information regarding the reaction mechanism and structure/activity relationships of the catalyst. Further, *ex situ* approach also enables the researcher to work with simplified systems under predefined conditions. Consequently, surface morphology and topology were analyzed with field emission scanning electron microscopy (FE-SEM) FEI QUANTA™ 450 FEG type 2033/14 (Czech Republic) unit with 30 kV accelerating voltage. An energy dispersive Xray spectrometer (EDX) from the same unit revealed the surface elemental composition of the catalysts.

XRD and BET analyses elucidated the structural and textural properties of the catalysts. Phillips X'pert diffractometer (The Netherlands) with $\text{CuK}\alpha$ radiation ($\lambda = 1.54056 \text{ \AA}$) at a scanning speed of $0.05^\circ \text{ s}^{-1}$ within 2θ range of 5 to 70° at 40 mA and 40 kV analyzed the XRD patterns. A Micromeritics TriStar II (USA) with accelerated surface area porosity (ASAP) 3020 at -196.15° C was used to determine the specific surface area of the catalytic materials using liquid nitrogen. Degassing the catalysts at 120° C for 3 h under a vacuum eliminated any physisorbed volatiles and impurities. Rapid (scan speed 3 velocities, 2.2 to 20 kHz) identification and quantification of the catalysts was performed with a Bruker Fourier transform infrared (FT-IR) Tensor 27 IR (Germany). The apparatus has a spectral range of 7500 to 370 cm^{-1} with more than 1 cm^{-1} apodized resolution and a standard KBr beam splitter. Ammonia temperature programmed desorption (NH_3 -TPD) by AutoChem 2920 (Micromeritics) evaluated the acidic profiles on the catalysts. To ascertain the exact amount of gas consumed during the experiment, the equipment was calibrated by $10\% \text{ NH}_3$ in He before the analysis. After placing 0.10 g in a quartz U-tube, N_2 flow (50 mL/min) at 110° C for 1 h degassed the synthesized

material. After cooling to 60 °C, the samples were saturated with NH₃ by the (20 mL/min) flow of 10% NH₃ in He for 40 min. N₂ gas flowing at 50 mL/min for 30 min over catalyst purged the physisorbed NH₃. Raising the temperature from 60 to 700 °C with a ramp of 10 °C/min under N₂, flowing at 50 mL/min revealed the TPD profile. TCD detector revealed the amount of NH₃ consumed which determines the Brønsted and Lewis acid sites in the catalyst.

5.3.2 Production of fatty acid methyl esters from used frying oil

Heating the catalysts at 150 °C for 1 h before the reaction to evacuate adsorbed water and other volatiles. With the aid of catalyst, 23.40 ml of used frying oil, UFO (866 g/mol) was esterified and transesterified simultaneously with methanol at 100 to 220 °C, while the pressure varied according to the process temperature inside the reactor. The reactors employed for conducting the reaction were a 100 mL autoclaves (250 °C, 100 bar) supplied by AmAr Equipment Pvt., Ltd. (Mumbai). Constant stirring ensured contact between the catalyst and the reaction mixture. A reflux condenser attached to the autoclave maintained the temperature during the reaction. Preliminary optimization (Fig. 1) showed that a 6:1 methanol-to-oil molar ratio and 2 wt.% catalyst loading are optimal reaction conditions. However, this study employed a molar ratio of 5:1 because the difference in conversion was minimal. This minimizes the use of resource, energy, and cost. Simple decanting and centrifugation recovered the FAME at the end of the 5 h reaction time.

The study employed GC-MS (Serial # CN10946045; Model 7890A; US), and EN 14103:2003 (E) analytical method in determining methyl ester contents with 100-mg neat mixture (Supelco® No. 18919) containing 37 components (C₄ to C₂₄ FAMES; 2 to 4% relative concentration) as reference standard. This was dissolved in 99% heptane at 0.01

to 0.10% (w/v) concentration. Then, 1 mL hexane placed in vials with screw caps having PTFE-faced septa dissolves an accurately weighed 10 mg sample, prior to the addition of 10 μ L of 2 N KOH in methanol.

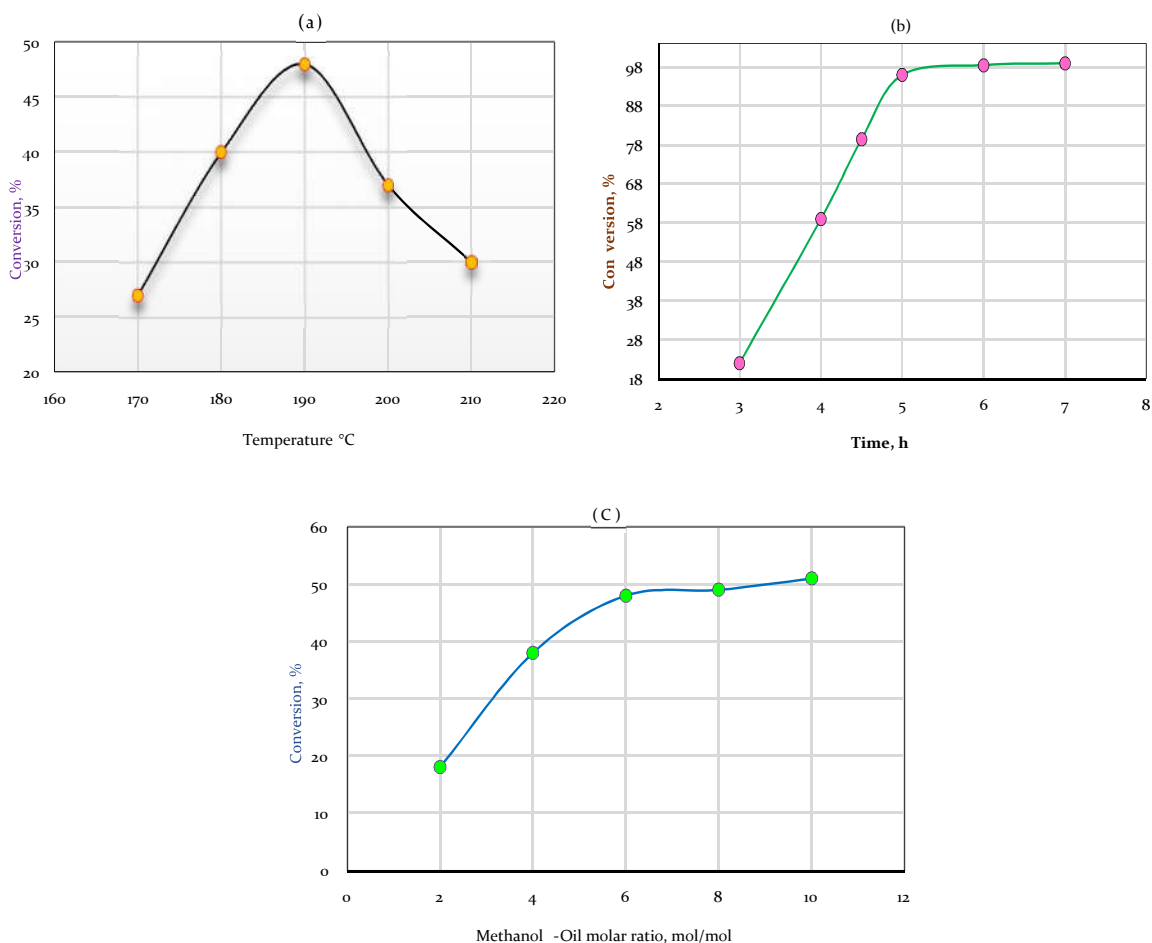


Figure 5.5: Preliminary optimization on (a) temperature, (b) time and (c) methanol-to-oil molar ratio.

After vortex for 30 s, and centrifugation, one μ L of the supernatant was transferred into TSP micro vial. The GC analyzer has the following working conditions: DB 23 column ($L = 0.30 \text{ mm} \times \text{ID} = 0.32 \text{ mm} \times 0.25 \text{ }\mu\text{m}$ film thickness of 5% diphenyl, 95% dimethyl polysiloxane) and methyl heptadecanoate, C_{17} (99% minimum purity; 14 min retention time) as the internal standard; 210 $^{\circ}\text{C}$ injection temperature and helium as carrier gas. Equation 1 facilitated the determination of the ester content (C), expressed as a mass fraction in percentage.

$$C = \frac{(\sum A) - A_{E1}}{A_{E1}} \times \frac{C_{E1} \times V_{E1}}{m} \times 100\% \quad (5.1)$$

Where: $\sum A$ is the total peak area from the methyl ester in C₁₄ to that in C_{24:1}

A_{E1} is the peak area corresponding to methyl heptadecanoate

C_{E1} is the concentration of the methyl heptadecanoate, in mg/mL

V_{E1} is the volume of the methyl heptadecanoate, in mL

m is the mass of the sample, in mg

5.4 Results and discussion

5.4.1 X-ray diffraction analysis

The XRD diffractograms (Figures 5.6 and 5.7) of synthesized SZ catalysts revealed a tetragonal-monoclinic phase transition. The XRD patterns also show the significant impact of calcination temperature and precursor concentration on the crystal phase and crystallite size. Further, tetragonal phase exhibited more prominent characteristic peak areas than its monoclinic phase counterpart. In addition, the intensity of the peaks reflected both adsorption and amount of phase in the synthesized materials. Usually tetragonal phase transition occurs at above 1170 °C. However, according to (Osendi et al., 1985; Tangchupong et al., 2010), SZ precipitation preparation method produces monoclinic-tetragonal phase transformation of zirconia at lower temperature.

Therefore, the low temperature employed during synthesis in this study facilitated the transition of monoclinic phase to tetragonal phase, which retards crystallization of zirconia support (Fa et al., 1997; Vishwanathan et al., 2008). Furthermore, the higher surface energy of the monoclinic phase compared to that of tetragonal phase ensures the metastable tetragonal phase transformation (Tangchupong et al., 2010). All the XRD patterns displayed presence of monoclinic and tetragonal phases except SZr-Ti-Yb-500-

4/s (Figure 5.6b). This is despite the variance in the preparatory methods and precursor types utilized. The amount and chemical composition of the latter material was different from all other samples. This explains the differences observed from the crystallographic structures. Expectedly, the tetragonal phase (111) reflection at $2\theta = 31.02^\circ$ XRD patterns of the SZ broadens with higher pH. However, the (111) reflection of the monoclinic phase at $2\theta = 28.18^\circ$ especially for the sample prepared at higher pH indicated unstable tetragonal phase because probably the crystallite size were not small enough (Pacheco & Fripiat, 2000). Conversely, SZ prepared at higher pH exhibited lower monoclinic phases. Further, SZr-Ti-Yb-500-4/s that was synthesized with repeated addition of ammonium hydroxide exhibited lower crystalline structures with major anatase titania. The sample however, displayed similar pore size distribution to SZr-500-4/s but with 20 fold higher S_{BET} (Table 5.2). The two materials were both soaked for 2 h in sufficient H_2SO_4 .

Consequently, the difference in sintering process, which causes higher S_{BET} (Table 5.1), confirmed the phase transformation exhibited by the XRD pattern of SZr-Ti-Yb-500-4/s. Interestingly, the materials processed in sufficient, but under longer soaking period exhibited higher acidity and pore diameter. For instance, entries 2 and 3 (Table 5.1) showed higher pore sizes and active site dispersion than those soaked in excess. This informed the preparation of SZr-Ti-Yb-500-4/s, which despite its lower width/height SZ peak ratio and crystallite size exhibited the highest S_{BET} and acidity. Similarly, the sample in entry 9, displayed higher S_{BET} and acidity than the one in entry 10 Table 5.1. Therefore, it is plausible to assert that higher SO_4^{2-} concentration in SZr-Ti-Yb-500-4/s, facilitated the retardation of tetragonal phase transforming into monoclinic phase.

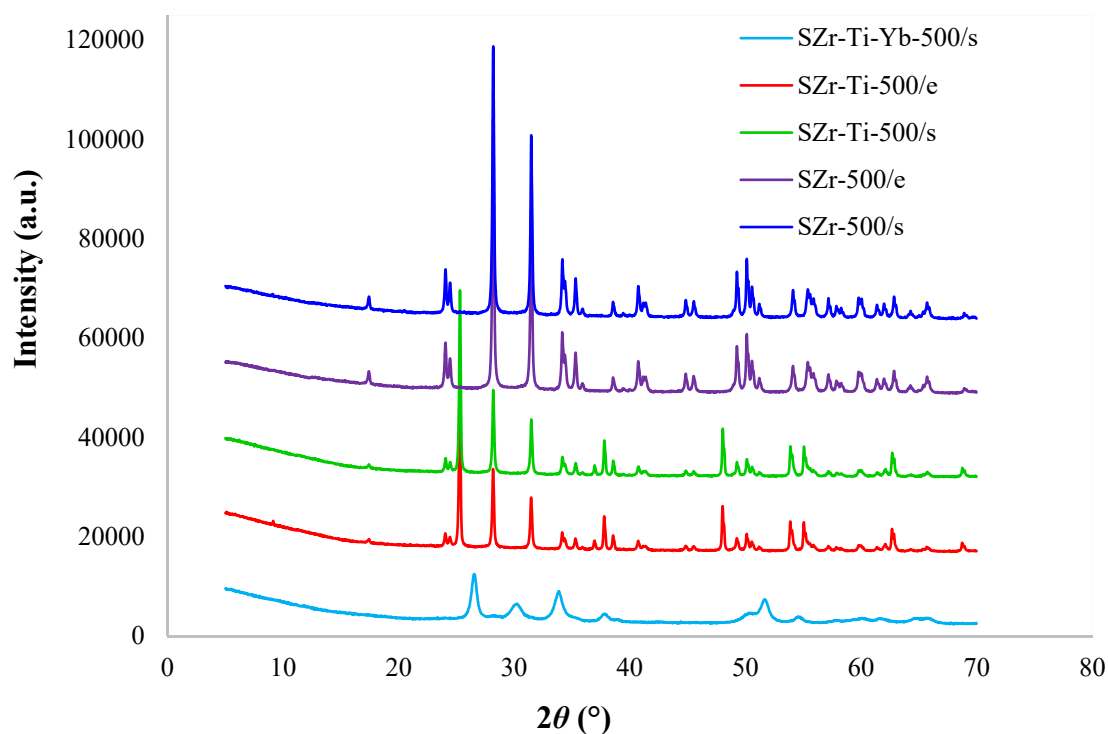


Figure 5.6: X-ray diffraction patterns for SZr-Ti-Yb-500-4/s, SZr-500/e, SZr-500-4/s, SZr-Ti-500-4/e, and SZr-Ti-500-4/s.

It is also evident from the peak intensities that reflectance of adsorption and amount of phase in the mixture of SZr-Ti-Yb-500-4/s were lower than for the other materials. SZr-Ti-500-4/e, SZr-Ti-500-4/s and SZr-500-5/7 displayed zirconia predominantly in monoclinic phase with little tetragonal phase with respect to intensity. The monoclinic phase had highest intensity at $2\theta = 28.16$ (61.21%) while that of the tetragonal is at $2\theta = 50.09$ (13.27%). In contrast, SZr-500-4/e, SZr-500-4/s, SZr-500-5/14 and SZr-500-5/10 exhibited zirconia predominantly in tetragonal phase with little monoclinic phase with respect to intensity. The tetragonal phase has the highest intensity at $2\theta = 30.19$ (81.74%) while that of the monoclinic was at $2\theta = 28.17$ (64.43%). Figures (5.2a and 5.2b) also highlight the effect that slight modification in catalyst preparatory conditions has on the morphology of the material. These morphological changes could be favorable or detrimental to the catalytic activity of the catalysts. Such alterations affected the domain sizes and lattice strains (i.e., the contribution from crystalline sizes and strains) displayed

by the peaks. The peaks also revealed the concentrations of active metal in the different modified catalysts. The intensity of monoclinic phase ZrO_2 (Baddeleyite) appeared in XRD patterns of all the materials except SZr-Ti-Yb-500-4/s. This evidenced the better selectivity and activity performances influenced by the high S_{BET} , which reflects small crystallite size. However, monoclinic phase was more prominent on SZr-500-4/10 than for others (Figure 5.6a) though with minimal effect.

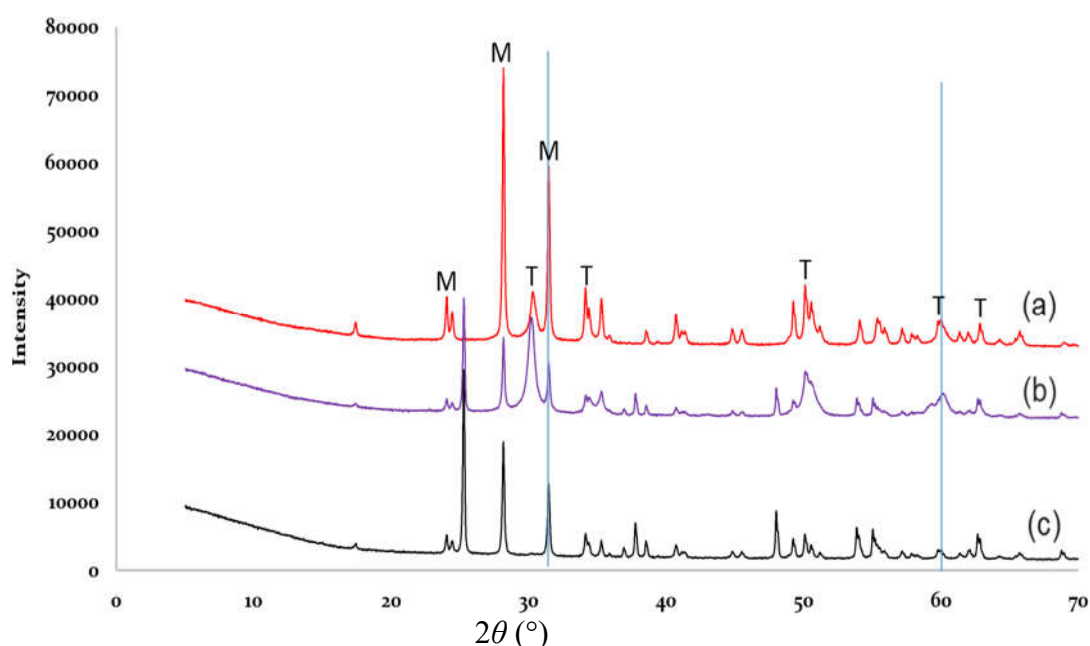


Figure 5.7: X-ray diffraction patterns for (a) SZr-500-5/7, (b) SZr-500-5/14, and (c) SZr-500-5/10.

A good system of channeled pores for diffusion, and enhanced textural properties are some essential requirements for zirconia and ZrO_2 mixed oxides heterogeneous catalysis. Interestingly, the XRD shoulder with the maximum intensity was centered at 27.78° , and situated at the same peak position that exhibits Bragg's diffraction angle graphically. Further, the position matches what is expected for the strongest Bragg reflection of the crystalline monoclinic ZrO_2 phase (baddeleyite). Similarly, the XRD peak centered at 31.58° is in consonance with the expected position for the second strongest Bragg reflection of baddeleyite. These facts suggest that incipient ordered structure at 27.78° and

the associated shoulder at 31.58 are responsible for activity and stability of the modified zirconia.

5.4.2 Surface physical property measurements

Table 5.2 presents the textural properties and acidity of the mesoporous SZ catalysts. The difference in chemical composition of the catalytic materials plausibly explains the significant variations in textural and catalytic activities. Thus, for instance, the S_{BET} of SZr-500-5/10 was $15.0543 \text{ m}^2/\text{g}$ while SZr-500-5/7 had $7.6917 \text{ m}^2/\text{g}$ S_{BET} value. However, the pore size distribution ($2 < dp < 50 \text{ nm}$) of all the synthesized catalysts revealed mesoporous structure which permits the TG molecule access to the active sites within the materials (Table 5.2 and Figure 5.8).

Table 5.2: Textural properties and acidity of synthesized sulfated zirconia

Sample ID	Surface area (m^2/g)	Pore vol. (cm^3/g)	Pore size (nm)	Acidity ($\times 10^{-3} \text{ mmol/g}$)
SZr-500-4/e	5.30 ± 0.5	0.020	21.21	20 ± 0.02
SZr-500-4/s	3.43 ± 0.2	0.017	37.04	40 ± 0.02
SZr-500-1/e	3.84 ± 0.3	0.018	20.35	10 ± 0.01
SZr-Ti-500-4/e	8.12 ± 1.3	0.043	24.98	50 ± 0.03
SZr-Ti-500-4/s	8.33 ± 1.4	0.047	28.52	70 ± 0.03
SZr-Ti-Yb-600-4/s	60.33 ± 2.3	0.323	21.38	330 ± 0.05
SZr-550-5/7	7.69 ± 1.4	0.034	21.44	80 ± 0.03
SZr-550-5/7R	9.05 ± 1.3	0.039	20.27	40 ± 0.03
SZr-550-5/14	41.22 ± 1.9	0.071	6.83	280 ± 0.04
SZr-550-5/10	15.05 ± 1.7	0.038	9.65	70 ± 0.03

Figures 5.8a and 5.8b shows nitrogen sorption isotherms of the SZ obtained after calcination in air at 500°C . The isotherms followed the type III of the IUPAC classification with pores in the range of 1.5 to 100nm. This indicates the mesoporous nature of the synthesized materials, which are typical of materials with weak fluid-wall attractive forces. The slopes show increased adsorbate uptake at higher pressures as gas fills pores, while inflection point occurs typically near completion of the first

monolayer. Expectedly, the voids between the zirconia nanocrystals showed a H₂ type hysteresis loop befitting of inkbottle pores. The isotherms of SZr-500-5/7, SZr-500-5/7R, SZr-500-5/10, and SZr-500-5/14 shifted to higher adsorbed volumes with increasing aging and pH. This indicated increase in specific surface area, S_{BET} of the materials (Table 5.2). For instance, the S_{BET} for the materials aged for 7, 10, and 14 days produced 9, 15, and 41 m²/g, respectively. This corroborated the report by Cassiers et al. (2003) that large specific surface area needs higher post-treatment of ca. pH 12.

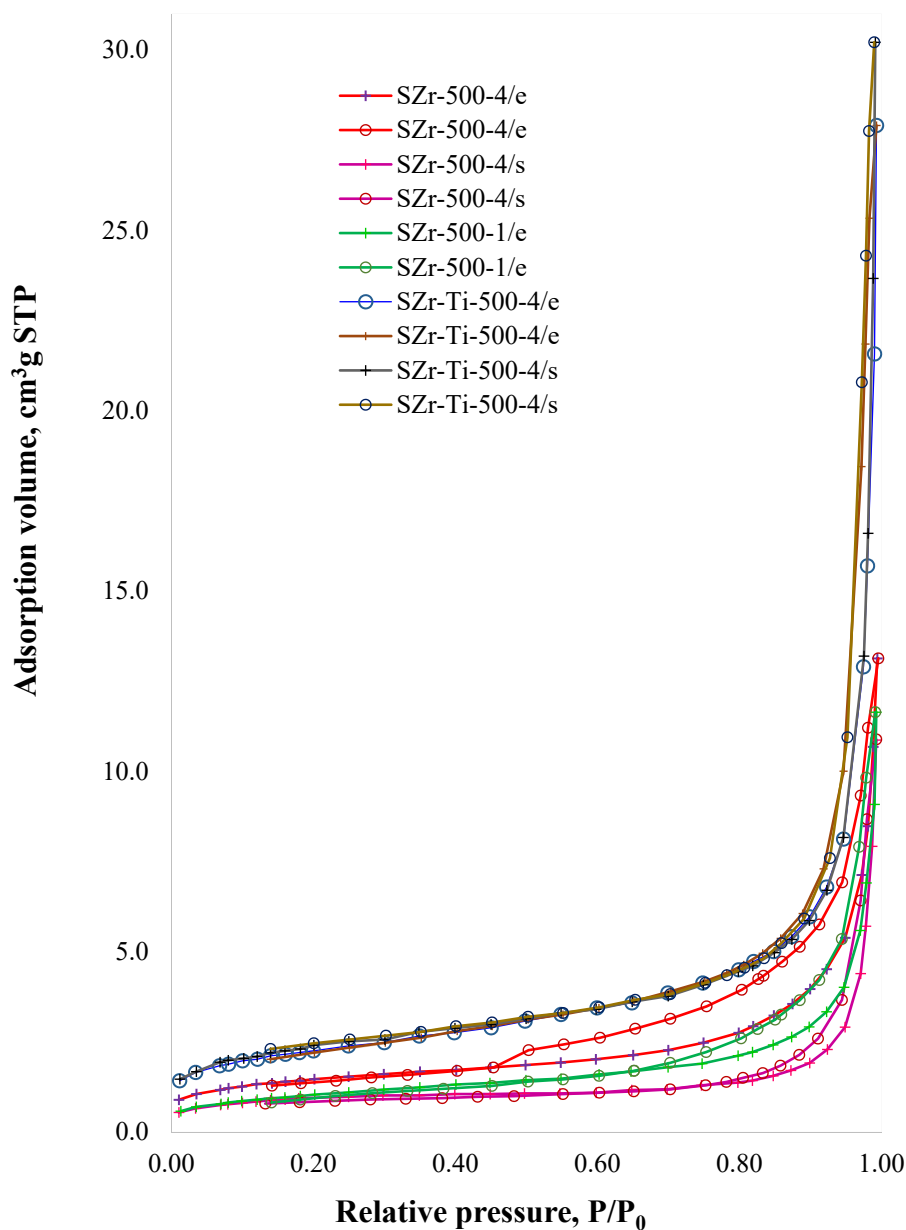


Figure 5.8(a): N₂ adsorption-desorption isotherms of mesoporous SZ synthesized under different conditions.

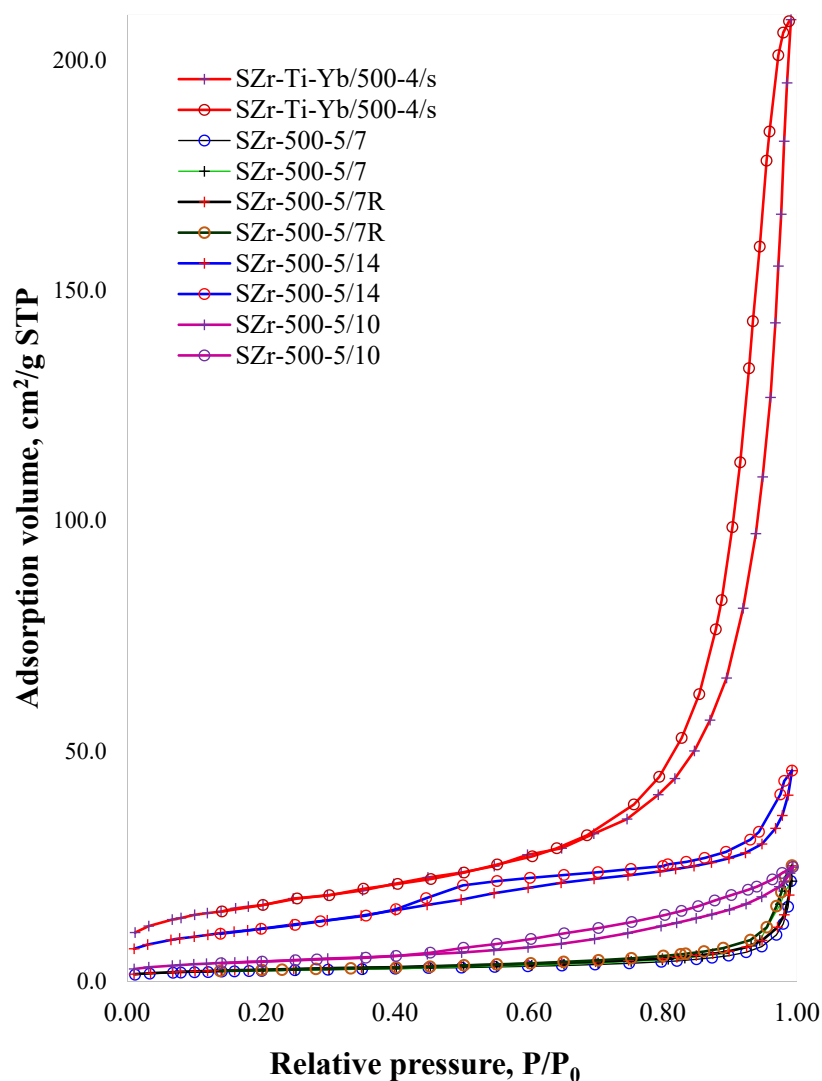


Figure 5.8(b): N₂ adsorption-desorption isotherms of mesoporous SZ synthesized under different conditions.

Intriguingly, the study obtained inverse correlations from the pore size distributions (Figures 5.9a and 5.9b) which shifted to smaller diameters with increasing aging and pH (Table 5.2). Materials aged for 7 days (pH 1.25) produced about 21 nm, against 7 nm for materials aged for 14 days (pH 5). Interestingly, impregnating 5 wt.% titanium into the zirconium hydroxide had a pronounced effect on the S_{BET} of the SZ. However, this modification had negligible effect on the pore size distribution of the calcined materials (Table 5.2; Figure 5.9a, and 5.9b). Similar shifts were observed in the pore size distributions and the isotherms from both Ti-free materials and those impregnated with titania.

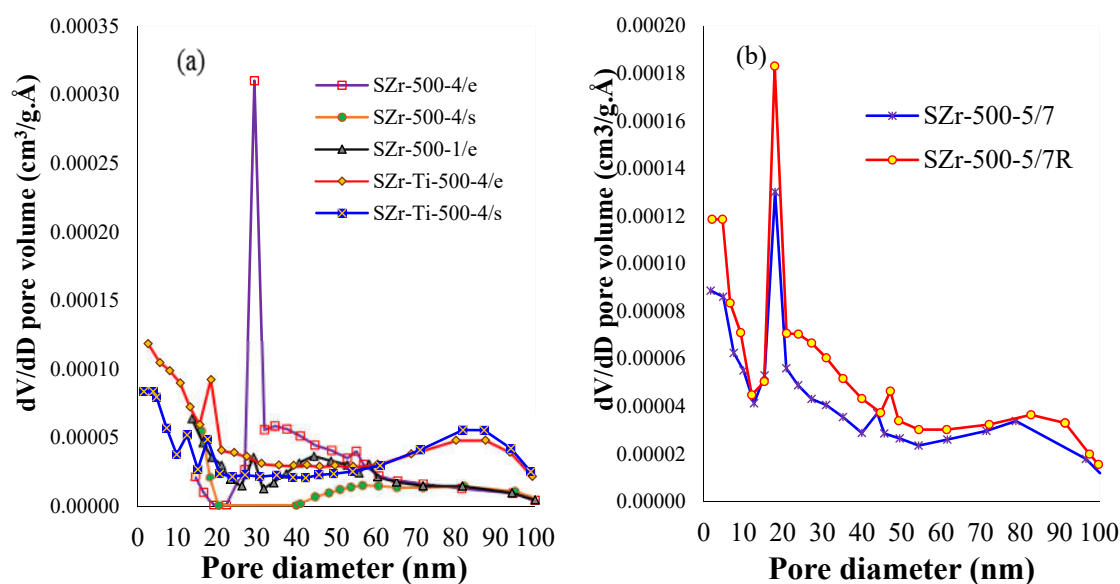


Figure 5.9: Pore size distribution curves of mesoporous SZ prepared from different preparatory conditions.

To further evaluate the effect of incorporating transition-metal on the structural and acidic properties on activity of SZ, 1.5 wt % ytterbium (III) nitrate hydrate was used in preparing SZr-Ti-Yb-500-4/s. The corresponding material exhibited the highest S_{BET} of $60 \text{ m}^2/\text{g}$ and a high pore size distribution (21 nm) comparable to the other materials (Figure 5.10). Further, this SZ exhibited the highest acidity of $33 \times 10^{-2} \text{ mmol/g}$. These observations suggest that longer aging period of the precipitating agent within aggregates of nanocrystals in the interparticle voids leads higher S_{BET} and lower crystal size. The pore system of the resulting material was significantly higher than the samples without Yb; whereas at relative pressures < 0.8 , the nitrogen sorption isotherm remained similar (Figures 5.3 to 5.5). The higher sorption capacity of SZ doped with Yb at higher relative pressures confirmed the existence of mesopores with a broad size distribution. Similarly, this is evident from the pore size distribution (Figure 5.5) which instead of the expected 3-8 nm, it revealed a broad distribution of mesopores of 3-60 nm. The authors attributed this observation to volumes between the interparticle voids and nanocrystal aggregates. Consequently, Yb incorporation narrows the pore size distribution because of even crystal

size distribution and even Zr aggregate size (Figure 5). An earlier study by Cassiers et al. (2003) showed the effect that scaffolding DDA support has on mesoscale of zirconia.

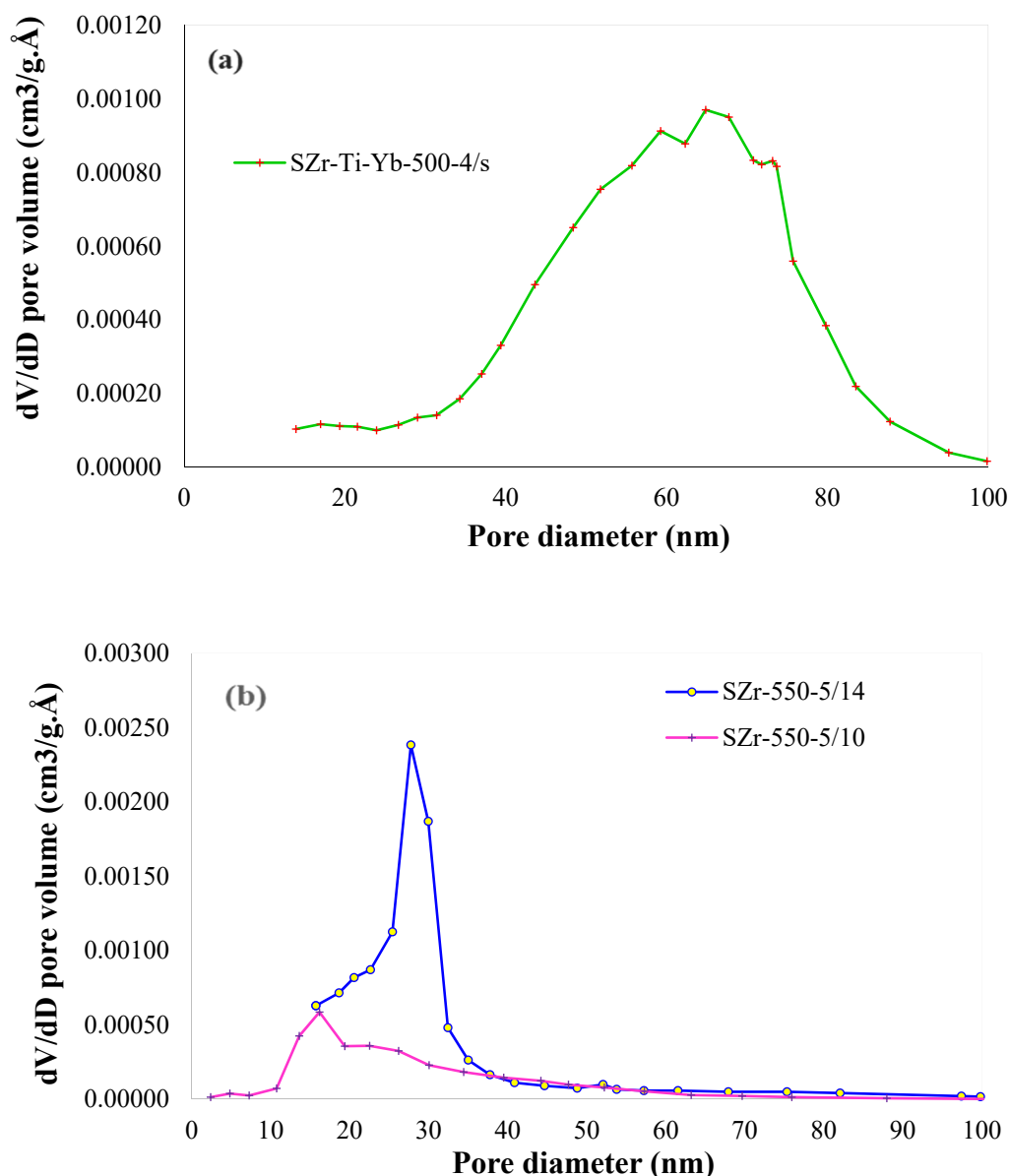


Figure 5.10: Pore size distribution curves of mesoporous SZ prepared from different preparatory conditions.

A notable increase in the number of acid sites was observed in the Zr-Ti mixed oxide catalysts compared to SZ without titania. This is despite the shorter aging period of the former (15 min) against the latter (120 min). These observations are in complete accordance with previous reports (Manríquez et al., 2004) that mixed oxides generate more acid sites than single oxides. One of two mechanisms premised this hypothesis: (a)

zirconium atoms substituting some of the titanium atoms or (b) large dispersion effect on the surface of the mixed oxide by the ZrO_2 or TiO_2 . To investigate the activity of the surface acid sites on the SZ further, see discussion on the catalytic results (Section 5.4.4). Simultaneous esterification of FFA and transesterification of TG was validated the acid catalytic activity of the synthesized SZ.

Figure 5.11a illustrates the surface microstructure of SZr-500-4/e as studied using FESEM, showing solid particles of uniform dimensions homogeneously processed from different constituents. The EDX analysis of the surface elemental composition revealed the presence of zirconium (99.63 wt.%) and sulfur (0.16 wt.%; see Appendix A) (Fig. 5.11b).

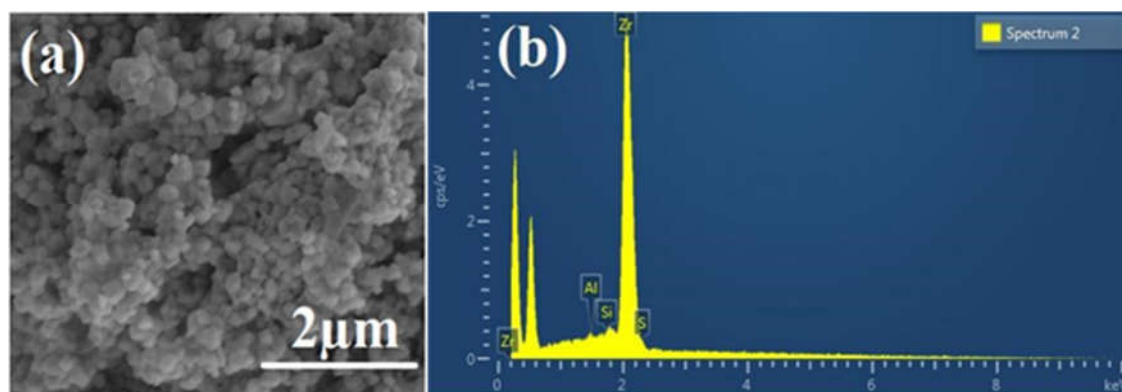


Figure 5.11: (a) Results of the surface microstructural analysis of the SZr-500-4/e *via* FE-SEM and (b) surface elemental composition of the SZr-500-4/e determined *via* EDX analysis

Similarly, Fig. 5.12(a) presents the surface microstructure (size and shape of topographic features) of sulfonated SZr-500-4/s catalyst studied using FE-SEM. The surface morphology has been homogeneously processed into solid particles. The surficial elemental composition by EDX analysis (Fig. 12b) also revealed the presence of 98.14 wt.% zirconium and 0.10 wt.% sulfur. The surficial appearance of SZr-500-4/e revealed a lesser dispersion of surface elements than SZr-500-4/s. Interestingly, the acid site

density of the latter was also higher than that of the former. However, the catalyst calcined for one hour (SZr-500-1/e) revealed a similar surficial micrograph (Fig. 5.13)

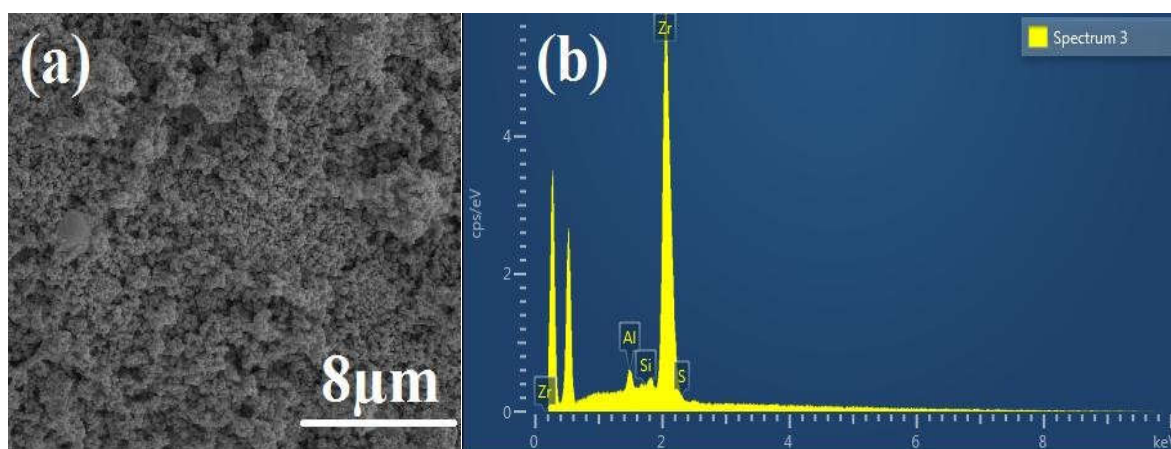


Figure 5.12: (a) Results of the surface microstructural analysis of the SZr-500-4/s *via* SEM and (b) surficial elemental composition of the SZr-500-4/s *via* EDX analysis

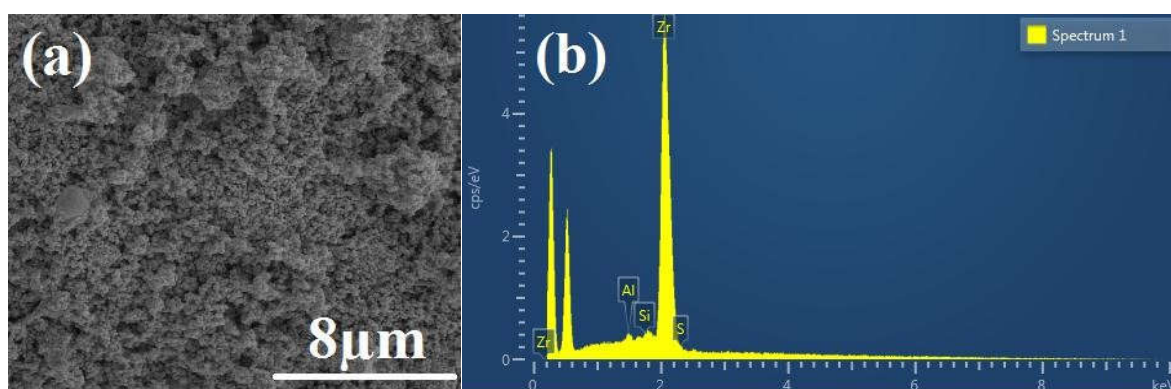


Figure 5.13: (a) Results of the surface microstructural analysis of the SZr-500-1/e (15 min) *via* SEM and (b) surficial elemental composition of the SZr-500-1/e (15 min) *via* EDX analysis

Fig. 5.14(a) presents the surface microstructure (size and shape of topographic features) of S/Zr-Ti/500/e catalyst. Calcination incorporated and stabilized the titanium oxide into crystal lattices of zirconium oxide structure. Fig. 5.14(b) presents a cross-sectional surficial composition and distribution of elements on SZr-Ti-500/e *via* EDX analysis. However, the micrograph of the catalyst prepared with sufficient acid revealed more dispersed surficial metal elements (Figure 5.15a). Expectedly, micrograph representing SZr-Ti-Yb-500-4/s displayed a somewhat amorphous phase (Fig 5.16a).

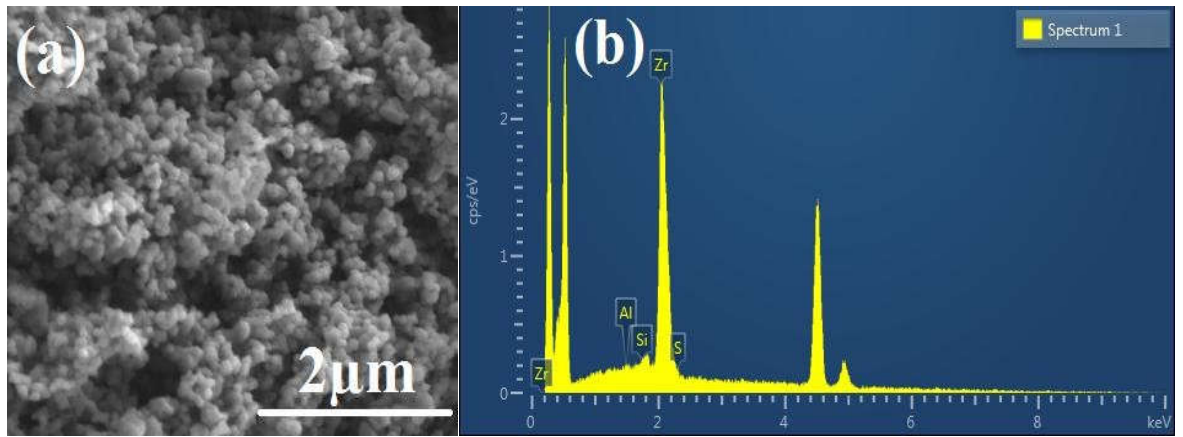


Figure 5.14: (a) Results of the surface microstructural analysis of the SZr-Ti-500/e (15 min) *via* SEM and (b) surficial elemental composition of the SZr-Ti-500/e *via* EDX analysis

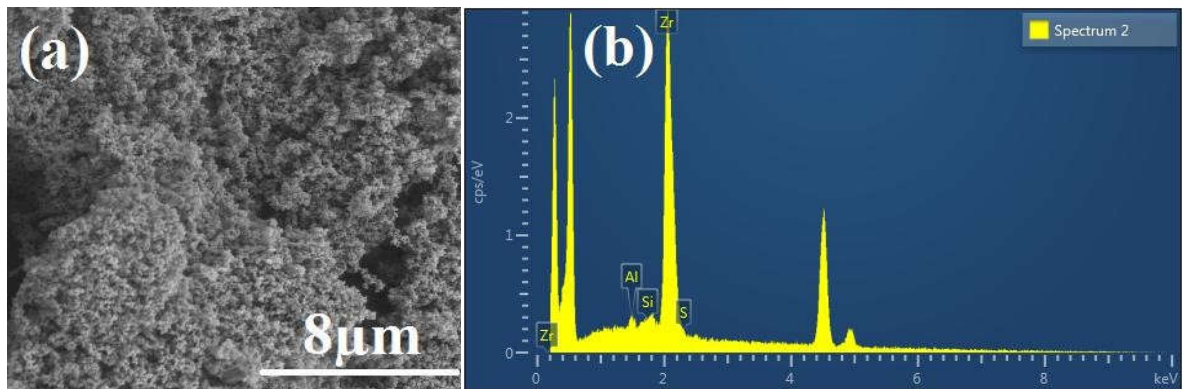


Figure 5.15: (a) Results of the surface microstructural analysis of the SZr-Ti-500/s (15 min) *via* SEM and (b) surficial elemental composition of the SZr-Ti-500/s *via* EDX analysis

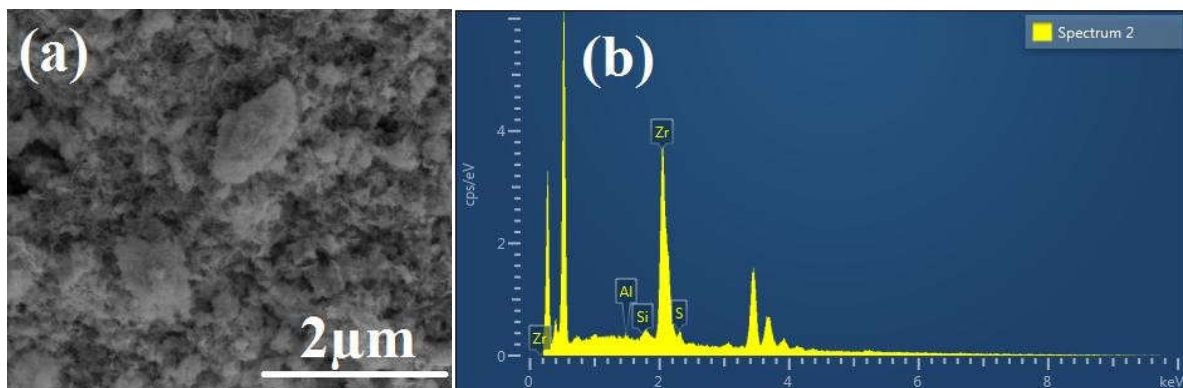


Figure 5.16: (a) Results of the surface microstructural analysis of the SZr-Ti-Yb/500-4/s *via* SEM and (b) surficial elemental composition of the SZr-Ti-Yb/500-4/s *via* EDX analysis

As expected, the differences between the micrographs of SZr-500-5/7 (Figure 5.17a) and SZr-500-5/7R (Figure 5.18a) were hardly noticeable. Intriguingly however, the surficial

structures of SZr-500-5/14 and that of SZr-500-5/10 (Figure 5.19a) were markedly dissimilar.

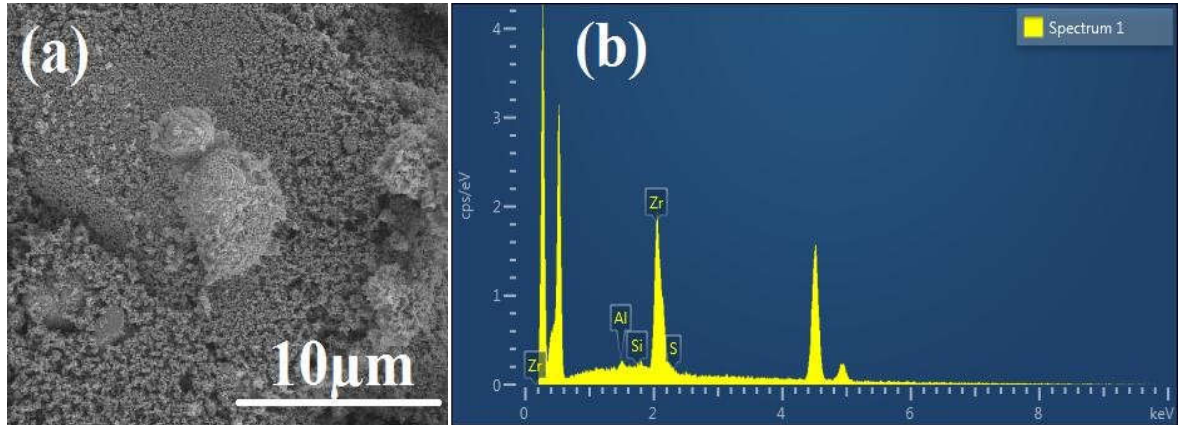


Figure 5.17: (a) Results of the surface microstructural analysis of the SZr-500-5/7 *via* SEM and (b) surficial elemental composition of the SZr-500-5/7 *via* EDX analysis

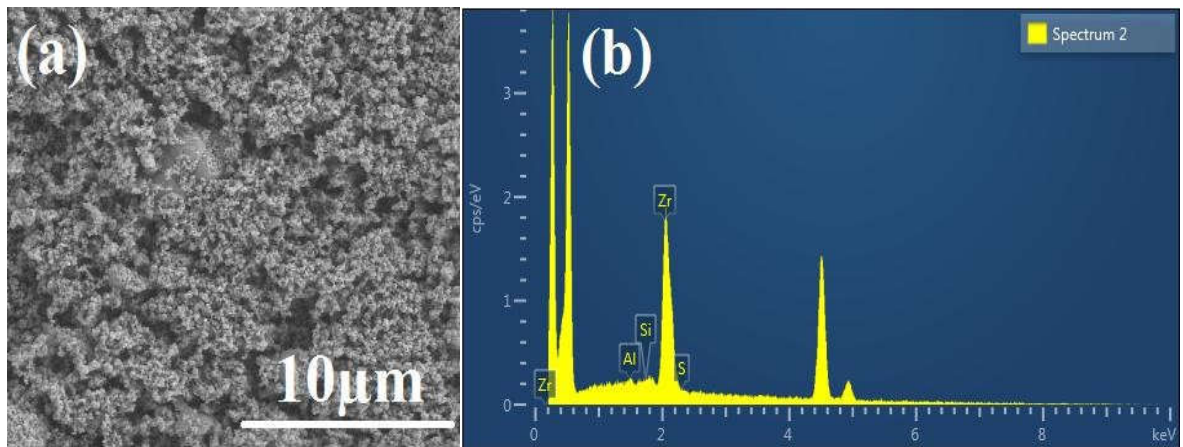


Figure 5.18: (a) Results of the surface microstructural analysis of the SZr-500-5/7R *via* SEM and (b) surficial elemental composition of the SZr-500-5/7R *via* EDX analysis

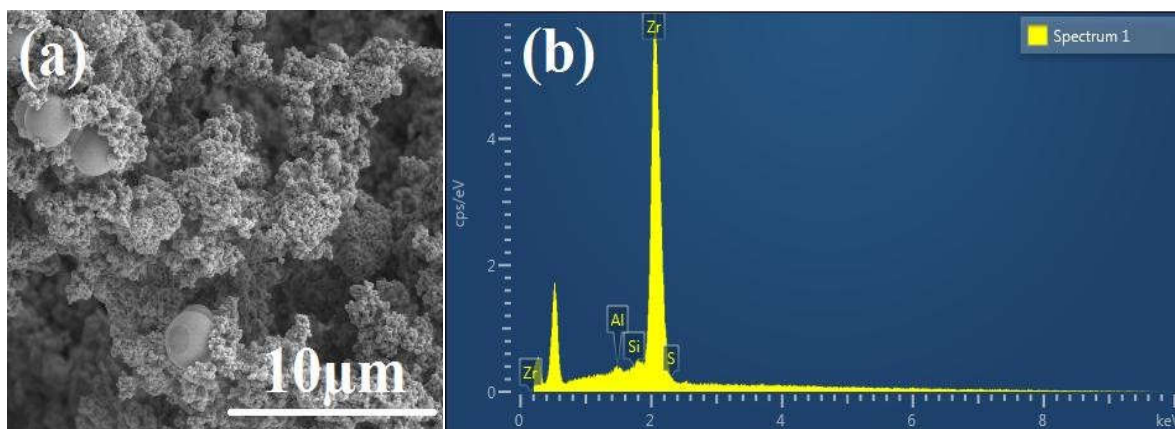


Figure 5.19: (a) Results of the surface microstructural analysis of the SZr-500-5/10 *via* SEM and (b) surficial elemental composition of the SZr-500-5/10 *via* EDX analysis

5.4.3 Ammonia temperature-programmed desorption

Impregnating zirconium with Ti and Yb as described in Section 5.3 above aimed at synthesizing catalytically active materials. The acid strength of the SZ was experimentally investigated by temperature-programmed ammonia desorption (NH₃-TPD) shows representative NH₃-TPD profiles of some of the SZ calcined at 500 to 600 °C. A low-temperature desorption peak with a maximum around 400 °C was detected. Except for SZr-Ti-Yb-500-4/s, the NH₃-TPD thermograms revealed flat and broad NH₃ desorption peaks. These indicate the presence of broad acid sites distribution on the synthesized catalysts. The shapes of the NH₃-TPD profiles were consistent with those reported for comparable mesoporous zirconium-titanium oxide nanospheres (Rezaei et al., 2007 and 2008; Guan et al., 2013). All synthesized materials except SZr-Ti-Yb-500-4/s, exhibited predominantly weak Lewis acids property (Barthos et al., 1996) because Brønsted sites are desorbed at temperatures higher than 400 °C (Zou and Lin, 2004; Das et al., 2003). These authors assigned broad peaks at temperatures below 600 °C as a conglomerate of overlapping component peaks.

The peaks may include ammonia desorption from bound strong Lewis acid sites, NH_4^+ ions decomposition and those released from weak Lewis acid sites. The latter desorption may also include coordinately unsaturated titanium and zirconium ions. The low-temperature peak desorption of bulk titanium oxide is assigned to the weak support interaction which corroborated report by (Mile et al., 1990; Manríquez et al., 2004). However, SZr-Ti-Yb-500-4/s generated strong Lewis and Brønsted acidity from its sulfate groups (Figure 5.20). Evidently, this material possessed more acid sites than the other materials because of its available protons for donation. Table 5.2 presents the strength of the acid sites calculated from the ammonia thermodesorption curves.

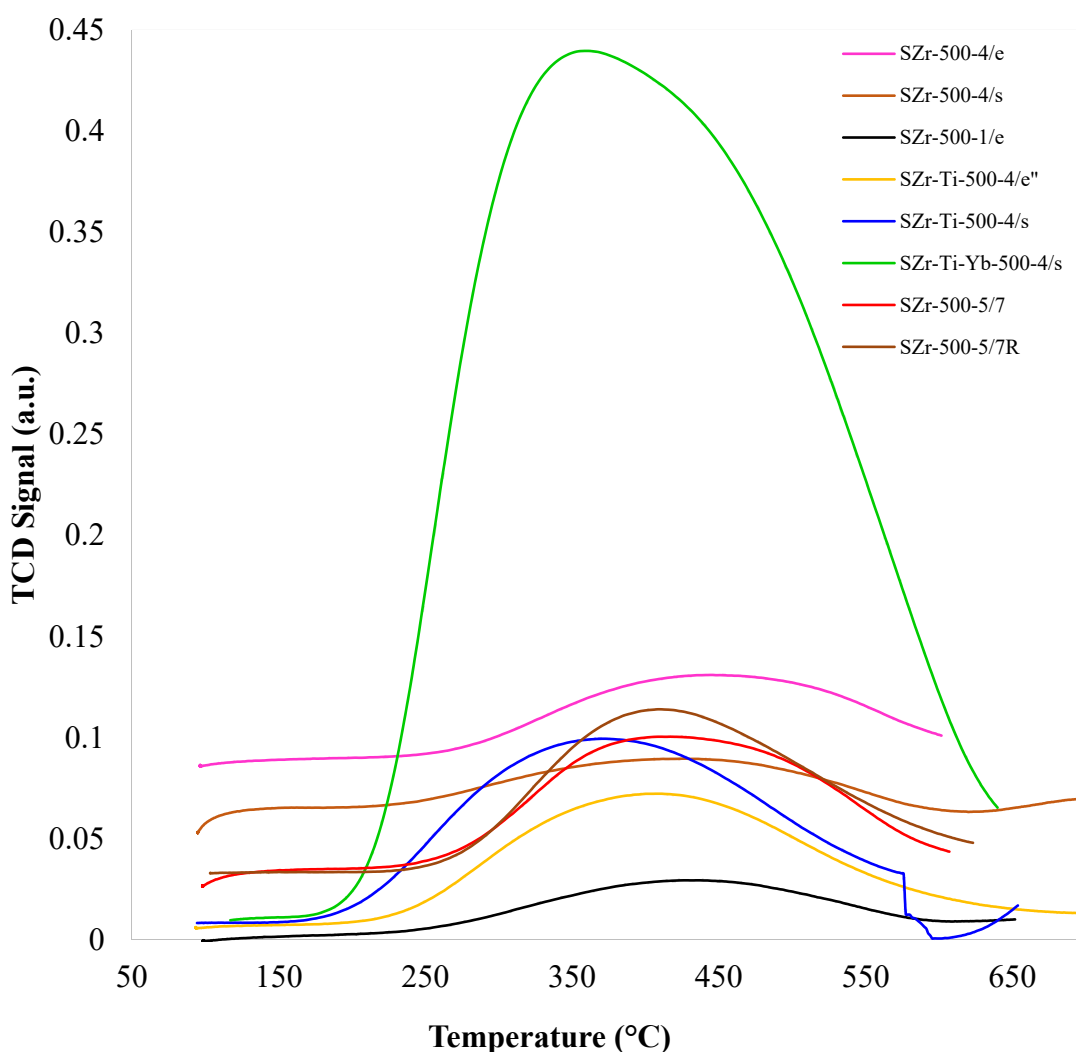


Figure 5.20: NH_3 -temperature-programmed desorption profiles for the synthesized catalysts.

5.4.4 Activity of mesoporous SZ catalysts in transesterifying high FFA-containing feedstock

It is instructive to note that impregnating sulfate onto zirconium oxide produces acidic solid catalysts. The high conversions (Figures 5.21) displayed by the synthesized materials reflect the role of this incorporation. This is despite the moderate S_{BET} values of the synthesized catalysts (Table 5.2). The study attributed acidity of the SZ to the SO_4^{2-} ions on surface acid sites of the materials. This further affirmed the presence of sulfate active sites within the surface structure of the catalysts as reported by Hino et al., (2006). However, the zirconia support provided the essential acid sites (Viinikainen et al., 2009). It is therefore plausible to assert that acidity of materials synthesized in this study have direct correlation to surface hydroxyl groups. Soaking for the same period (15 min) in excess 0.5-M H_2SO_4 led to a decrease in acidity from $(70 \text{ to } 50) \times 10^{-3} \text{ mmol/g}$ and average pore diameter from about 29 to 25 nm.

However, the S_{BET} remained essentially unaffected at $8.33 \text{ m}^2/\text{g}$ for sample (SZr-Ti-500-4/e) prepared in excess acid and $8.12 \text{ m}^2/\text{g}$ for SZr-Ti-500-4/s synthesized in sufficient 0.5-M H_2SO_4 . Similarly, both materials exhibited negligible change in pore volumes (Table 5.2). Expectedly, a TG molecule requires a critical diameter or the smallest access cylinder of 2 to 4 nm (Kiss et al., 2007). Srilatha et al. (2011), reported severe internal diffusion resistance while (López, Goodwin, Bruce, & Lotero, 2005) obtained 57% conversion from SZ with S_{BET} of $134.4 \pm 5.3 \text{ m}^2/\text{g}$.

Premised on underlying difficulty of TG molecules to access inner pores of the catalysts, it is plausible to assert that amount and dispersion of active sites, which are reflective of acidity, are responsible for transesterification activity reported in this study. Furthermore, variation in titanium loading by an order of magnitude did not have significant effect on

the acid site density. These findings agreed with those reported by Viinikainen et al. (2009). Incidentally, S_{BET} increases with aging period (Table 5.2, Figure 5.8). This ensures consequent stabilization and high dispersion of the nano-particles into tetragonal phase. Hence, the observed lower sintering and coking from the catalysts despite their low specific surface area.

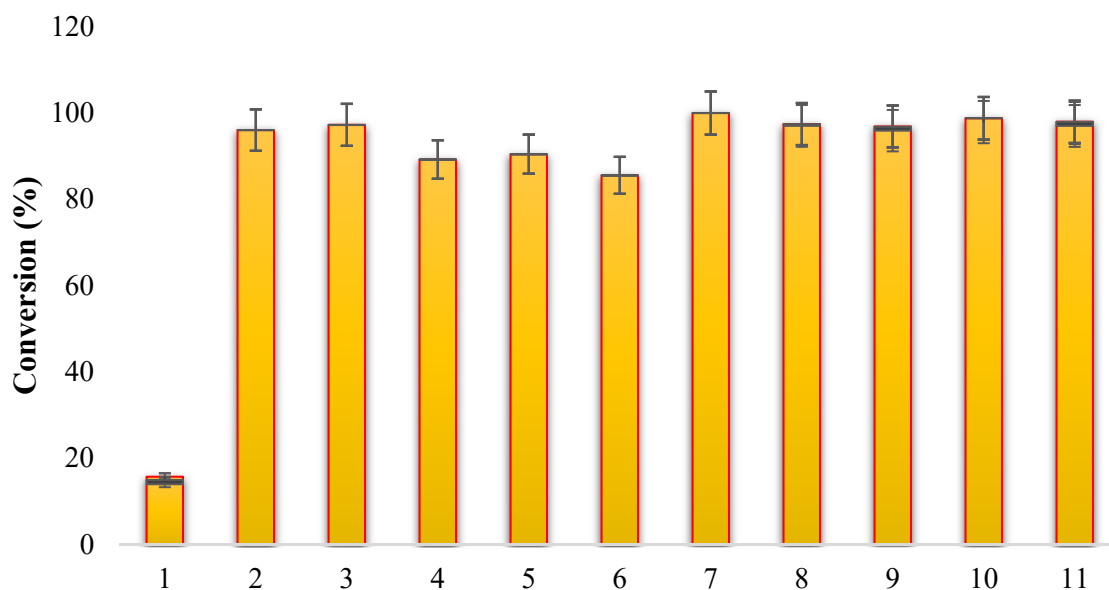


Figure 5.12: Different activity of SZ employed at 200 °C for 5 h (1 = Unsulfated Zr; 2 = SZr-500-4/e; 3 = SZr-500-4/s; 4 = SZr-500-1/e; 5 = SZr-Ti-500-4/e; 6 = SZr-Ti-500-4/s; 7 = SZr-Ti-Yb-500-4/s; 8 = SZr-500-5/7; 9 = SZr-500-5/7R, 10 = Zr-500-5/14, 11 = SZr-500-5/10)

Though all the samples exhibited good performances when evaluated for transesterification of UFO (Figure 5.21), SZr-Ti-Yb/500-4/s displayed higher activity compared to others. We ascribed this to its superior acidity. However, interaction between the tetragonal phase of the zirconia support (facilitated by highly dispersed nanoparticles) and higher mesopores determines the acidity and activity of the SZ. Further, we attributed the high acid-catalyzed activity of the other catalysts to a combination of acidity and the dominant presence of tetragonal phase as shown by the XRD patterns. This indicates that

monoclinic phase does not favor transesterification of UFO as much as tetragonal phase of the evaluated materials. This is in consonance with the report of Ramu, et al. (2004).

Interestingly, the presence of ytterbium facilitated higher specific surface area and acidic sites on the catalysts. However, loading titanium onto zirconia decreases the density of the surface acid sites. Thus, the activity of SZr-Ti-500-1/e, SZr-Ti-500-4/e, and SZr-Ti-500-4/s were comparatively lower than were obtainable from the other catalysts. The difference in chemical composition of the catalytic materials plausibly explains the significant variations in textural and catalytic activities. Incidentally, SZr-Ti-500-1/e displayed the lowest acid density. Thus, for instance, the S_{BET} of SZr-500-5/10 was 15.05 m²/g (97.98% conversion) while SZr-500-1/e with 3.84 m²/g S_{BET} value had a lower conversion of 85.55%. The catalysts were regenerated by decantation, methanol washing, drying, and calcining. Expectedly, compared to the others the catalyst, SZr-Ti-Yb-500-4/s retained most of its activity and displayed better performance after 5 recycles (Figure 5.22). Evidently, Yb-doped SZ ensured the high stability, and good reusability of the synthesized catalyst. This is despite the presence of Ti, which decreases the surface acid sites density. However, as the surface loses its sulfate ions after several cycles, deactivation sets in on the materials.

Transforming feedstocks of low economic value into high yield FAMEs with increased desired product selectivity, and enhanced recycling and reusability opportunities demonstrates the advantage of solid acid catalysts. Incidentally, the strategy of doping SZ with Yb proves economical. It employed moderate reaction conditions such as relatively low catalyst loading, and a 5:1 alcohol-to-oil ratio to convert more than 99% high FFA feedstock. This is interesting when compared with other SZ solid acid catalysts employed under similar condition and feedstock.

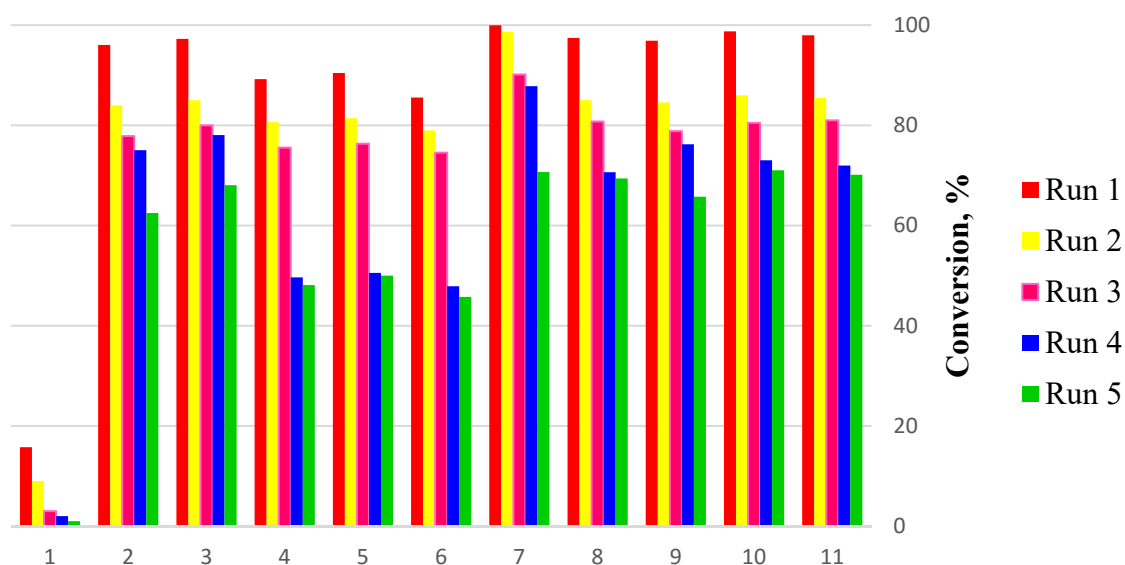


Figure 5.12: Performance of regenerated SZ employed at 200 °C for 5 h (1 = Unsulfated Zr; 2 = SZr-500-4/e; 3 = SZr-500-4/s; 4 = SZr-500-1/e; 5 = SZr-Ti-500-4/e; 6 = SZr-Ti-500-4/s; 7 = SZr-Ti-Yb-500-4/s; 8 = SZr-500-5/7; 9 = SZr-500-5/7R, 10 = Zr-500-5/14, 11 = SZr-500-5/10)

For instance, Park et al. (2008), obtained 70% conversion with WO_3/ZrO_2 ($S_{\text{BET}} = 40 \text{ m}^2/\text{g}$; pore size = 11 nm). Despite the high S_{BET} of 258 m^2/g , Peng *et al.* (2008), achieved 90% conversion with SZr-Ti-Si. This was achieved with a 9:1 methanol-to-oil molar ratio at 200 °C for 4 h and a catalyst loading of 3 wt.%. Conversely, it is noteworthy to mention the result by Feng et al. (2010). The authors achieved 90% conversion cation exchange resin ($S_{\text{BET}} = 77 \text{ m}^2/\text{g}$; pore size = 56 nm) under a low temperature of 64 °C from FFA-containing feedstock. However, the study employed 20 wt.% catalyst after 4 h and 6:1 methanol-to-oil molar ratio.

5.5 Conclusion

In summary, this study demonstrated a facile route for synthesizing efficient solid acid catalysts for transesterifying UFO. Doping SZ with ytterbium is a key feature of this synthesis strategy. The process stabilizes the mesostructured channels and crystallographic phase, and produces high amount and good dispersion of the active sites that ensures higher catalytic performance. The excellent results obtained from this study

highlight the need for further research in this area. Other significant findings include: (1) slight modification in catalyst preparation condition yields different catalytic activity. Such modifications affected the domain size and lattice strain of the material. (2) The observed low specific surface area was probably due to shorter precipitating period. However, the encouraging conversions obtained suggest that activity for transesterification does not depend solely on textural property of the catalytic material. (3) Amount and dispersion of active sites, which are reflective of acidity of SZ, play significant role in facilitating higher conversion of TG into biodiesel. (4) The study also showed how to achieve a flexibility of properties from unlimited number of possible manipulations from one catalyst precursor. These observations highlight the possibility of improving on the reported formulations to facilitate higher intrinsic efficiency in biodiesel production.

CHAPTER 6: FACILE SYNTHESIS OF SULFATED MESOPOROUS Zr/ZSM-5 WITH IMPROVED BRØNSTED ACIDITY AND SUPERIOR ACTIVITY OVER SZr/Ag, SZr/Ti, AND SZr/W IN TRANSFORMING USED FRYING OIL INTO BIODIESEL

This chapter describes the synthesis and characterization of a new sulfated Zr/ZSM-5 with improved Brønsted acidity. It compared its activity with SZr/Ag, SZr/Ti, and SZr/W for the transesterification of used frying oil to biodiesel. This was presented as Article 4: *Facile synthesis of sulfated mesoporous Zr/ZSM-5 with improved Brønsted acidity and superior activity over SZr/Ag, SZr/Ti, and SZr/W in transforming UFO into biodiesel.* This study investigated an innovative approach of enhancing acidity of SZ composite catalysts that could withstand unfavorable constituents such as high percentage of high free fatty acid. This was premised on the basis of the interplay between metal function of modified oxo-anions and pore structure of zeolites and its strong acidic properties. The Journal of Taiwan Institute of Chemical Engineers has accepted this study for publication as a research article.

6.1 Introduction

As the price of Brent oil plummeted below USD40/barrel in the third quarter of 2015, the prominence, and sustenance of biofuels in general, and biodiesel in particular, faces greater challenges. The heavily footed subsidy that fossil fuels enjoy from governmental agencies exacerbates this problem further. Consequently, for biodiesel to maintain its indomitability as sustainable energy alternative beyond the 21st century, urgent and concerted efforts must be initiated from reactor engineering and catalysis (Hassan, Sani, Abdul Aziz, Sulaiman, & Daud, 2015). From materials chemistry perspective, many studies have investigated the performances of a wide range of bifunctional solid acids

catalysts such as WO_3/ZrO_2 (Guldhe et al., 2014), WO_3/SnO_2 (Xie and Wang, 2013), $\text{Mo-Mn}/\text{Al}_2\text{O}_3$ -15 wt% MgO (Farooq et al., 2013), WO_3/ZrO_2 (Furuta et al., 2004; Park et al., 2008), and $\text{SO}_4^{2-}/\text{TiO}$ (Refaat, 2011) designed to incorporate synergetic effect in catalysis. However, despite the capability of converting different feedstock oils to FAME, there is need for improvements.

For instance, WO_3/SnO_2 required 43 methanol-to-oil ratio to achieve a 78% yield (Xie & Wang, 2013), WO_3/ZrO_2 gave $\sim 100\%$ conversion after 20 h at 200 °C (Furuta et al., 2004) and 70% conversion from used frying oil, UFO (Park et al., 2008). Similarly, the difficulty in synthesis and high production cost of $\text{SO}_4^{2-}/\text{TiO}$ hinder its industrial application (Refaat, 2011). WO_3/ZrO_2 converted more than 90% soybean oil during transesterification at 250 °C (Furuta et al., 2004) while $\text{SO}_4^{2-}/\text{TiO}$, $\text{SO}_4^{2-}/\text{ZrO}$ and WO_3/ZrO_2 converted 100, 99, and 94% n-octanoic acid respectively during esterification at 175 °C. In addition, longer reaction time (2047 min) was necessary for obtaining 50% conversion with tungstated zirconia with the acid site densities exhibiting ca. 95% of the original values. The long duration promoted adsorption of intermediates and products with subsequent deactivation.

Conversely, some results obtained from transesterification with zeolites were not as encouraging. For instance, despite high alcohol-to-oil molar ratio (14.5:1), Shu et al. (2007), reported only 48.9 wt.% conversion into fatty acid methyl esters, FAME after 4 h with zeolite beta modified with La^{3+} . Equally, Mordenite (HMOR) and H^+ ion exchanged ZSM-5 (HMF1) zeolite catalysts (Chung and Park, 2009) converted 80% of oleic acid with > 0.06 mmol/g acid amount to biodiesel. High reaction temperature of 500 °C was necessary to achieve ca. 100% conversion over H-ZSM5 [$S_{\text{BET}} = 377 \text{ m}^2/\text{g}$, acidity density = $382 \text{ } \mu\text{mol/gcat}$] after 20 min (Danuthai et al., 2009). Consequently, Kiss, et al. (2006),

posited that lower catalytic activity of zeolites is due to the small pores that limits diffusion of large fatty acid molecules. However, (Dasari et al., 2003) obtained 95% conversion without catalyst, albeit at high pressures of 45 – 65 MPa and high temperatures of 350 – 500°C. Nonetheless, (Sasidharan and Kumar, 2004) were able to obtain 85% and 80% conversion from beta-keto esters with solid acid La-Beta and H-Y zeolites respectively. Evidently, the nature of the oil employed by (Sasidharan and Kumar, 2004) also contributed to the encouraging results. Moreover, the high-silica in Zeolite Socony Mobil-5, ZSM-5 [Mordenite framework inverted (MFI) type and a member of the pentasil family] gives it special properties. Depending on the Si/Al ratio, ZSM-5 is moderately hydrophilic to highly hydrophobic unlike types A, X and Y zeolites, which are very hydrophilic. Another important factor that ensures this desirable property is the type and number of cations compensating the lattice charge. Further, the hydrogen form is obtainable without losing significant Al directly *via* zeolite exchange in dilute acid because of its acid (down to pH = 3) and temperature (> 1000°C) stability.

Further, the acidity of crystalline aluminosilicate zeolites may be fine-tuned by appropriate manipulation of SiO₂/Al₂O₃ molar ratio. Such manipulations have significant effect on the activity (i.e. the hydrophobicity and acidity of the zeolite), performance, and its affinity for water. Interestingly, the structure of ZSM-5 also allows the introduction of alternative T-atoms such B, Be, Al, Si, Ga, Fe, Ge, etc. during synthesis (Breck, 1974). The nature of positive simple counter-ions from these T-atoms also determines the acidic catalytic power of the zeolite. Thus, its catalytic properties are amenable to adjustments for the desired catalytic process, which include interchanging other elements within the framework constituents, or by modifying the zeolitic material. These intriguing attributes of ZSM-5 explain its acceptability as efficient catalytic material with wide range of applications in the laboratory as well as the industry. However, these advantages do come

with attendant problems. These include deactivation and a drop in conversion from reaction of organic species catalyzed by zeolite with lower Si/Al ratio, which causes higher affinity towards water.

However, despite the numerous encouraging results highlighted above, attendant viscosity and poor miscibility of light alcohols with low-grade oil feedstocks hampers the use of new heterogeneous catalysts. This explains why to date, the wide range of commercially available polymeric and inorganic solid acids have lower activity when compared with their base-catalyzed routes (Lotero et al., 2005). This necessitates the application of higher reaction temperatures to achieve appreciable conversions. Other limitations include rapid on-stream deactivation because of impurities in high concentrations, such as moisture, acid, and heavy metals.

Aside these arduous challenges, regional availability is another contending issue that determines the quest and cost for utilizing non-edible, low grade oil sources. Notwithstanding their comparable lower activity, solid acids are less susceptible to FFA contaminants common with unrefined feedstocks than their solid base equivalents (Lotero et al., 2005). Moreover, they are able to simultaneously esterify free fatty acids, FFA into esters and transesterify triglycerides, TG into FAME without pretreatment, and saponification; thus minimizing the processing steps in biodiesel production (Narasimharao et al., 2007; Suwannakarn, et al., 2009; Kouzu, et al., 2011). Intriguingly, zirconium is active at lower temperatures than zeolite catalysts, while zeolite is generally more acidic than zirconia. Notwithstanding this and the extensive research on the factors affecting the acidity of sulfated zirconia, SZr there is no information in open literature that concerns biodiesel production with mesoporous SZr dispersed over ZSM-5. Consequently, the present contribution aims to demonstrate the superiority of mesoporous

sulfated zirconia comprised of Brønsted acid sites dispersed on ZSM-5 over Ag, Ti and W supports. To achieve this, the present study investigated an innovative approach of enhancing acidity of sulfated, robust bifunctional composite catalysts that could withstand unfavorable constituents highlighted above. This was premised on the basis of the interplay between metal function of modified oxo-anions and pore structure of zeolites and its strong acidic properties.

6.2 Literature review

Seemingly, depending on which factors one considers, the debate surrounding the super acidity or otherwise of SZ is unending. This is because it is not possible to exclude the presence of other planes or defects sites from the structure. However, the complete dissociation of strong H_2SO_4 on a strong zirconia basic surface to produce sulfate ions should not be surprising.

6.2.1 Superacidity of SZ and other modified aluminosilicate catalysts

Consequently, deprotonation will always occur within accessible basic sites, producing the very strong surface acids (hydroxyl groups) on the surface of the zirconia. Yet, Haase and Sauer (1998) showed from the Brønsted site deprotonation energies that zeolite is more acidic than these sites. This was the reason Fărcașiu et al. (1996) concluded that the exceptional catalytic activity of SZ stems from its redox properties rather than its acidity. Thus, the debate persists. On the other hand, Ward and Ko (1994), proposed structures of both Brønsted and Lewis acid sites on sulfated zirconia as shown in Figure 6.1.

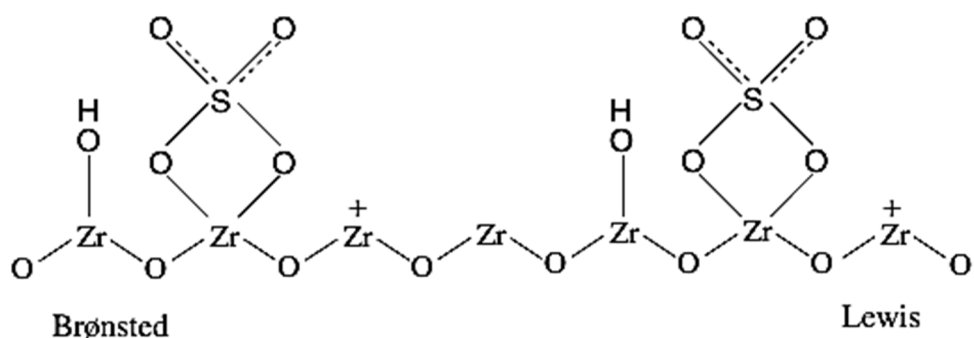


Figure 6.1: Presence of Bronsted and Lewis acid sites on SZ (Ward and Ko, 1994).

Wang and Mou (2008), classified SZ species into three:

- 1) Based on the number of directly bonded oxygen, Lewis acid sites with most electron deficiency exhibit the highest binding energy. These are species type-1.
- 2) These species have middle value of binding energies similar to the binding energy of Zr-O-Zr because they are located at Zr center bonded to a sulfate or Al-O-. They are termed as species type-2.
- 3) The species type-3 possesses lesser binding energy. Consequently, Brønsted acid sites Zr-OH are species 3 because of the presence of acidic H in Zr-OH. Thus, neighboring Zr-OH and sulfate groups serve as good points for the formation of Brønsted acid sites.

Therefore, the sum of specie 2 and 3 determines the amount of Brønsted acid sites on the surface. This is because alumina loading decreases the ratio of Lewis acid to Brønsted acid sites as Al substitution of Zr-OH sites eliminates Lewis acid sites as well as generates stronger Al-OH Brønsted acid sites.

A threefold consequence is possible with alumina addition:

- (1) Al-content facilitates only moderate increase in the amount of surface acid as revealed from NH_3 -TPD results. This implies that change of acidic properties causes the increased activity.
- (2) Type of acidity distribution changed despite the moderate increase on the amount and strength of acidity upon Al-loading. For instance, the formation of more Brønsted acid sites because of the elimination of Lewis acids by Al^{3+} and surface binding of Al to zirconia enhances the activity of catalysts (Kim et al., 2006). Similarly, Cerrato et al. (2006), independently, derived the same conclusion on Ga-promoted sulfated zirconia system.
- (3) High Al-loading affects the degree of dispersion of zirconia. Highly dispersed zirconia monolayer may be less active in catalysis.

The weakening of the O–H bond by the neighboring sulfate group produces Brønsted acid sites on sulfated zirconia-alumina, SZA. Contrarily, the electron-withdrawing by the neighboring sulfate group, which coordinates deficient Zr(IV) center produces Lewis acid sites (Ward and Ko, 1994). The summary of the foregoing observations is that activity enhances as sulfur content increases because of the initial Al-loading. Nevertheless, the initial favorable formation of carbenium ions (high activity) with increased Brønsted acid sites formation could turn out unfavourable with extensive Al-loading. This is because excessive dispersion of monolayer zirconia reduces the activity to a lesser value compared to the sulfated tetragonal zirconia nanoparticles (Wang and Mou, 2005). It is therefore worthy to mention the findings of Kim et al. (2006). The authors found that average residence time of the reaction intermediate increases significantly upon adding Al with consequent increase in activity. Zalewski et al. (1999) posited the possibility that Al-loading causes surface defects, which facilitates the adsorption of butane intermediates.

Furthermore, the hydrogen environment enhances the catalytic stability while carbene fragments accumulating on the surface aids catalyst deactivation. The implication of this is the need for adjusting the hydrogen partial pressure to achieve optimum stability.

6.2.3 Sulfated zirconia supported on zeolite – the way forward?

Sulfated zirconia (SO_4^{2-}/ZrO_2 , abbreviated as SZ) is gaining considerable attention more than most other solid acid catalysts. This is because the activity and selectivity of SZ in transforming hydrocarbons at low-temperature is higher than what is obtainable from its counterparts (Song and Sayari, 1996; Davis et al., 1994). Further, sulfated zirconia is more environmental friendly compared to liquid acid catalysts such as HF and H_2SO_4 . However, controlling the textural properties of SZ synthesized *via* conventional routes is difficult. This explains the observation by (Corma et al., 1994) that surface area of active SZ in the tetragonal crystalline phase is less than $100\text{ m}^2/\text{g}$. Further, available specific surface area and degree of surface sulfation limit the concentration and number of active sites of SZ. Moreover, the degree of dispersion is one of the most important factor that affects the performance of the solid acid catalysts. This is because it affects the density and number of active sites on the catalytic material. Large surface area on ordered mesoporous materials facilitates the dispersion and decomposition of a large amount of zirconium sulfate to form tetragonal sulfated zirconia nanoparticles. Consequently, the nanochannels of ZSM-5 could restrict large zirconia nanoparticles. Therefore, synthesizing ZSM-5 supported on SZ without steric limitation is a feat worth exploring.

6.3 Materials and methods

The following describes the easy, and undemanding catalyst preparation employed for this study. Sigma-Aldrich, Germany supplied all chemical reagents. To ensure reproducibility, all sample preparations were carried out in replicates.

6.3.1 Catalyst preparation

A required amount of ammonium hydroxide solution precipitated the active constituents from zirconium oxynitrate hydrate (99%) at pH of 10 under vigorous stirring. Subsequently, the filtrate was washed with de-ionized water to minimize the nitrate ion concentration. For comparison and optimization, about 2.5 to 25% each of AgNO_3 ($\geq 99.0\%$), titanium nitride (TiN ; $< 3\ \mu\text{m}$), ammonium metatungstate hydrate, $(\text{NH}_4)_6\text{H}_2\text{W}_{12}\text{O}_{40}\cdot x\text{H}_2\text{O}$ (99.99% trace metals basis), and ZSM-5 ($\text{Si}/\text{Al} = 20.01$) were separately soaked in the precipitated zirconium solution at ambient conditions for 4 h. The solution contained exact amount of liquid which filled the pore volume of the support. This facilitated good contact (impregnation) between the metal precursors and the porous support. The supernatant was decanted after proper saturation and infusion of the metal elements. Thereafter, sufficient (not in excess) 0.5-M H_2SO_4 was added to the impregnated mixed oxides, and kept at room temperature to ensure the incorporation of appropriate doubly charged sulfate oxo-anions. After drying in an oven at $120\ ^\circ\text{C}$ for 24 h, the samples were calcined separately at $550\ ^\circ\text{C}$ for 4 h. This process was optimized and catalytic materials were designated SZr/Ag, SZr/Ti, SZr/W, and SZr/ZSM-5. The following discussion would mainly be regarding these four samples, and in some instances, in comparison with the ZSM-5.

6.3.2 Catalyst characterization

Field emission scanning electron microscopy (FE-SEM) FEI QUANTATM 450 FEG type 2033/14 (Czech Republic) unit with 30 kV accelerating voltage analyzed the surface morphology and topology. An energy dispersive X-ray spectrometer (EDX) from the same unit revealed the surface elemental composition variation of the catalysts. The samples were evenly distributed on a double sided, black carbon tape glued on an aluminum stub and put under vacuum for 10 min prior to the analysis. Similarly, powder

XRD and BET analyses elucidated the structural and textural properties of the catalysts respectively. Phillips X'pert diffractometer (The Netherlands) with $\text{CuK}\alpha$ radiation ($\lambda = 1.54056 \text{ \AA}$) at a scanning speed of $0.05^\circ \text{ s}^{-1}$ within 2θ range of 5 to 70° at 40 mA and 40 kV analyzed the XRD patterns, the crystal phase and structure of the samples. A Micromeritics TriStar II (USA) with accelerated surface area porosity (ASAP) 3020 at -196.15°C in liquid nitrogen, determine the specific surface area, pore size and the pore volume of the catalytic materials. Degassing the catalysts at 120°C for 3 h under a vacuum eliminated any physisorbed volatiles and impurities. These were kept in liquid nitrogen temperature for nitrogen adsorption.

An AutoChem 2920 (Micromeritics) evaluated the acid density profiles *via* ammonia temperature-programmed desorption (NH_3 -TPD). Calibrating the equipment with $10\% \text{ NH}_3$ in He before the analysis guarantees ascertaining the exact amount of gas consumed during the experiment. For each analysis, He flow (20 mL/min) for 1 h at 700°C degasses about 0.10 g of the synthesized material housed in a quartz U-tube. After cooling to 80°C , $10\% \text{ NH}_3$ in He flowing at 20 mL/min for 40 min saturates the sample. A steady temperature ramp of 120°C ensured proper NH_3 adsorption. Changing the gas flow to He at 20 mL/min for 30 min over the catalyst removed the physisorbed NH_3 . Elevating the temperature ramp from 80°C to 700°C at 10°C/min under flowing He at 20 mL/min after the baseline stabilizes produces distinct TPD profile. Similarly, the TCD detector revealed the amount of NH_3 consumed, which determines the acid strength of the Brønsted and Lewis acid sites on the catalysts. IR spectra of adsorbed pyridine were taken on a Bruker Fourier transform infrared (FT-IR) Tensor 27 spectrometer (Germany). The apparatus has a spectral range of 7500 to 370 cm^{-1} with more than 1 cm^{-1} apodized resolution and a standard ATr beam splitter. The samples were outgassed at 300°C for 4

h under vacuum, and cooled to room temperature. Pyridine was then admitted into the samples and the IR spectra of adsorbed pyridine were recorded at room temperature.

6.3.3 Production of fatty acid methyl esters

Heating the catalysts at 200 °C for 1 h before the reaction ensured activation by evacuating any adsorbed water and other volatiles. Thereafter, the catalytic activity of the catalysts in simultaneous esterification and transesterification of UFO (FFA = 48 wt.%) with methanol was determined in a 100 mL autoclave stainless-steel reactor supplied by AmAr Equipment Pvt., Ltd. (Mumbai). Constant stirring at 550 rpm ensured good contact between the catalyst and the reaction mixture. A water bath attached to the autoclave maintained the reaction temperature in the range of 190 – 200 °C during the reaction. Preliminary optimization showed that a 5:1 methanol-to-oil molar ratio and 2 wt.% catalyst loading were optimal for the reaction. At the end of the 5 h reaction time, it took more than 6 h for the product [ester or oil phase (biodiesel) and the upper aqueous phase (glycerol)] to settle into two distinct layers because of the initial translucent nature of biodiesel. The two distinct phases were separated by simple decanting. Centrifugation, water washing, and drying with anhydrous sodium sulfate facilitated the recovery of the FAME by purifying it from excess methanol and other impurities such as residual catalyst.

The study employed GC-MS (Serial # CN10946045; Model 7890A; US), and EN 14103:2003 (E) analytical method in determining methyl ester contents with 100-mg neat mixture (Supelco® No. 18919) containing 37 components (C₄ to C₂₄ FAMES; 2 to 4% relative concentration) as reference standard. This was dissolved in 99% heptane at 0.01 to 0.10% (w/v) concentration. Then, 1 mL hexane placed in vials with screw caps having PTFE-faced septa dissolves an accurately weighed 10 mg sample, prior to the addition of

10 μL of 2 N KOH in methanol. After vortex for 30 s, and centrifugation, one μL of the supernatant was transferred into TSP micro vial. The GC analyzer has the following working conditions: DB 23 column ($L = 0.30 \text{ mm} \times \text{ID} = 0.32 \text{ mm} \times 0.25 \text{ }\mu\text{m}$ film thickness of 5% diphenyl, 95% dimethyl polysiloxane) and methyl heptadecanoate, C_{17} (99% minimum purity; 14 min retention time) as the internal standard; 210 $^{\circ}\text{C}$ injection temperature and helium as carrier gas. Equation 6.1 facilitated the determination of the ester content (C), expressed as a mass fraction in percentage.

$$C = \frac{(\sum A) - A_{E1}}{A_{E1}} \times \frac{C_{E1} \times V_{E1}}{m} \times 100\% \quad (6.1)$$

Where: $\sum A$ is the total peak area from the methyl ester in C_{14} to that in $\text{C}_{24:1}$;

A_{E1} is the peak area corresponding to methyl heptadecanoate;

C_{E1} is the concentration of the methyl heptadecanoate, in mg/mL ;

V_{E1} is the volume of the methyl heptadecanoate, in mL ;

m is the mass of the sample, in mg .

6.4 Results and discussion

The following discussion concerns the various characterization such as NH_3 -TPD, IR spectroscopy, and structural analyses performed on the catalysts to ascertain which properties have significant influence in converting the UFO into FAMEs.

6.4.1 Results of catalyst characterization

6.4.1.1 Surface acid density measurement *via* NH_3 -TPD

Temperature-programmed ammonia desorption, NH_3 -TPD revealed information regarding the distribution and type of acid sites on the catalysts (Table 1). Figures 1(a) and 1(b) show representative NH_3 -TPD profiles of the parent ZSM-5, and SZr/W,

SZr/Ag, and SZr/Ti modified catalysts calcined at 550 °C for 4 h. We classified the acid sites corresponding to base desorption at 100-240 °C, 240-340 °C, and 340-500 °C as weak, intermediate, and strong acid sites, respectively. The peak pattern of modified SZr/ZSM-5 reveals similar profile as the parent ZSM-5. Expectedly, the parent ZSM-5 contained 5-fold more acid number than the composite SZr/ZSM-5, and even more than the other mixed oxides. The probable explanation for the significant decrease in the acidity of the SZr/ZSM-5 is the combining effect of the hydroxyl Al(OH)Si bridging groups with ZrO₂ species (Kaeding & Butter, 1980). However, SZr/ZSM-5 exhibited higher acidity than the other materials because of its available protons for donation. Notably, SZr/W generated strong Brønsted and Lewis acidity because of the extensive polymerization of W species from its sulfate groups. This explains the difference between SZr/W and SZr/Ag, SZr/Ti. However, SZr/W, SZr/Ag, and SZr/Ti have comparable acidity. Except for SZr/Ti (flat and broad), the NH₃-TPD curves revealed sharp NH₃ desorption peaks. This indicated the presence of broad acid sites distribution on the synthesized catalysts. The shapes of the NH₃-TPD profiles were consistent with those reported for comparable mesoporous zirconium titanium oxide nanospheres (Zou and Lin, 2004; Rezaei et al., 2007 and 2008; Guan et al., 2013).

Table 6.1: Textural properties and acidity of synthesized sulfated zirconia revealed by BET and NH₃-TPD methods respectively.

Sample ID	Surface area (m ² /g)	Pore vol. (cm ³ /g)	Pore size (nm)	Acidity (mmol/g)
ZSM-5	385.20	0.154	3.04	3.71176
SZr/ZSM-5	107.25	0.116	5.10	0.75187
SZr/Ag	15.97	0.080	20.11	0.13572
SZr/Ti	12.90	0.046	14.53	0.08604
SZr/W	72.13	0.097	5.37	0.04783

The source compounds that supply aluminum during the synthesis of zeolites determine the acidity of mesoporous zeolites. Similarly, zeolite type, Si/Al ratio, and metal loading have significant effect on both total acidity (mmol/g) and the acid strength distribution of

the catalyst. This explains the high acidity (3.71 mmol/g) of the source ZSM-5 employed in the present study. Incidentally, (Čejka, et al., 1995) reported higher acidity of 4.99 mmol/g for H-ZSM-5 (Si/Al ratio = 36; average crystal size = 6 μm). Further, (Song et al., 1996) obtained similar total acidity (2.42, 1.53, 2.90, and 3.12 mmol/g) from [sodium aluminate (Si/Al ratio = 49), H-mordenite (Si/Al ratio = 21.0), HY-2 (Si/Al ratio = 5.0), and HY-2 (Si/Al ratio = 5.0)] respectively. Markedly, all synthesized materials, except SZr/Ag and SZr/W, predominantly exhibited the weak Lewis acid property. This is because Brønsted sites get desorbed at temperatures higher than 400 °C. Zou and Lin (2013), and Das et al., (2003) assigned broad peaks at temperatures below 600 °C to a conglomerate of overlapping component peaks. These peaks may include ammonia desorption from bound strong Lewis acid sites, NH_4^+ ions decomposition and those released from weak Lewis acid sites. The latter desorption may also include coordinately unsaturated titanium and zirconium ions.

A notable increase in the number of acid sites was observed in the mixed oxide catalysts compared to single oxide SZr. The low-temperature peak desorption of bulk titanium oxide is representative of the weak support interaction, which corroborated a report by Manríquez et al., 2004 that mixed oxides generate more acid sites than single oxides. This is premised on one of two mechanisms; (a) zirconium atoms substituting some of the oxide atoms or (b) large dispersion effect on the surface of the mixed oxide by the ZrO_2 or the other oxide. The strength of the acid site density was in the following order: ZSM-5 > SZr/ZSM-5 » SZr/Ag > SZr/Ti > SZr/W. This sequence highlights the natural acidity of ZSM-5 in comparison to the generated Brønsted acid sites on the other mixed oxides introduced by sulfate anions on the surface of the catalysts. The discussion in the results section further illustrated the effect of acid strength on the activity of the simultaneous esterification of FFA and transesterification of TG. Mostly, infrared adsorption

experiments with basic probe molecules such as ammonia, pyridine, and acetonitrile differentiate Brønsted or Lewis acid sites.

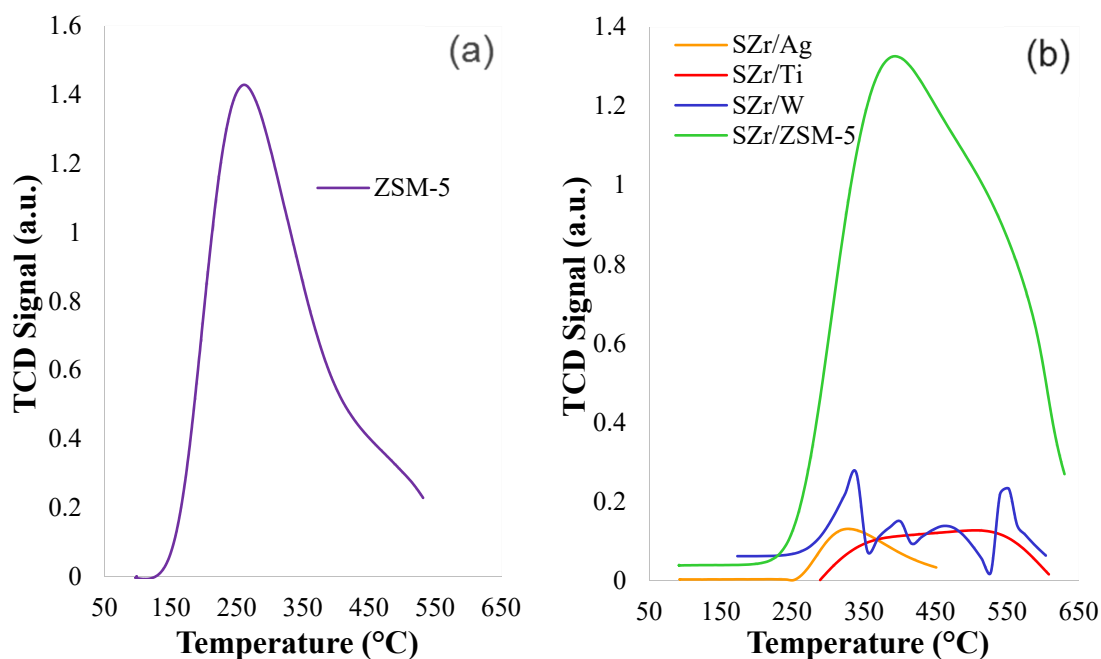


Figure 6.1: (a) NH₃-temperature-programmed desorption profiles for the parent ZSM-5, and (b) SZr/Ag, SZr/Ti, SZr/W, SZr/ZSM-5 synthesized catalysts.

However, the measurement conditions employed such as desorption temperature, determine the results of the analysis. Further, the adsorption of ammonia is not specific to Brønsted sites. These highlight the possibility of non-Brønsted sites adsorbing more, and hence exhibiting stronger acidity than Brønsted sites. Hence, TPD results are helpful, but with careful interpretation of data. Evidently, no single method can give all the details of the acidity of solid acid catalyst. For example, (Jacobs and Von Ballmoos, 1982) distinguished the Brønsted sites in H-ZSM-5 by a well-defined stretching frequency, 3605 cm⁻¹ while (Ward, 1969; Angell and Schaffer, 1965) distinguished those in H-Y by 3640 and 3540 cm⁻¹ stretching. Nonetheless, it is difficult to quantify the concentrations of these sites because of the overlapping features in the spectra. Evaluating the concentration of the protonated bases in the solid is one way of circumventing this challenge. The

characterization of pyridine adsorption by infrared spectroscopy is one most popular application of this technique (Parry, 1963). Therefore, this study employed NH₃-TPD and IR – Spectroscopy of chemisorbed pyridine to get accurate picture about the acidity of the synthesized catalysts.

6.4.1.2 Acid density probed by IR – spectroscopy of chemisorbed pyridine

Pyridine adsorption measured by IR spectroscopy revealed the strength and types of acid sites of catalysts. The formation of stoichiometric adsorption complex on the acid sites by pyridine makes this acid measurement distinctive. Pyridine accepts proton to form pyridinium ion on the Brønsted sites whereas an adduct forms at the Lewis sites by donating lone pair of electrons. Partial hydrolysis of some framework aluminum atoms occurs after steam treatment at 300 °C to form non-tetrahedral symmetric aluminum atoms. These act as strong electron withdrawal centers for the remaining tetrahedral framework aluminum atoms that facilitate the formation of stronger Brønsted acids. Further, the technique exploits the modification in chemical nature of the adsorbed species. Moreover, the pyridine adsorbed on Brønsted sites and Lewis sites have different wavenumbers because of difference in bonding nature. The ring stretching vibration at ca. 1540 (1515–1565 cm⁻¹) and 1450 cm⁻¹ (1435–1470 cm⁻¹) to protonated pyridine, *i.e.* pyridinium cation (Brønsted acid sites) and coordinated pyridine (Lewis acid sites) appear, respectively. Figure 2 presents the acidity distribution (variation of IR bands in 1400–1700 cm⁻¹ region) of ZSM-5, SZr/ZSM-5, SZr/Ag, SZr/Ti, and SZr/W.

Expectedly, the parent ZSM-5 exhibited stronger sites of both Brønsted and Lewis acids than the remaining four samples. The profiles of synthesized catalytic materials reveal similar patterns as the parent sample. The trend of the Brønsted acid site strength was similar to the one obtained by NH₃-TPD in the following order: ZSM-5 > SZr/ZSM-5 > SZr/Ti > SZr/Ag > SZr/W. However, the trend was different for the Lewis acid site

strength in the following order: ZSM-5 > SZr/ZSM-5 > SZr/Ag > SZr/Ti > SZr/W. The three prominent bands in the 1425–1575 region are representative of: (a) the C–C stretch at $\sim 1450\text{ cm}^{-1}$ arising from a coordinatively bonded pyridine complex that designates the presence of Lewis sites. (b) The C–C stretching vibration of the pyridinium ion at $\sim 1540\text{ cm}^{-1}$ that is typically used for identifying Brønsted sites. (c) The peak at $\sim 1490\text{ cm}^{-1}$ formed from the interaction of pyridine species with both Brønsted and Lewis acid sites. All the samples exhibited the IR bands due to hydrogen-bonded pyridine at 1447 cm^{-1} , but only the parent ZSM-5 and modified SZr/ZSM-5 showed peaks at 1599 cm^{-1} . This is because of the difference in the Si/Al ratios of the samples. Similarly, the peaks at 1455 and 1623 cm^{-1} exhibited by all the samples indicate pyridine adsorbed on Lewis acid sites, while those at 1533 and 1647 cm^{-1} highlight pyridine adsorbed on Brønsted acid sites. Pyridine associated with both Lewis and Brønsted acid sites appear at 1490 cm^{-1} . Previously, Jin and Li, 2009; Emeis, 1993 reported similar analysis on the distribution of acid sites (Table 6.2).

Table 6.2: Wave number frequencies and extinction coefficients of IR absorption spectra designated to typical probe molecules adsorbed on acid sites (Emeis, 1993; Suzuki et al., 2007)

		Brønsted	Lewis
Ammonia	Frequency (cm^{-1})	1460	1620
	IR mode	$\delta(\text{NH}_4^+)_{\text{asym.}}$	$\delta(\text{NH}_3)_{\text{asym.}}$
	Extinction coefficient (ϵ)	$14.7\text{ m}^2\text{ mol}^{-1}$	$2.2\text{ m}^2\text{ mol}^{-1}$
Pyridine ($\text{C}_5\text{H}_5\text{N}$)	Frequency (cm^{-1})	1540	1450
	IR mode	Ring stretch (PyH^+)	Ring stretch (Py)
	Extinction coefficient (ϵ)	$0.72\text{ m}^2\text{ mol}^{-1}$	$2.23\text{ m}^2\text{ mol}^{-1}$
D3-cetonitrile (CD_3CN)	Frequency (cm^{-1})	2297	2325, 2310
	IR mode	$\nu(\text{C}\equiv\text{N})\text{-B}$	$\nu(\text{C}\equiv\text{N})\text{-L}_{\text{strong, weak}}$
	Extinction coefficient (ϵ)	$2.05\text{ cm}\mu\text{mol}^{-1}$	$3.60\text{ cm}\mu\text{mol}^{-1}$

Evidently, the acidity of the materials determined by NH_3 -TPD supersedes that of their counterparts determined by the pyridine adsorbed IR method. This is plausibly because of the differences in the molecular size of the basic probe molecules. Ammonia molecule penetrates through more pores because of its smaller molecules than the larger molecules

of pyridine (Lu et al., 2003). Table 2 presents a summary of the frequencies and reported extinction coefficients assigned to adsorbed species on acid sites.

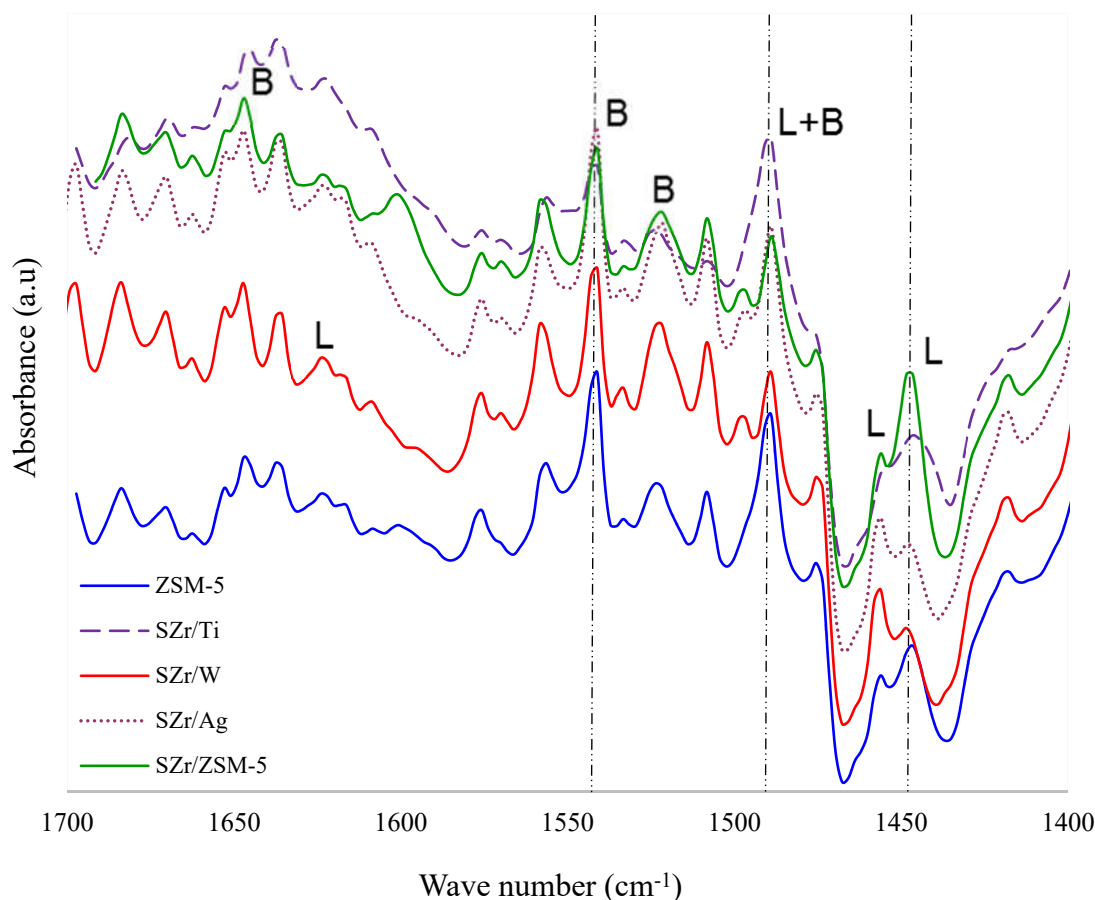


Figure 2. Room-temperature infrared spectra of adsorbed pyridine on ZSM-5, SZr/ZSM-5, SZr/Ag, SZr/Ti, and SZr/W after outgassing at 300 °C for 4 h.

6.4.1.3 Powder X-ray diffraction analysis

The highly crystalline characteristic peaks at 2θ value of 7.87, 8.81, 23.09, 23.86, 24.34, 29.20 and 29.88 confirmed ZSM-5 support according to the JCPDS Card No. 00-044-0002 (Pan et al., 2014). The powder X-ray pattern peaks of the ZSM-5 showed typical MFI topology, whereas the modified SZr/ZSM-5 patterns indicated retained ZrO_2 crystallinity and novel crystalline phases (Figure 6.2). The loss of intense ZSM-5 peaks was due to the effects of acid treatment, ZrO_2 and ZSM-5 inter-particle interaction and calcination during the synthesis stage as earlier noted. This indicates that ZrO_2 species were not merely dispersed on the zeolite, but might have replaced some of the alternative

T-atoms. This interaction resulted in the almost disappearance of peaks with high intensities around $2\theta = 7^\circ, 8^\circ, 23^\circ$ and 24° , and emergence of typical zirconium peaks at $28^\circ, 30^\circ, 50^\circ$ and 60° . This further confirmed that ZrO_2 particles were not merely dispersed but rather, caused changes in the lattice structure of the zeolite.

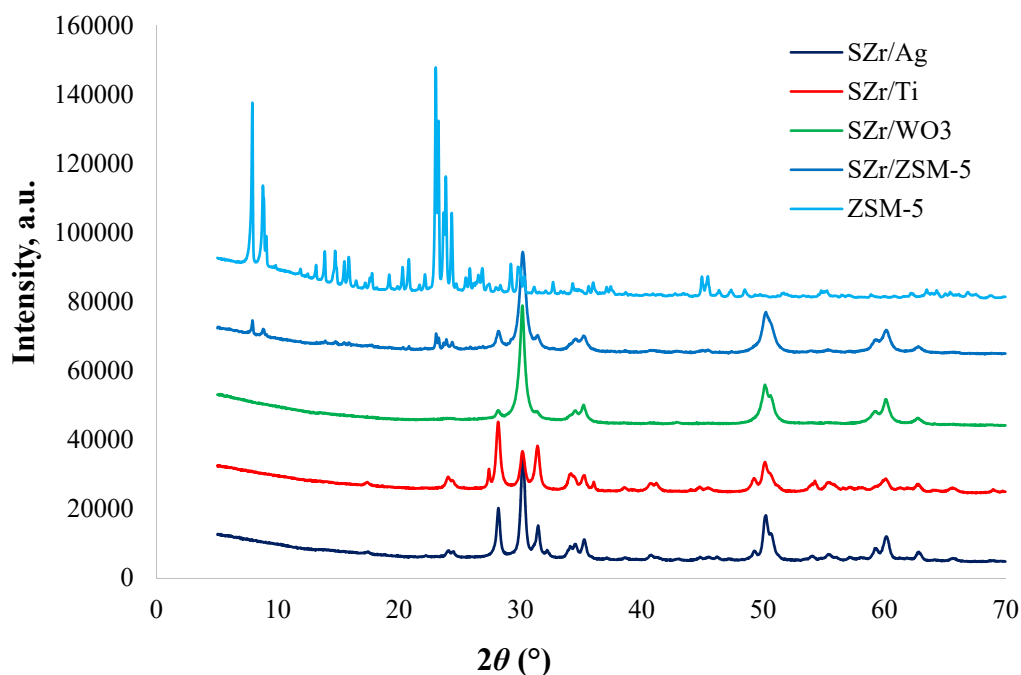


Figure 6.2: X-ray diffraction patterns for the parent ZSM-5 and the optimized SZr/Ag, SZr/Ti, SZr/W, SZr/ZSM-5 catalysts synthesized under the same conditions.

The XRD diffractograms of all the samples revealed a tetragonal-monoclinic phase transition. The XRD patterns also showed the significant impact of calcination temperature and precursor concentration on the crystal phase and crystallite size. The formation of the monoclinic phase (peaks at $2\theta = 28.21^\circ$ and $2\theta = 31.51^\circ$) because of the increase of the crystallite size as function of temperature lowers the content of tetragonal phase ($2\theta = 30^\circ$). This is in agreement with the Garvie Theory (Santos et al., 2008). Further, except for SZr/Ti, it is evident that characteristic tetragonal peak at $2\theta = 30^\circ$ was more prominent than those of the monoclinic phases were. However, the remaining monoclinic peaks were more prominent than the reduced tetragonal phases. In addition, the intensity of the peaks reflected both adsorption and the amount of phase in the

synthesized materials. For instance, the monoclinic phase present on the parent TiN at $2\theta = 37^\circ, 43^\circ, 62^\circ, 75^\circ$ and 79° disappeared after the modification with zirconia. Tetragonal phase typical of zirconia at $2\theta = 24^\circ, 28^\circ, 34^\circ$, and 50° replaced these phases. Furthermore, the lower surface energy of the tetragonal phase when compared to monoclinic phase ensured transformation of the metastable tetragonal phase (Osendi et al., 1985).

6.4.1.3 Measurement of physicochemical properties

The measurement of the specific surface area, S_{BET} was according to the BET method from the nitrogen adsorption isotherms obtained at -196.15°C . Table 6.1 presents the textural properties and acidity of the mesoporous mixed oxide catalysts. Figure 3a presents the nitrogen sorption isotherms of all the samples. The parent ZSM-5 sample exhibited a characteristic monolayer formation at lower relative pressure followed by few molecular layers typical of Type I isotherm. This is because at higher pressures, adsorbate fills the micropores and restricts additional adsorption as represented by the plateau on Figure 4(a). However, the BET surface area, all synthesized samples decreased significantly compared to the parent ZSM-5. Conversely, the pore size, which facilitates diffusion benefits, was in the following order: $\text{SZr/Ag} > \text{SZr/Ti} > \text{SZr/W} > \text{SZr/ZSM-5} > \text{ZSM-5}$. All the synthesized catalysts revealed mesoporous ($2 < dp < 50\text{ nm}$) structures that permits the TG molecule (which requires a critical diameter of 2 to 4 nm) access to the active sites within the materials (Table 6.1, Figure 6.3). The difference in chemical composition of the catalytic materials plausibly explains the significant variations in textural and catalytic activities (Figures 6.3a and 6.3b). Thus, for instance, the pore size of SZr/ZSM-5 (5.10 nm) is lower than those of the other mixed oxide catalysts are (Sani et al., 2015c). These results suggest that the channels of SZr/ZSM-5 could get occluded easily and may result in mass transfer limitation. This is because a TG molecule requires

a critical diameter or the smallest access cylinder of 2 to 4 nm (Kiss et al., 2006; Fernández et al., 2007).

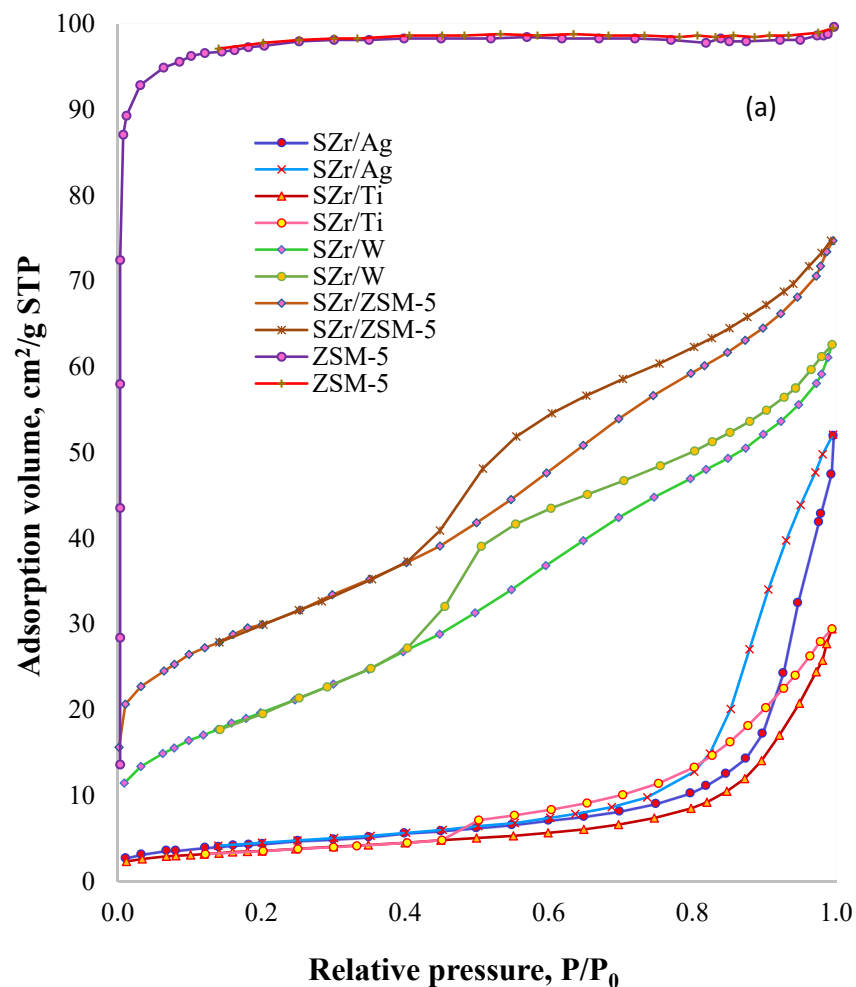


Figure 6.3: (a) N₂ adsorption-desorption isotherms for SZr/Ag, SZr/Ti, SZr/W, SZr/ZSM-5, and ZSM-5 respectively, synthesized under the same conditions.

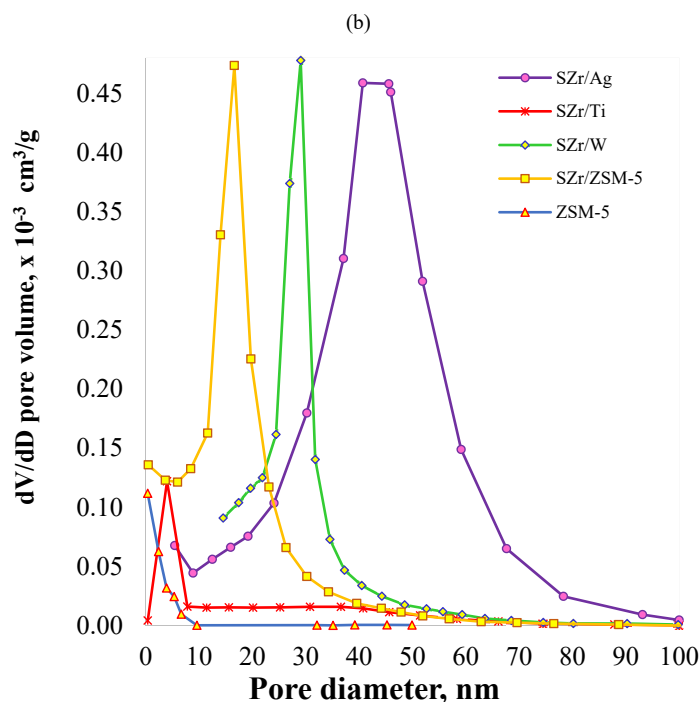


Figure 6.3: (b) Pore size distribution curves for mesoporous SZr/Ag, SZr/Ti, SZr/W, SZr/ZSM-5, and ZSM-5 respectively, synthesized under the same conditions.

The adsorption isotherm of all samples with exception of ZSM-5, followed type-IV IUPAC classification for mesoporous materials with capillary condensation taking place at higher pressures of adsorbate depicting a hysteresis loop (Sing et al., 1985). The steep N_2 -uptake emphasized crystalline agglomeration of the plate-like, nano-sized particles containing slit-shaped pores. This resulted from inter-particle interaction and voids formed by the agglomeration that are typical of H_3 hysteresis loop during the catalyst synthesis. This observation is in accordance to the IUPAC classification, which is generally observed for mesoporous solids, thereby confirming the enhanced textural properties of SZr/ZSM-5 as seen in Table 6.1.

Conversely, the low P/P_0 region for ZSM-5 revealed distinct increase in adsorbate volume with a tight hysteresis loop in the high P/P_0 region. This highlighted the occurrence of micropores evident from Figure 3(b). Provided the effect of thermal or acid treatments were not excessive to destroy the alumino-silicate structural template,

amorphization *via* morphological variation of erstwhile crystalline material, usually facilitates textural property enhancement (Sato et al., 1999). However, the pattern of parent ZSM-5 was apparently destroyed after the modification that produced SZr/ZSM-5. Consequently, we attributed the superior properties observed on SZr/ZSM-5 from Table 1, BET results (Figure 4) and SEM analysis (Figures 5 to 7) in comparison to other materials on the acidity of SZr/ZSM-5. This is because despite the destruction of crystallographic phase of ZSM-5 from SZr/ZSM-5, the process stabilized the mesostructure channels, and ensured higher catalytic performance on SZr/ZSM-5 than that of SZr/Ti, SZr/Ag, and SZr/W synthesized under similar conditions. These outcomes bring to light the effect that hydrogen H^+ has on Brønsted acidity and their influence on their ability to catalyze the transesterification reaction.

The compared acidities of the other catalysts evidenced the observation regarding the acidic catalytic power of the zeolite influenced by nature of the cations. Provided the effect of thermal or acid treatments were not excessive to destroy the alumino-silicate structural template, amorphization *via* morphological variation of erstwhile crystalline material, usually facilitates textural property enhancement. These improvements are obvious from results on Table 6.1, the BET result (Figure 6.3) and SEM analysis (Figures 6.4 to 6.6). The enhanced surface area is considered an advantage for transesterification of feedstock containing high FFA value. This is because higher effective surface area, guarantees high dispersion of active ZrO_2 which complements the high acid density (Table 6.1).

6.4.1.4 Scanning electron microscopy

Scanning electron micrographs, SEM (Figures 6.4 to 6.11) illustrates the surface microstructure of all the catalysts and the morphology of parent ZSM-5 as studied *via* FE-SEM. The FE-SEM micrographs (Figure 6.4a to 6.6b) revealed a change in the morphology of parent ZSM-5 and zirconia upon modification with species of both components and sulfate ions. Similarly, the variations in elemental compositions are vividly noticeable from the EDX graphs. The morphology of ZSM-5 suggested agglomerates of micro-sized hexagonal crystal prisms. However, Zr incorporation, acid treatment and calcination, caused large degree of morphological variation in the SZr/ZSM-5 (Figure 6.6). This is probably because of the combined effects H_2SO_4 attack, inter-particle interaction with Zr and calcination during the synthesis stage that decreased the Si/Al ratio from 1.00 to 0.45 as observed from the EDX results.

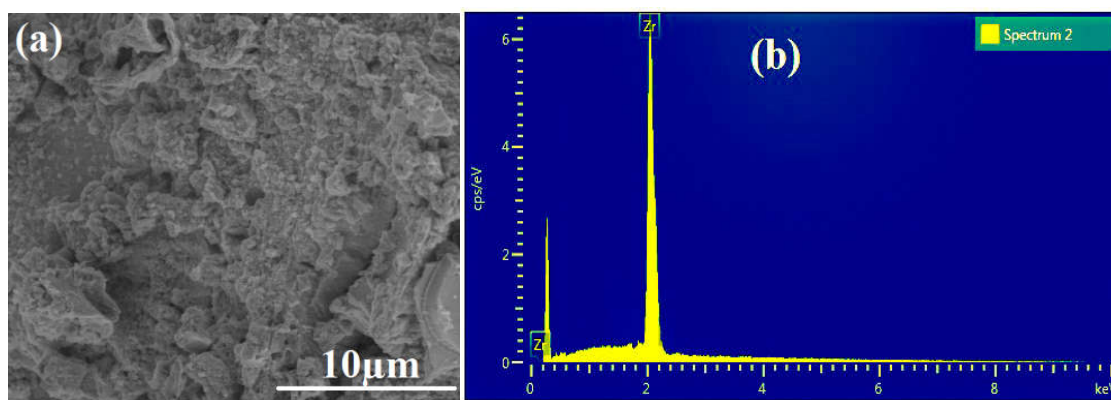


Figure 6.4: (a) Results of the surface microstructural analysis of the ZrO_2 *via* FE-SEM and (b) surface elemental composition of the ZrO_2 determined *via* EDX analysis

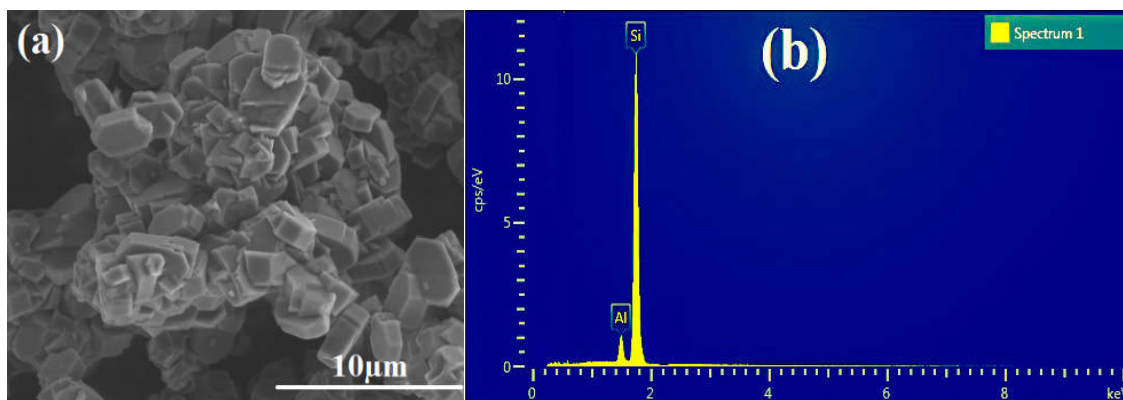


Figure 6.5: (a) Results of the surface microstructural analysis of the ZSM-5 *via* FE-SEM and (b) surface elemental composition of the ZSM-5 determined *via* EDX analysis

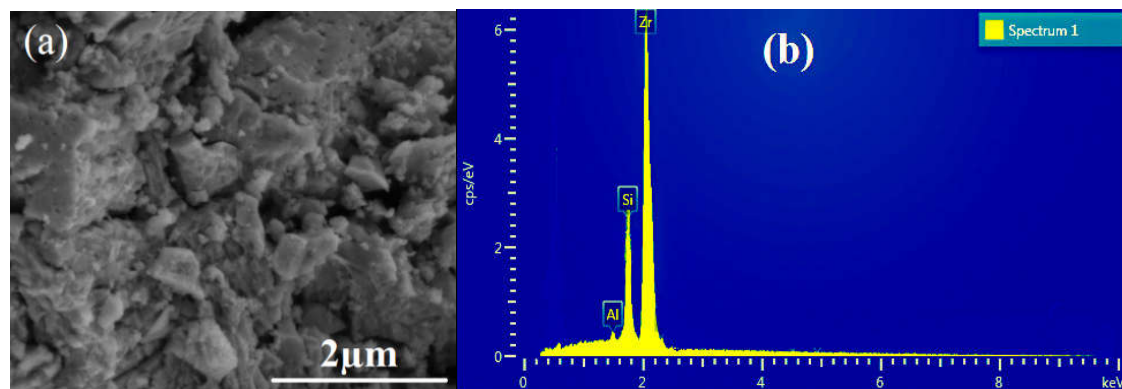


Figure 6.6: (a) Results of the surface microstructural analysis of the SZr/ZSM-5 *via* FE-SEM and (b) surface elemental composition of the SZr/ZSM-5 determined *via* EDX analysis

The different constituents were homogeneously processed into solid particles of uneven dimensions. The EDX analysis of the surface elemental composition (Fig. 6.7b) revealed the presence of zirconium (87.17 wt.%), silica (9.72 wt.%), aluminium (1.49 wt.%) and sulfur (1.26 wt.%). Fissures and faults appeared on the surface of SZr/ZSM-5 which were absent from the parent ZSM-5 and zirconium micrographs. These confirmed secondary pores formation that are beneficial in minimizing diffusion associated with zeolites (Sato, Nishimura, & Shimada, 1999).

Further, agglomeration or the adhesion of particles to each other because of van der Waals forces of attraction is significantly higher in nanoparticles. Fine particles, particularly nanoscale particles have characteristic large surface areas. These often agglomerate to form either secondary particles or lumps that minimize the interfacial energy or total surface area of the system. Figure 7(a) evidenced such agglomeration. Similarly, Figures 6.7a and 6.8a revealed the surface microstructure of AgNO_3 and SZr/Ag as studied *via* FE-SEM. The different constituents were homogeneously processed into solid particles of uniform dimensions. The EDX analysis of the surface elemental composition (Fig. 6.7b and 6.7b) revealed the presence of zirconium (99.63 wt.%) and sulfur (0.16 wt.%). Cracks were evident on the surface of the composite catalyst mainly because of its stronger acidity. This clarified the higher mesoporosity and activity of SZr/Ag when compared with that of SZr/Ti and SZr/W .

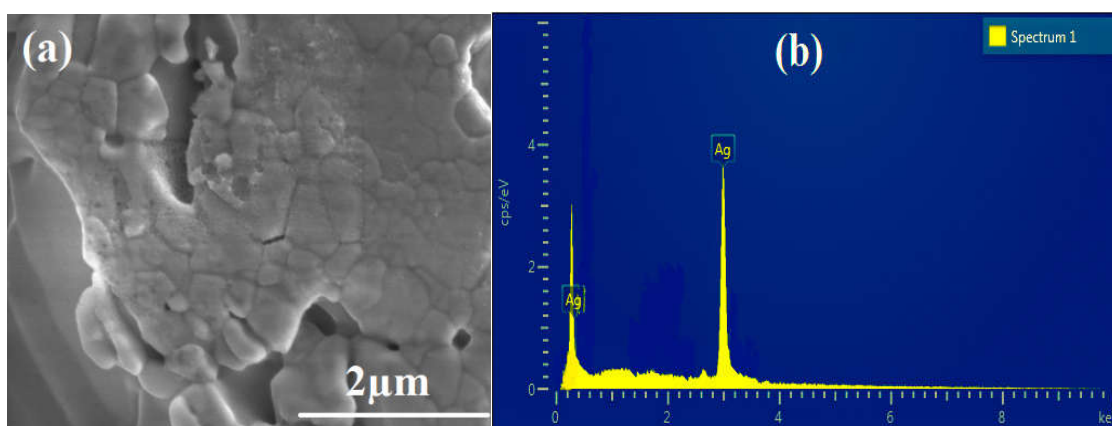


Figure 6.7: (a) Results of the surface microstructural analysis of the AgNO_3 *via* FE-SEM and (b) surface elemental composition of the AgNO_3 determined *via* EDX analysis

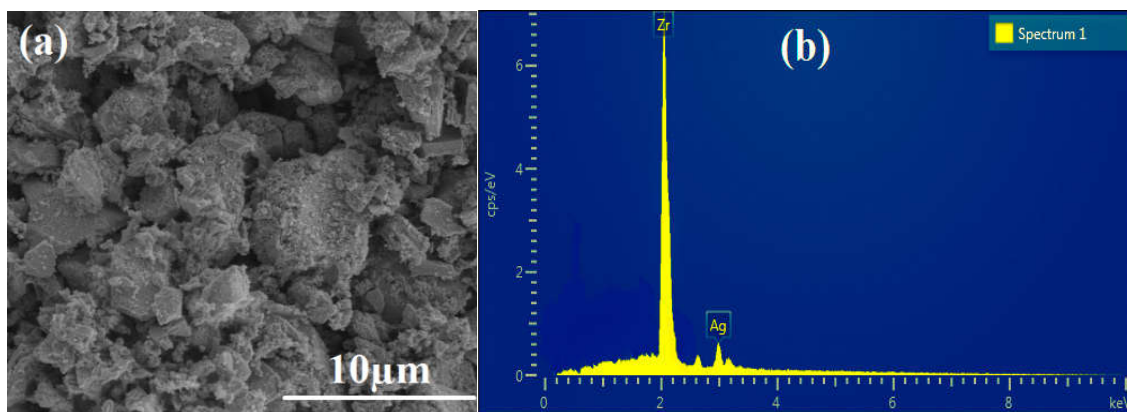


Figure 6.8: (a) Results of the surface microstructural analysis of the SZr/Ag *via* FE-SEM and (b) surface elemental composition of the SZr/Ag determined *via* EDX analysis

Similarly, Fig. 6.8(a) presents the size and shape of topographic features of SZr/Ti catalyst studied *via* FE-SEM. The surface morphology was also homogeneously processed into solid particles. The surficial elemental composition by EDX analysis (Fig. 6.8b) also revealed the presence of 92.92 wt.% zirconium, 6.45 wt.% and 0.36 wt.% sulfur (Appendix A).

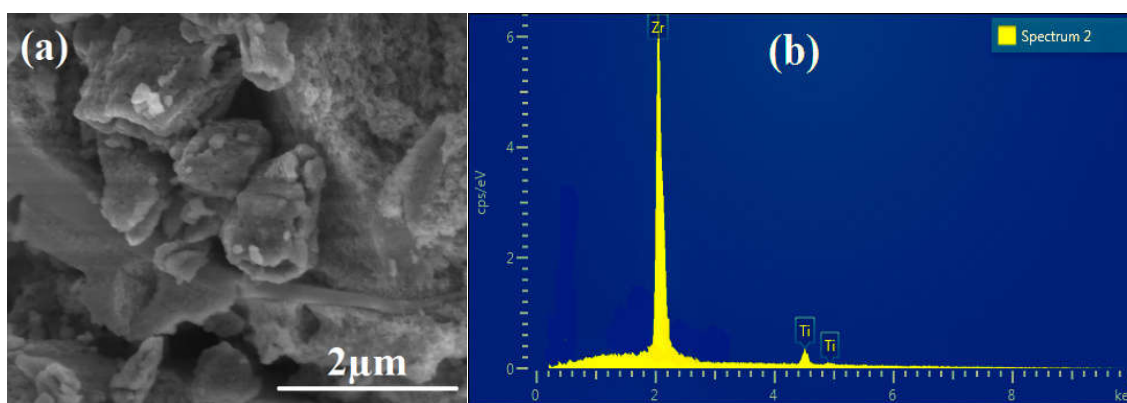


Figure 6.9: (a) Results of the surface microstructural analysis of the SZr/Ti *via* FE-SEM and (b) surface elemental composition of the SZr/Ti determined *via* EDX analysis

Figures 6.10a and 6.11a present the surface microstructure of the parent $(\text{NH}_4)_6\text{H}_2\text{W}_{12}\text{O}_{40} \cdot x\text{H}_2\text{O}$ and SZr/W catalyst. High calcination temperature made the zirconium oxide structure to incorporate fully into the crystal lattices of the tungstate oxide. Fig. 6.10b presents a cross-sectional surficial composition and distribution of elements on SZr/W *via* EDX analysis. However, the micrograph of the catalyst prepared

with sufficient acid revealed more dispersed surficial metal elements (Figure 11a). Expectedly, a somewhat amorphous phase of the parent material transformed into crystalline phase as displayed by the micrograph representing SZr/W (Figure 6.11b).

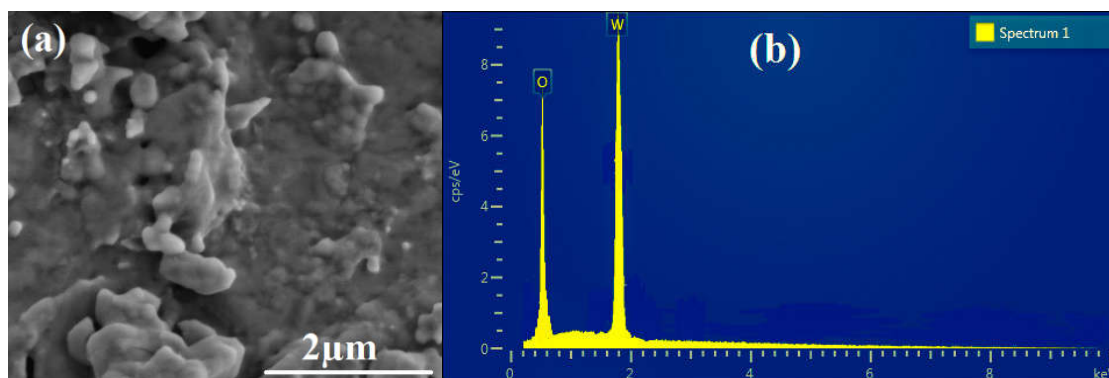


Figure 6.10: (a) Results of the surface microstructural analysis of the $(\text{NH}_4)_6\text{H}_2\text{W}_{12}\text{O}_{40} \cdot x\text{H}_2\text{O}$ *via* FE-SEM and (b) surface elemental composition of the $(\text{NH}_4)_6\text{H}_2\text{W}_{12}\text{O}_{40} \cdot x\text{H}_2\text{O}$ determined *via* EDX analysis

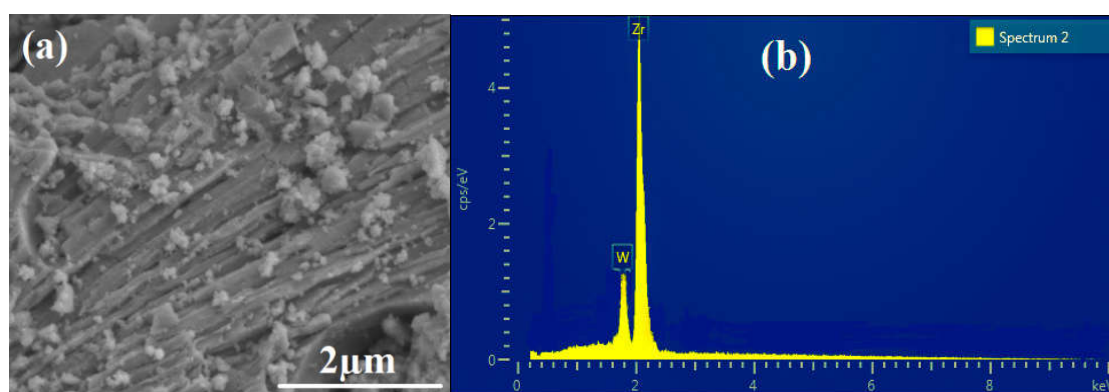
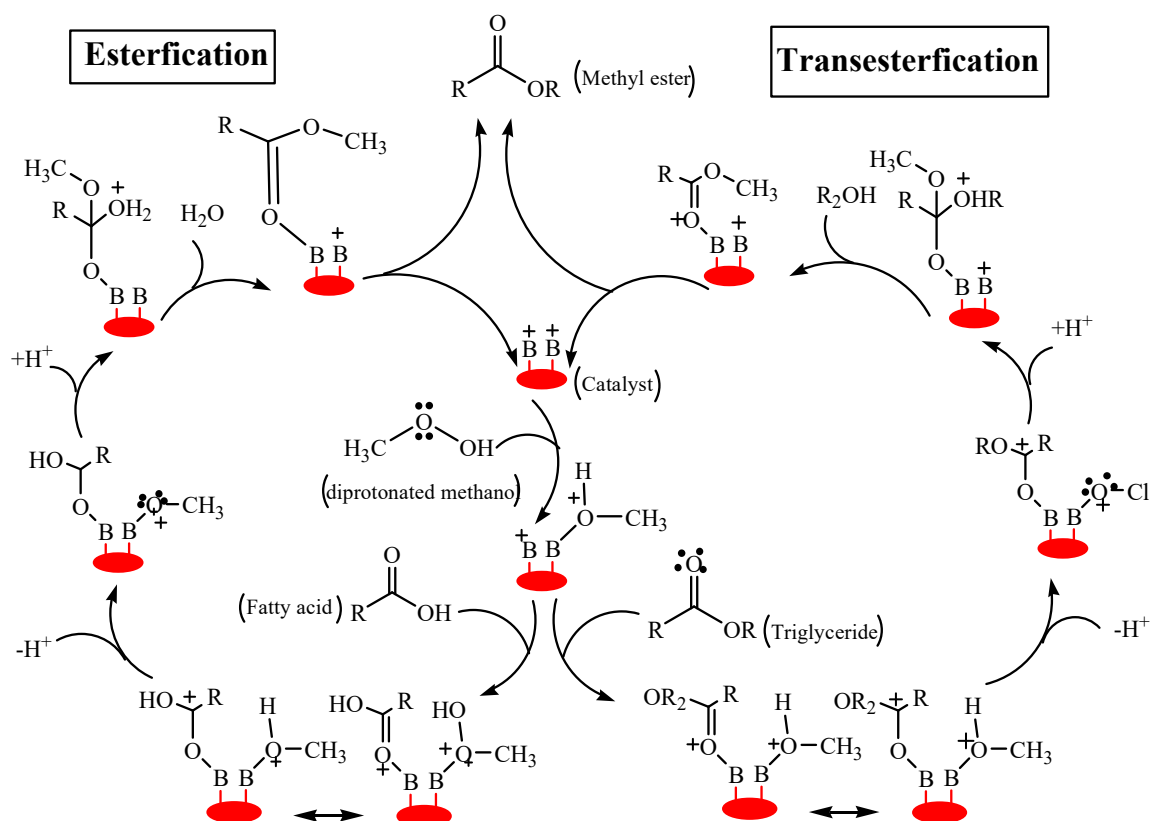


Figure 6.11: (a) Results of the surface microstructural analysis of the SZr/W *via* FE-SEM and (b) surface elemental composition of the SZr/W determined *via* EDX analysis

6.4.2 Comparative transesterification activity over the composite sulfated zirconia catalysts

The preferential adsorption of TG and FFA on the Brønsted acid sites of sulfated zirconia facilitates the simultaneous transesterification and esterification reaction and explains the poorer performance exhibited by SZr/W. Hence, the reaction investigated in this study follows the Langmuir-Hinshelwood mechanism (scheme 6.1) (Rattanaphra et al., 2010).

This mechanism (sequence of actual events that occur in transforming reactant molecules into products) harnesses the activation of the adsorbed reactants. Under this mechanism, the adsorbed atoms or “*adatoms*” are highly reactive even though they are not free radicals. Consequently, the mechanism facilitates the interchange of atoms from a second, different molecular species when adsorbed onto the same surface.



Scheme 6.1: The Langmuir-Hinshelwood mechanism (Rattanaphra et al., 2010)

Thus, Brønsted acid protonates the hydroxyl group on the methanol while carbocation results from the protonation of TG and FFA from the adjacent site on catalyst surface. A nucleophile emerges from the deprotonation of methanol oxygen that generates a tetrahedral intermediate from attacking the carbocation. Consequently, during esterification, the tetrahedral intermediate eliminates water to form ester. Similarly, it generates a new ester during transesterification by eliminating glycerol. The same mechanism aided by the highly hydrophobic SZr/ZSM-5, applies to di- and tri-glycerides.

Morterra, et al. (1995) posited a linear relationship between increased acidity and the feedstock conversions. Figure 6.12 presents the activity of catalysts in the simultaneous transesterification of UFO. The study revealed an order of conversion ($\text{SZr/ZSM-5} > \text{SZr/Ag} > \text{SZr/Ti} > \text{SZr/W} \gg \text{ZSM-5}$) that showed significant correlation to the acidity and structure of the materials. This further affirms the presence of sulfate active sites within the surface structure of the catalysts as reported by (Hino, Kurashige, Matsuhashi, & Arata, 2006). However, the pore size of SZr/ZSM-5 might have minimized conversion beyond expectation because of possible occlusion. This is because the catalyst possesses 5.10 nm pore size.

However, a TG molecule requires a critical diameter or the smallest access cylinder of 2 to 4 nm (Fernandez et al., 2007; Kiss et al., 2006). Srilatha et al. (2011), reported severe internal diffusion resistance, while López et al. (2005) obtained 57% conversion with SZ, which exhibited $134.4 \pm 5.3 \text{ m}^2/\text{g } S_{\text{BET}}$. Premised on the underlying difficulty of the TG molecules to access the inner pores of the catalysts for efficient contact, it is plausible to assert that amount and dispersion of active sites, which is reflective of acidity, was responsible for transesterification activity reported in this study. It is also instructive to note that infusing sulfate onto zirconium oxide produces acidic solid catalysts. However, doping zirconia with acidic ZSM-5 further increases its acidity. Hence, the high conversions displayed by the synthesized material reflect the role of this incorporation. It is therefore plausible to assert that acidity of materials synthesized in this study have direct correlation to surface hydroxyl groups.

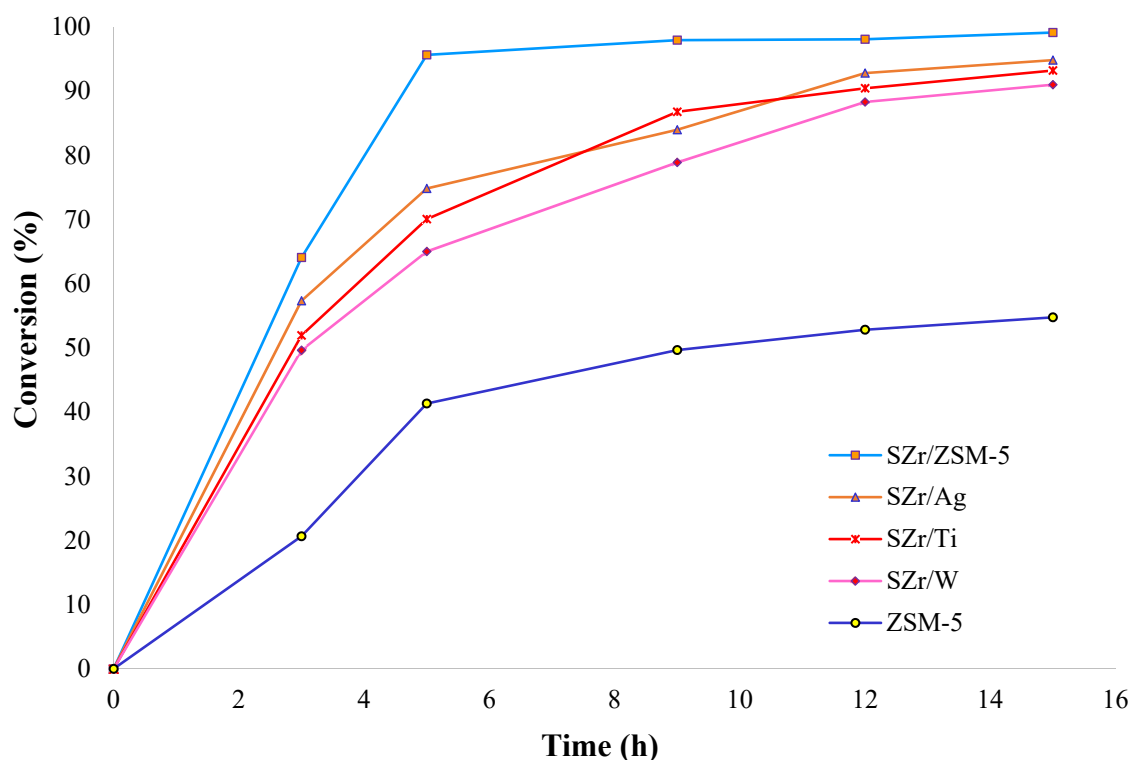


Figure 6.12: Catalytic activities of 2 wt.% mesoporous SZr/Ag, SZr/Ti, SZr/W, SZr/ZSM-5, and ZSM-5 catalysts at 5:1 methanol-to-oil ratio and 200 °C

6.4.3 Palmitic acid transesterification kinetics SZr/ZSM-5

Both Brønsted (proton donor) and Lewis acids (electron pair acceptor) have the capability to esterify free fatty acids (Brown, 2000; Cardoso et al., 2008). Contrary to the initiation of the reaction mechanism of esterification in homogeneous systems by protonation of the carbonyl group, there exists a remarkable difference in the reaction mechanism over Brønsted and Lewis acids. As mentioned earlier, the transesterification of palmitic acid with methanol on SZr/ZSM-5 obeyed Langmuir-Hinshelwood mechanism kinetics with palmitic acid and methanol adsorbed on the active sites respectively. The rate-determining step was the adsorption reaction between methanol and palmitic acid in the bulk fluid. This implies the equilibrium condition between the adsorption and desorption reactions and the possibility of achieving ca. 100% conversion.

A gas chromatography equipped with a Cotrun GC9800N flame ionization detector and OV-17 (30 m x 0.25 mm x 0.25 µm) capillary tube analyzed the biodiesel yield (Table 6.3) quantitatively under injector, oven, and detector temperatures of 280, 250, and 250 °C respectively. The biodiesel yields were calculated from Equations 6.3 to 6.5.

$$M_i = \frac{f_i A_i M_s}{A_s} \quad (6.3)$$

$$Y_i = \frac{f_i A_i M_s}{A_s \times M_{sample}} \times 100\% \quad (6.4)$$

$$Y_{Biodiesel} = \sum Y_i \quad (6.5)$$

Where M_s , and A_s represents the mass and peak area of the internal standard respectively. M_i , A_i and f_i represent the mass, peak area, and the correction factor of each component (methyl palmitate, $f=1.089$; methyl oleate, $f=1.018$; methyl stearate, $f=1.044$; linoleic acid methyl ester, $f=0.9584$ and linolenic acid methyl ester, $f=0.8532$) in the sample. Y_i and M_{sample} represents the yield of each component and mass of sample respectively; while $Y_{biodiesel}$ denotes the total biodiesel yield. The calculated mean molecular weight of fatty acids was 276 g/mol while that of the oil was 866 g/mol respectively.

Table 6.3: Working conditions for the GC analyzer

Column	DB 23 (L = 0.30 mm × ID = 0.32 mm × 0.25 µm film thickness of 5% diphenyl, 95% dimethyl polysiloxane)
Guard column	0.5 m with same phase as the analytical column connected to the injector (volume = 0.5 µL)
Gas flow	
He, carrier gas	2 µL/min
air	374 mL/min
H ₂	27 mL/min
Injection temperature	210 °C
Flame ionization detector temperature	250 °C
Oven temperature program	50 to 200 °C for 5 min at 15 °C/min; 200 to 240 °C for 18 min at 3 °C/min)

Similarly, the turnover frequency, TOF (see Table 6.4) was calculated from Equation 6.5.

$$TOF = \frac{mol_{actual}}{m_{cat} \times f_m \times t} = \frac{\text{number of molecules of a given product}}{(\text{number of active sites}) \times (\text{times})} \quad (6.5)$$

Where mol_{actual} denotes the amount in moles of the biodiesel; m_{cat} represents the mass of catalyst; f_m denotes the surface amounts of acid sites while t represents the reaction time. Turnover frequency expresses the efficiency of a catalyst. It is a chemical reaction rate and not a rate constant. TOF represents the number of times the overall catalytic reaction in question takes place per catalytic site per unit time (usually in sec). Hence, TOF holds only for a fixed set of reaction conditions (e.g., form and structure of the catalyst, temperature, pressure, ratio, and concentration of the reacting species and time). Thus, it is necessary to specify all the prevailing conditions of the catalytic reaction used in calculating a particular TOF. Table 6.4 presents the physical properties and yield of biodiesel obtained from UFO compared to diesel.

Table 6.4: Physical properties and biodiesel yield obtained from UFO compared to diesel

Quality	Unit	EN14214	UFO	Diesel	Encinar et al.	Centinkaya et al.	This study	TOF
Acid number	mg KOH/g		146.67	0.11				
Iodine number	mg KOH/g		13.20	-				
Saponification No.	mg KOH/g		268.20	-				
Density @15 °C	g/cm ³	0.86 to 0.90	0.92	0.83	0.890 @ 25 °C	0.8823 to 0.8874	0.88	
Flash point	°C	>101	269	69	177	176	176	
Cloud point	°C	-	21.00	0	4.7	9	5.2	
Pour point	°C	-	18.00	< -12	-3.9	-3	-3	
Viscosity @40 °C	mm ² /s	3.5 to 5.0	30.05	3.53	4.8	5.29 to 6.46	4.56	
Acid value, max	mg KOH/g	0.5			-	0.289		
Water content, max	ppm	500			-	480.07		
FFA composition ^a	wt%							
Palmitic (C16:0)			11.8				12.13	
Palmitoleic (C16:1)			4.4				6.34	
Stearic (C18:0)			4.6				4.55	
Oleic (C18:1)			49.5				55.92	
Linoleic (C18:2)			25.3				20.61	
Mean molecular wt	g/mol		866					
Conversion; Yield	%							x 10 ⁻³ s ⁻¹
Zr/ZSM-5							99.12; 91	39.2
SZr/Ag							94.84; 89	38.0
SZr/Ti							93.21; 85	23.4
SZr/W							91.01; 84	15.1
ZSM-5							54.76; 42	9.62

^aOther fatty acids [Myristic (C14:0), Linolenic(C18:3), Arachidic (C20:0), Eicosenic (C20:1), Behenic (C22:0), Erucic (C22:1), Tetracosanic (C24:0)] were present in amounts ca. < 1%.

Further, the facile process employed in present study is encouraging considering the lower reaction parameters employed (200 °C, 5 h, 5:1 molar ratio and 2 wt.% catalyst loading). It eliminates the yield loss and chemical costs associated with acid-catalyzed esterification pretreatment and caustic stripping (Table 6.5) alluded to by Chai et al., (2014). This lowers the energy consumption and chemical costs. Against the backdrop of affordability and sustainability, it is important to highlight some reports related to the present study for comparison. Danuthai et al., (2009), converted ca. 100% methyl octanoate over H-ZSM-5 at a very high temperature of 500 °C for 5 h. Whereas, Chung et al. (2009), obtained 80% conversion from Soybean oil mixed with oleic acid over H⁺ ion exchanged ZSM-5 at 60 °C for 6 h. Moreover, the deactivation limitation associated with sulfated zirconia due to leaching of sulfate ions was not observed from this study.

Further, it is worthy of note that conventional zirconia produced negligible conversion under the same conditions. The encouraging conversion of 95% obtained with SZr/Ti from the present study corroborated the findings by (López et al., 2008). This is despite the employed calcination temperature of 550 °C. Kiss et al. (2006), reported 500 °C and 400 to 500 °C as optimum calcination temperature for SZ and TiZ respectively, with subsequent loss of activity at higher temperature due to loss of sulfate ions and decreased catalyst's surface area. However, the material showed poor reusability because of active basic sites poisoning from carboxylic acids. This hinders its suitability for transesterification especially with feedstocks containing higher acid values such as UFO. In comparison also, WO₃/ZrO₂ gave ~100% conversion from 4.5:1 methanol-to-soybean oil at 200 °C after 20 h (Furuta et al., 2004). In a different study similar to the current report, Park et al. (2008) obtained 70% conversion from UFO over WO₃/ZrO₂.

Table 6.5: Comparative FFA pretreatment cost (López, et al., 2005)

FFA % in oil		2.5%	5%	10%	15%
Caustic stripping	Yield loss	2.5%	5%	10%	15%
	Cost (\$/gal)	0.119	0.238	0.476	0.715
	Cost (\$/L)	0.031	0.063	0.126	0.189
Acid esterification	Yield loss	1%	1%	1%	1%
	Cost (\$/gal)	0.040	0.080	0.160	0.240
	Cost (\$/L)	0.011	0.021	0.042	0.063

Notes: All chemical costs (H_2SO_4 = \$5/gal, methanol = \$1.6/gal, sodium methylate = \$4/gal) and biodiesel selling price (\$4/gal after various local and federal tax credit and other incentives) were based on recent industrial scale values with 80% assumed efficiency for methanol recovery.

Though all the samples exhibited good performances when evaluated for transesterification of UFO after 5 h (Figure 6.12), SZr/ZSM-5 exhibited highest activity than the other catalysts. This is despite possessing smaller pore size. We attributed this to enhanced acid strength imparted on SZr/ZSM-5 by the zeolite, as well as its suitable S_{BET} when compared to its counterparts. The NH_3 -TPD and IR spectra of pyridine adsorption analyses showed lower acid density for SZr/Ti and SZr/W than that of SZr/ZSM-5. Consequently, the interaction between the zirconia (facilitated by highly dispersed nanoparticles) and higher mesopores of the zeolite support determined the observed acidity and activity. This is because acidity, which arises from electron deficiency of the supported catalysts to a combination of acidity (0.14, 0.09, and 0.05 mmol/g) and the good S_{BET} (20.11, 14.53, and 5.37 nm) exhibited by SZr/Ag, SZr/Ti, and SZr/W respectively.

6.5 Conclusion

This study developed a facile route for synthesizing efficient solid acid catalysts for transesterifying UFO-containing high FFA under moderate reaction conditions. Albeit, doping SZ with SZr/ZSM-5 is a key feature of this synthesis strategy, which proved superior to prior formulations. This is because despite the destruction of ZSM-5 crystallographic phase, the process stabilized the mesostructure channels, and ensured higher catalytic performance on SZr/ZSM-5 such as 99.12% conversion, 91% yield, and

a TOF of $39.2 \times 10^{-3} \text{s}^{-1}$. Interestingly, the activity of SZr/ZSM-5 was markedly higher than that of SZr/Ti, SZr/Ag, and SZr/W synthesized under similar conditions. The process provided solutions to the economic concerns associated with accessing fossil fuel reserves *via* simultaneous transesterification and esterification of waste oil into low cost and readily implementable biodiesel as sustainable alternative source of energy for transportation. Furthermore, the use of waste oil is essential in solving the contending issue of regional availability. Interestingly, the activity of SZr/ZSM-5 was markedly higher than that of SZr/Ti, SZr/Ag, and SZr/W. Other significant findings include:

- 1) Factors essential for efficient transesterification include acidic site, sufficient surface area with mesoporous channels and tetragonal phase of zirconia.
- 2) The interplay between metal species of modified oxo-anions and pore structure of acidic zeolites and its strong properties enhances acidity of sulfated composite catalysts.
- 3) The encouraging conversions obtained suggested that activity for transesterification does not depend solely on textural property of the catalytic material.
- 4) Amount and dispersion of active sites, which are reflective of acidity of the catalysts, play significant role in facilitating higher conversion of TG into biodiesel.
- 5) The study also showed how to achieve a flexibility of properties from unlimited number of possible manipulations from one catalyst precursor. These encouraging observations highlighted the possibility of improving on the reported formulations to facilitate higher intrinsic efficiency in biodiesel production. The catalysts synthesized from the present study have potential applications in other acid-catalyzed reactions such as selective catalytic reactions, SCR for abating

environmentally harmful NO_x emissions from mobile or stationary power sources. This is because of the presence of sulfate ions and their resistance to H₂O, which are inevitable components of diesel exhaust gas.

CHAPTER 7: OVERALL CONCLUSION

Finally, this chapter summarizes the overall research findings from all the four articles with their respective implications. The chapter also offers recommendations for future research. Agreeably, biodiesel as an alternative fuel for diesel engines is produceable from virtually any fat or oil feedstock *via* a simple chemical process. However, the choice of technology adopted for the production is dependent on feedstock type and cost, catalyst activity and recovery, quality and desired capacity, and alcohol recovery. Feedstock cost is the dominant factor in the production process; gulping up to 88% of the production cost, while capital cost contributes only ca. 7%. The availability of cheap and abundant feedstocks such as microalgal and used frying oils reduces the overall cost of production. However, these cheap sources come with inherent challenges that incur other costs in maintaining product quality. Accordingly, catalysis provides the required panacea because chemical reaction kinetics is the major factor that has direct effect on weak acidity, incomplete and slow reactions *vis-à-vis* the high contents of FFA from such feedstocks. Evidently, to increase biodiesel yield and lower the operational costs, certain technological advancements and sustained governmental policies are essential. These include:

- (i) Establishing proficient systems for the production of vast quantities of feedstocks at affordable costs.
- (ii) Developing novel catalysts with higher activities that could facilitate greater yields in shorter time with lesser refining difficulties.
- (iii) Radical innovations for separating and refining crude biodiesel.
- (iv) Enacting new policies that will favor sustained biodiesel production.
- (v) Minimizing costs, energy and water usage by implementing the excellent findings from the research communities.

Consequently, this study argued that points (i), (ii), and (v) above are achievable within the period of the study, and available facilities. Thus, the study highlighted that:

1. It is possible to synthesize and characterize solid acid catalysts from palm tree biomass as cheap and environmentally benign alternatives for biodiesel production.
2. It possible to enhance the activity of sulphated zirconia despite its attaining state-of-the-art status by investigating the effect of different precursors in activating the active sites of the material.
3. The combined catalytic attributes of zirconia and zeolite have the potential of reducing the challenges associated with other solid acid catalysts.

The study subsequently addressed the foregoing issues thus:

- a. Synthesized, characterized and evaluated the use of sulfonated mesoporous catalysts from palm tree biomass such as palm fronds, spikelets, empty fruit bunches and palm waste fruits in esterifying the high free fatty acids of used frying oil into biodiesel. Interestingly, all the catalysts exhibited high activity, with sEFB/300 and sPTS/400 converting more than 98% FFA into FAMES. This is outstanding considering the lower reaction parameters of 5 h, 5:1 methanol-to-oil ratio, and a moderate temperature range between 100 and 200 °C. It is instructive to highlight these against similar reports by other authors, such as 80% conversion from 18:1 methanol-oil molar ratio after 3 h. The present study further illustrates the prospect of converting wastes into highly efficient, benign, and recyclable solid acid catalysts; especially when compared against the backdrop of the sustainability issue of fossil oil. Further, the implication of utilizing these wastes and by-products highlights appropriate means of reducing pollution as well as production costs.

- b. Synthesized and modified sulfated zirconia and compared the effect of doping SZ with ytterbium, and the variation in preparatory methods on acidity and catalytic activity for simultaneous esterification and transesterification reactions in biodiesel production. Double sulfation ensured sulfate incorporation while minor precursor amounts enhanced activity of the materials. Despite the low specific surface area, which was due to short aging period, large mesoporosity, high amount, and dispersion of the active sites ensured remarkable activity. SZr-Ti-Yb/500-4/s catalyst converted > 99 % used frying oil containing ca. 48 wt.% FFA. Consequently, this highlights the prospect of producing biodiesel at lower cost.
- c. Synthesized and characterized sulfated Zr/ZSM-5 with improved Brønsted acidity and compared its activity over SZr/Ag, SZr/Ti, and SZr/W for the transesterification reaction of used frying oil to form methyl ester. For the first time, this study explored the effect of dispersing zirconium on ZSM-5 for the simultaneous esterification and transesterification of used frying oil for biodiesel production. The material exhibited moderate to strong acidic sites and a system of interconnected system of large pores. The study manipulated the interplay between the metal function of the modified oxo-anions and pore structure of zeolites and its strong acidic properties as an innovative approach for enhancing acidity of sulfated zirconia. Albeit, doping SZ with SZr/ZSM-5 is a key feature of this synthesis strategy, which proved superior to prior formulations. This is because the process stabilizes the mesostructure channels, crystallographic phase, and ensured higher catalytic performance such as 99.12% conversion, 91% yield, and a TOF of $39.2 \times 10^{-3} \text{s}^{-1}$.

The study evidenced a notable increase in the acid strength from the mixed oxide catalysts compared to single SZ oxide. Compared to prior arts, Zr/ZSM-5 converted > 95% of used frying oil (48 wt.% FFA) under lower reaction parameters (5 h, 5:1

methanol-to-oil ratio and 200 °C). The catalytic activity of the materials was directly dependent on the amount and dispersion of Brønsted acid active sites, which are reflective of SZ acidity. This implies that change of acidic properties causes the increased activity. Hence, the high conversions displayed by the synthesized materials reflect the role of this incorporation. It is therefore plausible to assert that acidity of materials synthesized in this study have direct correlation to surface hydroxyl groups. The performances of the synthesized catalysts (Table 7.1) have answered some important questions regarding SZ solid acid catalysis such as higher reaction conditions, methanol-to-oil ratio, and temperature requirements. Further, it opened up new areas regarding inherent limitations such as weak acidity, and slow reaction rates; that *hitherto* were deemed saturated.

Table 7.1: Summary of the different catalysts and their respective performances

Catalyst		Surface Area (m ² /g)	Pore Size (nm)	Pore Volume (cm ³ /g)	Total Acid (-SO ₃ H) Density (mmol/g)	Conversion @ 100 °C, 15 h (%)
Esterification	sPTF/SA/400	28.11	10.17	0.03	0.79	87.39
	sPTF/SA/300	27.78	10.02	0.03	1.13	87.87
	sPTF/400	17.80	9.20	0.03	1.09	83.27
	sPTS/400	12.70	5.16	0.02	1.30	91.26
	sEFB/400	236.37	4.15	0.11	1.86	86.27
	sEFB/300	246.46	4.18	0.12	2.34	91.64
	sWPF/400	28.11	10.09	0.03	1.54	86.50
						Conversion @ 200 °C, 15 h (%)
Transesterification	SZr-500-4/e	5.30	21.21	0.02	20 x 10 ⁻³	96.03
	SZr-500-4/s	3.43	37.04	0.02	40 x 10 ⁻³	97.24
	SZr-500-1/e	3.84	20.35	0.02	10 x 10 ⁻³	89.23
	SZr-Ti-500-4/e	8.12	24.98	0.04	50 x 10 ⁻³	90.44
	SZr-Ti-500-4/s	8.33	28.52	0.05	70 x 10 ⁻³	85.54
	SZr-Ti-Yb-500-4/s	60.33	21.38	0.32	330 x 10 ⁻³	99.96
	SZr-500-5/7	7.69	21.44	0.03	80 x 10 ⁻³	97.01
	SZr-500-5/7R	9.05	20.27	0.04	40 x 10 ⁻³	95.90
	SZr-500-5/14	41.22	6.83	0.07	280 x 10 ⁻³	97.88
	SZr-500-5/10	15.05	9.65	0.04	70 x 10 ⁻³	96.99
	ZSM-5	385.20	3.04	0.15	3.71	54.76
	SZr/ZSM-5	107.25	5.10	0.12	0.75	99.12
	SZr/Ag	15.97	20.11	0.08	0.14	94.84
	SZr/Ti	12.90	14.53	0.05	0.09	93.21
	SZr/W	72.13	5.37	0.10	0.05	91.01

SZ doped with Yb ($60.33 \text{ m}^2/\text{g}$, $330 \times 10^{-3} \text{ mmol/g}$) and the one supported on ZSM-5 ($107.25 \text{ m}^2/\text{g}$, 0.75 mmol/g) gave conversions of ca. 100%. Plausibly, the carbenium ions, which require very strong acid sites in all the catalysts, outnumbered the carbonium ions that require high temperature for the reaction to reach completion. This evidenced the short residence time and low reaction temperature observed from the work. The study also showed how to achieve a flexible set of properties from unlimited number of possible manipulations using one catalyst precursor. These observations highlight the possibility of improving on the reported formulations to facilitate higher intrinsic efficiency in biodiesel production.

7.1 Recommendations for future works

Though this work articulately reported a compelling advancement of knowledge on the complex realms of solid acid catalysis, it is nonetheless imperative to pre-empt inevitable critiques on some recommendations worthy of investigating. These include:

- i. Devising a technique to minimize or recover the concentrated sulfuric acid utilized in sulfonating carbon-based mesoporous catalysts.
- ii. Utilizing probe molecules techniques augmented with multifarious nuclei such as ^1H , ^{13}C and ^{31}P for investigating surface acidities of the solid acid catalysts.
- iii. Utilizing computational and real-time *in situ* observation techniques to predict catalytic performances under real reaction conditions.
- iv. Studies on how to determine the most suitable turn over frequency, TOF calculations, and the adsorbate-induced surface-reconstruction relationship for solid acid-catalyzed biodiesel production.

These will lead to compressive understanding of the factors that influence activity during catalysis. Location of acidic sites and types, concentrations, strengths of Brønsted and Lewis acid during a chemical reaction could be precisely determined and characterized. Advances required for the rational design of catalysts with interconnected system of large pores that will minimize diffusional effects of the long alkyl molecules will thus, be achievable. Further, develop catalysts that can preferentially exclude polar by-products and prevent deactivation of the catalytic sites.

REFERENCES

- Agarwal, A. K. (2007). Biofuels (alcohols and biodiesel) applications as fuels for internal combustion engines. *Progress in energy and combustion science*, 33(3), 233-271.
- Agarwal, A. K., & Das, L. M. (2001). Biodiesel development and characterization for use as a fuel in compression ignition engines. *Journal of engineering for gas turbines and power*, 123(2), 440-447.
- Aguilar-Garnica, E., Silva-Romero, Y. E., Hernández-Montelongo, R., García-Sandoval, J. P., & Aceves-Lara, C. A. (2014). Kinetic analysis for the esterification of high free fatty acid feedstocks with a structural identifiability approach. *European Journal of Lipid Science and Technology*, 116(11), 1598-1607. DOI: 10.1002/ejlt.201400059
- Al-Rifai, N., Cao, E., Dua, V., & Gavrilidis, A. (2013). Microreaction technology aided catalytic process design. *Current Opinion in Chemical Engineering*, 2(3), 338-345.
- Angell, C. L., & Schaffer, P. C. (1965). Infrared Spectroscopic Investigations of Zeolites and Adsorbed Molecules. I. Structural OH Groups¹. *The Journal of Physical Chemistry*, 69(10), 3463-3470.
- Antizar-Ladislao, B., & Turrion-Gomez, J. L. (2008). Second-generation biofuels and local bioenergy systems. *Biofuels, Bioproducts and Biorefining*, 2(5), 455-469.
- Antizar-Ladislao, B., & Turrion-Gomez, J. L. (2010). Decentralized energy from waste systems. *Energies*, 3(2), 194-205.
- Arata, K., & Hino, M. (1990). Preparation of superacids by metal oxides and their catalytic action. *Materials Chemistry and Physics*, 26(3), 213-237.
- Ardizzzone, S., Bianchi, C. L., Cappelletti, G., & Porta, F. (2004). Liquid-phase catalytic activity of sulfated zirconia from sol-gel precursors: the role of the surface features. *Journal of Catalysis*, 227(2), 470-478.
- Armaroli, N., & Balzani, V. (2007). The future of energy supply: challenges and opportunities. *Angewandte Chemie International Edition*, 46(1-2), 52-66.
- Armor, J. N. (1991). New catalytic technology commercialized in the USA during the 1980s. *Applied catalysis A: General*, 78(2), 141-173.

- Armor, J. N. (2001). New catalytic technology commercialized in the USA during the 1990s. *Applied Catalysis A: General*, 222(1), 407-426.
- Atadashi, I. M., Aroua, M. K., Aziz, A. A., & Sulaiman, N. M. N. (2011). Membrane biodiesel production and refining technology: a critical review. *Renewable and Sustainable Energy Reviews*, 15(9), 5051-5062.
- Aziz, M. A., Uemura, Y., and Sabil, K. M. (2011). Characterization of oil palm biomass as feed for torrefaction process. *National Postgraduate Conference (NPC)*, September, IEEE. DOI: 10.1109/NatPC.2011.6136260
- Babou, F., Coudurier, G., & Vedrine, J. C. (1995). Acidic properties of sulfated zirconia: an infrared spectroscopic study. *Journal of Catalysis*, 152(2), 341-349.
- Balat, M., & Balat, H. (2008). A critical review of bio-diesel as a vehicular fuel. *Energy conversion and management*, 49(10), 2727-2741.
- Barthos, R., Lonyi, F., Onyestyak, G. Y., & Valyon, J. (2000). An IR, FR, and TPD study on the acidity of H-ZSM-5, sulfated zirconia, and sulfated zirconia-titania using ammonia as the probe molecule. *The Journal of Physical Chemistry B*, 104(31), 7311-7319.
- Basiron, Y., Jalani, B. S., & Chan, K. W. (2000). *Advances in Oil Palm Research*. Malaysian Palm Oil Board, Bangi. 1-782, 783-1526.
- Bekkum, H. V., Jansen, J. C., & Flanigen, E. M. (1991). Introduction to zeolite science and practice.
- Bensitel, M., Saur, O., Lavalley, J. C., & Morrow, B. A. (1988). An infrared study of sulfated zirconia. *Materials chemistry and physics*, 19(1), 147-156.
- Berchmans, H. J., & Hirata, S. (2008). Biodiesel production from crude *Jatropha curcas* L. seed oil with a high content of free fatty acids. *Bioresource technology*, 99(6), 1716-1721. DOI: 10.1016/j.biortech.2007.03.051
- Blasco, T., Corma, A., Martinez, A., & Martinez-Escolano, P. (1998). Supported heteropolyacid (HPW) catalysts for the continuous alkylation of isobutane with 2-butene: The benefit of using MCM-41 with larger pore diameters. *Journal of catalysis*, 177(2), 306-313.
- Borges, M. E., & Díaz, L. (2012). Recent developments on heterogeneous catalysts for biodiesel production by oil esterification and transesterification reactions: a review. *Renewable and Sustainable Energy Reviews*, 16(5), 2839-2849.

- Breck, D. W. (1984). *Zeolite molecular sieves structure, chemistry and use*. Krieger. J Wiley & Sons, New York.
- Brito, A., Borges, M. E., & Otero, N. (2007). Zeolite Y as a heterogeneous catalyst in biodiesel fuel production from used vegetable oil. *Energy & Fuels*, 21(6), 3280-3283.
- Brown, W. H. 2000. *Introduction to organic chemistry*. 2nd ed. Saunders College Publishing, Orlando.
- Budarin, V. L., Clark, J. H., Luque, R., & Macquarrie, D. J. (2007). Versatile mesoporous carbonaceous materials for acid catalysis. *Chemical communications*, (6), 634-636. DOI: 10.1039/B614537J
- Caetano, C. S., Fonseca, I. M., Ramos, A. M., Vital, J., & Castanheiro, J. E. (2008). Esterification of free fatty acids with methanol using heteropolyacids immobilized on silica. *Catalysis Communications*, 9(10), 1996-1999.
- Campanati, M., Fornasari, G., & Vaccari, A. (2003). Fundamentals in the preparation of heterogeneous catalysts. *Catalysis Today*, 77(4), 299-314.
- Cardoso, A. L., Neves, S. C. G., & Da Silva, M. J. (2008). Esterification of oleic acid for biodiesel production catalyzed by SnCl₂: a kinetic investigation. *Energies*, 1(2), 79-92.
- Carrero, A., Vicente, G., Rodríguez, R., Linares, M., & Del Peso, G. L. (2011). Hierarchical zeolites as catalysts for biodiesel production from *Nannochloropsis* microalga oil. *Catalysis Today*, 167(1), 148-153.
- Cassiers, K., Linssen, T., Aerts, K., Cool, P., Lebedev, O., Van Tendeloo, G., ... & Vansant, E. F. (2003). Controlled formation of amine-templated mesostructured zirconia with remarkably high thermal stability. *Journal of Materials Chemistry*, 13(12), 3033-3039.
- Čejka, J., Richter, M., & Kölsch, P. (1995). Characterization of external surface properties of zeolite ZSM-5 modified by 12-tungstosilicic acid. *Studies in Surface Science and Catalysis*, 94, 246-253.
- Cerrato, G., Morterra, C., Delgado, M. R., Areán, C. O., Signoretto, M., Somma, F., & Pinna, F. (2006). Ga-promoted sulfated zirconia systems. II. Surface features and catalytic activity. *Microporous and mesoporous materials*, 94(1), 40-49.

- Chai, M., Tu, Q., Lu, M., & Yang, Y. J. (2014). Esterification pretreatment of free fatty acid in biodiesel production, from laboratory to industry. *Fuel Processing Technology*, 125, 106-113.
- Chakrabarti, A., & Sharma, M. M. (1993). Cationic ion exchange resins as catalyst. *Reactive Polymers*, 20(1), 1-45.
- Chan, K. W., Watson, I., and Lim, K. C. (1980). Use of oil palm waste material for increased production. In: *Proceeding of the Conference on Soil Science and Agricultural Development in Malaysia*, Kuala Lumpur, Malaysia. 213-241.
- Chen, G., & Fang, B. (2011). Preparation of solid acid catalyst from glucose–starch mixture for biodiesel production. *Bioresource technology*, 102(3), 2635-2640.
- Chen, W. H., Tu, Y. J., & Sheen, H. K. (2010). Impact of dilute acid pretreatment on the structure of bagasse for bioethanol production. *International Journal of Energy Research*, 34(3), 265-274.
- Cheng, J. J., & Timilsina, G. R. (2011). Status and barriers of advanced biofuel technologies: a review. *Renewable Energy*, 36(12), 3541-3549.
- Chisti, Y. (2007). Biodiesel from microalgae. *Biotechnology advances*, 25(3), 294-306.
- Chorkendorff, I., & Niemantsverdriet, J. W. (2006). *Concepts of modern catalysis and kinetics*. John Wiley & Sons.
- Chung, K. H., & Park, B. G. (2009). Esterification of oleic acid in soybean oil on zeolite catalysts with different acidity. *Journal of Industrial and Engineering Chemistry*, 15(3), 388-392.
- Clark, J. H. (2002). Solid acids for green chemistry. *Accounts of Chemical Research*, 35(9), 791-797.
- Clark, J. H., & Macquarrie, D. J. (1996). Environmentally friendly catalytic methods. *Chem. Soc. Rev.*, 25(5), 303-310.
- Clark, J. H., Cullen, S. R., Barlow, S. J., & Bastock, T. W. (1994). Keynote article. Environmentally friendly chemistry using supported reagent catalysts: structure–property relationships for clayzic. *Journal of the Chemical Society, Perkin Transactions 2*, (6), 1117-1130.

- Clark, J. H., Monks, G. L., Nightingale, D. J., Price, P. M., & White, J. F. (2000). A new solid acid-based route to linear alkylbenzenes. *Journal of catalysis*, 193(2), 348-350.
- Clements, L. D., & Gerpen, J. V. (2004). Biodiesel production technology. *NREL-National Renewable Energy Laboratory. NREL/SR-510-36244*.
- Corma, A. (2003). State of the art and future challenges of zeolites as catalysts. *Journal of Catalysis*, 216(1), 298-312.
- Corma, A., Fornes, V., Juan-Rajadell, M. I., & Nieto, J. L. (1994). Influence of preparation conditions on the structure and catalytic properties of $\text{SO}_4^{2-}/\text{ZrO}_2$ superacid catalysts. *Applied Catalysis A: General*, 116(1), 151-163.
- Corma, A., Martinez, A., & Martinez, C. (1994). Influence of process variables on the continuous alkylation of isobutane with 2-butene on superacid sulfated zirconia catalysts. *Journal of catalysis*, 149(1), 52-60.
- Dal Santo, V., Liguori, F., Pirovano, C., & Guidotti, M. (2010). Design and use of nanostructured single-site heterogeneous catalysts for the selective transformation of fine chemicals. *Molecules*, 15(6), 3829-3856.
- Damyanova, S., Pawelec, B., Arishtirova, K., Huerta, M. M., & Fierro, J. L. G. (2008). Study of the surface and redox properties of ceria-zirconia oxides. *Applied Catalysis A: General*, 337(1), 86-96.
- Danuthai, T., Jongpatiwut, S., Rirksomboon, T., Osuwan, S., & Resasco, D. E. (2009). Conversion of methylesters to hydrocarbons over an H-ZSM5 zeolite catalyst. *Applied Catalysis A: General*, 361(1), 99-105.
- Das, D., Mishra, H. K., Dalai, A. K., & Parida, K. M. (2003). Isopropylation of benzene over sulfated ZrO_2 - TiO_2 mixed-oxide catalyst. *Applied Catalysis A: General*, 243(2), 271-284.
- Dasari, M. A., Goff, M. J., & Suppes, G. J. (2003). Noncatalytic alcoholysis kinetics of soybean oil. *Journal of the American oil chemists' society*, 80(2), 189-192.
- Davis, B. H., Keogh, R. A., & Srinivasan, R. (1994). Sulfated zirconia as a hydrocarbon conversion catalyst. *Catalysis Today*, 20(2), 219-256.
- Dawodu, F. A., Ayodele, O. O., Xin, J., & Zhang, S. (2014). Application of solid acid catalyst derived from low value biomass for a cheaper biodiesel production. *Journal of Chemical Technology and Biotechnology*, 89(12), 1898-1909. DOI: 10.1002/jctb.4274

- Dehkhoda, A. M., West, A. H., & Ellis, N. (2010). Biochar based solid acid catalyst for biodiesel production. *Applied Catalysis A: General*, 382(2), 197-204. DOI: 10.1016/j.apcata.2010.04.051
- Delfort, B., Hillion, G., Le Pennec, D., & Lendresse, C. (2006). Process for transesterification of vegetable oils or animal oils by means of heterogeneous catalysts based on zinc or bismuth, titanium and aluminum. *U.S. Patent No. 7,151,187*. Washington, DC: U.S. Patent and Trademark Office.
- Di Serio, M., Cozzolino, M., Tesser, R., Patrono, P., Pinzari, F., Bonelli, B., & Santacesaria, E. (2007). Vanadyl phosphate catalysts in biodiesel production. *Applied Catalysis A: General*, 320, 1-7.
- Di Serio, M., Tesser, R., Pengmei, L., & Santacesaria, E. (2007). Heterogeneous catalysts for biodiesel production. *Energy & Fuels*, 22(1), 207-217.
- DIN EN ISO 660. (2009). "Animal and vegetable fats and oils - Determination of acid value and acidity," *European Committee for Standardization*.
- Dupont, P., & Lefebvre, F. (1996). Esterification of propanoic acid by butanol and 2-ethylhexanol catalyzed by heteropolyacids pure or supported on carbon. *Journal of Molecular Catalysis A: Chemical*, 114(1), 299-307.
- Dutch National Research School. (April 2009). Combination Catalysis Controlled by Chemical Design, Future Perspectives in Catalysis. (NRSC-Catalysis), Eindhoven, The Netherlands.
- Emeis, C. A. (1993). Determination of integrated molar extinction coefficients for infrared absorption bands of pyridine adsorbed on solid acid catalysts. *Journal of Catalysis*, 141(2), 347-354.
- Environmental Protection Agency, U. S. A comprehensive analysis of biodiesel impacts on exhaust. EPA; (2002). Available on-line: <http://www.epa.gov/otaq/models/analysis/biodsl/p02001.pdf>.
- Fa, D., Li, J. Q., & Cameron, S. (1997). Preparation of sulfated zirconia catalysts with improved control of sulfur content II. Effect of sulfur content on physical properties and catalytic activity. *Applied Catalysis A: General*, 154(1), 173-184.
- Fărcașiu, D., Ghenciu, A., & Li, J. Q. (1996). The Mechanism of conversion of saturated hydrocarbons catalyzed by sulfated metal oxides: reaction of adamantane on sulfated zirconia. *Journal of Catalysis*, 158(1), 116-127.

- Farooq, M., Ramli, A., & Subbarao, D. (2013). Biodiesel production from waste cooking oil using bifunctional heterogeneous solid catalysts. *Journal of Cleaner Production*, 59, 131-140.
- Feng, Y., He, B., Cao, Y., Li, J., Liu, M., Yan, F., & Liang, X. (2010). Biodiesel production using cation-exchange resin as heterogeneous catalyst. *Bioresource technology*, 101(5), 1518-1521.
- Fernández, M. B., Tonetto, G. M., Crapiste, G., & Damiani, D. E. (2007). Kinetics of the hydrogenation of sunflower oil over alumina supported palladium catalyst. *International Journal of Chemical Reactor Engineering*, 5(1), 10.
- Freedman, B. E. H. P., Pryde, E. H., & Mounts, T. L. (1984). Variables affecting the yields of fatty esters from transesterified vegetable oils. *Journal of the American Oil Chemists Society*, 61(10), 1638-1643.
- Freyhardt, C. C., Tsapatsis, M., Lobo, R. F., Balkus, K. J., & Davis, M. E. (1996). A high-silica zeolite with a 14-tetrahedral-atom pore opening.
- Fukuda, H., Kondo, A., & Noda, H. (2001). Biodiesel fuel production by transesterification of oils. *Journal of bioscience and bioengineering*, 92(5), 405-416.
- Furuta, S., Matsushashi, H., & Arata, K. (2004). Biodiesel fuel production with solid superacid catalysis in fixed bed reactor under atmospheric pressure. *Catalysis communications*, 5(12), 721-723.
- Furuta, S., Matsushashi, H., & Arata, K. (2006). Biodiesel fuel production with solid amorphous-zirconia catalysis in fixed bed reactor. *Biomass and Bioenergy*, 30(10), 870-873.
- Garcia, C. M., Teixeira, S., Marciniuk, L. L., & Schuchardt, U. (2008). Transesterification of soybean oil catalyzed by sulfated zirconia. *Bioresource Technology*, 99(14), 6608-6613.
- Geng, L., Yu, G., Wang, Y., & Zhu, Y. (2012). Ph-SO₃H-modified mesoporous carbon as an efficient catalyst for the esterification of oleic acid. *Applied Catalysis A: General*, 427, 137-144. DOI: 10.1016/j.apcata.2012.03.044
- Ghadge, S. V., & Raheman, H. (2006). Process optimization for biodiesel production from mahua (*Madhuca indica*) oil using response surface methodology. *Bioresource technology*, 97(3), 379-384. DOI: 10.1016/j.biortech.2005.03.014

- Giarola, S., Zamboni, A., & Bezzo, F. (2012). Environmentally conscious capacity planning and technology selection for bioethanol supply chains. *Renewable Energy*, 43, 61-72.
- Gladden, L. F. (2013). Magnetic resonance in reaction engineering: beyond spectroscopy. *Current Opinion in Chemical Engineering*, 2(3), 331-337.
- Graedel, T. E. (2007). Chapter 4. Green Chemistry and Sustainable Development, in Handbook of Green Chemistry and Technology. J. H. Clark & D. Macquarrie (Eds), Blackwell Science Ltd, Oxford, UK. doi: 10.1002/9780470988305.ch.4, p. 56.
- Guan, B., Wang, X., Xiao, Y., Liu, Y., & Huo, Q. (2013). A versatile cooperative template-directed coating method to construct uniform microporous carbon shells for multifunctional core-shell nanocomposites. *Nanoscale*, 5(6), 2469-2475.
- Guldhe, A., Singh, B., Rawat, I., & Bux, F. (2014). Synthesis of biodiesel from *Scenedesmus* sp. by microwave and ultrasound assisted in situ transesterification using tungstated zirconia as a solid acid catalyst. *Chemical Engineering Research and Design*, 92(8), 1503-1511.
- Gurmit, S., Lim, K. H., Teo, L., & David, L. K. (1999). Oil palm and the environment, a Malaysian perspective. *Malaysian Oil Palm Growers' Council*.
- Haase, F., & Sauer, J. (1998). The surface structure of sulfated zirconia: Periodic ab initio study of sulfuric acid adsorbed on ZrO₂ (101) and ZrO₂ (001). *Journal of the American Chemical Society*, 120(51), 13503-13512.
- Hara, M., Yoshida, T., Takagaki, A., Takata, T., Kondo, J. N., Hayashi, S., & Domen, K. (2004). A carbon material as a strong protonic acid. *Angewandte Chemie International Edition*, 43(22), 2955-2958.
- Harmer, M. A., & Sun, Q. (2001). Solid acid catalysis using ion-exchange resins. *Applied Catalysis A: General*, 221(1), 45-62.
- Hassan, K. B., Husin, M. A., Darus, B., & Jalani S. (1997). An estimated availability of oil palm biomass in Malaysia. *PORIM Occasional Paper* 37, 100.
- Hassan, S. N., Sani, Y. M., Aziz, A. A., Sulaiman, N. M. N., & Daud, W. M. A. W. (2015). Biogasoline: An out-of-the-box solution to the food-for-fuel and land-use competitions. *Energy Conversion and Management*, 89, 349-367. DOI: 10.1016/j.enconman.2014.09.050

- Hattori, H. (2010). Solid acid catalysts: roles in chemical industries and new concepts. *Topics in Catalysis*, 53(7-10), 432-438.
- He, H., Wang, T., & Zhu, S. (2007). Continuous production of biodiesel fuel from vegetable oil using supercritical methanol process. *Fuel*, 86(3), 442-447.
- Helwani, Z., Othman, M. R., Aziz, N., Kim, J., & Fernando, W. J. N. (2009). Solid heterogeneous catalysts for transesterification of triglycerides with methanol: a review. *Applied Catalysis A: General*, 363(1), 1-10.
- Hernández-Montelongo, R., García-Sandoval, J. P., & Aguilar-Garnica, E. (2015). On the non-ideal behavior of the homogeneous esterification reaction: A kinetic model based on activity coefficients. *Reaction Kinetics, Mechanisms and Catalysis*, 1-19. 10.1007/s11144-015-0848-x
- Hill, J., Nelson, E., Tilman, D., Polasky, S., & Tiffany, D. (2006). Environmental, economic, and energetic costs and benefits of biodiesel and ethanol biofuels. *Proceedings of the National Academy of Sciences*, 103(30), 11206-11210.
- Hino, M., Kobayashi, S., & Arata, K. (1979). Solid catalyst treated with anion. 2. Reactions of butane and isobutane catalyzed by zirconium oxide treated with sulfate ion. Solid superacid catalyst. *Journal of the American chemical society*, 101(21), 6439-6441.
- Hino, M., Kurashige, M., Matsushashi, H., & Arata, K. (2006). The surface structure of sulfated zirconia: Studies of XPS and thermal analysis. *Thermochimica acta*, 441(1), 35-41.
- Holewinski, A., Xin, H., Nikolla, E., & Linic, S. (2013). Identifying optimal active sites for heterogeneous catalysis by metal alloys based on molecular descriptors and electronic structure engineering. *Current Opinion in Chemical Engineering*, 2(3), 312-319.
- Hou, K., Zhang, A., Gu, L., Liu, M., & Guo, X. (2012). Efficient synthesis and sulfonation of ordered mesoporous carbon materials. *Journal of colloid and interface science*, 377(1), 18-26.

<http://www.bfdic.com/en/Features/Features/79.html> (Accessed on 10/03/2015)

http://www.exxonmobil.com/Corporate/files/news_pub_eo.pdf

- International Energy Agency (IEA), World energy outlook 2007. Available from: http://www.iea.org/textbase/nppdf/free/2007/weo_2007.pdf, 2007 (accessed 15.12.12).
- Ishida, M., and Abu Hassan, O. (1992). Effect of urea treatment level on nutritive value of oil palm fronds silage in Kedah. *Kelantan bulls*, 3, p. 68, in: Proceedings of the 6th AAAP Animal Science Congress, AHAT, Bangkok, Thailand.
- Izumi, Y., & Onaka, M. (1992). Organic syntheses using aluminosilicates. *Advances in catalysis*, 38, 245-282.
- Jacobs, P. A., & Von Ballmoos, R. (1982). Framework hydroxyl groups of H-ZSM-5 zeolites. *The Journal of Physical Chemistry*, 86(15), 3050-3052.
- Janaun, J., & Ellis, N. (2011). Role of silica template in the preparation of sulfonated mesoporous carbon catalysts. *Applied Catalysis A: General*, 394(1), 25-31. DOI: 10.1016/j.apcata.2010.12.016
- Jin, F., & Li, Y. (2009). A FTIR and TPD examination of the distributive properties of acid sites on ZSM-5 zeolite with pyridine as a probe molecule. *Catalysis Today*, 145(1), 101-107.
- Jin, T., Yamaguchi, T., & Tanabe, K. (1986). Mechanism of acidity generation on sulfur-promoted metal oxides. *The Journal of Physical Chemistry*, 90(20), 4794-4796.
- Jitputti, J., Kitiyanan, B., Rangsunvigit, P., Bunyakiat, K., Attanatho, L., & Jenvanitpanjakul, P. (2006). Transesterification of crude palm kernel oil and crude coconut oil by different solid catalysts. *Chemical Engineering Journal*, 116(1), 61-66.
- Jothiramalingam, R., & Wang, M. K. (2009). Review of recent developments in solid acid, base, and enzyme catalysts (heterogeneous) for biodiesel production via transesterification. *Industrial & Engineering Chemistry Research*, 48(13), 6162-6172.
- Kaeding, W. W., & Butter, S. A. (1980). Production of chemicals from methanol: I. Low molecular weight olefins. *Journal of Catalysis*, 61(1), 155-164.
- Kafuku, G., & Mbarawa, M. (2010). Biodiesel production from Croton megalocarpus oil and its process optimization. *Fuel*, 89(9), 2556-2560.
- Kaneda, K., Ebitani, K., Mizugaki, T., & Mori, K. (2006). Design of high-performance heterogeneous metal catalysts for green and sustainable chemistry. *Bulletin of the Chemical Society of Japan*, 79(7), 981-1016.

- Karatepe, Y., Nese, S. V., Keçebas, A., Yumurtaci M. (2012). The levels of awareness about the renewable energy sources of university students in Turkey. *Renewable Energy*, 44, 174-179.
- Kastner, J. R., Miller, J., Geller, D. P., Locklin, J., Keith, L. H., & Johnson, T. (2012). Catalytic esterification of fatty acids using solid acid catalysts generated from biochar and activated carbon. *Catalysis Today*, 190(1), 122-132.
- Kawabata, T., Kato, M., Mizugaki, T., Ebitani, K., & Kaneda, K. (2005). Monomeric metal aqua complexes in the interlayer space of montmorillonites as strong lewis acid catalysts for heterogeneous carbon-carbon bond-forming reactions. *Chemistry-A European Journal*, 11(1), 288-297.
- Keggin, J. F. (1934, March). The structure and formula of 12-phosphotungstic acid. In *Proceedings of the Royal Society of London A: Mathematical, Physical and Engineering Sciences* (Vol. 144, No. 851, pp. 75-100). The Royal Society.
- Kim, S. Y., Lohitharn, N., Goodwin, J. G., Olindo, R., Pinna, F., & Canton, P. (2006). The effect of Al₂O₃-promotion of sulfated zirconia on n-butane isomerization: An isotopic transient kinetic analysis. *Catalysis Communications*, 7(4), 209-213.
- Kiss, A. A., Dimian, A. C., & Rothenberg, G. (2006). Solid acid catalysts for biodiesel Production-Towards sustainable energy. *Advanced Synthesis & Catalysis*, 348(1-2), 75-81.
- Kiss, A. A., Dimian, A. C., & Rothenberg, G. (2007). Biodiesel by catalytic reactive distillation powered by metal oxides. *Energy & Fuels*, 22(1), 598-604.
- Kiss, A. A., Omota, F., Dimian, A. C., & Rothenberg, G. (2006). The heterogeneous advantage: biodiesel by catalytic reactive distillation. *Topics in Catalysis*, 40(1-4), 141-150.
- Knothe, G. (2010). Biodiesel and renewable diesel: a comparison. *Progress in Energy and Combustion Science*, 36(3), 364-373.
- Koberg, M., & Gedanken, A. (2012). Optimization of bio-diesel production from oils, cooking oils, microalgae, and castor and jatropha seeds: probing various heating sources and catalysts. *Energy & Environmental Science*, 5(6), 7460-7469.
- Koster, R., van der Linden, B., Poels, E., & Blik, A. (2001). The mechanism of the gas-phase esterification of acetic acid and ethanol over MCM-41. *Journal of Catalysis*, 204(2), 333-338.

- Kouzu, M., Nakagaito, A., & Hidaka, J. S. (2011). Pre-esterification of FFA in plant oil transesterified into biodiesel with the help of solid acid catalysis of sulfonated cation-exchange resin. *Applied Catalysis A: General*, 405(1), 36-44.
- Kozhevnikov, I. V. (1998). Catalysis by heteropoly acids and multicomponent polyoxometalates in liquid-phase reactions. *Chemical Reviews*, 98(1), 171-198.
- Kozhevnikov, I. V. (2002). Catalysts for fine chemical synthesis. *Catalysis by polyoxometalates*, 2. Wiley, Chichester, England.
- Krawczyk, T. (1996). Biodiesel-alternative fuel makes inroads but hurdles remain. *Inform*, 7(8), 801-829.
- Kuo, C. H., & Lee, C. K. (2009). Enhancement of enzymatic saccharification of cellulose by cellulose dissolution pretreatments. *Carbohydrate Polymers*, 77(1), 41-46.
- Lam, M. K., & Lee, K. T. (2010). Accelerating transesterification reaction with biodiesel as co-solvent: A case study for solid acid sulfated tin oxide catalyst. *Fuel*, 89(12), 3866-3870.
- Lam, M. K., Lee, K. T., & Mohamed, A. R. (2009). Sulfated tin oxide as solid superacid catalyst for transesterification of waste cooking oil: an optimization study. *Applied Catalysis B: Environmental*, 93(1), 134-139.
- Lam, M. K., Lee, K. T., & Mohamed, A. R. (2010). Homogeneous, heterogeneous and enzymatic catalysis for transesterification of high free fatty acid oil (waste cooking oil) to biodiesel: a review. *Biotechnology advances*, 28(4), 500-518.
- Larock, R. C. (1989). Comprehensive Organic Transformations: A Guide to Functional Group Preparations. *VCH Publishers*, New York. ISBN: 9780895737106
- Lee, A. F., & Wilson, K. (2015). Recent developments in heterogeneous catalysis for the sustainable production of biodiesel. *Catalysis Today*, 242, 3-18.
- Lee, K. Y., Arai, T., Nakata, S., Asaoka, S., Okuhara, T., & Misono, M. (1992). Catalysis by heteropoly compounds. 20. An NMR study of ethanol dehydration in the pseudoliquid phase of 12-tungstophosphoric acid. *Journal of the American Chemical Society*, 114(8), 2836-2842.
- Lin, V. S. Y., & Radu, D. R. (2006). Use of functionalized mesoporous silicates to esterify fatty acids and transesterify oils. *U.S. Patent No. 7,122,688*. Washington, DC: U.S. Patent and Trademark Office.

- Liu, J., Wang, Q., Wang, S., Zou, D., & Sonomoto, K. (2012). Utilisation of microwave-NaOH pretreatment technology to improve performance and L-lactic acid yield from vinasse. *Biosystems Engineering*, 112(1), 6-13.
- Liu, R., Wang, X., Zhao, X., & Feng, P. (2008). Sulfonated ordered mesoporous carbon for catalytic preparation of biodiesel. *Carbon*, 46(13), 1664-1669. DOI: 10.1016/j.carbon.2008.07.016
- Liu, T., Li, Z., Li, W., Shi, C., & Wang, Y. (2013). Preparation and characterization of biomass carbon-based solid acid catalyst for the esterification of oleic acid with methanol. *Bioresource technology*, 133, 618-621. DOI: 10.1016/j.biortech.2013.01.163
- Lobo, R. F., Tsapatsis, M., Freyhardt, C. C., Khodabandeh, S., Wagner, P., Chen, C. Y., ... & Davis, M. E. (1997). Characterization of the extra-large-pore zeolite UTD-1. *Journal of the American Chemical Society*, 119(36), 8474-8484.
- Lónyi, F., Valyon, J., Engelhardt, J., & Mizukami, F. (1996). Characterization and catalytic properties of sulfated $\text{ZrO}_2\text{-TiO}_2$ mixed oxides. *Journal of Catalysis*, 160(2), 279-289.
- López, D. E., Goodwin, J. G., Bruce, D. A., & Furuta, S. (2008). Esterification and transesterification using modified-zirconia catalysts. *Applied Catalysis A: General*, 339(1), 76-83.
- López, D. E., Goodwin, J. G., Bruce, D. A., & Lotero, E. (2005). Transesterification of triacetin with methanol on solid acid and base catalysts. *Applied Catalysis A: General*, 295(2), 97-105.
- López, D. E., Goodwin, J. G., Bruce, D. A., & Lotero, E. (2005). Transesterification of triacetin with methanol on solid acid and base catalysts. *Applied Catalysis A: General*, 295(2), 97-105.
- López, D. E., Suwannakarn, K., Bruce, D. A., & Goodwin, J. G. (2007). Esterification and transesterification on tungstated zirconia: effect of calcination temperature. *Journal of Catalysis*, 247(1), 43-50.
- Lotero, E., Liu, Y., Lopez, D. E., Suwannakarn, K., Bruce, D. A., & Goodwin, J. G. (2005). Synthesis of biodiesel via acid catalysis. *Industrial & engineering chemistry research*, 44(14), 5353-5363.
- Lotero, E., Liu, Y., Lopez, D. E., Suwannakarn, K., Bruce, D. A., & Goodwin, J. G. (2005). Synthesis of biodiesel via acid catalysis. *Industrial & engineering chemistry research*, 44(14), 5353-5363.

- Lou, W. Y., Zong, M. H., & Duan, Z. Q. (2008). Efficient production of biodiesel from high free fatty acid-containing waste oils using various carbohydrate-derived solid acid catalysts. *Bioresource Technology*, 99(18), 8752-8758.
- Lu, R., Tangbo, H., Wang, Q., & Xiang, S. (2003). Properties and characterization of modified HZSM-5 zeolites. *Journal of Natural Gas Chemistry*, 12(1), 56-62.
- Luque, R., Herrero-Davila, L., Campelo, J. M., Clark, J. H., Hidalgo, J. M., Luna, D., ... & Romero, A. A. (2008). Biofuels: a technological perspective. *Energy & Environmental Science*, 1(5), 542-564.
- Luque, R., Lovett, J. C., Datta, B., Clancy, J., Campelo, J. M., & Romero, A. A. (2010). Biodiesel as feasible petrol fuel replacement: a multidisciplinary overview. *Energy & Environmental Science*, 3(11), 1706-1721.
- M. Pacheco, U.S. Senate Full Committee Hearing - Renewable Fuel Standards (National Renewable Energy Laboratory, National Bioenergy Center, 19 June 2006); available at http://energy.senate.gov/public/index.cfm?IsPrint=true&FuseAction=Hearings.Testimony&Hearing_ID=1565&Witness_ID=4427. On corn ethanol.
- Ma, F., & Hanna, M. A. (1999). Biodiesel production: a review. *Bioresource technology*, 70(1), 1-15.
- Maciá-Agulló, J. A., Sevilla, M., Diez, M. A., & Fuertes, A. B. (2010). Synthesis of Carbon-based Solid Acid Microspheres and Their Application to the Production of Biodiesel. *ChemSusChem*, 3(12), 1352-1354.
- Maesen, T., & Marcus, B. (2001). The zeolite scene—an overview. *Studies in surface science and catalysis*, 137, 1-9. Elsevier Science BV, Amsterdam.
- Maksimov, G. M. (1995). Advances in the synthesis of polyoxometalates and in the study of heteropolyacids. *Russian Chemical Reviews*, 64(5), 445.
- Manriquez, M. E., López, T., Gómez, R., & Navarrete, J. (2004). Preparation of TiO₂–ZrO₂ mixed oxides with controlled acid–basic properties. *Journal of Molecular Catalysis A: Chemical*, 220(2), 229-237.
- Mata, T. M., Martins, A. A., & Caetano, N. S. (2010). Microalgae for biodiesel production and other applications: a review. *Renewable and sustainable energy reviews*, 14(1), 217-232.

- McNeff, C. V., McNeff, L. C., Yan, B., Nowlan, D. T., Rasmussen, M., Gyberg, A. E., ... & Hoyer, T. R. (2008). A continuous catalytic system for biodiesel production. *Applied Catalysis A: General*, 343(1), 39-48.
- Metcalf, I. S., North, M., Pasquale, R., & Thursfield, A. (2010). An integrated approach to energy and chemicals production. *Energy & Environmental Science*, 3(2), 212-215.
- Mile, B., Stirling, D., Zammitt, M. A., Lovell, A., & Webb, M. (1990). TPR studies of the effects of preparation conditions on supported nickel catalysts. *Journal of molecular catalysis*, 62(2), 179-198.
- Misono, M. (1987). Heterogeneous catalysis by heteropoly compounds of molybdenum and tungsten. *Catalysis Reviews Science and Engineering*, 29(2-3), 269-321.
- Misono, M., & Nojiri, N. (1990). Recent progress in catalytic technology in Japan. *Applied catalysis*, 64, 1-30.
- Misono, M., Ono, I., Koyano, G., & Aoshima, A. (2000). Heteropolyacids. Versatile green catalysts usable in a variety of reaction media. *Pure and applied chemistry*, 72(7), 1305-1311.
- Mitchell, S., Michels, N. L., Majano, G., & Pérez-Ramírez, J. (2013). Advanced visualization strategies bridge the multidimensional complexity of technical catalysts. *Current Opinion in Chemical Engineering*, 2(3), 304-311.
- Moles, P. Sulphated zirconia as a catalyst for isomerisation reactions. Reprinted from Speciality Chemicals 2014, Nov/Dec.
- Morterra, C., Cerrato, G., Emanuel, C., & Bolis, V. (1993). On the Surface Acidity of Some Sulfate-Doped ZrO₂ Catalysts. *Journal of Catalysis*, 142(2), 349-367.
- Morterra, C., Cerrato, G., Pinna, F., & Signoreto, M. (1995). Crystal phase, spectral features, and catalytic activity of sulfate-doped zirconia systems. *Journal of Catalysis*, 157(1), 109-123.
- Nakajima, K., & Hara, M. (2012). Amorphous carbon with SO₃H groups as a solid Brønsted acid catalyst. *ACS catalysis*, 2(7), 1296-1304.
- Nakpong, P., & Wootthikanokkhan, S. (2010). High free fatty acid coconut oil as a potential feedstock for biodiesel production in Thailand. *Renewable Energy*, 35(8), 1682-1687.

- Narasimharao, K., Brown, D. R., Lee, A. F., Newman, A. D., Siril, P. F., Tavener, S. J., & Wilson, K. (2007). Structure–activity relations in Cs-doped heteropolyacid catalysts for biodiesel production. *Journal of catalysis*, 248(2), 226-234.
- Narayan, C. M. (2002). Vegetable oil as engine fuels - prospect and retrospect. *Proceedings on Recent Trends in Automotive Fuels*, Nagpur, India. 2001-01-1807/4227.
- National Renewable Energy Laboratory (NREL), (2006). US Department of Energy, U.S. Biodiesel handling and use guidelines; available at <http://www.nrel.gov/docs/fy06osti/40555.pdf>.
- Navio, J. A., Colón, G., Macias, M., Campelo, J. M., Romero, A. A., & Marinas, J. M. (1998). Catalytic properties of sulfated and non-sulfated ZrO₂–SiO₂: effects of the sulfation submitted before or after the calcination process, in the cyclohexene isomerization reaction. *Journal of Molecular Catalysis A: Chemical*, 135(2), 155-162.
- Ni, J., & Meunier, F. C. (2007). Esterification of free fatty acids in sunflower oil over solid acid catalysts using batch and fixed bed-reactors. *Applied Catalysis A: General*, 333(1), 122-130.
- Nigam, P. S., & Singh, A. (2011). Production of liquid biofuels from renewable resources. *Progress in Energy and Combustion Science*, 37(1), 52-68.
- Nusterer, E., Blöchl, P. E., & Schwarz, K. (1996). Interaction of water and methanol with a zeolite at high coverages. *Chemical physics letters*, 253(5), 448-455.
- Okuhara, T. (2002). Water-tolerant solid acid catalysts. *Chemical Reviews*, 102(10), 3641-3666.
- Omota, F., Dimian, A. C., & Blik, A. (2003a). Fatty acid esterification by reactive distillation. Part 1: equilibrium-based design. *Chemical Engineering Science*, 58(14), 3159-3174.
- Omota, F., Dimian, A. C., & Blik, A. (2003b). Fatty acid esterification by reactive distillation: Part 2 – kinetics-based design for sulphated zirconia catalysts. *Chemical Engineering Science*, 58(14), 3175-3185.
- Ong, H. C., Mahlia, T. M. I., Masjuki, H. H., & Norhasyima, R. S. (2011). Comparison of palm oil, *Jatropha curcas* and *Calophyllum inophyllum* for biodiesel: a review. *Renewable and Sustainable Energy Reviews*, 15(8), 3501-3515.

- Orjuela, A., Kolah, A., Lira, C. T., & Miller, D. J. (2011). Mixed Succinic Acid/Acetic Acid Esterification with Ethanol by Reactive Distillation. *Industrial & Engineering Chemistry Research*, 50(15), 9209-9220.
- Orjuela, A., Yanez-Mckay, A., Lira, C. T., and Miller, D. J. (2012). Carboxylic acid recovery and methods related thereto. *U.S. Patent*. EP2507200 A1, Oct 10.
- Osendi, M. I., Moya, J. S., Serna, C. J., & Soria, J. (1985). Metastability of tetragonal zirconia powders. *Journal of the American Ceramic Society*, 68(3), 135-139.
- Pacheco, G., & Fripiat, J. J. (2000). Physical chemistry of the thermal transformation of mesoporous and microporous zirconia. *The Journal of Physical Chemistry B*, 104(50), 11906-11911.
- Pan, F., Lu, X., Zhu, Q., Zhang, Z., Wang, T., & Chen, S. (2014). A fast route for synthesizing nano-sized ZSM-5 aggregates. *Journal of Materials Chemistry A*, 2(48), 20667-20675.
- Park, J. Y., Kim, D. K., & Lee, J. S. (2010). Esterification of free fatty acids using water-tolerable Amberlyst as a heterogeneous catalyst. *Bioresource technology*, 101(1), S62-S65.
- Park, Y. M., Lee, D. W., Kim, D. K., Lee, J. S., & Lee, K. Y. (2008). The heterogeneous catalyst system for the continuous conversion of free fatty acids in used vegetable oils for the production of biodiesel. *Catalysis Today*, 131(1), 238-243.
- Pauling, L. (1960). *The nature of the chemical bond and the structure of molecules and crystals: an introduction to modern structural chemistry* (Vol. 18). Cornell University Press.
- Peng, B. X., Shu, Q., Wang, J. F., Wang, G. R., Wang, D. Z., & Han, M. H. (2008). Biodiesel production from waste oil feedstocks by solid acid catalysis. *Process Safety and Environmental Protection*, 86(6), 441-447.
- Peng, F., Zhang, L., Wang, H., Lv, P., & Yu, H. (2005). Sulfonated carbon nanotubes as a strong protonic acid catalyst. *Carbon*, 43(11), 2405-2408.
- Peng, L., Philippaerts, A., Ke, X., Van Noyen, J., De Clippel, F., Van Tendeloo, G., ... & Sels, B. F. (2010). Preparation of sulfonated ordered mesoporous carbon and its use for the esterification of fatty acids. *Catalysis Today*, 150(1), 140-146.
- Pinto, A. C., Guarieiro, L. L., Rezende, M. J., Ribeiro, N. M., Torres, E. A., Lopes, W. A., ... & Andrade, J. B. D. (2005). Biodiesel: an overview. *Journal of the Brazilian Chemical Society*, 16(6B), 1313-1330.

- Piriou, B., Vaitilingom, G., Veyssière, B., Cuq, B., & Rouau, X. (2013). Potential direct use of solid biomass in internal combustion engines. *Progress in Energy and Combustion Science*, 39(1), 169-188.
- Pizzio, L. R., Caceres, C. V., & Blanco, M. N. (1998). Acid catalysts prepared by impregnation of tungstophosphoric acid solutions on different supports. *Applied Catalysis A: General*, 167(2), 283-294.
- Poonjarernsilp, C., Sano, N., & Tamon, H. (2014). Hydrothermally sulfonated single-walled carbon nanohorns for use as solid catalysts in biodiesel production by esterification of palmitic acid. *Applied Catalysis B: Environmental*, 147, 726-732.
- Pramanik, K. (2003). Properties and use of *Jatropha curcas* oil and diesel fuel blends in compression ignition engine. *Renewable energy*, 28(2), 239-248.
- Prauchner, M. J., & Rodríguez-Reinoso, F. (2012). Chemical versus physical activation of coconut shell: a comparative study. *Microporous and Mesoporous Materials*, 152, 163-171.
- Rabumi, W. (1998). "Chemical composition of oil palm empty fruit bunch and its decomposition in tile field," Thesis Submitted to Universiti Putra Malaysia.
- Rahimi, N., & Karimzadeh, R. (2011). Catalytic cracking of hydrocarbons over modified ZSM-5 zeolites to produce light olefins: A review. *Applied Catalysis A: General*, 398(1), 1-17.
- Ramadhas, A. S., Jayaraj, S., & Muraleedharan, C. (2004). Use of vegetable oils as IC engine fuels—a review. *Renewable energy*, 29(5), 727-742.
- Ramadhas, A. S., Jayaraj, S., & Muraleedharan, C. (2005). Biodiesel production from high FFA rubber seed oil. *Fuel*, 84(4), 335-340.
- Ramu, S., Lingaiah, N., Devi, B. P., Prasad, R. B. N., Suryanarayana, I., & Prasad, P. S. (2004). Esterification of palmitic acid with methanol over tungsten oxide supported on zirconia solid acid catalysts: effect of method of preparation of the catalyst on its structural stability and reactivity. *Applied Catalysis A: General*, 276(1), 163-168.
- Ranganathan, S. V., Narasimhan, S. L., & Muthukumar, K. (2008). An overview of enzymatic production of biodiesel. *Bioresource Technology*, 99(10), 3975-3981.
- Rattanaphra, D., Harvey, A., & Srinophakun, P. (2010). Simultaneous conversion of triglyceride/free fatty acid mixtures into biodiesel using sulfated zirconia. *Topics in Catalysis*, 53(11-12), 773-782.

- Refaat, A. A. (2011). Biodiesel production using solid metal oxide catalysts. *International Journal of Environmental Science & Technology*, 8(1), 203-221.
- Rezaei, M., Alavi, S. M., Sahebdehfar, S., Bai, P., Liu, X., & Yan, Z. F. (2008). CO₂ reforming of CH₄ over nanocrystalline zirconia-supported nickel catalysts. *Applied Catalysis B: Environmental*, 77(3), 346-354.
- Rezaei, M., Alavi, S. M., Sahebdehfar, S., Xinmei, L., Qian, L., & Yan, Z. F. (2007). CO₂-CH₄ reforming over nickel catalysts supported on mesoporous nanocrystalline zirconia with high surface area. *Energy & fuels*, 21(2), 581-589.
- Riemer, T., Spielbauer, D., Hunger, M., Makhemer, G., & Knözinger, H. (1994). Superacid properties of sulfated zirconia as measured by Raman and ¹H MAS NMR spectroscopy. *Journal of the Chemical Society. Chemical communications*, (10), 1181-1182.
- Rocchiccioli-Deltcheff, C., Amirouche, M., Hervé, G., Fournier, M., Che, M., & Tatibouët, J. M. (1990). Structure and catalytic properties of silica-supported polyoxomolybdates: II. Thermal behavior of unsupported and silica-supported 12-molybdosilicic acid catalysts from IR and catalytic reactivity studies. *Journal of Catalysis*, 126(2), 591-599.
- Sani, Y. M., Abdul Aziz, A., & Daud, W. M. A. W. (2012). Biodiesel feedstock and production technologies: Successes, challenges and prospects. In: *Biodiesel - Feedstocks, Production, and Applications*, Z. Fang (ed.), InTech, Croatia. DOI: [10.5772/52790](https://doi.org/10.5772/52790)
- Sani, Y. M., Abdul Aziz, A., & Daud, W. M. A. W. (2013). Solid acid-catalyzed biodiesel production from microalgal oil—the dual advantage. *Journal of Environmental Chemical Engineering*, 1(3), 113-121.
- Sani, Y. M., Alaba, P. A., Raji-Yahya, A. O., Aziz, A. A., & Daud, W. M. A. W. (2015). Acidity and catalytic performance of Yb-doped/Zr in comparison with/Zr catalysts synthesized via different preparatory conditions for biodiesel production. *Journal of the Taiwan Institute of Chemical Engineers*, <http://dx.doi.org/10.1016/j.jtice.2015.07.016>.
- Sani, Y. M., Aziz, A. A., & Daud, W. M. A. W. (2014). Activity of solid acid catalysts for biodiesel production: a critical review. *Applied Catalysis A: General*, 470, 140-161.
- Sani, Y. M., Daud, W. M. A. W. Abdul Aziz, A. R. (2012). Biodiesel Feedstock and Production Technologies: Successes, Challenges and Prospects. In: *Biodiesel—Feedstocks, Production and Applications*. Z. Fang (Ed.), ISBN: 978-953-51-0910-5 <http://dx.doi.org/10.5772/52790>

- Sani, Y. M., Raji-Yahya, A. O., Alaba, P. A., Aziz, A. R. A., & Daud, W. M. A. W. (2015a). Palm Frond and Spikelet as Environmentally Benign Alternative Solid Acid Catalysts for Biodiesel Production. *BioResources*, 10(2), 3393-3408.
- Sani, Y. M., Raji-Yahya, A. O., Alaba, P. A., Aziz, A. R. A., & Daud, W. M. A. W. (2015). Palm frond and spikelet as environmentally benign alternative solid acid catalysts for biodiesel production. *BioResources*, 10(2), 3393-3408.
- Santos, V., Zeni, M., Bergmann, C. P., & Hohemberger, J. M. (2008). Correlation between thermal treatment and tetragonal/monoclinic nanostructured zirconia powder obtained by sol–gel process. *Rev. Adv. Mater. Sci*, 17(1/2), 62-70.
- Sarkar, N., Ghosh, S. K., Bannerjee, S., & Aikat, K. (2012). Bioethanol production from agricultural wastes: An overview. *Renewable Energy*, 37(1), 19-27.
- Sasidharan, M., & Kumar, R. (2004). Transesterification over various zeolites under liquid-phase conditions. *Journal of Molecular Catalysis A: Chemical*, 210(1), 93-98.
- Sato, K., Nishimura, Y., & Shimada, H. (1999). Preparation and activity evaluation of Y zeolites with or without mesoporosity. *Catalysis letters*, 60(1-2), 83-87.
- Schwab, A. W., Bagby, M. O., & Freedman, B. (1987). Preparation and properties of diesel fuels from vegetable oils. *Fuel*, 66(10), 1372-1378.
- Şensöz, S., Angin, D., & Yorgun, S. (2000). Influence of particle size on the pyrolysis of rapeseed (*Brassica napus* L.): fuel properties of bio-oil. *Biomass and Bioenergy*, 19(4), 271-279.
- Sensoz, S., Demiral, I., & Gercüel, H. F. (2006). Olive bagasse (*Olea europaea* L.) pyrolysis. *Bioresource Technology*, 97(3), 429-436.
- Serrano-Ruiz, J. C., Ramos-Fernández, E. V., & Sepúlveda-Escribano, A. (2012). From biodiesel and bioethanol to liquid hydrocarbon fuels: new hydrotreating and advanced microbial technologies. *Energy & Environmental Science*, 5(2), 5638-5652.
- Shahid, E. M., & Jamal, Y. (2011). Production of biodiesel: a technical review. *Renewable and Sustainable Energy Reviews*, 15(9), 4732-4745.
- Shapouri, H., Duffield, J. A., & Wang, M. Q. (2002). *The energy balance of corn ethanol: an update* (No. 34075). United States Department of Agriculture, Economic Research Service.

- Sharma, M. M. (1995). Some novel aspects of cationic ion-exchange resins as catalysts. *Reactive and Functional Polymers*, 26(1), 3-23.
- Sharma, Y. C., Singh, B., & Upadhyay, S. N. (2008). Advancements in development and characterization of biodiesel: a review. *Fuel*, 87(12), 2355-2373.
- Shay, E. G. (1993). Diesel fuel from vegetable oils: status and opportunities. *Biomass and Bioenergy*, 4(4), 227-242.
- Sheehan, J., Camobreco, V., Duffield, J., Graboski, M., Shapouri, H., (1998). Life Cycle Inventory of Biodiesel and Petroleum Diesel for use in an Urban Bus. Prepared for the US Department of Energy's Office of Fuels Development and US Department of Agriculture's Office of Energy by the National Renewable Energy Laboratory, Golden, CO. (Available at: <http://www.nrel.gov/docs/legosti/fy98/24089.pdf> (Accessed on July 1, 2014).
- Sheldon, R. A., & Van Bekkum, H. (Eds.). (2008). *Fine chemicals through heterogeneous catalysis*. John Wiley & Sons.
- Sheldon, R. A., Arends, I., & Hanefeld, U. (2007). *Green chemistry and catalysis*. John Wiley & Sons.
- Shimizu, K. I., Miyagi, M., Kan-no, T., Hatamachi, T., Kodama, T., & Kitayama, Y. (2005). Michael reaction of β -ketoesters with vinyl ketones by iron (III)-exchanged fluorotetrasilicic mica: catalytic and spectroscopic studies. *Journal of Catalysis*, 229(2), 470-479.
- Shu, Q., Nawaz, Z., Gao, J., Liao, Y., Zhang, Q., Wang, D., & Wang, J. (2010). Synthesis of biodiesel from a model waste oil feedstock using a carbon-based solid acid catalyst: reaction and separation. *Bioresource technology*, 101(14), 5374-5384.
- Shu, Q., Yang, B., Yuan, H., Qing, S., & Zhu, G. (2007). Synthesis of biodiesel from soybean oil and methanol catalyzed by zeolite beta modified with La^{3+} . *Catalysis Communications*, 8(12), 2159-2165.
- Sing, K. S. W., Everett, D. H., Haul, R. A. W., Moscou, L., Pierotti, R. A., Rouquerol, J., and Siemieniewska, T. (1985). Reporting physisorption data for gas/solid systems with special reference to the determination of surface area and porosity (Recommendations 1984). *Pure and applied chemistry*, 57(4), 603-619.
- Smith, K., El-Hiti, G. A., Jayne, A. J., & Butters, M. (2003). Acetylation of aromatic ethers using acetic anhydride over solid acid catalysts in a solvent-free system. Scope of the reaction for substituted ethers. *Organic & biomolecular chemistry*, 1(9), 1560-1564.

- Song, C., Lai, W. C., Schmitz, A. D., & Reddy, K. M. (1996). *Characterization of acidic properties of microporous and mesoporous zeolite catalysts using TGA and DSC* (No. CONF-960376--). American Chemical Society, Washington, DC (United States).
- Song, X., & Sayari, A. (1996). Sulfated zirconia-based strong solid-acid catalysts: recent progress. *Catalysis Reviews*, 38(3), 329-412.
- Sonntag, N. O. V. (1979). Reactions of fats and fatty acids. Bailey's industrial oil and fat products, vol. Swern, D.
- Sreeprasanth, P. S., Srivastava, R., Srinivas, D., & Ratnasamy, P. (2006). Hydrophobic, solid acid catalysts for production of biofuels and lubricants. *Applied Catalysis A: General*, 314(2), 148-159.
- Srilatha, K., Kumar, C. R., Devi, B. P., Prasad, R. B. N., Prasad, P. S., & Lingaiah, N. (2011). Efficient solid acid catalysts for esterification of free fatty acids with methanol for the production of biodiesel. *Catalysis Science & Technology*, 1(4), 662-668.
- Suganuma, S., Nakajima, K., Kitano, M., Kato, H., Tamura, A., Kondo, H., Yanagawa, S., Hayashi, S., and Hara, M. (2011). SO₃H-bearing mesoporous carbon with highly selective catalysis. *Microporous and Mesoporous Materials*, 143(2), 443-450.
- Suharto, T. E. (2009). Synthesis of Catalytically Active High Surface Area Sulfated Zirconia. *Jurnal Matematika & Sains*, 8(4), 171-173.
- Sulaiman, O., Salim, N., Nordin, N. A., Hashim, R., Ibrahim, M., & Sato, M. (2012). The potential of oil palm trunk biomass as an alternative source for compressed wood. *BioResources*, 7(2), 2688-2706.
- Sun, Y., Ma, S., Du, Y., Yuan, L., Wang, S., Yang, J., ... & Xiao, F. S. (2005). Solvent-free preparation of nanosized sulfated zirconia with Brønsted acidic sites from a simple calcination. *The Journal of Physical Chemistry B*, 109(7), 2567-2572.
- Sunita, G., Devassy, B. M., Vinu, A., Sawant, D. P., Balasubramanian, V. V., & Halligudi, S. B. (2008). Synthesis of biodiesel over zirconia-supported isopoly and heteropoly tungstate catalysts. *Catalysis Communications*, 9(5), 696-702.
- Suwannakarn, K., Lotero, E., Ngaosuwan, K., & Goodwin Jr, J. G. (2009). Simultaneous free fatty acid esterification and triglyceride transesterification using a solid acid catalyst with in situ removal of water and unreacted methanol. *Industrial & Engineering Chemistry Research*, 48(6), 2810-2818.

- Suzuki, K., Sastre, G., Katada, N., & Niwa, M. (2007). Quantitative measurements of bronsted acidity of zeolites by ammonia IRMS-TPD method and density functional calculation. *Chemistry Letters*, 36(8), 1034-1035.
- Takagaki, A., Toda, M., Okamura, M., Kondo, J. N., Hayashi, S., Domen, K., & Hara, M. (2006). Esterification of higher fatty acids by a novel strong solid acid. *Catalysis Today*, 116(2), 157-161.
- Tanabe, K., & Hölderich, W. F. (1999). Industrial application of solid acid–base catalysts. *Applied Catalysis A: General*, 181(2), 399-434.
- Tanabe, K., & Yamaguchi, T. (1994). Acid-base bifunctional catalysis by ZrO₂ and its mixed oxides. *Catalysis today*, 20(2), 185-197.
- Tanabe, K., Hattori, H., & Yamaguchi, T. (1991). Surface properties of solid superacids. *ChemInform*, 22(26). 1.
- Tangchupong, N., Khaodee, W., Jongsomjit, B., Laosiripojana, N., Praserttham, P., & Assabumrungrat, S. (2010). Effect of calcination temperature on characteristics of sulfated zirconia and its application as catalyst for isosynthesis. *Fuel Processing Technology*, 91(1), 121-126.
- Toda, M., Takagaki, A., Okamura, M., Kondo, J. N., Hayashi, S., Domen, K., & Hara, M. (2005). Green chemistry: biodiesel made with sugar catalyst. *Nature*, 438(7065), 178-178.
- Topsøe, H. (2003). Developments in operando studies and in situ characterization of heterogeneous catalysts. *Journal of Catalysis*, 216(1), 155-164.
- Tsigdinos, G.A. (1978). Heteropoly compounds of molybdenum and tungsten. *Topics in Current Chemistry*. 76, 1-64.
- Uzun, B. B., Pütün, A. E., & Pütün, E. (2006). Fast pyrolysis of soybean cake: product yields and compositions. *Bioresource technology*, 97(4), 569-576.
- Uzun, B. B., Pütün, A. E., & Pütün, E. (2006). Fast pyrolysis of soybean cake: product yields and compositions. *Bioresource technology*, 97(4), 569-576.
- Vaccari, A. (1998). Preparation and catalytic properties of cationic and anionic clays. *Catalysis Today*, 41(1), 53-71.
- Vaccari, A. (1999). Clays and catalysis: a promising future. *Applied Clay Science*, 14(4), 161-198.

- Valkenberg, M. H., & Hölderich, W. F. (2002). Preparation and use of hybrid organic–inorganic catalysts. *Catalysis Reviews*, 44(2), 321-374.
- van de Waal, J. C. & van Bekkum, H. in: Sherrington, D. C., & Kybett, A. P. (Eds.). (2001). *Supported catalysts and their applications* (Vol. 266). Royal Society of Chemistry.
- Veljković, V. B., Lakićević, S. H., Stamenković, O. S., Todorović, Z. B., & Lazić, M. L. (2006). Biodiesel production from tobacco (*Nicotiana tabacum* L.) seed oil with a high content of free fatty acids. *Fuel*, 85(17), 2671-2675.
- Venkat Reddy, C. R., Oshel, R., & Verkade, J. G. (2006). Room-temperature conversion of soybean oil and poultry fat to biodiesel catalyzed by nanocrystalline calcium oxides. *Energy & Fuels*, 20(3), 1310-1314.
- Viinikainen, T., Rönkkönen, H., Bradshaw, H., Stephenson, H., Airaksinen, S., Reinikainen, M., ... & Krause, O. (2009). Acidic and basic surface sites of zirconia-based biomass gasification gas clean-up catalysts. *Applied Catalysis A: General*, 362(1), 169-177.
- Vishwanathan, V., Balakrishna, G., Rajesh, B., Jayasri, V., Sikhivihilu, L. M., & Coville, N. J. (2008). Alkylation of catechol with methanol to give guaiacol over sulphate-modified zirconia solid acid catalysts: The influence of structural modification of zirconia on catalytic performance. *Catalysis Communications*, 9(14), 2422-2427.
- Wan Zahari, M., Mohd. Ariff, O., Mohd. Sukri, I., Oshibe, A., and Hayakawa, H. (2000). Oil palm by-products and urea molasses mineral blocks as feed resources for buffaloes in Malaysia. In: Proceedings of the 3rd Asian Buffalo Congress, Kandy, Sri Lanka.
- Wang, J. H., & Mou, C. Y. (2005). Alumina-promoted mesoporous sulfated zirconia: A catalyst for n-butane isomerization. *Applied Catalysis A: General*, 286(1), 128-136.
- Wang, J. H., & Mou, C. Y. (2008). Characterizations of aluminum-promoted sulfated zirconia on mesoporous MCM-41 silica: butane isomerization. *Microporous and Mesoporous Materials*, 110(2), 260-270.
- Wang, X., Liu, R., Waje, M. M., Chen, Z., Yan, Y., Bozhilov, K. N., & Feng, P. (2007). Sulfonated ordered mesoporous carbon as a stable and highly active protonic acid catalyst. *Chemistry of materials*, 19(10), 2395-2397.

- Wang, Y., Ou, S., Liu, P., Xue, F., & Tang, S. (2006). Comparison of two different processes to synthesize biodiesel by waste cooking oil. *Journal of Molecular Catalysis A: Chemical*, 252(1), 107-112.
- Ward, D. A., & Ko, E. I. (1994). One-step synthesis and characterization of zirconia-sulfate aerogels as solid superacids. *Journal of Catalysis*, 150(1), 18-33.
- Ward, J. W. (1969). The nature of active sites on zeolites: X. The acidity and catalytic activity of X zeolites. *Journal of Catalysis*, 14(4), 365-378.
- West, A. H., Posarac, D., & Ellis, N. (2008). Assessment of four biodiesel production processes using HYSYS. Plant. *Bioresource Technology*, 99(14), 6587-6601.
- White, R. L., Sikabwe, E. C., Coelho, M. A., & Resasco, D. E. (1995). Potential role of penta-coordinated sulfur in the acid site structure of sulfated zirconia. *Journal of Catalysis*, 157(2), 755-758.
- Wilson, K., Adams, D. J., Rothenberg, G., & Clark, J. H. (2000). Comparative study of phenol alkylation mechanisms using homogeneous and silica-supported boron trifluoride catalysts. *Journal of Molecular Catalysis A: Chemical*, 159(2), 309-314.
- Wilson, K., Renson, A., & Clark, J. H. (1999). Novel heterogeneous zinc triflate catalysts for the rearrangement of α -pinene oxide. *Catalysis letters*, 61(1-2), 51-55.
- Wong, H. K., & Wan Zahari, M. (1997). Nutritive value of palm kernel cake and cocoa pod husks for growing cattle. *Journal of Tropical Agriculture and Food Science*, 25, 125-131.
- Xie, W., & Wang, T. (2013). Biodiesel production from soybean oil transesterification using tin oxide-supported WO₃ catalysts. *Fuel Processing Technology*, 109, 150-155.
- Xing, R., Liu, Y., Wang, Y., Chen, L., Wu, H., Jiang, Y., ... & Wu, P. (2007). Active solid acid catalysts prepared by sulfonation of carbonization-controlled mesoporous carbon materials. *Microporous and Mesoporous Materials*, 105(1), 41-48.
- Xu, L., Wang, Y., Yang, X., Yu, X., Guo, Y., & Clark, J. H. (2008). Preparation of mesoporous polyoxometalate-tantalum pentoxide composite catalyst and its application for biodiesel production by esterification and transesterification. *Green Chemistry*, 10(7), 746-755.
- Yamaguchi, T., Jin, T., & Tanabe, K. (1986). Structure of acid sites on sulfur-promoted iron oxide. *The Journal of Physical Chemistry*, 90(14), 3148-3152.

- Yan, S., Salley, S. O., & Ng, K. S. (2009). Simultaneous transesterification and esterification of unrefined or waste oils over ZnO-La₂O₃ catalysts. *Applied Catalysis A: General*, 353(2), 203-212.
- Yan, X., Inderwildi, O. R., & King, D. A. (2010). Biofuels and synthetic fuels in the US and China: a review of well-to-wheel energy use and greenhouse gas emissions with the impact of land-use change. *Energy & Environmental Science*, 3(2), 190-197.
- Yu, H., Jin, Y., Li, Z., Peng, F., & Wang, H. (2008). Synthesis and characterization of sulfonated single-walled carbon nanotubes and their performance as solid acid catalyst. *Journal of Solid State Chemistry*, 181(3), 432-438.
- Yu, T., Chang, H. B., Lai, W. P., & Chen, X. F. (2011). Computational study of esterification between succinic acid and ethylene glycol in the absence of foreign catalyst and solvent. *Polym. Chem.*, 2(4), 892-896.
- Zabeti, M., Daud, W. M. A. W., & Aroua, M. K. (2009). Activity of solid catalysts for biodiesel production: a review. *Fuel Processing Technology*, 90(6), 770-777.
- Zalewski, D. J., Alerasool, S., & Doolin, P. K. (1999). Characterization of catalytically active sulfated zirconia. *Catalysis Today*, 53(3), 419-432.
- Zhang, F., Johnson, D. M., & Johnson, M. A. (2012). Development of a simulation model of biomass supply chain for biofuel production. *Renewable Energy*, 44, 380-391.
- Zhang, J., & Jiang, L. (2008). Acid-catalyzed esterification of *Zanthoxylum bungeanum* seed oil with high free fatty acids for biodiesel production. *Bioresource Technology*, 99(18), 8995-8998.
- Zhang, M., Sun, A., Meng, Y., Wang, L., Jiang, H., & Li, G. (2015). High activity ordered mesoporous carbon-based solid acid catalyst for the esterification of free fatty acids. *Microporous and Mesoporous Materials*, 204, 210-217.
- Zhang, Y. H. P. (2008). Reviving the carbohydrate economy via multi-product lignocellulose biorefineries. *Journal of industrial microbiology & biotechnology*, 35(5), 367-375.
- Zhang, Y. H. P. (2009). A sweet out-of-the-box solution to the hydrogen economy: is the sugar-powered car science fiction? *Energy & Environmental Science*, 2(3), 272-282.

- Zeng, Z., Chen, J., Cui, L., Xue, W., & Che, Y. (2012). Recent developments on the mechanism and kinetics of esterification reaction promoted by various catalysts. Dr. Vivek Patel (Ed.), ISBN: 978-953-51-0132-1, INTECH Open Access Publisher, [DOI: 10.5772/38106](https://doi.org/10.5772/38106).
- Zięba, A., Drelinkiewicz, A., Chmielarz, P., Matachowski, L., & Stejskal, J. (2010). Transesterification of triacetin with methanol on various solid acid catalysts: A role of catalyst properties. *Applied Catalysis A: General*, 387(1), 13-25.
- Zong, M. H., Duan, Z. Q., Lou, W. Y., Smith, T. J., & Wu, H. (2007). Preparation of a sugar catalyst and its use for highly efficient production of biodiesel. *Green Chemistry*, 9(5), 434-437.
- Zou, H., & Lin, Y. S. (2004). Structural and surface chemical properties of sol-gel derived TiO₂-ZrO₂ oxides. *Applied Catalysis A: General*, 265(1), 35-42.

List of publications and conference papers

- Sani, Y. M., Daud, W. M. A. W. Abdul Aziz, A. R. (2012). Biodiesel Feedstock and Production Technologies: Successes, Challenges and Prospects. In: Biodiesel—Feedstocks, Production and Applications. Z. Fang (Ed.), ISBN: 978-953-51-0910-5 <http://dx.doi.org/10.5772/52790>
- Sani, Y. M., Daud, W. M. A. W., & Abdul Aziz, A. (2013). Solid acid-catalyzed biodiesel production from microalgal oil—the dual advantage. *Journal of Environmental Chemical Engineering*, 1(3), 113-121. [doi:10.1016/j.jece.2013.04.006](https://doi.org/10.1016/j.jece.2013.04.006)
- Sani, Y. M., Daud, W. M. A. W., & Aziz, A. A. (2014). Activity of solid acid catalysts for biodiesel production: A critical review. *Applied Catalysis A: General*, 470, 140-161. [doi:10.1016/j.apcata.2013.10.052](https://doi.org/10.1016/j.apcata.2013.10.052)
- Sani, Y. M., Raji-Yahya, A. O., Alaba, P. A., Aziz, A. R. A., & Daud, W. M. A. W. (2015a). Palm frond and spikelet as environmentally benign alternative solid acid catalysts for biodiesel production. *BioResources*, 10(2), 3393-3408. [doi:10.15376/biores.10.2.3393-3408](https://doi.org/10.15376/biores.10.2.3393-3408)
- Sani, Y. M., Alaba, P. A., Raji-Yahya, A. O., Aziz, A. A., & Daud, W. M. A. W. (2015c). Acidity and catalytic performance of Yb-doped/Zr in comparison with/Zr catalysts synthesized via different preparatory conditions for biodiesel production. *Journal of the Taiwan Institute of Chemical Engineers*, <http://dx.doi.org/10.1016/j.jtice.2015.07.016>.
- Sani, Y. M., Alaba, P. A., Raji-Yahya, A. O., Aziz, A. R. A., & Daud, W. M. A. W. Facile synthesis of sulfated mesoporous Zr/ZSM-5 with improved Brønsted acidity and superior activity over SZr/Ag, SZr/Ti, and SZr/W in transforming UFO into biodiesel. *Journal of the Taiwan Institute of Chemical Engineers*. [doi:10.1016/j.jtice.2015.10.010](https://doi.org/10.1016/j.jtice.2015.10.010)

International Conferences

1. Sani, Y.M., Raji-Yahya, A. O., Alaba, P.A., Abdul Aziz, A. R., & Daud, W.M.A.W. (2015). Palm Frond and Spikelet as Environmentally Benign Alternative Solid Acid Catalysts for Biodiesel Production. International Institute of Engineers (IIER), 7th International Conference on Engineering & Natural Science, Dubai, UAE (1st March, 2015).

2. Sani, Y.M., Alaba, P.A., Abdul Aziz, A. R., & Daud, W.M.A.W. (2014). Effect of Preparation Method in Activating Active Sites and Catalytic Activity of $\text{SO}_4^{2-}/\text{ZrO}_2$ in Biodiesel Production. 7th RCChE 2014 Regional Conference on Chemical Engineering, AUN SEED NET, Yogyakarta, Indonesia (2nd-3rd December, 2014)

List of other related publications

- Hassan, S. N., Sani, Y. M., Aziz, A. A., Sulaiman, N. M. N., & Daud, W. M. A. W. (2015). Biogasoline: An out-of-the-box solution to the food-for-fuel and land-use competitions. *Energy Conversion and Management*, 89, 349-367. DOI: [10.1016/j.enconman.2014.09.050](https://doi.org/10.1016/j.enconman.2014.09.050)
- Alaba, P.A., **Sani, Y.M.**, Mohammed, I.Y., Daud, W.M.A.W. (2015). Insight into catalyst deactivation mechanism and suppression techniques in thermocatalytic deoxygenation of bio-oil over zeolites. *Reviews in Chemical Engineering*. 6, 521-639. DOI: [10.1515/revce-2015-0025](https://doi.org/10.1515/revce-2015-0025)
- Alaba, P.A., **Sani, Y.M.**, Mohammed, I.Y. Yousif Abakr, Daud, W.M.A.W. (2015). Synthesis and Application of Hierarchical Mesoporous HZSM-5 for Biodiesel Production from Shea Butter. *Journal of the Taiwan Institute of Chemical Engineers*. <http://dx.doi.org/10.1016/j.jtice.2015.09.006>
- Alaba, P.A., **Sani, Y.M.**, Daud, W.M.A.W. (2015). Synthesis and characterization of hierarchical nanoporous HY zeolite from acid activated kaolin. *Chinese Journal of Catalysis*. 36, 1846–1851. doi:[10.1016/S1872-2067\(15\)60962-7](https://doi.org/10.1016/S1872-2067(15)60962-7)
- Alaba, P.A., Sani, Y.M., Daud, W.M.A.W. (2015). Kaolinite properties and advances for solid acid and basic catalyst synthesis. *RSC Advances*. 5, 101127-101147. DOI: [10.1039/C5RA18884A](https://doi.org/10.1039/C5RA18884A)



Activity of solid acid catalysts for biodiesel production: A critical review



Yahaya Muhammad Sani^{a,b}, Wan Mohd Ashri Wan Daud^{a,*}, A.R. Abdul Aziz^a

^a Chemical Engineering Department, Faculty of Engineering, University Malaya, 50603 Kuala Lumpur, Malaysia

^b Department of Chemical Engineering, Ahmadu Bello University, Zaria 870001, Nigeria

ARTICLE INFO

Article history:

Received 17 June 2013

Received in revised form 22 October 2013

Accepted 26 October 2013

Available online 6 November 2013

Keywords:

Solid acid catalysts

Catalytic activity

Turnover frequency

Reaction conditions

Biodiesel

ABSTRACT

Homogeneous acid catalysts received wide acceptability because of their fast reaction rates. However, postproduction costs incurred from aqueous quenching, wastewater and loss of catalysts led to the search for alternatives. Until recently, heterogeneous base catalyzed-biodiesel production also gained the attention of most researchers. This was because the process minimized the problems of homogeneous catalysis in terms of catalyst regeneration and recycling in continuous processes. However, despite these advances, the ultimate aim of producing biodiesel at affordable cost is yet to be realized. Further, the process requires refined feedstocks which account for as high as 88% of the final production costs. Thus, the focus of many research efforts is towards the rational design and development of solid acid catalysts aimed at reducing biodiesel production costs. Therefore, this study reviewed current literature on the activities and advantages of solid acid catalysts used in biodiesel production. It discussed in details how the preparation method and prevailing reaction conditions affect the catalytic activity of the catalyst. The review concluded by suggesting way forward from the traditional trial-and-error method to a rational means of determining catalytic activities.

© 2013 Elsevier B.V. All rights reserved.

Contents

1. Introduction	141
2. Issues with heterogeneous base and homogeneous acid catalysts	141
3. Solid acid catalysts	142
3.1. Mixed oxides	142
3.1.1. Acidic montmorillonite (pillared) clays	142
3.1.2. Mixed metal oxides	142
3.2. Catalysts with sulfonic acid groups	148
3.3. Heteropoly acids and polyoxometalates (isopoly and heteropoly anions)	149
3.4. Zeolites and zeotype materials	150
4. Biodiesel production via solid acid catalysis	151
4.1. Turnover frequency (TOF)	151
4.2. Activity of solid acid catalysts under varying conditions	153
4.2.1. Effect of structure promoters, preparation method and reaction conditions	153
4.2.2. Effect of calcination temperature and acid strength	154
4.2.3. Effect of preparation method on CCSA bearing COOH, SO ₃ H and phenolic OH groups	156
4.2.4. Fixed bed reactor for continuous operations	157
4.2.5. Industrial production of biodiesel	157
5. Current status, future challenges and prospects	158
6. Conclusion	158
Acknowledgments	159
References	159

* Corresponding author. Tel.: +603 7967 5297; fax: +603 7967 5319.
E-mail address: ashri@um.edu.my (W.M.A.W. Daud).



Review

Solid acid-catalyzed biodiesel production from microalgal oil—The dual advantage

Yahaya Muhammad Sani^{a,b}, Wan Mohd Ashri Wan Daud^{a,*}, A.R. Abdul Aziz^a^a Chemical Engineering Department, Faculty of Engineering, University Malaya, 50603 Kuala Lumpur, Malaysia^b Department of Chemical Engineering, Ahmadu Bello University, Zaria 870001, Nigeria

ARTICLE INFO

Article history:
Received 1 February 2013
Accepted 15 April 2013

Keywords:
Microalgal oil
Solid acid catalysts
Transesterification
Biodiesel
Prospects
Challenges.

ABSTRACT

The major challenges facing the commercialization of biodiesel are: readily available and profitable feedstock and cost-effective production process. Although conventional oilseed feedstocks provided biodiesel yields of more than 98%, sufficient land for cultivating such feedstocks is a major challenge. Moreover, the use of refined feedstocks is uneconomical because of refining costs and priority as food. Algae (including macro- and microalgae) are the focus of many current research interests because they have the potential to provide sufficient fuel for global consumption. Beside their high lipid contents and fast growth rate, microalgae have the potential to mitigate the competition for land-use and food-for-fuel conflicts. They are also able to reduce the greenhouse effects via CO₂ sequestration. Critical survey of the literature suggests that microalgal oil has the potential to produce higher biodiesel yields with about 25% reduction in production costs. However, the oil from microalgae contains high free fatty acids which require pretreatment if conventional homogeneous catalysts are employed. Heterogeneous base catalysts are also not suitable due to soap formation and post-production processes, hence the need for solid acid catalysts. Therefore, this article provides a review on solid-acid catalysts used in processing microalgal oil for biodiesel production. Also discussed in details are the challenges and prospects of the production process. With more advances in technology and long-term commitment to investments, heterogeneous acid-catalyzed microalgal-biodiesel can become the ideal process for the future.

© 2013 Elsevier Ltd. All rights reserved.

Contents

Introduction	113
Biodiesel from algae as an alternative fuel	114
Present and future status of microalgal biodiesel production	114
Issues surrounding conventional transesterification processes	116
Solid acid catalysts used in microalgal oil biodiesel production	116
Biodiesel yields from heterogeneous acid-catalyzed microalgal oil	117
The dual advantage: potentials of heterogeneous acid-catalyzed microalgal biodiesel production	118
Issues surrounding solid acid catalysis	118
Future prospects and challenges	118
Conclusion	119
Conflict of interest	119
Acknowledgements	119
References	119

Introduction

Industrialization and transportation are two indicators used in reflecting the global civilization status [1,2]. Human civilization transformed from using animal forces (which relied on biomass from plants) to external combustion engines (which relied on solid

* Corresponding author. Tel.: +60 3 79675297; fax: +60 3 79675319.
E-mail address: ashri@um.edu.my (Daud).



Review

Biogasoline: An out-of-the-box solution to the food-for-fuel and land-use competitions

S.N. Hassan^{a,b}, Y.M. Sani^{a,c}, A.R. Abdul Aziz^{a,*}, N.M.N. Sulaiman^a, W.M.A.W. Daud^a^a Department of Chemical Engineering, University of Malaya, 50603 Kuala Lumpur, Malaysia^b Faculty of Chemical & Natural Resources Engineering, University Malaysia, 26300 Pahang, Malaysia^c Department of Chemical Engineering, Ahmadu Bello University, 870001 Zaria, Nigeria

ARTICLE INFO

Article history:

Received 31 December 2013

Accepted 17 September 2014

Keywords:

Biogasoline

Bioethanol

Biodiesel

Food-for-fuel

Microalgae

Rubber seed oil

ABSTRACT

Societal developments are hinged on the energy supplied by fossil fuels. However, the supply of these fuels is finite in the foreseeable future. This is aside the associated environmental degradation and economic sustainability of these fuels. These negative consequences and challenges spurred the search for sustainable energy sources such as biofuels. However, affordable feedstocks and efficient synthesis for renewable fuels remain indispensable and yet challenging line of research. Therefore, breakthroughs in plant biotechnology and mass production are essential prerequisites for ensuring the sustainability of biofuels as alternatives to petroleum-based energy. Conversely, public outcry concerning the food-for-fuel conflicts and land-use change hinder the popularity of such biofuel energy sources. Therefore, this paper reviewed the prospects of biogasoline production as sustainable alternative to ethanol and a compliment to biodiesel. Apart from reduction in greenhouse gas emissions, biogasoline promises to be cheaper and more environmental friendly. Further, inedible feedstocks such as microalgae and rubber seed oil would ensure higher net energy gain. Consequently, these will help resolve the food-for-fuel conflicts and land-use competitions. However, achieving the biofuel central policy depends on advances in processing the renewable energy sources.

© 2014 Elsevier Ltd. All rights reserved.

Contents

1. Introduction	350
2. Challenges associated with biofuel production and utilization	351
2.1. Land-use change and associated implications	351
2.1.1. Biogasoline land requirement	352
2.2. Food-for-fuel conflicts	353
2.3. Unavoidable utilization of fossil fuels & gasoline formulations	354
2.4. GHG emissions	354
3. Determinants that influence the demand and supply of biofuels	355
3.1. Prevailing market conditions	355
3.2. Socio-economic factors, health effects and environmental concerns	355
3.3. Governmental policies	356
3.4. Irregular distribution of global oil reserves	356
3.5. Need for long-term durability tests on vehicles powered by unblended biofuels	356
4. Is there a light at the end of the tunnel?	357
4.1. Biodiesel and bioethanol are only part of, but not the panacea	357
5. Biogasoline	357
5.1. Catalytic cracking of triglyceride-based feedstocks	358
5.2. Biogasoline via fluid catalytic cracking of microalgal oil	358
5.3. Properties, characterization and availability of RSO	359

* Corresponding author. Tel.: +60 3 7967 5300; fax: +60 3 7967 5319.

E-mail address: azizraman@um.edu.my (A.R. Abdul Aziz).<http://dx.doi.org/10.1016/j.enconman.2014.09.050>

0196-8904/© 2014 Elsevier Ltd. All rights reserved.

Biodiesel Feedstock and Production Technologies: Successes, Challenges and Prospects

Y.M. Sani, W.M.A.W. Daud and A.R. Abdul Aziz

Additional information is available at the end of the chapter

<http://dx.doi.org/10.5772/52790>

1. Introduction

In order to achieve the biodiesel central policy of protecting the environment, replacing petroleum diesel and protecting and/or creating jobs, a good understanding of biodiesel history is essential. This is because consumers always tend to buy cheap rather than “green” fuels. Moreover, it is more difficult for a new technology to dislodge one that has reached societal standard. The more the popular technology is used, the more it improves; becoming less expensive due to wider market potentials. Petrodiesel has become the “life-blood” of our economy. It would be almost impossible to find a commercial product today that does not consume diesel fuel during its production and distribution [1-4]. Therefore, the aim of this chapter is to provide an overview on the history and motivation, successes, challenges and prospects of biodiesel as source of energy. This will provide a global outlook in making biodiesel an economical and eco-friendly alternative to petroleum diesel.

The historical developments of the biofuel industry in general and biodiesel in particular, is unlike many industries. This is because the driving factors for its advances are more of economics and politics than technological [5]. As early as 1853, transesterification was conducted on vegetable oil in the search for a cheap method to produce glycerine for producing explosives during World War II by E. Duffy and J. Patrick [6-8]. In 1937, G. Chavanne, Belgian scientist patented the “Procedure for the transformation of vegetable oils for their uses as fuels”. “Biodiesel” as a concept was thus established [9]. It is a simple process where alkoxy group of an ester compound (oil or fat) is exchanged with an alcohol. However, it was not until 1977 that first patent on commercial biodiesel production process was applied for by Expedito Parente; a Brazilian scientist [10].

Prior to the discovery of and boom in fossil fuels, power was mainly generated from steam. However, the use of hydro-energy consumes large resources coupled with the inefficiencies

Palm Frond and Spikelet as Environmentally Benign Alternative Solid Acid Catalysts for Biodiesel Production

Yahaya M. Sani,^{a,b} Aisha O. Raji,^b Peter A. Alaba,^a A. R. Abdul Aziz,^a and Wan Mohd A. Wan Daud^{a,*}

A carbonization-sulfonation method was utilized in synthesizing sulfonated mesoporous catalysts from palm tree biomass. Brunauer-Emmett-Teller (BET), powder X-ray diffraction (XRD), energy dispersive X-ray (EDX), and field emission scanning emission microscopy (FE-SEM) analyses were used to evaluate the structural and textural properties of the catalysts. Further, Fourier transform infrared (FT-IR) spectroscopy and titrimetric analyses measured the strong acid value and acidity distribution of the materials. These analyses indicated that the catalysts had large mesopore volume, large surface area, uniform pore size, and high acid density. The catalytic activity exhibited by esterifying used frying oil (UFO) containing high (48%) free fatty acid (FFA) content further indicated these properties. All catalysts exhibited high activity, with SPTS/400 converting more than 98% FFA into fatty acid methyl esters (FAMEs). The catalyst exhibited the highest acid density, 1.2974 mmol/g, determined by NaOH titration. This is outstanding considering the lower reaction parameters of 5 h, 5:1 methanol-to-oil ratio, and a moderate temperature range between 100 and 200 °C. The study further illustrates the prospect of converting wastes into highly efficient, benign, and recyclable solid acid catalysts.

Keywords: Biomass; Mesoporous carbon sulfonation; Solid acid catalyst; High free fatty acid; Esterification

Contact information: a: Department of Chemical Engineering, University of Malaya, 50603 Kuala Lumpur, Malaysia; b: Department of Chemical Engineering, Ahmadu Bello University, 870001, Nigeria; * Corresponding author: ashri@um.edu.my

INTRODUCTION

Despite the recent fall in the price of Brent crude oil, the search for a sustainable and ecologically benign alternative persists. This is due to the pollution caused by crude oil exploration and the combustion of refined oil products (Sani *et al.* 2013; Hassan *et al.* 2015), coupled with weaker demand for petroleum fuels. One alternative being aggressively researched is the transesterification of triglycerides (TG) with methanol into biodiesel or fatty acids methyl esters (FAME) (Ghadge and Raheman 2006). However, feedstocks for this process containing large amounts of free fatty acids (FFAs), such as used frying oil (UFO), animal fats, and vegetable oils, usually incur postproduction costs in soap separation after alkali-catalyzed transesterification. This substantially decreases the biodiesel yield (Park *et al.* 2010). Reducing the FFA content of these feedstocks to approximately 1% (acid value of less than 2 mg KOH/g) is necessary before transesterification (Lotero *et al.* 2005; Zhang and Jiang 2008).

Similarly, there are several drawbacks to the two-step process of acid-catalyzed pre-esterification of FFA into esters with H₂SO₄ followed by alkali-catalyzed transesterification (Ramadhas *et al.* 2005; Ghadge and Raheman 2006; Veljkovic *et al.*



Contents lists available at ScienceDirect

Journal of the Taiwan Institute of Chemical Engineers

journal homepage: www.elsevier.com/locate/jtice

Facile synthesis of sulfated mesoporous Zr/ZSM-5 with improved Brønsted acidity and superior activity over SZr/Ag, SZr/Ti, and SZr/W in transforming UFO into biodiesel

Yahaya Muhammad Sani^{a,b}, Peter Adeniyi Alaba^a, Aisha Olatope Raji-Yahya^b, A.R. Abdul Aziz^{a,*}, Wan Mohd Ashri Wan Daud^a

^a Department of Chemical Engineering, University of Malaya, 50603 Kuala Lumpur, Malaysia

^b Department of Chemical Engineering, Ahmadu Bello University, 870001 Zaria, Nigeria

ARTICLE INFO

Article history:

Received 11 April 2015

Revised 9 September 2015

Accepted 6 October 2015

Available online xxx

Keywords:

Zirconia

Zeolite

Solid acid catalyst

High free fatty acid

Biodiesel

ABSTRACT

On the basis of the interplay between the metal function of oxo-anions, and structure of zeolites and its acidic properties, we report an innovative approach for enhancing acidity of sulfated zirconia, SZ. This concerns the superiority of SZ comprised of single-Brønsted acid sites dispersed on ZSM-5 over Ag, Ti and W. The influence of doping ZrO₂ on MFI framework of ZSM-5 was studied against other composite catalysts characterized by temperature-programmed desorption of ammonia (NH₃-TPD), IR spectra of pyridine adsorption, N₂ sorption, powder X-ray diffraction, elemental analysis via FE-SEM and EDX. Results showed uniform pore size, high mesopore volume, high surface area, and acid densities on the catalysts. Despite lower pore size distribution, Zr/ZSM-5 exhibited highest total acidity (0.75 mmol/g), and activity in converting >95% used frying oil (48 wt.%) over SZr/Ag, SZr/Ti, and SZr/W. This is outstanding considering the lower reaction parameter of 5 h, 5:1 methanol-to-oil ratio, and 200 °C compared to prior arts. Evidently, structure and strength of Brønsted acids have direct effect on the catalytic activity of the materials. This study also illustrated prospects of converting wastes into biodiesel, which is important especially against the backdrop of the current plummeting price of Brent crude oil.

© 2015 Taiwan Institute of Chemical Engineers. Published by Elsevier B.V. All rights reserved.

1. Introduction

As the price of Brent oil plummeted below USD45/barrel in the third quarter of 2015, the prominence, and sustenance of biofuels in general, and biodiesel in particular, faces greater challenges. The heavily footed subsidy that fossil fuels enjoy from governmental agencies exacerbates this problem further. Consequently, for biodiesel to maintain its indomitability as sustainable energy alternative beyond the 21st century, urgent and concerted efforts must be initiated from reactor engineering and catalysis [1,2]. From materials chemistry perspective, many studies have investigated the performances of a wide range of bifunctional solid acids catalysts such as WO₃/ZrO₂ [3], WO₃/SnO₂ [4], Mo-Mn/Al₂O₃-15 wt.% MgO [5], WO₃/ZrO₂ [6,7] and SO₄²⁻/TiO₂ [8] designed to incorporate synergistic effect in catalysis. However, despite the capability of converting

different feedstock oils to fatty acid methyl esters, FAME there is need for improvements.

For instance, WO₃/SnO₂ required 43 methanol-to-oil ratio to achieve a 78% yield [4], WO₃/ZrO₂ gave ~100% conversion after 20 h at 200 °C [6] and 70% conversion from used frying oil, UFO [7]. Similarly, the difficulty in synthesis and high production cost of SO₄²⁻/TiO₂ hinder its industrial application [8]. WO₃/ZrO₂ converted more than 90% soybean oil during transesterification at 250 °C [6] while SO₄²⁻/TiO₂, SO₄²⁻/ZrO₂, and WO₃/ZrO₂ converted 100, 99, and 94% *n*-octanoic acid respectively during esterification at 175 °C. In addition, longer reaction time (2047 min) was necessary for obtaining 50% conversion with tungstated zirconia with the acid site densities exhibiting ca. 95% of the original values. The long duration promoted adsorption of intermediates and products with subsequent deactivation.

Conversely, some results obtained from transesterification with zeolites were not as encouraging. For instance, despite high alcohol-to-oil molar ratio (14.5:1), Shu et al. [9] reported only 48.9 wt.% FAME conversion after 4 h with zeolite beta modified with La³⁺. Equally, Mordenite (HMOR) and H⁺ ion exchanged ZSM-5 (HMFI) zeolites [10] converted 80% of oleic acid with >0.06 mmol/g acid amount

* Corresponding author Tel.: +60 3 7967 5300; fax: +60 3 79675319.

E-mail addresses: ymsani@siswa.um.edu.my (Y.M. Sani), adeniyipee@live.com (P.A. Alaba), raji.aisha@gmail.com (A.O. Raji-Yahya), azizraman@um.edu.my, raja.shazrin@gmail.com (A.R. Abdul Aziz), ashri@um.edu.my (W.M.A.W. Daud).

<http://dx.doi.org/10.1016/j.jtice.2015.10.010>

1876-1070/© 2015 Taiwan Institute of Chemical Engineers. Published by Elsevier B.V. All rights reserved.

Please cite this article as: Y.M. Sani et al., Facile synthesis of sulfated mesoporous Zr/ZSM-5 with improved Brønsted acidity and superior activity over SZr/Ag, SZr/Ti, and SZr/W in transforming UFO into biodiesel, Journal of the Taiwan Institute of Chemical Engineers (2015), <http://dx.doi.org/10.1016/j.jtice.2015.10.010>



Contents lists available at ScienceDirect

Journal of the Taiwan Institute of Chemical Engineers

journal homepage: www.elsevier.com/locate/jtice

Acidity and catalytic performance of Yb-doped $\text{SO}_4^{2-}/\text{Zr}$ in comparison with $\text{SO}_4^{2-}/\text{Zr}$ catalysts synthesized *via* different preparatory conditions for biodiesel production

Yahaya Muhammad Sani^{a,b}, Peter Adeniyi Alaba^a, Aisha Olatope Raji-Yahya^b, A.R. Abdul Aziz^a, Wan Mohd Ashri Wan Daud^{a,*}

^a Department of Chemical Engineering, University of Malaya, 50603 Kuala Lumpur, Malaysia

^b Department of Chemical Engineering, Ahmadu Bello University, 870001 Zaria, Nigeria

ARTICLE INFO

Article history:

Received 8 April 2015

Revised 15 June 2015

Accepted 15 July 2015

Available online xxx

Keywords:

Catalyst preparation

Bifunctional catalyst

Acid activation

Solid acid catalyst

Biodiesel

ABSTRACT

Highly efficient, robust and mesoporous sulfated zirconia, SZ catalysts were prepared by co-precipitation and incipient-wetness routes with sufficient and in-excess acid. The study investigated the effect of pH, precursor type, and concentration, on SZ and compared their acidity and performance with ytterbium-doped SZ toward transesterification. N_2 sorption, elemental analysis, XRD, and ammonia temperature-programmed desorption (NH_3 -TPD) revealed the properties of the catalytic materials. The specific surface area increases independently of the presence of Ti up to $60.33 \text{ m}^2/\text{g}$, with increasing pH while pore size of the tetragonal crystallites decreases from 37.04 to 6.83 nm . Soaking the material in sufficient $0.5\text{-M H}_2\text{SO}_4$ produced $37.04 \text{ nm } S_{\text{BET}}$ in contrast to 21.21 nm from soaking in excess. Double sulfation ensured sulfate incorporation while moderate precursor amounts enhanced activity of the materials. Interestingly, despite low specific surface area, which was due to short aging period, large mesoporosity, high amount, and dispersion of active sites on Yb-doped SZ, SZr-Ti-Yb-500-4/s ensured remarkable activity. The catalyst converted ca. 99% of used frying oil containing ca. 48 wt. % FFA. Consequently, this highlights the prospect of producing biodiesel at lower cost especially with current dwindling price of crude oil.

© 2015 Taiwan Institute of Chemical Engineers. Published by Elsevier B.V. All rights reserved.

1. Introduction

The potency of public concern in the 21st century forces decision makers to enact policies not primarily based on science and technology. Concerns such as environmental impacts and socioeconomic challenges help to shape public opinion toward new demands which require novel catalytic solutions [1,2]. Inherent with these new challenges are the potentials for greater efficiency and sustainability of such systems [3]. Moreover, the searches for newer solutions have led experts to explore in details, the attributes of different materials, systems and devices [4]. One key task is in achieving phase-homogeneous solids with uniform morphological and chemical properties. This challenge is a fundamental prerequisite to any rational catalyst design. Further, the current dwindling price of crude oil is an indication that catalysis needs extensive experimentation to give biofuel the needed competitive edge. Consequently, it is necessary to

devise catalytic processes with ca. 100% yields. These will help to establish the potentials of catalysts as well as ensure the prominence of biofuels such as biodiesel. Despite these challenges, last century witnessed catalysis as the major backbone for most industrial processes such as petrochemistry (especially, petroleum catalytic refining) and bulk chemistry. Incidentally, the high activity of sulfated zirconia (SZ) attracted substantial attention for converting triglycerides (TGs) into biodiesel at moderate to high temperatures. SZ is the subject of numerous reports since its discovery in 1979 [5]. Considering the numerous reports available in the open literature, it is plausible to assert that SZ has attained a 'state-of-the-art' status. Further, most reports considered SZ as superacids because of their catalytic activity in simultaneously esterifying free fatty acids (FFA) and transesterifying triglycerides (TG) from high-FFA containing feedstocks into biodiesel.

However, despite numerous encouraging results, some aspects of SZ catalytic reactivity and physicochemical properties remain debatable. Some authors [6–8] argue that despite the presence of sulfate anions, the hydroxyl groups on the SZ surface are less acidic than the bridged hydroxyls in zeolites. They further claimed that besides Lewis sites, the surface of zirconia contains basic sites in the form of coordinated unsaturated oxygen atoms. They attributed this

* Corresponding author. Tel.: +601 1263 76195, +60 3796 75297; fax: +60 3796 75319.

E-mail addresses: ymsani@siswa.um.edu.my (Y.M. Sani), adeniyipee@live.com (P.A. Alaba), raji.aisha@gmail.com (A.O. Raji-Yahya), ashri@um.edu.my (W.M.A.W. Daud).

<http://dx.doi.org/10.1016/j.jtice.2015.07.016>

1876-1070/© 2015 Taiwan Institute of Chemical Engineers. Published by Elsevier B.V. All rights reserved.

Please cite this article as: Y.M. Sani et al., Acidity and catalytic performance of Yb-doped $\text{SO}_4^{2-}/\text{Zr}$ in comparison with $\text{SO}_4^{2-}/\text{Zr}$ catalysts synthesized *via* different preparatory conditions for biodiesel production, Journal of the Taiwan Institute of Chemical Engineers (2015), <http://dx.doi.org/10.1016/j.jtice.2015.07.016>

Cite this: *RSC Adv.*, 2015, 5, 101127

Kaolinite properties and advances for solid acid and basic catalyst synthesis

Peter Adeniyi Alaba,^a Yahaya Muhammad Sani^{ab} and Wan Mohd Ashri Wan Daud^{*a}

Historically, clay mineral catalysts have found industrial applications since the early 1930s. However, inherent limitations such as impurities, porosity, low surface area and acidity hindered their wide and sustained acceptability, this is despite their economic advantages. Interestingly, the use of kaolinite as precursor in active catalyst synthesis has been a breakthrough for several industrial processes such as petrol chemistry; especially in catalytic refining and bulk chemistry. The same is also true for processes that require solid acid catalysts, catalyst support, co-catalyst or promoter application for positive environmental impact and economic viability. Therefore, this article reviews the physicochemical properties of kaolinite and their amenability to modification towards enhancing their catalytic properties. The article also discussed modification methods such as mechanochemical activation (dealumination), thermal activation, intercalation and chemical activation. With more advances in technology and long-term commitment to investments, kaolinite will become the ideal catalyst and precursor for synthesizing novel catalysts for a sustainable “greener” future.

Received 14th September 2015
Accepted 17th November 2015

DOI: 10.1039/c5ra18884a

www.rsc.org/advances

1. Introduction

Kaolinite is a 1 : 1 layer phyllosilicate clay mineral that makes up about 10–95% of the mineral kaolin. Its structure possesses a sheet of gibbsite-like $\text{Al}(\text{OH})_3$ (octahedrally coordinated) and

a sheet of SiO_4 tetrahedral combined with longitudinal sideline chains forming a dioctahedral structure called 1 : 1 layer phyllosilicate.^{1–3} Fig. 1 shows the structural model of kaolinite.⁴ Theoretically, its chemical formula is $\text{Si}_2\text{Al}_2\text{O}_5(\text{OH})_4$ ($\text{Al}_2\text{O}_3 \cdot 2\text{H}_2\text{O}$ or $\text{Al}_2\text{O}_3 \cdot 2\text{SiO}_2 \cdot 2\text{H}_2\text{O}$).^{5–7} Other components of kaolin includes mica and quartz as well as metal oxides such as K_2O , CaO , TiO_2 , Fe_2O_3 , Na_2O , MgO , MnO , and P_2O_5 as impurities. It is a versatile hydrated aluminosilicate with a wide variety of industrial applications such as in catalysis, photocatalysis,⁸ ion exchange,⁹ decolorization,^{10–12} adsorption,^{12,13} catalyst supports

^aDepartment of Chemical Engineering, University of Malaya, 50603 Kuala Lumpur, Malaysia. E-mail: ashri@um.edu.my; adeniyipee@live.com; ymsani@abu.edu.ng; Fax: +60 3 79675319; Tel: +60 1 126376195; +60 3 79675297

^bDepartment of Chemical Engineering, Ahmadu Bello University, 870001 Nigeria



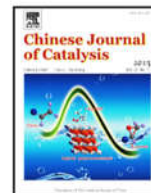
Peter Adeniyi Alaba was born in Kwara State, Nigeria in 1980 and carried out undergraduate at the Federal University of Technology Minna. He is currently concluded his post-graduate studies (Mphil.) at the University of Malaya under the supervision of Prof. Wan Mohd Ashri Wan Daud. He was appointed to a Graduate research assistantship at the University of Malaya in 2013 till

date. His research interests lie in rational design of tailored solid acid catalysts for efficient biofuel production, environmental engineering, CFD, and computational chemistry.



Yahaya Muhammad Sani was born and raised in Zaria, a city rich in cultural heritage & the capital of the Hausa kingdom of Zazzau in Nigeria. He received his B.Eng. Chem. Eng. from Ahmadu Bello University, the 2nd largest on the African continent (2002), MSc degrees in Biotechnology (Newcastle University, UK; 2007), & Chem. Eng. (A.B.U. Zaria; 2008) prior to obtaining a PhD from

University of Malaya, Malaysia. He joined A.B.U. Zaria in 2005 with research interest on catalysis, and renewable & sustainable energy. He is a registered Engineer certified by Council for the Regulation of Engineering, & a corporate member of the Nigerian Society of Engineers.

available at www.sciencedirect.comjournal homepage: www.elsevier.com/locate/chnjc

Article

Synthesis and characterization of hierarchical nanoporous HY zeolites from acid-activated kaolin

Peter Adeniyi Alaba^a, Yahaya Muhammad Sani^{a,b}, Wan Mohd Ashri Wan Daud^{a,*}^a Department of Chemical Engineering, University of Malaya, 50603 Kuala Lumpur, Malaysia^b Department of Chemical Engineering, Ahmadu Bello University, 870001 Nigeria

ARTICLE INFO

Article history:

Received 1 May 2015

Accepted 15 August 2015

Published 20 November 2015

Keywords:

HY zeolite

Kaolin

Hierarchical mesopore

Hierarchical factor

Relative crystallinity

ABSTRACT

Hierarchical nanoporous HY zeolites were synthesized from acid-activated kaolin. The hierarchical factor (HF) was maximized by varying the aging and crystallization time. This was achieved by maximizing the external surface area without greatly reducing the micropore volume. The resulting products were characterized using X-ray diffraction (XRD), X-ray fluorescence, N₂ adsorption, and NH₃ temperature-programmed desorption. The nanoporous HY zeolite with the highest HF was obtained by aging for 48 h and a crystallization time of 24 h. The acidity and crystallinity varied depending on the operating parameters. Incorporation of an appropriate amount of NaCl was also vital in maximizing the HF, crystallinity, and acidity. The sample crystallinities were determined by comparing their XRD peak intensities with those of a conventional Y zeolite. The results show that optimizing this process could lead to a widely acceptable commercial route for HY zeolite production.

© 2015, Dalian Institute of Chemical Physics, Chinese Academy of Sciences.
Published by Elsevier B.V. All rights reserved.

1. Introduction

Faujasitic zeolites have gained immense popularity within the research community and commercially. This is because they have a uniform pore size, high specific surface area (SSA), and thermal stability [1]. They also have tunable pores and acidities, and are therefore useful in various petrochemical processes [2]. However, their average pore size is low, which limits their use in processes that involve bulky molecules. Such processes include organic waste treatment, and heavy crude oil and bio-oil upgrading. This is because of their mass transfer hurdle in bulky chemical reactions [3]. Several researchers have reported strategies for overcoming this transport limitation for bulky molecules. These include dealumination, desilication, synthesis of mesoporous zeolites and microporous zeolites, and use of structure-directing agents [4]. The use of commercially available dual-pore materials obtained from crystal-

line composite materials and crystalline physical mixtures has also been investigated [5,6].

However, these strategies do not give satisfactory results in terms of acidity, and structural, thermal, and hydrothermal stability [7]. Recently, one of the most potent strategies has been the synthesis of nanocrystalline materials with more than one porosity level, termed hierarchical nanoporous materials. These materials synergistically combine the properties of mesoporous and microporous zeolites [8,9]. Hierarchical nanoporous materials have high thermal and hydrothermal stability and pore channels with a bimodal pore system (micro- and mesopores) [7,10]. The connection of microporous and mesoporous channels in a highly ordered manner enables the microporous channels to reside in the matrix. This results in shorter diffusion paths for reactant molecules [11].

Several researchers have worked on the synthesis of these bimodal materials [7,12,13]. Tan et al. [7] investigated the syn-

* Corresponding author. Tel: +60 3796 76897, +60 3796 75297; Fax: +60 3796 75319; E-mail: ashri@um.edu.myDOI: 10.1016/S1872-2067(15)60962-7 | <http://www.sciencedirect.com/science/journal/18722067> | Chin. J. Catal., Vol. 36, No. 11, November 2015



Contents lists available at ScienceDirect

Journal of the Taiwan Institute of Chemical Engineers

journal homepage: www.elsevier.com/locate/jtice

Synthesis and application of hierarchical mesoporous HZSM-5 for biodiesel production from shea butter

Peter Adeniyi Alaba^a, Yahaya Muhammad Sani^{a,b}, Isah Yakub Mohammed^c,
Yousif Abdalla Abakr^c, Wan Mohd Ashri Wan Daud^{a,*}

^a Department of Chemical Engineering, University of Malaya, 50603 Kuala Lumpur, Malaysia

^b Department of Chemical Engineering, Ahmadu Bello University, 870001 Nigeria

^c Energy, Fuel and Power Technology Research Division, School of Engineering, the University of Nottingham Malaysia Campus, Jalan Broga, 43500 Semenyih, Selangor Darul Ehsan, Malaysia

ARTICLE INFO

Article history:

Received 23 April 2015

Revised 8 September 2015

Accepted 11 September 2015

Available online xxx

Keywords:

Hierarchical mesoporous ZSM-5 zeolite

Desilication

Transesterification

Shea butter

ABSTRACT

Here, we report the upgrading of shea butter to biodiesel with hierarchical mesoporous ZSM-5 zeolites (HMZeol). Shea butter is a triglyceride (mainly oleic and steric acid) extracted from African shea tree nut. The catalysts synthesis was by desilication of conventional ZSM-5 with an aqueous solution of NaOH (0.3 and 0.4 M). XRF, XRD, NH_3 -TPD and N_2 adsorption unveiled the effect of desilication of the parent zeolite. The study investigated the effect of NaOH concentration on matrix area, pore size, mesopore volume and Si/Al ratio. HMZeol showed superior activity on biodiesel yield when compared with the parent ZSM-5 zeolite. The catalytic material treated with 0.4 M NaOH (0.4HMZeol) gave 74% biodiesel yield at 5:1 methanol/oil molar ratio, 1 wt% catalyst, and 200 °C for 3 h reaction time while ZSM-5 gave 46.05% yield under the same reaction conditions. Further increase in the reaction time to 12 h for 0.4HMZeol, 0.3HMZeol and ZSM-5 gave 82.12, 79.21, and 72.13% biodiesel yield respectively. These results showed that hierarchical mesoporous HZSM-5 is a promising solid acid catalyst for biodiesel production via transesterification.

© 2015 Taiwan Institute of Chemical Engineers. Published by Elsevier B.V. All rights reserved.

1. Introduction

Depleting global petroleum reserves, greenhouse gas (GHG) emissions, and health-related issues are increasing the demand for alternative energy resources. Incidentally, the benign nature, renewability and economic prospects of biodiesel is gaining attention [1]. This makes biodiesel more advantageous than fossil-diesel. Moreover, it exhibits superior lubricating property, flash point and cetane number thereby, prolonging engine life [2,3]. Biodiesel is obtained from lipid feedstock derived long chain fatty acid mono alkyl ester such as algae-derived oil, animal fats and vegetable fats and oils. One of such source is shea butter. Shea butter is an ivory colored fat extracted from shea nut of sub-Saharan African shea tree (*Vitellaria paradoxa*) with high free fatty acid (FFA) content [4]. The FFA contents are majorly of oleic acid and steric acid. Shea butter enjoyed wide utilization in confectionery and cosmetic industry. This leads to rapid growth in shea market, about 350,000 tons of shea export in the past decade

[5], the cost of which is close to that of palm oil (as low as USD 720 per tons) [6]. Table 1 presents the properties of crude shea butter.

There are four strategies for biodiesel production; these include transesterification, thermal cracking, micro-emulsions, and hydrodeoxygenation. The most popular of these strategies is transesterification [2]. Generally, transesterification proceeds with the aid of homogeneous basic catalysts such as KOH, NaOH and other hydroxides [8]. The preference of homogeneous basic catalysts to their acidic counterparts is basically due to their better activity especially for triglycerides with low free fatty acid (FFA) content [2]. However, transesterification with homogeneous catalysts have various drawbacks. These include catalyst separation to purify the biodiesel, soap formation and separation of glycerol and water quenching which requires a large amount of water. These generates large amount of wastewater [3,9,10]. Solid acid catalyzed transesterification is a promising route that could overcome these shortcomings because of ease of separation. However, some authors reported the limitations of solid acid catalysts such as leaching and diffusion limitations [3,11–13]. Consequently, synthesis of mesoporous stable solid acid catalysts is necessary to avoid leaching of the active sites, which leads to catalyst deactivation.

Zeolites are crystalline microporous aluminosilicate minerals, which exhibit remarkable attributes such as high surface area and

* Corresponding author. Tel.: +601 1263 76195, +60 3796 75297;

fax: +60 3796 75319.

E-mail addresses: adeniyipee@live.com (P.A. Alaba), ymsani@siswa.um.edu.my (Y.M. Sani), ashri@um.edu.my (W.M.A.W. Daud).

<http://dx.doi.org/10.1016/j.jtice.2015.09.006>

1876-1070/© 2015 Taiwan Institute of Chemical Engineers. Published by Elsevier B.V. All rights reserved.

Please cite this article as: P.A. Alaba et al., Synthesis and application of hierarchical mesoporous HZSM-5 for biodiesel production from shea butter, Journal of the Taiwan Institute of Chemical Engineers (2015), <http://dx.doi.org/10.1016/j.jtice.2015.09.006>

Peter Adeniyi Alaba, Yahaya Muhammad Sani, Isah Yakub Mohammed
and Wan Mohd Ashri Wan Daud*

Insight into catalyst deactivation mechanism and suppression techniques in thermocatalytic deoxygenation of bio-oil over zeolites

DOI 10.1515/revce-2015-0025

Received May 7, 2015; accepted August 28, 2015

Keywords: acidity; biomass; coke; deactivation; deoxygenation; zeolite.

Abstract: The economic viability of the thermocatalytic upgrade of biomass-derived oxygenates is facing the challenge of low-quality products. This is because of leaching of active species, coking, and concomitant catalyst deactivation. These cumulate into the loss of catalytic activity with time on stream (TOS), which causes low degree of deoxygenation. Thus, this article reviews recent advances aimed at alleviating these setbacks to make the process viable for industrial scale-up. To understand the concept of catalyst deactivation and to offer solutions, the review scrutinized the deactivation mechanism diligently. The review also analyzes deactivation-suppression techniques such as nanocrystal zeolite cracking, hydrogen spilt-over (HSO) species, and composite catalysts (hybrid, hierarchical mesoporous zeolite, modified zeolites, and catalytic cracking deposition of silane). Interestingly, these deactivation-suppression techniques enhance catalytic properties mostly by reducing the signal strength of strong acid sites and increasing hydrothermal stability. Further, the approaches improve catalytic activity, selectivity, and TOS stability because of the lower formation of coke precursors such as polynuclear aromatics. However, despite these many advances, the need for further investigations to achieve excellent catalytic activity for industrial scale-up persists.

1 Introduction

The use of fossil fuels in several sectors, such as heat and power generation, and transportation create environmental hazards from emission of greenhouse gases (Graça et al. 2010). Furthermore, these fuels are nonrenewable, often scarce with unpredictable prices. Also, because of the excessive use of these conventional fuels, crude oil exploration is said to have reached its peak (Mohammad et al. 2013). Thus, the public outcry for urgent solutions explains the need to seek alternative and sustainable sources of energy. Biomass from fast pyrolysis possess high potentials for producing biofuels and other specialty chemicals for replacing fossil fuel-derived products (Demirbas 2009, Botas et al. 2012). Techniques currently explored in producing these biofuels include thermal cracking (pyrolysis), coblending with VGO, and micro-emulsion of biomass (Gómez et al. 2013). Fast pyrolysis is the most commonly used method for biofuel production from biomass because it is economically viable and thermally efficient (Apaydin-Varol et al. 2014). The product of this process include gaseous, liquid, and solid biofuels. The liquid biofuel could be biocrude, synthetic oils, and biodiesels (Demirbas 2007a, 2008a,b, Gerçel and Gerçel 2007, Gonzalez et al. 2008, Ye et al. 2008, Balat 2009). However, the major drawback of biofuel from pyrolysis is the oxygen contents, which is responsible for its low heating value, instability, and high acidity (Pütün et al. 2006, Demirbas 2007b, Phung et al. 2012, Shi et al. 2014). This constituent lowers the quality of the biofuel and thereby restricts its application. Despite this, however, the popularity and the public acceptance of biofuels are on the increase. The major reasons for this include sustainability of fuels derived from renewable sources that support ecosystem and human health as well as long-term goals on tolerable emissions. Other reasons include availability,

*Corresponding author: Wan Mohd Ashri Wan Daud, Department of Chemical Engineering, University of Malaya, 50603 Kuala Lumpur, Malaysia, e-mail: ashri@um.edu.my

Peter Adeniyi Alaba: Department of Chemical Engineering, University of Malaya, 50603 Kuala Lumpur, Malaysia

Yahaya Muhammad Sani: Department of Chemical Engineering, University of Malaya, 50603 Kuala Lumpur, Malaysia; and Department of Chemical Engineering, Ahmadu Bello University, 870001 Nigeria

Isah Yakub Mohammed: Energy, Fuel and Power Technology Research Division, School of Engineering, The University of Nottingham Malaysia Campus, Jalan Broga, 43500 Semenyih, Selangor Darul Ehsan, Malaysia

APPENDIX

Appendix A: Energy dispersive X-ray, EDX analysis

SZr-500-4/e

Element	Line Type	Apparent Concentration	k Ratio	Wt%	Wt% Sigma	Atomic %
Al	K series	0.01	0.00010	0.27	0.18	0.85
Si	K series	0.01	0.00006	0.13	0.20	0.39
S	K series	0.09	0.00079	2.50	0.40	6.73
Zr	L series	3.56	0.03563	97.11	0.48	92.02
Total:				100.00		100.00

SZr-500-1/e

Element	Line Type	Apparent Concentration	k Ratio	Wt%	Wt% Sigma	Atomic %
Al	K series	0.17	0.00120	2.31	0.15	7.18
Si	K series	0.00	0.00000	0.00	0.00	0.00
S	K series	0.09	0.00078	1.85	0.30	4.83
Zr	L series	4.64	0.04637	95.84	0.33	87.99
Total:				100.00		100.00

SZr-500-5/7

Element	Line Type	Apparent Concentration	k Ratio	Wt%	Wt% Sigma	Atomic %
Al	K series	0.04	0.00027	1.10	0.31	3.51
Si	K series	0.00	0.00001	0.02	0.33	0.07
S	K series	0.04	0.00031	1.60	0.59	4.32
Zr	L series	2.22	0.02218	97.28	0.73	92.10
Total:				100.00		100.00

SZr-500-5/7R

Element	Line Type	Apparent Concentration	k Ratio	Wt%	Wt% Sigma	Atomic %
Al	K series	0.01	0.00008	0.33	0.29	1.10
Si	K series	0.00	0.00002	0.06	0.32	0.20
S	K series	0.00	0.00002	0.08	0.59	0.23
Zr	L series	2.30	0.02303	99.53	0.73	98.47
Total:				100.00		100.00

SZr-500-5/10

Element	Line Type	Apparent Concentration	k Ratio	Wt%	Wt% Sigma	Atomic %
Al	K series	0.03	0.00023	0.61	0.19	1.97
Si	K series	0.01	0.00012	0.27	0.22	0.84
S	K series	0.04	0.00034	1.10	0.36	3.00
Zr	L series	3.55	0.03551	98.03	0.46	94.19
Total:				100.00		100.00

SZr-500-5/14

Element	Line Type	Apparent Concentration	k Ratio	Wt%	Wt% Sigma	Atomic %
Al	K series	0.04	0.00028	0.46	0.12	1.54
Si	K series	0.00	0.00002	0.03	0.14	0.11
S	K series	0.00	0.00000	0.00	0.00	0.00
Zr	L series	5.71	0.05713	99.50	0.18	98.35
Total:				100.00		100.00

ZSM-5

Element	Line Type	Apparent Concentration	k Ratio	Wt%	Wt% Sigma	Atomic %
Al	K series	0.38	0.00271	6.24	0.19	6.49
Si	K series	4.93	0.03907	93.42	0.26	93.22
S	K series	0.01	0.00011	0.34	0.19	0.29
Zr	L series	0.00	0.00000	0.00	0.00	0.00
Total:				100.00		100.00

ZrO₂

Element	Line Type	Apparent Concentration	k Ratio	Wt%	Wt% Sigma	Atomic %
Al	K series	0.00	0.00001	0.04	0.25	0.15
Si	K series	0.00	0.00000	0.00	0.00	0.00
S	K series	0.00	0.00002	0.08	0.48	0.23
Zr	L series	2.28	0.02280	99.87	0.54	99.62
Total:				100.00		100.00

sEFB/400

Element	Line Type	Apparent Concentration	k Ratio	Wt%	Wt% Sigma	Atomic %
C	K series	5.28	0.05283	70.57	0.43	78.44
O	K series	2.95	0.00993	22.25	0.40	18.57
S	K series	0.96	0.00826	7.18	0.21	2.99
Total:				100.00		100.00

sPTS/400

Element	Line Type	Apparent Concentration	k Ratio	Wt%	Wt% Sigma	Atomic %
C	K series	4.09	0.04090	65.85	0.68	72.16
O	K series	2.88	0.00969	33.53	0.68	27.59
S	K series	0.05	0.00041	0.62	0.19	0.25
Total:				100.00		100.00

sPTF/SA/400

Element	Line Type	Apparent Concentration	k Ratio	Wt%	Wt% Sigma	Atomic %
C	K series	5.12	0.05122	58.26	0.33	66.14
O	K series	6.19	0.02082	37.74	0.32	32.16
S	K series	0.55	0.00476	4.00	0.13	1.70
Total:				100.00		100.00

sPTF/SA/300

Element	Line Type	Apparent Concentration	k Ratio	Wt%	Wt% Sigma	Atomic %
C	K series	5.25	0.05245	59.22	0.33	67.03
O	K series	5.97	0.02009	36.85	0.32	31.31
S	K series	0.54	0.00468	3.93	0.12	1.67
Total:				100.00		100.00

WO₃

Element	Line Type	Apparent Concentration	k Ratio	Wt%	Wt% Sigma	Atomic %
O	K series	3.84	0.01292	23.60	0.28	77.40
Al	K series	0.04	0.00029	0.27	0.06	0.52
Si	K series	0.00	0.00000	0.00	0.00	0.00
S	K series	0.00	0.00000	0.00	0.00	0.00
Ti	K series	0.00	0.00000	0.00	0.00	0.00
Zr	L series	0.08	0.00084	1.21	0.34	0.70
Ag	L series	0.00	0.00002	0.02	0.28	0.01
W	M series	6.13	0.06128	74.89	0.43	21.37
Total:				100.00		100.00

SZrAg

Element	Line Type	Apparent Concentration	k Ratio	Wt%	Wt% Sigma	Atomic %
Al	K series	0.02	0.00013	0.16	0.08	0.55
Si	K series	0.00	0.00000	0.00	0.00	0.00
S	K series	0.07	0.00063	0.88	0.16	2.51
Zr	L series	6.71	0.06706	84.73	0.54	84.88
Ag	L series	0.92	0.00924	14.23	0.53	12.05
Total:				100.00		100.00

SZrTi

Element	Line Type	Apparent Concentration	k Ratio	Wt%	Wt% Sigma	Atomic %
Al	K series	0.02	0.00018	0.24	0.09	0.71
Si	K series	0.00	0.00000	0.00	0.00	0.00
S	K series	0.02	0.00020	0.32	0.17	0.80
Ti	K series	1.06	0.01059	13.78	0.46	23.10
Zr	L series	6.02	0.06021	85.26	0.60	75.08
Ag	L series	0.02	0.00024	0.41	0.41	0.30
Total:				100.00		100.00

SZrWO₃

Element	Line Type	Apparent Concentration	k Ratio	Wt%	Wt% Sigma	Atomic %
Al	K series	0.01	0.00010	0.13	0.10	0.45
Si	K series	0.00	0.00000	0.00	0.00	0.00
S	K series	0.09	0.00079	1.26	0.20	3.71
Ti	K series	0.00	0.00000	0.00	0.00	0.00
Zr	L series	6.05	0.06050	86.86	0.64	89.81
Ag	L series	0.00	0.00000	0.00	0.00	0.00
W	M series	0.76	0.00760	11.75	0.61	6.03
Total:				100.00		100.00

SZrZSM-5

Element	Line Type	Apparent Concentration	k Ratio	Wt%	Wt% Sigma	Atomic %
Al	K series	0.07	0.00051	0.69	0.09	1.89
Si	K series	0.88	0.00699	8.56	0.20	22.55
S	K series	0.08	0.00066	1.10	0.18	2.53
Ti	K series	0.03	0.00029	0.40	0.29	0.61
Zr	L series	5.95	0.05952	89.26	0.38	72.41
Ag	L series	0.00	0.00000	0.00	0.00	0.00
W	M series	0.00	0.00000	0.00	0.00	0.00
Total:				100.00		100.00

AgNO₃

Element	Line Type	Apparent Concentration	k Ratio	Wt%	Wt% Sigma	Atomic %
Al	K series	0.05	0.00038	0.63	0.12	2.48
Si	K series	0.01	0.00007	0.10	0.11	0.37
S	K series	0.01	0.00006	0.08	0.12	0.26
Zr	L series	0.03	0.00030	0.48	0.36	0.55
Ag	L series	6.48	0.06479	98.71	0.41	96.33
Total:				100.00		100.00